Mechanisms of resistance to lapatinib in HER2-positive breast cancer

A thesis submitted for the degree of PhD

by Martina McDermott, BSc

June 2012

The work in this thesis was carried out under the supervision of

Dr. Norma O'Donovan

&

Prof. John Crown

National Institute for Cellular Biotechnology

School of Biotechnology

Dublin City University

I hereby certify that this material, which I now submit for assessment on the programme of study leading to the award of PhD, is entirely my own work, that I have exercised reasonable care to ensure that the work is original, and does not to the best of my knowledge breach any law of copyright, and has not been taken from the work of others save and to the extent that such work has been cited and acknowledged within the text of my work.

Signed: _____

ID No.: _____

Date: _____

Acknowledgements

First of all, my sincerest thanks to my supervisor Dr Norma O'Donovan. You encouraged me to begin the PhD and have guided me throughout the process. Without your help and gentle prodding I'd never have completed it! Thanks also to Prof. John Crown for giving me the opportunity to do my PhD in your group; I've learnt so much from being a part of it. Special thanks to little Ciara and Keelin; without you both keeping your mum so busy I'd never have gotten to disappear to LA for a year :)

I can't mention LA without saying thank you to Dr Neil O'Brien. Thanks for the surfing lessons, drinking sessions and trips to Vegas, but most of all thanks for inspiring me so much. You've been a great mentor and friend throughout the PhD. Hopefully someday we'll get the chance to work together again. To Karen McDonald, thanks for making LA so much fun, I never expected to make such a great friend and I miss having you around the place making everyone laugh.

Special thanks to Dr. Lee Anderson in UCLA who performed the aCGH analysis in this study, Mick and Paul for helping with the SILAC proteomics, Susan Kennedy and Alison Prendergast who performed the FISH and Karen McDonald for helping with lysates for the panel of cell lines.

Thanks to everyone who's been a part of our group over the years, especially to Alex, Denis and Brigid for all the help and guidance when experiments when wrong or I couldn't face doing yet another replicate. Thanks to Thamir, Brendan, and Zulfi, and the newer members of the group Alexandra, Trish and Karen for the laughs and fun you've brought to the group!

Thanks to Sandra and Erica for realising that I wasn't going anywhere and eventually learning the student with the long-hair's name! and for coming to LA to visit me and not causing earthquakes or bomb-scares! It's great to have made such great friends in the centre, especially Kathy. You helped make the last year bearable even though I drove you demented with the mess I made of the apartment. Thanks for putting up with me and making sure I remembered to have fun! And most of all thanks for getting a job in South Carolina too so I can make a mess of that apartment too!!

Thanks to everyone else in the centre for making my time here so memorable including, Fiona, Naomi, Laura, Justine, Karen, Geraldine and to Carol and Yvonne for all your help.

Lastly special thanks to my family, especially my parents, thank you for encouraging me throughout my education to always try my hardest and to achieve my goals. Thanks for helping to support me financially and for always being at the end of the phone whenever I needed help. To mam, you are the strongest, bravest most amazing person I know, I'll be in awe of you always, and I dedicate this thesis to you!

Table of Contents

Abbreviations

4E-BP1	eukaryotic initiation factor 4E-binding protein 1
ABC	adenosine tri-phosphate binding cassette
aCGH	Array comparative genomic hybridisation
ACN	acetonitrile
ACS	accelerated cellular senescence
ADAM	A disintegrin and a metalloprotease domain protein
ADCC	antibody-dependent cell-mediated cytotoxicity
ADP	adenosine di-phosphate
AIF	apoptosis inducing factor
AKT/PKB	protein kinase B
AMP	adenosine mono-phosphate
AMPK	adenosine mono-phosphate activated protein kinase
APBI	accelerated partial breast irradiation
ATM	ataxia telangiectasia mutated
ATP	adenosine tri-phosphate
BAD	BCL-2 antagonist of cell death
BAK	BCL-2 antagonist killer
BAX	BCL-2 associated protein X
BCA	bicinchoninic acid
BCRP	breast cancer-related protein
BCT	breast conserving therapy
BIM	BCl-2 interacting protein
BrdU	bromodeoxyrudine
CDK	cyclin-dependent kinase
CDKI	cyclin-dependent kinase inhibitor
CNS	central nervous system
CNV	copy number variation
DAPI	4',6-diamidino-2-phenylindole
DIGE	Difference in-gel electrophoresis
DMF	N-N-dimethylformamide

DNK-PK	double-stranded DNA-dependent protein kinase
DTEP	drug-tolerant expanded persistor
DTT	dithiothreitol
EBP1	erbb3-binding protein 1
ECD	extracellular domain
eEF2	eukaryotic elongation factor 2
eEF2k	eukaryotic elongation factor 2 kinase
EGFR/HER1/erBB1	epidermal growth factor receptor 1
eiF4E	eukaryotic translation initiation factor 4E
ephA2	ephrin receptor
ER	oestrogen receptor
ERK1/MAPK3	mitogen activated protein kinase 3
ERK2/MAPK1	mitogen activated protein kinase 13
FCS	foetal calf serum
FISH	fluorescent in situ hybridisation
FITC	Fluorescein isothiocyanate
FOXO	Forkhead box class O
GADPH	glyceraldehyde-3-phosphoate dehydrogenase
GDP	guanosine diphosphate
Grb2	growth factor receptor bound 2
Grb7	growth factor receptor bound 7
GSDMA	gasdermin
GSK3	glycogen synthase kinase 3
GTP	guanosine triphosphate
HCl	hydrochloric acid
HER2/erBB2	epidermal growth factor receptor 2
HER3/erBB3	epidermal growth factor receptor 3
HER4/erBB4	epidermal growth factor receptor 4
HGF	hepatocyte growth factor
HM	hydrophobic motif
IAP	inhibitor of apoptosis protein

IBC	inflammatory breast cancer
IGF	insulin-like growth factor
IGF-IR	insulin-like growth factor receptor
IHC	Immunohistochemistry
ILK	integrin-linked kinase
LC	Liquid Chromatography
LC-MS/MS	Liquid Chromatography and tandem mass spectrometry
LTQ	Linear trap quadrupole
MAP	mitogen activated protein
MAPK	mitogen-activated protein kinase
MBC	metastatic breast cancer
MCL-1	myeloid cell leukaemia 1
MDMA	mouse double minute 2 homolog
MEK/MAPKK	mitogen-activated protein kinase kinase
miRNA	microRNA
MK2	mitogen activated protein kinase-activated protein kinase 2
MLN64	metastatic lymph node 64
MS	Mass spectrometry
MS/MS	Tandem Mass Spectrometry
mTOR	mammalian target of rapamycin
mTORC1	mammalian target of rapamycin complex 1
mTORC2	mammalian target of rapamycin complex 2
NF-κβ	nuclear factor kappa beta
NK	natural killer
NSCLC	non-small cell lung cancer
NTC	non-target control
OATP	organic anion transporting polypeptide
ORR	overall response rate
P13K	phosphatidylinositol-3 kinase
P13K2	phosphatidylinositol-4,5-biphosphate
p70S6k	ribosomal S6 kinase 1

PANTHER	Protein analysis through evolutionary relationships
PBS	Phosphate buffered saline
PCR	polymerase chain reaction
pCr	pathological complete response
PDK1	phosphoinositide-dependent kinase 1
PDK2	phosphoinositide-dependent kinase 2
PFS	progression free survival
P-gp	p-glycoprotein
PH	pleckstrin homology
PI3K3	phosphatidylinositol-3,4,5-triphosphate
PKC	protein kinase C
PMSF	phenylmethanesulfonylfluoride
PR	progesterone receptor
PRAS40	proline-rich AKT substrate of 40 kD
PTEN	Phosphatase and tensin homolog
qrt-PCR	quantitative real-time polymerase chain reaction
raptor	regulatory associated protein of mTOR
RelA	reticuloendotheliosis protein A
Rheb	Ras-homolog enriched in brain
rictor	rapamycin-insensitive companion of mTOR
ROS	reactive oxygen species
RT	reverse transcriptase
-RTC	minus reverse transcriptase control
RTK	receptor tyrosine kinase
RT-PCR	reverse transcription polymerase chain reaction
SAPK4	mitogen activated protein kinase 13
SDS	Sodium dodecyl sulphate
SELENBP1	selenium-binding protein 1
Ser	serine
SERM	selective oestrogen receptor modulator
SET/I2PP2A	inhibitor of protein phosphatase 2A

Shc	SRC-homology 2-containing proto-oncogene
SILAC	Stable Isotope labelling of amino acids in cell culture
SLCO	solute carrier anion transporter
Sos	Son of sevenless
STARD3	star-related lipid transfer domain containing protein 3
TFA	Trifluoroacetic acid
Thr	threonine
TKI	tyrosine kinase inhibitor
TNF	tumour necrosis factor
TOP2A	topoisomerase 2A
TRAIL	TNF-related apoptosis inducing factor
TRITC	Tetramethyl Rhodamine Iso-Thiocyanate
Tyr	tyrosine
UHP	ultra-high purity
VEGF	vascular endothelial growth factor
WBI	whole breast irradiation
X-gal	5-bromo-4-chloro-3-indolyl-βD-galactopyranoside
XIAP	X inhibitor of apoptosis protein

Abstract

Lapatinib is a tyrosine kinase inhibitor of HER2 which blocks downstream signaling pathways in HER2 positive breast cancer cell lines, tumor xenografts and HER2 positive breast cancer patients. However, pre-clinical and clinical studies have shown that HER2 positive patients can exhibit either innate or acquired lapatinib resistance. Previous work in our laboratory resulted in the generation of lapatinib-resistant SKBR3 cells which exhibit decreased phosphorylation of eEF2 compared to parental cells. The aims of this study were to develop additional models of lapatinib resistance, characterise the cell lines and identify and validate alterations which may contribute to lapatinib resistance.

HCC1954-L cells are a novel cell line model of acquired lapatinib resistance, developed through low-dose continuous conditioning with lapatinib. Using array CGH technology, HCC1954-L cells were found to have increased amplification and expression of STARD3. The decreased phosphorylation of eEF2 in SKBR3-L cells was found to be regulated by Ser359 phosphorylation of eEF2k in an mTOR-independent manner, suggesting a role for alterations in eEF2k and eEF2 in acquired lapatinib resistance. SILAC-proteomic analysis with SKBR3-par and SKBR3-L cells identified alterations in a number of different proteins of which CDK1, GAPDH, HER2, SELENBP1, SET and EBP1 were validated. Lapatinib conditioning of HCC1419 cells revealed a novel potential mechanism of lapatinib action – the induction of a senescent-like phenotype, which was reversed when lapatinib was removed from the media, suggesting a possible mechanism of lapatinib resistance, which may be dependent on p53 and p16 expression. Alterations in the phosphorylation of AKT, ERK, p70S6k and eEF2 correlated with lapatinib sensitivity in a panel of ~HER2-amplifed breast cancer cell lines.

In conclusion, our data suggests several novel mechanisms of lapatinib resistance which warrant further investigation in *in vivo* models of HER2 positive breast cancer and ultimately in patients.

Chapter 1

Introduction

1.1 Introduction

Cancer is a term given to a group of diseases characterised by abnormal cell growth, increased rate of cell proliferation and decreased cell apoptosis. Cell division/proliferation is an essential function of cells and is strictly regulated by a variety of external signals, including contact with neighbouring cells, contact with the extracellular matrix, and secreted growth factors and hormones. Cancer begins when a single cell begins to divide abnormally, resulting in exponential growth of cancer cells which form a tumour or neoplasm [1].

Breast cancer is the most prevalent form of invasive cancer, (excluding non-melanoma skin cancer), diagnosed in women in Ireland, with an average annual incidence of 2673, equating to 125.4 women per 100,000 (2007 – 2009). Breast cancer was second only to lung cancer as the leading cause of cancer death in Ireland in 2007 [2]. It was estimated that 230,480 women would be diagnosed with and 39,520 women would die of breast cancer in the USA in 2011 [3].

1.2 Breast cancer subtypes

Breast tumours consist of several pathological subtypes with different histological appearances of the malignant cells, different clinical presentations and outcomes, and the patients show a diverse range of responses to a given treatment [4]. Until recently, breast cancer was sub-classified on the basis of cellular morphology and the presence or absence of several receptors, namely the oestrogen receptor (ER), progesterone receptor (PR) and the epidermal growth factor receptor 2 (HER2) [5]. In recent years, gene expression studies using DNA micro-arrays have been used to further classify breast cancer subtypes based on the gene expression pathways of an intrinsic gene list of 496 genes. The variation in expression in this set of genes was used to group breast cancer tumour samples into various subtypes [6]. The identified subtypes differ in prognosis and the therapeutic targets they express [7]. Five distinct types of breast cancer have been identified using these techniques, including two ER-positive groups called luminal (A and B). Luminal tumours share features with luminal epithelial cells arising from the inner layer of the duct lining. A third group identified were called HER2 positive as they exhibited over-expression of HER2. A fourth group of tumours were found to have a high expression of basal epithelial-cell genes and a low expression of luminal epithelial-cell genes, this group is known as the normal type. The fifth subgroup is the basal-like; this group lacks expression of ER, PR and HER2. A

number of studies have shown that the HER-2 positive and the basal-like sub-types have a poorer prognosis than either luminal or normal-like tumours [8-10].

1.3 Epidermal Growth Factor Receptor 2 (HER2)

The HER2-*neu* (c-ERBB-2) proto-oncogene encodes HER2, a 185-kilodalton glycoprotein associated with tyrosine kinase activity [11]. The epidermal growth factor family of transmembrane receptors (ERBB or HER) are potent mediators of normal cell growth and development. This family of receptors has four known members EGFR (HER1 or ERBB1), HER2 (ERBB2), HER3 (ERBB3) and HER4 (ERBB4). The receptors are composed of an extracellular ligand binding domain, an α-helical transmembrane domain and an intracellular protein tyrosine kinase domain [12].

1.3.1 Role of HER2 in normal development

The HER receptors are widely expressed and functionally important in multiple tissues, particularly in mammalian development. HER2 plays a role in neuregulin (heregulin) signalling and is expressed in the developing nervous system [13]. HER2 plays a central role in the formation of the sympathetic nervous system, and HER2 mutant mouse embryos die at mid-gestation, soon after the effects of early defects in sympathetic nervous system development become apparent [14]. HER2 plays an essential role in the prevention of dilated cardiomyopathy as mice with a ventricular deletion of HER2 displayed multiple independent parameters of dilated cardiomyopathy [15, 16].

1.3.2 HER2 in breast cancer

HER2 is frequently overexpressed in breast cancer. The HER2 gene is either amplified or overexpressed at the protein level in approximately 25% of breast cancers [17]. Tumours are classed as HER2 positive if they achieve; immunohistochemistry (IHC) staining of 3+, a fluorescent *in situ* hybridisation (FISH) result of more than 6 HER2 gene copies per nucleus or a FISH ratio of more than 2.2 [18]. The FISH ratio is calculated as the ratio of HER2 gene signals to chromosome 17 signals. HER2 status in breast cancer correlates positively with tumour size, lymph node status, high tumour grade, DNA aneuploidy, p53 mutation, high proliferative index, high urokinase-type plasminogen activator expression, and reduced ER and PR levels [19, 20]. HER2 overexpression is associated with a poor clinical outcome [17].

1.3.3 Activation of HER2

HER receptors are activated by a number of ligands, referred to as EGF-related peptide growth factors [21]. These are produced as transmembrane precursors, and are processed and released by proteolysis. This cleavage, referred to as ectodomain shedding, is an important step in the control of ligand availability and receptor activation [22]. The known EGF ligands that bind to the HER receptors are EGF, transforming growth factor-α, amphiregulin, heparin-binding EGF, betacellulin, epiregulin, and heregulin [12, 23]. Ligand binding to HER receptors induces the formation of receptor homo- and heterodimers and the activation of the intrinsic kinase domain, resulting in phosphorylation on specific residues within the cytoplasmic tail. These phosphorylated residues serve as docking sites for a range of proteins, the recruitment of which leads to the activation of intracellular signalling pathways [12]. Receptor dimerisation is essential for the function and signalling activity of these receptors. The receptors can form either hetero- or homodimers, and heterodimers have a greater signalling potency than homodimers. The HER2-HER3 heterodimer is considered the most potent HER-dimer with respect to the strength of interaction, ligand induced tyrosine phosphorylation and downstream signalling [24, 25]. The receptors normally exist as inactive monomers with the molecules folded in such a way as to prevent dimerisation [26].

Ligand binding to the extracellular domain induces a conformational change in the receptor which exposes the dimerisation domain. After dimerisation, transactivation of the tyrosine kinase portion of the dimer occurs as each receptor activates its partner by phosphorylation leading to the activation of numerous downstream signalling cascades [Figure 1-1]. EGFR and HER4 both have an active kinase domain and known ligands to activate them [12]. Although HER3 can bind several ligands it is frequently reported to lack an active kinase domain rendering it incapable of binding ATP [27]. However, recent studies have shown that HER3 is locked in an inactive conformation and is capable of binding ATP yet remains catalytically inactive [28]. In the HER family, dimerisation of kinase domains occurs in an asymmetric conformation, leading to the allosteric activation of one kinase domain by the other [29]. The activating kinase domain does not have a catalytic role suggesting that the HER3 kinase domain may function as a highly specialised allosteric activator of other HER receptors [30]. HER2 has an active kinase domain but no known ligand. It exhibits the strongest kinase activity of the HER family [31]. HER-2/HER-3 dimers are thought to be the most active

and potent signalling heterodimers of the family. In addition, HER-2-containing dimers undergo slower dissociation and endocytosis, and are more frequently recycled back to the cell surface, prolonging the potent signals [32, 33]. The potential ligand binding site in HER-2 also differs significantly from that of EGFR and HER-3, resulting in a receptor structure that is constitutively poised in an active conformation. It has also been reported that HER2 fails to form homodimers as a result of this altered structure [34]. The constitutively active formation of HER2 makes it the preferred partner for heterodimerisation [35].

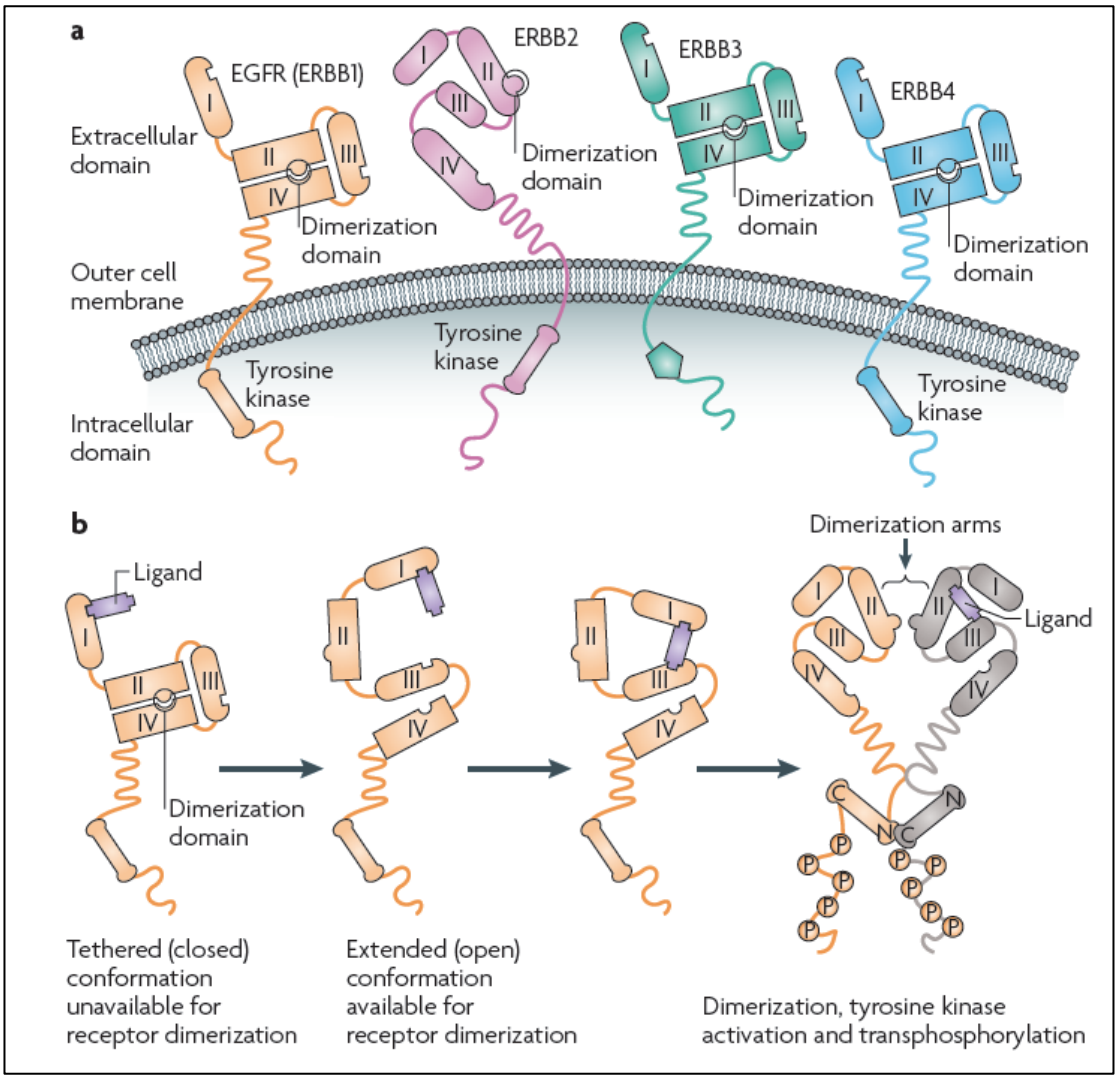

Figure 1-1: (a) EGFR, HER3 and HER4 exist in a tethered "closed" conformation in which dimerisation is inhibited in the absence of ligand binding. HER2 has no known ligand and exists in an "open" conformation making it constitutively active and poised for dimerisation. (b) Ligand binding to HER receptors seems to induce a conformational change in the folded structure of the molecule that exposes the dimerisation domain, a required step for dimer formation and functional activation of EGFR, HER3 and HER4. The kinase domain interaction is asymmetric with the amino-terminal lobe of one tyrosine kinase interacting with the carboxy-terminal lobe of the other. Note, HER3 is depicted here as having an inactive kinase domain. [Reproduced from [36]].

1.4 HER2 signalling pathways

The best characterised signalling pathways activated by the HER family are the phosphatidylinositol-3 kinase/AKT (PI3K/AKT) and the Ras/mitogen-activated protein kinase (Ras/MAPK) pathways [Figure 1-2].

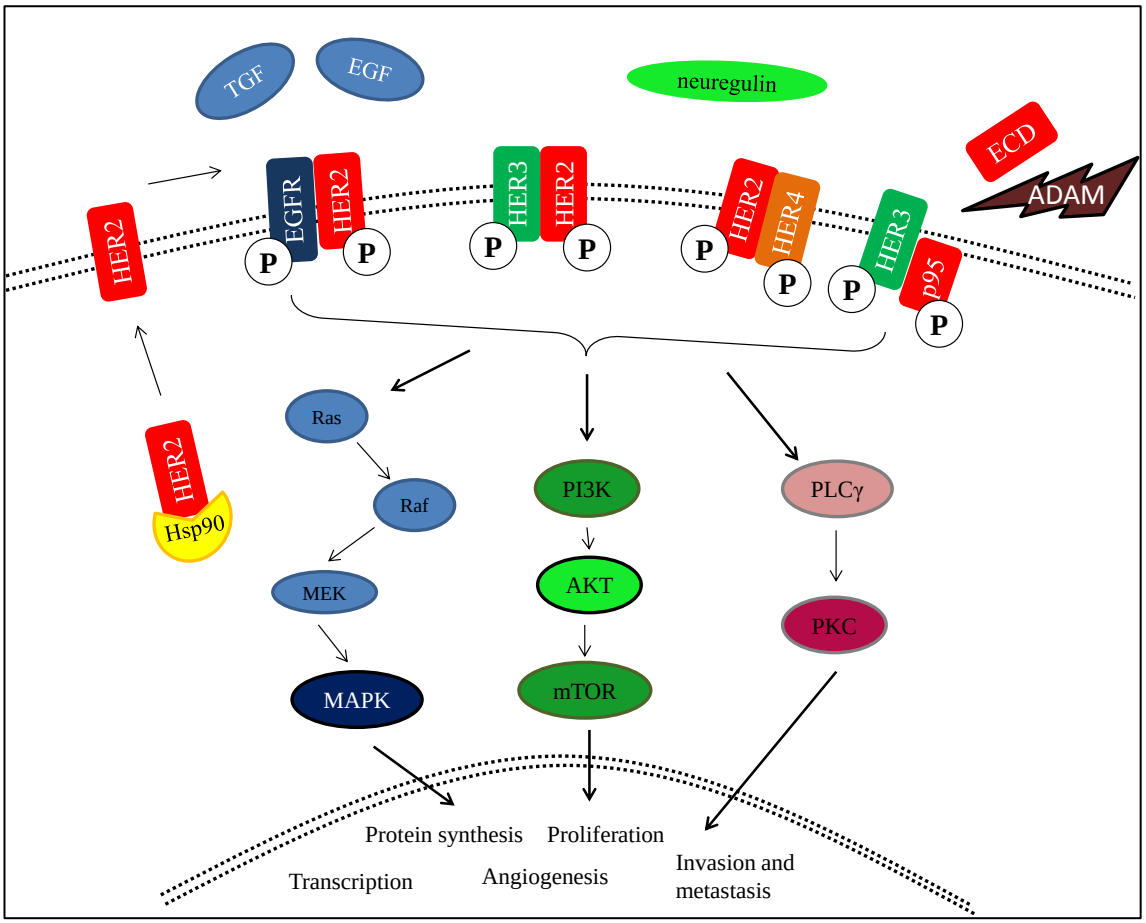

Figure 1-2: Activation of HER2 signalling pathway: HER2 is transported to the plasma membrane by heat shock protein (Hsp) 90. Ligand binding induces HER2 heterodimerisation with EGFR, HER3 and HER4 activating the P13K/AKT, MAPK and PKC pathways, promoting proliferation and cell survival. Cleavage of HER2 by A Disintegrin and A Metalloprotease (ADAM) proteases produces an extracellular domain (ECD), which is shed, and a truncated membrane-bound p95 fragment which is capable of heterodimerisation and activates downstream signalling pathways. [Adapted from [37]].

1.4.1 MAPK signalling pathway

Each of the HER receptors contain at least one docking site for Src homology 2-containing proto-oncogene (Shc) in the cytoplasmic tail of the receptor. Shc is the most common HER2 interacting protein and HER2 has 5 docking sites for Shc. Shc has 3 known isoforms and it mediates signalling from numerous receptor tyrosine kinases (RTKs) [38]. Phosphorylation of Shc causes it to associate with Growth Factor Receptor Bound 2 (Grb2) [39]. Grb2 can also bind directly to HER2 at tyrosine 1139. In the cytosol, Grb2 is bound to the guanine nucleotide exchange factor Son-of-Sevenless, (named for its homolog in drosophila), (Sos). The Grb2-Sos complex binds to the

membrane bound protein Ras. Inactive Ras is bound to GDP, activated Grb2-Sos catalyses the exchange of GDP to GTP leading to the activation of Ras [40]. This allows Ras to bind several effector proteins, including B-Raf. Activated B-Raf phosphorylates and activates MEK1 (also known as MAPK kinase). This in turn activates the extracellular signal-related kinases ERK-1 and ERK-2 (p42/44 MAPK). This leads to activation of members of the activator protein 1 (AP-1) family, the best characterised of which are jun and fos. Once activated, jun and fos translocate to the nucleus where they form a complex and bind to an AP-1 motif of DNA. This leads to the expression of many genes which mediate cellular processes including proliferation, differentiation and cell survival [Figure 1-3].

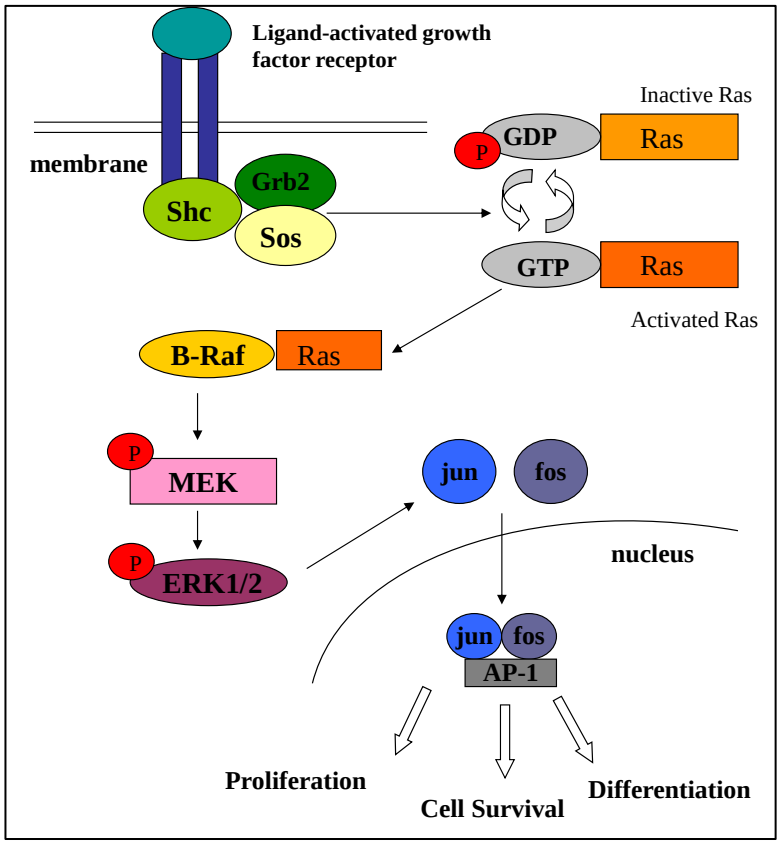

Figure 1-3: Schematic representation of growth factor receptor mediated activation of the MAPK signalling cascade.

1.4.2 PI3K/AKT signalling pathway

Phosphatidylinositol-3 kinases, (PI3Ks), constitute a lipid kinase family characterised by their ability to phosphorylate an inositol ring 3'-hydroxyl (-OH) group in inositol phospholipids. Class-I PI3Ks are heterodimers composed of a catalytic subunit (p110) and an adaptor/regulatory subunit (p85). This class is further divided into the subclass IA, which is activated by RTKs and the subclass IB, which is activated by receptors coupled with G proteins. Activation of PI3K occurs through binding of its p85 regulatory subunit to a phosphotyrosine residue on an RTK. While HER2 does not contain a docking site for PI3K, HER3 contains 6 PI3K docking sites in its intracellular domain [41]. PI3K can also bind to activated Ras-GTP which in turn activates PI3K. The p110 subunit of active PI3K binds to phosphatidylinositol-4,5-bisphosphate (PIP_2), which is anchored to the lipid layer of the cell membrane by two fatty acids. PI3K phosphorylates PIP_2 to phosphatidylinositol-3,4,5-trisphosphate (PIP_3) [42]. PIP_2 and PIP_3 act as docking sites for proteins containing a pleckstrin homology (PH) domain. PH domains are found in many proteins, including the protein serine/threonine kinases 3'-phosphoinositide-dependent kinase-1 (PDK1) and AKT/PKB, both central for the transforming effects of deregulated PI3K activity [43]. AKT binds to PIP_3 resulting in its translocation to the plasma membrane where it is phosphorylated by PDK1 at Thr 308. Full activation of AKT requires a second phosphorylation at Ser 473 which lies within in the hydrophobic motif (HM) near the C-terminal regulatory domain of AKT [44]. So far, at least 10 kinases have been suggested to function as HM kinases or a so-called "PDK2". These kinases include: mitogen-activated protein (MAP), kinase-activated protein kinase 2 (MK2), integrin-linked kinase (ILK), p38 MAP kinase, protein kinase C (PKC), NEK6, the double-stranded DNA-dependent protein kinase (DNK-PK) and the ataxia telangiesctasia mutated (ATM) gene product [45]. However, recent studies now suggest that mammalian target of rapamycin complex 2 (mTORC2) is the exclusive kinase which phosphorylates AKT at Ser473 [44, 46-48]. Active AKT is released into the cytosol where it phosphorylates multiple effector proteins which mediate cell regulatory processes including apoptosis, protein synthesis and proliferation [Figure 1-4].

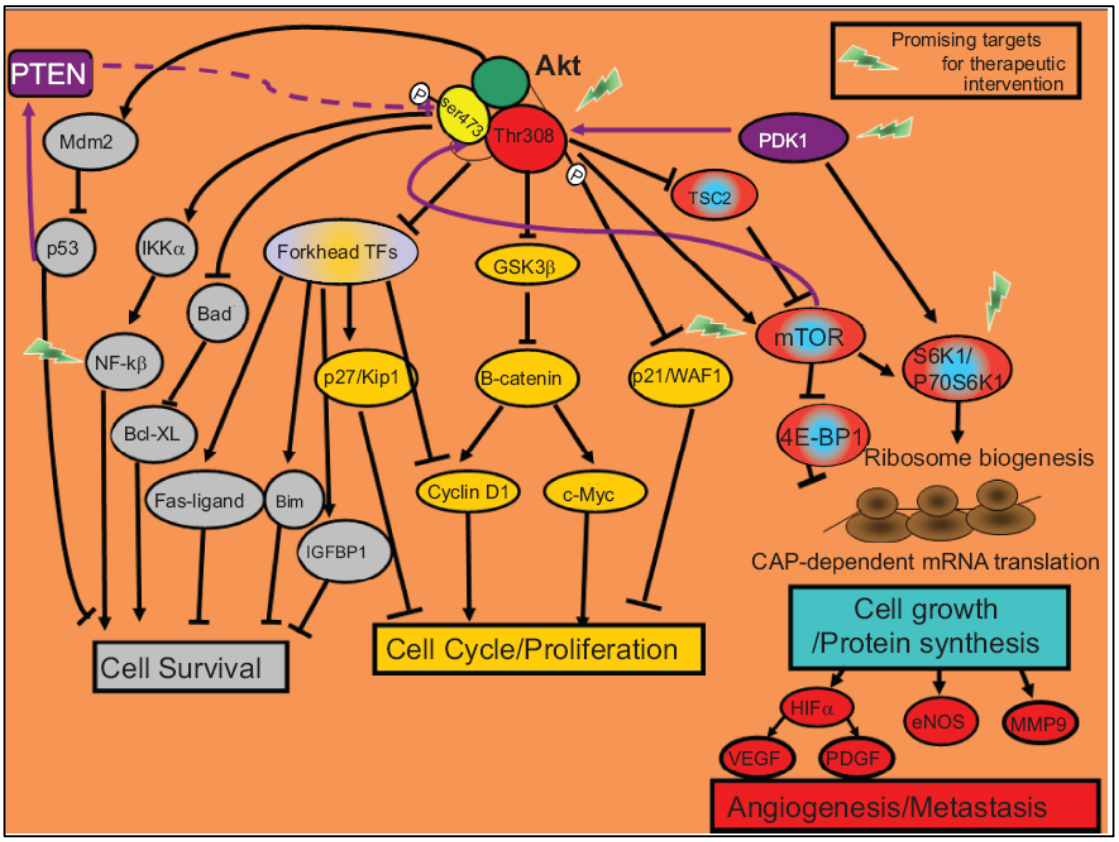

Figure 1-4: Schematic representation of the biological function of activated AKT. AKT regulates the activity of intracellular signalling proteins that trigger changes in the expression of proteins involved in cell survival, cell cycle and proliferation and protein synthesis [Reproduced from [49]].

1.4.3 Effects of activated AKT on cell regulatory processes

1.4.3.1 Inhibition of apoptosis

Active AKT phosphorylates the pro-apoptotic proteins Bcl-2 antagonist of cell death (BAD), pro-caspase 9 and members of the Forkhead family of transcription factors leading to their inactivation and subsequent inhibition of apoptosis [50]. AKT down regulates the pro-apoptotic protein p53 by activating mouse double minute 2 homolog (MDM2) which promotes p53 degradation [51]. AKT activation has also been linked to resistance to TNF-Related Apoptosis Inducing Ligand (TRAIL) induced apoptosis [52].

1.4.3.2 Cell cycle progression and cell proliferation

AKT inhibits glycogen synthase kinase-3 (GSK3) phosphorylation of β-catenin which results in the translocation of β-catenin to the nucleus where it induces the expression of Cyclin D leading to cell cycle progression [53]. AKT also phosphorylates $p21^{CIP1/WAF1}$

and $p27^{KIP1}$ which inhibits their anti-proliferative effects by retaining them in the cytoplasm [50]. These effects lead to cell cycle progression and cell proliferation.

1.4.3.3 Inhibition of tumour suppressors

AKT lowers the concentration of Forkhead Box Class O (FOXO) proteins, a family of tumour suppressors, via phosphorylation of FOXO proteins. Phosphorylated FOXO proteins are substrates of the enzyme ubiquitin ligase which transfers ubiquitin peptides onto the proteins causing them to be degraded by the proteosome. Therefore AKT blocks the FOXO tumour suppressive effect on cell proliferation [54-56].

1.4.4 AKT and regulation of protein synthesis

AKT plays a pivotal role in regulating protein synthesis through activation of the mammalian target of rapamycin (mTOR) pathway. mTOR forms two complexes, mTORC1 and mTORC2. mTORC1 is composed of mTOR, regulatory associated protein of mTOR (raptor), proline-rich AKT substrate of 40 kD (PRAS40) and mLST8/GβL [57]. mTORC2 is composed of mTOR, rapamycin-insensitive companion of mTOR (rictor) and mLST8/GβL. In addition to its role in the phosphorylation of AKT, mTORC2 is involved in the regulation of cell morphology and the cytoskeleton [58]. AKT activates Ras-homologue enriched in brain (Rheb) which results in the activation of mTORC1 [57]. Activated mTORC1 phosphorylates ribosomal S6 kinase 1 (p70S6k) and eukaryotic initiation factor 4E-binding protein (4E-BP1). p70S6k, promotes increased mRNA translation by phosphorylating ribosomal protein S6, and promotes protein synthesis by phosphorylating eukaryotic elongation factor 2 kinase (eEF2k) which inhibits its negative regulation of eukaryotic elongation factor 2 (eEF2) [59, 60]. mTORC1 phosphorylation of 4E-BP1 results in the release of eukaryotic translation initiation factor 4E (eIF4E) which enhances mRNA translation [61]. The activation of mTOR signalling and its downstream pathways are illustrated in [Figure 1-5].

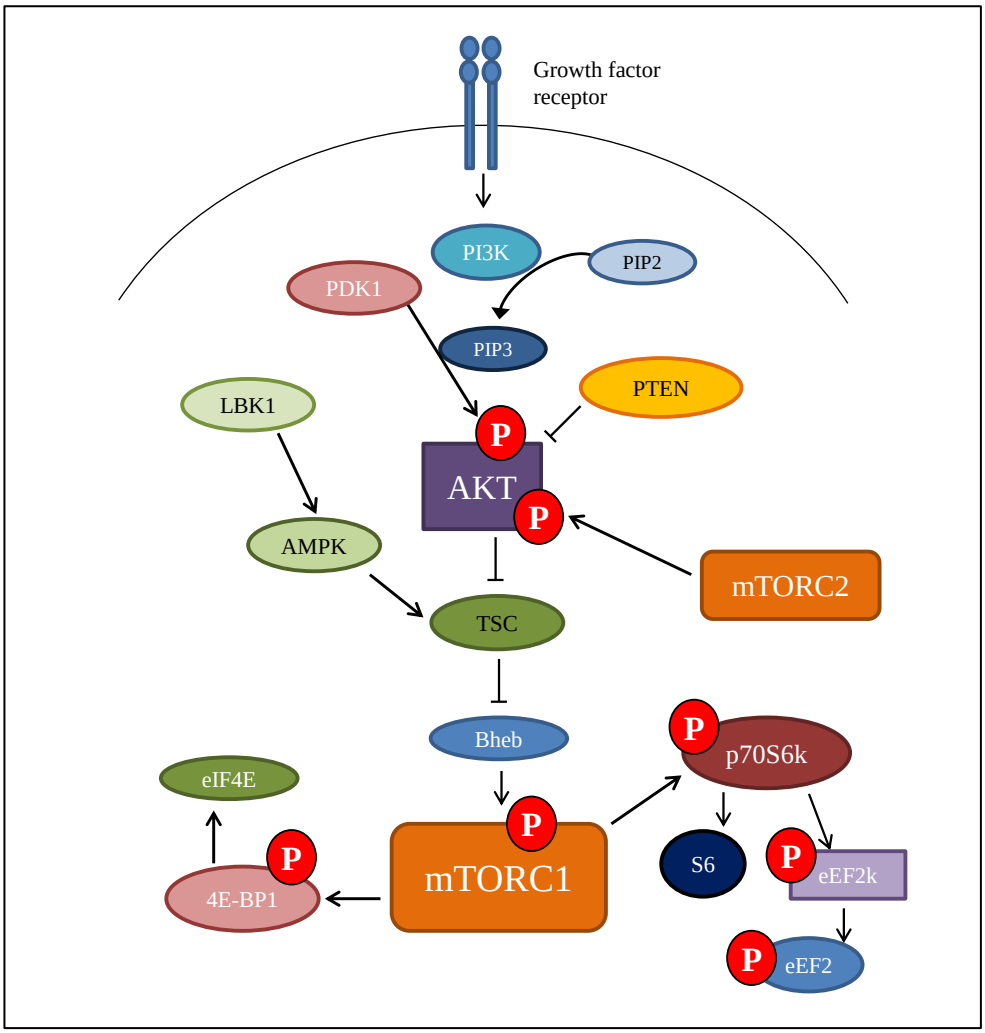

Figure 1-5: Schematic representation of AKT mediated activation of mTOR and subsequent downstream signalling pathways. Arrows represent activation while bars represent inhibition. This diagram has been adapted from [62].

1.5 Breast Cancer Treatment Strategies

The treatment of breast cancer can be categorised as either conventional or targeted therapy. Conventional therapy includes surgery, radiation therapy and chemotherapy while targeted therapy utilises drugs which specifically target cancerous cells.

1.2.1 Conventional Therapy

Surgery is one of the oldest methods of localised breast cancer treatment, of which there are two distinct strategies, breast conserving therapy (BCT) and mastectomy. BCT is the treatment of primary breast cancer without the removal of the entire breast tissue, also known as a lumpectomy [63]. A mastectomy involves the removal of the breast

(total mastectomy), the breast and auxiliary lymph nodes (modified radical mastectomy) or the breast, lymph nodes and pectoral muscles (radical mastectomy) [64]. Removal of the lymph nodes is not a curative measure but rather a means of determining if further treatment is required, as the presence of cancerous cells in the lymph nodes indicates a risk of metastasis, which is the movement or spread of cancer cells from one organ or tissue to another [65]. Randomised trials that compared mastectomy with BCT (with adjuvant radiotherapy) showed no difference in overall survival; however BCT is associated with a higher local recurrence rate [64].

Radiation therapy, like surgery, is primarily used in the treatment of localised breast cancers. The primary action of radiation therapy is to damage DNA, either directly or by the generation of reactive chemical species (such as oxygen free radicals) within cells. Whole breast irradiation (WBI), in conjunction with breast conserving surgery, reduces the risk of early breast cancer recurrence, leads to a significant improvement in overall survival and has become a standard treatment in the care of early breast cancer. However, the long duration of conventional WBI regimens negatively impacts on quality of life. An alternative approach is to deliver radiation to a limited volume of tissue cavity only (partial breast irradiation) and delivering a larger than standard dose of radiation with each treatment (accelerated partial breast irradiation, APBI). APBI focuses treatment on the lumpectomy bed. Many methods of delivering APBI have been developed including: multi-catheter interstitial brachytherapy, MammoSite balloon catheter, single insertion multicatheter devices, 3D conformal external-beam radiation therapy, permanent seed implant and intraoperative techniques using electrons or low-energy photons. Studies of APBI have demonstrated excellent local control and cosmetic outcomes in early-stage breast cancer patients [reviewed in [66], [67]].

Chemotherapy is the use of a chemical agent to kill cancer cells. The ultimate clinical effectiveness of any anticancer drug requires that it kill malignant cells *in vivo* at doses that allow enough cells in the patient's critical tissues (bone marrow and gastrointestinal tract) to survive to ensure that recovery can occur [68]. In general, anticancer drugs are most useful against malignant tumours with a high proportion of dividing cells. Thus, in practical terms, chemotherapy alone is primarily effective against leukaemia and lymphomas only. The most common tumours however, including those of breast cancer, usually have a low proportion of dividing cells and therefore are less susceptible to treatment with chemotherapy alone. Surgery and radiation therapy can often eradicate primary or localised tumours but they are not effective once the cancer has metastasised

to other parts of the body [69]. A systemic therapy such as chemotherapy is required to control and eliminate metastatic cancer. Chemotherapy drugs often show increased effectiveness when used in combinations [70]. The combinations of chemotherapeutic agents used in the treatment of breast cancer are described in Table 1-1. As the mode of action of anticancer drugs is to attack cells which are dividing at an increased rate, they also attack non-cancerous cells of the body which naturally divide quickly, for example, the bone marrow, the lining of the mouth and intestines, hair follicles and blood cells. This results in a number of known side effects including; hair loss, mouth sores, loss of appetite, nausea/vomiting, infections (due to low white blood cell counts), excessive bruising and bleeding (due to low platelet counts) and fatigue (due to low red blood cell counts) [68]. Some chemotherapeutic agents are also associated with chemotherapy-induced heart failure; many cancer survivors now have a higher risk of cardiovascular diseases than of recurrent cancer [71].

Table 1-1: Chemotherapeutic regimens utilised in the treatment of breast cancer. Information adapted from [72].

Abbreviation	**Components of chemotherapeutic regimen**
AC	doxorubicin [Adriamycin]; cyclosphamide
AC > T	doxorubicin; cyclosphamide; paclitaxel [Taxol]
CMF	cyclosphamide; methotrexate; 5-fluorouracil
FAC (CAF)	5-fluorouracil; doxorubicin; cyclosphamide
FEC-100	5-fluorouracil; epirubicin; cyclosphamide
GT	gemcitabine; paclitaxel
TAC	docetaxel [Taxotere]; doxorubicin; cyclosphamide
TC	docetaxel; cyclosphamide
EC	epirubicin; cyclophosphamide
AT	doxorubicin; docetaxel

1.2.2 Targeted Therapy

Since the late 1950s the predominant modalities in the treatment of breast cancer have been surgery, radiation and chemotherapy. Chemotherapy and radiation work primarily by damaging proliferating cells at the level of DNA replication and inducing apoptotic cell death as a secondary response to that damage. However, chemotherapy exhibits a

lack of selectivity and a relatively high toxicity which has given rise to a need for novel drugs with a more specific action [73]. In the late 1980s new signalling networks that regulate cell proliferation and survival were discovered including: membrane growth factor receptors, cytoplasmic signalling molecules, nuclear cell cycle proteins, modulators of apoptosis and angiogenesis promoters [69, 74]. Since then, many new drugs have been developed which target these proteins. The first targeted therapy for breast cancer, tamoxifen, which targets the oestrogen receptor, was discovered over 40 years ago [75]. The major classes of targeted therapeutic agents used in the treatment of breast cancer are, small molecule tyrosine kinase inhibitors (TKIs), selective oestrogen receptor modulators (SERMs), aromatase inhibitors and monoclonal antibodies (mAbs).

1.6 HER2 targeted therapy – monoclonal antibodies

HER2 positive breast cancer is associated with a poorer prognosis than HER2 negative breast cancer [17]. The discovery of trastuzumab, a monoclonal antibody which targets HER2 revolutionised the treatment of HER2 positive breast cancer.

1.6.1 Trastuzumab

Xenograft studies using HER2 positive driven tumours indicated that targeting these tumours with murine mAbs against HER2 was a viable treatment strategy. One of the most active murine mAbs, 4D5, was humanised to reduce immunogenicity yielding trastuzumab (Herceptin ®, Genentech), the first mAb approved for the treatment of breast cancer [76, 77] [Figure 1-6]. As a single agent trastuzumab achieved response rates of 26 – 34 % in HER2 positive metastatic breast cancer (MBC) patients and 11-15 % response in HER2 positive MBC patients who had progressed after chemotherapy [78-80]. A phase III study of trastuzumab in combination with chemotherapy in HER2 positive MBC patients resulted in a greater overall response rate (ORR), longer duration of response, longer survival and a 20 % decrease in the risk of death in patients treated with the combination compared to chemotherapy alone [81].

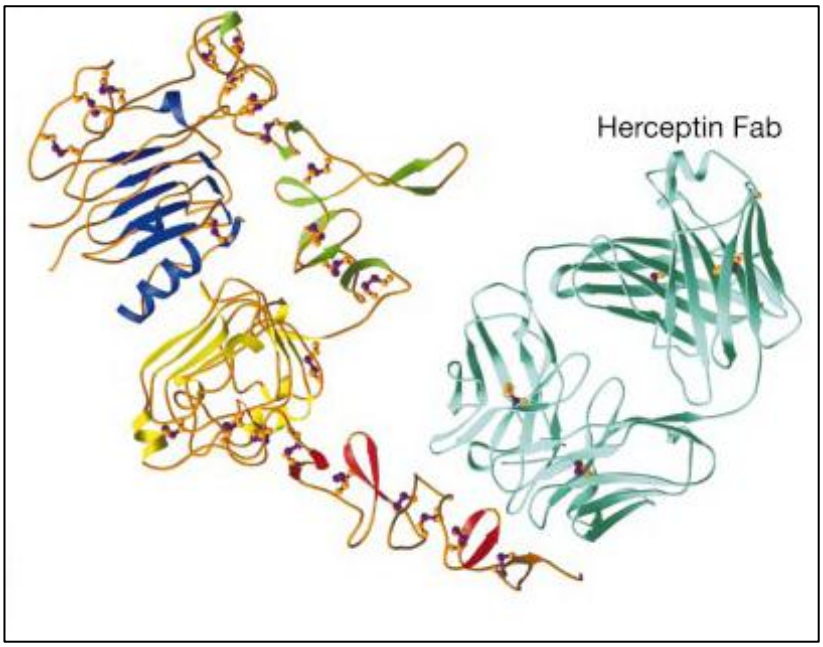

Figure 1-6: Ribbon diagram of the human HER2 and trastuzumab complex [Reproduced from [25]].

The proposed mechanisms of action for trastuzumab include:

1) Reduction of signalling through AKT and MAPK. Trastuzumab disrupts HER2-Src interactions which reduces PTEN phosphorylation thus increasing its activity. This results in a dephosphorylation of AKT and inhibition of proliferation [82].

2) ECD-shedding: HER2 is cleaved by proteins containing A Disintegrin and A Metalloprotease domain (ADAMs), the extracellular domain is shed and the truncated kinase domain (p95-HER2) retains the ability to form heterodimers with HER3 [83] and can be phosphorylated by heregulin [84]. Trastuzumab inhibits ECD-shedding *in vitro* [85] and the serum ECD levels of HER2 are lower in trastuzumab treated patients compared to those not treated with trastuzumab [86].

3) Trastuzumab sensitises cells to apoptotic agents: It is currently unclear as to whether or not trastuzumab induces apoptosis in tumours *in vivo* [87, 88] but it does sensitise tumour cells to apoptosis-inducing agents e.g. paclitaxel and etoposide [89]. Trastuzumab also enhances TRAIL-induced apoptosis [90], and prevents cells from repairing DNA damage caused by chemotherapy (e.g. cisplatin) or irradiation [91].

4) Inhibition of angiogenesis: HER2 overexpression correlates with elevated levels of vascular endothelial growth factor (VEGF) and increased angiogenesis [92]. Angiogenesis is the growth of new blood vessels from pre-existing ones and is essential to the continued growth of a tumour. In a mouse model of HER2 positive breast cancer, treatment with trastuzumab resulted in a decrease in VEGF and angiogenesis and a subsequent increase in the anti-angiogenesis factor thrombospondin-1 [93].

5) ADCC: Trastuzumab activates antibody-dependent cell-mediated cytotoxicity (ADCC) via recruitment of natural killer (NK) cells to the tumour. The NK cells express an Fcγ receptor (Fcγ-R) which binds to the Fc domain on trastuzumab. Trastuzumab showed lower activity in Fcγ-R-knockdown mouse compared to Fcγ-positive mice [94]. Response to trastuzumab was associated with increased ADCC activity in a neoadjuvant study of HER2 positive breast cancer [87]. A recent study also suggests that in breast cancer cells where HER2 is non-amplified but expressed at a low level, trastuzumab can bind resulting in an ADCC response [95].

As of January 2012 there were 499 clinical trials incorporating trastuzumab on clinicaltrials.gov. Several novel agents are being investigated in combination with trastuzumab including Hsp90 inhibitors, P13K/AKT/mTOR inhibitors, VEGF inhibitors, IGF-IR inhibitors and aromatase inhibitors. In addition, combining trastuzumab with other inhibitors of HER2 is currently being extensively investigated.

1.6.2 Pertuzumab

Pertuzumab represents a second generation of humanised monoclonal antibodies targeting HER2. Pertuzumab binds to an epitope in HER2 which is distinct to the trastuzumab binding domain [24, 25]. In contrast to trastuzumab, pertuzumab is able to inhibit the formation of HER2/HER3 heterodimers and activation of downstream signalling cascades [96-98]. Pertuzumab has been tested in combination with trastuzumab and docetaxel in the Cleopatra study. The combination of pertuzumab plus trastuzumab plus docetaxel, as compared with placebo plus trastuzumab plus docetaxel, when used as first-line treatment for HER2-positive metastatic breast cancer, significantly prolonged progression-free survival (PFS) from 12.4 months in the control group to 18.5 months in the pertuzumab arm, with no increase in cardiac toxic effects [99]. Pertuzumab is also being investigated in the neo-adjuvant setting in the Neosphere trial. Patients given pertuzumab and trastuzumab plus docetaxel had a significantly improved pathological complete response (pCR) rate (45.8 %), compared with those

given trastuzumab plus docetaxel (29.0 %), without substantial differences in tolerability [100]. These studies suggest an on-going role for pertuzumab in combination with trastuzumab for the treatment of HER2 positive breast cancer.

1.6.3 Trastuzumab-DMI

Trastuzumab-DM1 (T-DM1) is a novel antibody drug conjugate, whereby trastuzumab is linked to a microtubule agent, DM1 (a derivative of maytansine) using a non-reducible thioether linker. T-DM1 displayed superior activity compared to unconjugated trastuzumab [101]. The proposed mechanism of action of T-DM1 is to bind HER2 and enter the cell via endocytosis of HER2. T-DM1 then undergoes intralysosomal proteolytic degradation resulting in anti-tubulin associated cell death [101]. Single arm phase I and II trials confirmed T-DM1 had robust single-agent activity in patients with heavily pre-treated, HER2-positive metastatic breast cancer and that it was well tolerated at the recommended phase II dose (3.6 mg/kg every 3 weeks) [102, 103]. In a randomised phase II trial of T-DM1 versus trastuzumab and docetaxel in HER2-positive metastatic breast cancer, TDM-1 showed equivalent efficacy with clearly decreased toxicity [104] and an improvement in progression free survival [105]. T-DM1 can effectively inhibit the growth of HER2-positive cancer cells that are resistant to trastuzumab and lapatinib *in vitro* and *in vivo* [106-108]. Two large multicentre phase III clinical trials for T-DM1 are currently recruiting; MARIANNE and EMILIA. MARIANNE compares single agent T-DM1 with placebo, versus T-DM1 and pertuzumab, versus trastuzumab in combination with a taxane (docetaxel or paclitaxel) [109]. EMILIA compares single agent T-DM1 versus the combination of lapatinib and capecitabine in patients with metastatic breast cancer previously treated with anthracyclines, taxanes and trastuzumab [110].

1.7 HER2 targeted therapy – tyrosine kinase inhibitors

The development of trastuzumab revolutionised the treatment of HER2 positive breast cancer spurring on the development of another group of agents which target HER2, tyrosine kinase inhibitors (TKIs). TKIs differ from mAbs in several ways; TKIs can be administered orally versus intravenously for mAbs, TKIs bind the intracellular domain versus the extracellular domain for mAbs, the half-life of TKIs is usually shorter than that of mAbs, and mAbs are thought to be more specific than TKIs, as TKIs can frequently target more than one kinase [reviewed in [111]]. Table 1-2 summarises the

HER2-targeted therapies which are currently approved or under investigation for the treatment of HER2 positive breast cancer.

Table 1-2: The properties and current status of HER2-targeted therapies. TKI (rev) denotes a reversible TKI, TKI (irrev) denotes an irreversible TKI and mAb denotes a monoclonal antibody.

Drug	Company	Properties	Targets	Current Status in HER2 breast cancer
Trastuzumab	Genentech	mAb	HER2	Approved
Pertuzumab	Roche	mAb	HER2 and HER2-HER3 heterodimers	Phase III: Docetaxel-trastuzumab ± pertuzumab
T-DMI	Genentech	mAb conjugate	HER2	Phase III: Trastuzumab-taxane vs T-DM1 ± pertuzumab
				Phase III: T-DM1 vs lapatinib-capectabine
Lapatinib	GlaxoSmithKline	TKI (rev)	EGFR HER2	Approved: lapatinib-capecitabine in trastuzumab refractory MBC
				Phase III: Neo-adjuvant Lapatinib ± trastuzumab vs trastuzumab
				Phase III: Lapatinib ± trastuzumab vs trastuzumab
Neratinib	Pfizer	TKI (irrev)	EGFR HER2	Phase III: Neratinib vs placebo
Afatinib	Boehringer Ingelheim	TKI (irrev)	EGFR HER2 HER4	Phase III: Trastuzumab-vinorelbine vs Afatinib-vinorelbine
MM-111	Merrimack	bi-specific Ab	HER2 HER3	Phase I: MM-111 ± trastuzumab
U3-1287 (AMG888)	U3-Pharma	mAb	HER3	Phase I/II: Trastuzumab-paclitaxel ± AMG888
BMS-690514	Bristol-Myers Squibb	TKI (rev)	EGFR HER2 HER4 VEGFR	Phase II: letrozole-lapatinib vs letrozole-BMS-690514

1.7.1 Lapatinib

Lapatinib (Tyverb ®, Tykerb ®) is an orally active, low molecular weight TKI [Figure 1-7]. It is a selective, reversible inhibitor of EGFR and HER2; it binds to the ATP binding site of both receptors preventing signal transduction through both the MAPK and PI3K/AKT pathways, leading to an increase in apoptosis and decrease in cellular proliferation [112].

1.7.1.1 Pharmacodynamics of lapatinib

Lapatinib is a 4-anilinoquinazoline which binds selectively to EGFR and HER2. Lapatinib is one of the most specific kinase inhibitors approved for the treatment of cancer. When 20 kinase inhibitors (at 10 μM) were compared in an *in vitro* binding assay against a panel of 113 substrates, lapatinib was one of the most specific, targeting HER2 and EGFR with 10-fold greater affinity than any off-target substrates [113]. Lapatinib inhibits HER2 with an IC_{50} of 9.2 nM, EGFR with an IC_{50} of 10.8 nM, HER4 with an IC_{50} of 0.367 μM and c-Src with an IC_{50} of 3.5 μM making lapatinib a highly selective HER2/EGFR inhibitor [114].

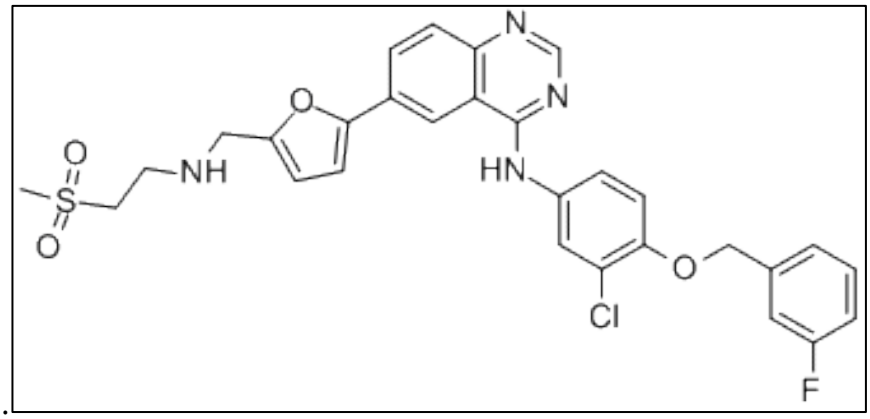

Figure 1-7: Chemical structure of lapatinib [Reproduced from [114]].

Lapatinib has a moderate rate of absorption after oral administration with peak plasma concentrations at several hours post-treatment, and is assumed to have a low bioavailability. Lapatinib is extensively distributed in human tissues, including tumour tissues, has a large volume of distribution at least 3-fold exceeding the volume of body water and is extensively (about 95%) protein bound to α_1-acid glycoprotein and albumin. Lapatinib undergoes metabolism via hepatic and intestinal cytochrome P450 and is eliminated by biotransformation [reviewed in [115]]. The serum concentrations of lapatinib peak four hours after treatment, increase with increasing dose and achieve steady state in 6 to 7 days, suggesting an effective half-life of 24 hours. At the dose of

1,250 mg daily the peak plasma concentration of lapatinib in patients was 2.4 µg/ml (2.5 µM), (ranging from 1.57 to 3.77 µg/ml) [116], and another study has shown that the steady-state trough concentrations of lapatinib range from 0.3 to 0.6 µg/ml (0.318 – 0.636 µM) [117], [118].

Lapatinib crosses the blood-brain barrier

Overexpression of HER2 has been correlated with an increased risk of developing central nervous system (CNS) metastases [119, 120]. CNS may be a potential sanctuary site in patients with HER2-postive disease treated with trastuzumab, as evidence suggests that trastuzumab does not penetrate the blood-brain barrier; trastuzumab levels in cerebrospinal fluid were 300-fold lower than those in plasma [121]. Gefitinib, which is structurally similar to lapatinib, demonstrated objective response in brain metastases in patients with non-small cell lung cancer (NSCLC) [122], suggesting that TKIs can cross the blood-brain barrier. In a preclinical mouse model lapatinib inhibited the formation of brain metastasis and reduced the phosphorylation of HER2 in the brain metastasis [123]. Lapatinib as a single agent showed modest CNS activity in a phase II clinical trial in women with brain metastasis from HER2 positive breast cancer, who had been previously treated with trastuzumab [124]

1.7.1.2 Early clinical trials with lapatinib

Phase I trials evaluating the safety and pharmacokinetics of lapatinib were conducted in patients with advanced malignancies exhibiting overexpression of EGFR and/or HER2 and provided evidence of lapatinib activity. These studies show that lapatinib is well tolerated at doses of up to 1600 mg/day. The predominant drug-related adverse events reported were diarrhoea and rash [117, 125]. Lapatinib was then examined in phase II trials, with a focus on breast cancer as most patients who exhibited a partial response to lapatinib in the phase I trials had breast cancer. As first-line therapy, lapatinib monotherapy resulted in objective response and clinical benefit rates of 24% and 43%, respectively in HER2-amplified locally advanced or metastatic breast cancer [126]. Lapatinib monotherapy also showed clinical activity and manageable toxicity in HER2-overexpressing breast cancer patients who had progressed on trastuzumab [127], confirming the results of another study which also reported no activity in chemotherapy-refractory HER2-negative breast cancer [128]. Although lapatinib shows modest clinical activity as a monotherapy, it was the increased efficacy observed when

used in combination with capecitabine versus capecitabine alone that first lead to its approval as a breast cancer therapy.

1.7.1.3 Lapatinib and capecitabine

Lapatinib, in combination with capecitabine, was approved by the US Food and Drug Administration (FDA) on March 13, 2007, for the treatment of patients with advanced or HER2-overexpressing metastatic breast cancer previously treated with trastuzumab and an anthracycline, or taxane. Capecitabine (Xeloda ®, Roche) is an orally-administered chemotherapeutic agent, that is enzymatically converted to 5-fluorouracil in the tumour, where it inhibits DNA synthesis and slows the growth of tumour tissue [129]. The efficacy of lapatinib in combination with capecitabine was first reported in a phase I study [130]. The pivotal trial, which led to regulatory approval of lapatinib, compared lapatinib plus capecitabine versus capecitabine alone, in HER2 positive, locally advanced or metastatic breast cancer, that had progressed after treatment with trastuzumab and an anthracycline, or taxane. The median time to progression was 8.4 months in the lapatinib plus capecitabine group compared with 4.4 months in the monotherapy group, without any increased toxicity [131]. Updated results suggested a trend towards improved overall survival and a reduction in the risk for progression to central nervous system disease in the combination group [132]. A final analysis of the trial results suggest a 20 % decrease in the risk of death for patients treated with the combination versus capecitabine alone [133]. Lapatinib in combination with capecitabine is the first (and so far only) therapy to be approved for the treatment of HER2-positive breast cancer that is refractory to trastuzumab in the metastatic setting.

1.7.1.4 Mechanism of action of lapatinib

Lapatinib inhibits both MAPK-ERK1/2 and PI3K-AKT signalling in lapatinib-treated HER2 positive breast cancer cell lines, tumour xenografts and in clinical tumour biopsies obtained from women with HER2 positive breast cancer treated with lapatinib [112]. Several proposed mechanisms of action of lapatinib are out-lined below.

<u>Inhibition of HER2 and EGFR signalling</u>

Sensitivity to lapatinib is independent of the levels of EGFR in HER2 overexpressing breast cancer cells. This indicates that the effects of lapatinib are as a result of inhibition of HER2 signalling rather than a combination of EGFR and HER2 inhibition. In patient samples, lapatinib responsiveness was also correlated with HER2 expression but not

EGFR expression. HER2 overexpressing patients benefitted from lapatinib regardless of EGFR expression [112, 114, 117, 134].

Induction of stress response pathways

As previously mentioned, HER2 is essential for cardiac development and function. Trastuzumab treatment is associated with increased incidence of cardiac-toxicity compared to chemotherapy alone [135], and anthracycline-trastuzumab combination therapy is associated with higher cardiac-toxicity compared to trastuzumab in combination with non-anthracycline-based chemotherapy [136]. In contrast, lapatinib treatment has been associated with a low-rate of cardiac toxicity [137]. GW2974, a lapatinib analogue, protects cardiac myocytes from apoptotic stimuli by activating AMP-regulated protein kinase (AMPK), which switches cells from an anabolic to a catabolic state of metabolism [138]. Trastuzumab does not activate AMPK which may explain, in part, why lapatinib is associated with a low incidence of cardiotoxicity compared to trastuzumab. This study suggests that activation of AMPK may be necessary to preferentially induce apoptosis in tumour cells while sparing cardiac cells [138].

Inhibition of drug efflux pumps

Drug efflux pumps are expressed in a broad spectrum of tissue, including cancerous tissue. Drug-efflux is largely mediated by the ATP-binding cassette (ABC) transporters p-glycoprotein (P-gp) and breast cancer-related protein BCRP [reviewed in [139]]. Lapatinib synergises with SN-38, (the active metabolite or irinotecan, a topoisomerase 1 inhibitor), leading to increased levels of apoptosis in a panel of breast, lung and testicular cancer cell lines [140]. The synergy between lapatinib and SN-38 was due to SN-38 intracellular accumulation via inhibition of BCRP by lapatinib. In addition, high dose lapatinib (10 μM) inhibited the efflux of mitoxantrone, a specific BCRP substrate, in a manner similar to fumitremorgin C, a BCRP inhibitor, suggesting that lapatinib is an inhibitor of BCRP [140]. Lapatinib treatment has also been shown to increase the expression of P-gp in a lung-cancer cell line with acquired resistance to paclitaxel, however the increased expression of P-gp was not associated with increase drug accumulation or activity [141].

Induction of apoptosis

Early studies with lapatinib report a 23-fold increase in apoptosis in HER2-amplified cells following lapatinib treatment [112], and later studies, by the same group, show an even greater enhancement of apoptosis when lapatinib is combined with trastuzumab [142]. Increased apoptosis in lapatinib and trastuzumab treated cells also correlates with decreased levels of survivin [143]. Lapatinib-mediated apoptosis has also been associated with the upregulation of the pro-apoptotic protein Bcl-2 interacting mediator of cell death (BIM) through inhibition of the MAPK signalling pathway in breast cancer cells with HER2 amplification [144]. Lapatinib-mediated apoptosis can also be increased through inhibition of the anti-apoptotic protein, myeloid cell leukaemia 1 (MCL-1) [145].

Survivin is an inhibitor of apoptosis protein (IAP) which when overexpressed can protect breast cancer cells from apoptotic stimuli [146]. Lapatinib inhibits survivin expression in HER2-overexpressing breast cancer cells leading to an increase in apoptosis. In contrast, neither trastuzumab nor gefitinib resulted in a down-regulation of survivin. The down-regulation of survivin was also seen in tumour samples of HER2-overexpressing breast cancer patients who participated in a phase 1 pilot study of lapatinib [147]. Failure to down-regulate survivin and/or increased accumulation of survivin in response to HER2 inhibition has been proposed as a possible mechanism of innate lapatinib and trastuzumab resistance [148].

Cell cycle arrest

Treatment of HER2 positive breast cancer cells with lapatinib results in cell cycle arrest, with cells accumulating in the G1 phase [114, 134]. Lapatinib treatment has also been shown to induce G1 arrest in gastric cancer [149], lung cancer [150] and in bladder cancer, specifically when used in combination with the chemotherapeutic regime gemcitabine, paclitaxel and cisplatin (GTC) [151].

Autophagy

Autophagy is a process involving the formation of membrane bound vacuoles containing lytic proteins which result in the degradation of cellular proteins and cytoplasmic organelles [152]. Treatment of breast cancer cells with lapatinib results in the induction of autophagy, which is dependent on the expression of eEF2k [153]. The authors of this study suggest that eEF2k-mediated autophagy plays a protective role for

breast cancer cells and that inhibition of autophagy in combination with lapatinib would result in a better therapeutic outcome. This is in contrast to another study showing that lapatinib in combination with a Bcl-2 inhibitor, obatoclax, caused synergistic cell killing by eliciting autophagic cell death indicating a non-protective role for autophagy in these cells [154]. Whether therapy-induced autophagy functions as a direct mechanism of cell death, or represents a self-defence mechanism for resisting therapy-mediated cell killing is still a matter for debate. The current belief is that autophagy is a cell survival mechanism activated in adverse conditions; continued exposure of the cells to adverse conditions may result in cell death, whereas alleviation of the conditions may result in cell survival [152]. The role of autophagy in response to lapatinib has not yet been fully elucidated.

1.7.1.5 Lapatinib in clinical trials

As of January 2012 there were 243 clinical trials with lapatinib listed on clinicaltrials.gov. The hypotheses, study design and results, where available, of several of the most interesting clinical trials, including those already completed and those still accruing, are summarised below.

Lapatinib with paclitaxel

Lapatinib in combination with paclitaxel, a microtubule interfering drug, has been evaluated as a first-line treatment for metastatic breast cancer (MBC). Patients with HER-2-negative or HER2-untested MBC did not benefit from the addition of lapatinib to paclitaxel. However, first-line therapy with paclitaxel-lapatinib significantly improved clinical outcomes in HER-2-positive patients [155]. First-line lapatinib and paclitaxel has shown ORR in previously untreated HER2-postive MBC patients [156]. Lapatinib in combination with paclitaxel has also shown clinical benefit in treatment-naive patients with inflammatory breast cancer (IBC) [157]. Lapatinib is being evaluated in combination with paclitaxel and gemcitabine as a neoadjuvant treatment for HER2 positive breast cancer patients. A phase I dose escalation study has been published indicating that the combination is tolerable [158]. There are currently 35 studies on clinicaltrials.gov examining combination of lapatinib and paclitaxel as a therapeutic intervention.

Lapatinib and docetaxel

Lapatinib in combination with another chemotherapeutic agent, docetaxel, is also being investigated for the treatment of HER2 positive breast cancer. Initial phase I studies of lapatinib in combination with docetaxel indicate that the combination is well-tolerated [159]. A phase I/II study evaluating lapatinib in combination with docetaxel as first-line treatment for advanced or metastatic HER2 breast cancer is currently ongoing [160]. Docetaxel and lapatinib are being compared to docetaxel trastuzumab in several phase I/II clinical trials including: a phase II neo-adjuvant study assessing TCH (Docetaxel, Carboplatin and Trastuzumab), TCL (Docetaxel, Carboplatin and Lapatinib) and the Combination of TCHL (Docetaxel, Carboplatin, Trastuzumab and Lapatinib) is currently underway in HER2 positive breast cancer patients [161].

Lapatinib with hormone therapy

Crosstalk between HER2 and ER signalling has been implicated in resistance to ER targeted therapy [reviewed in [162]], providing a rationale for combining HER2 inhibition with anti-ER based therapy. An initial phase I trial indicated the feasibility of safely combining lapatinib and letrozole [163]. Following this, a phase II trial comparing lapatinib plus letrozole, versus letrozole plus placebo resulted in significant improvement in PFS) in patients with ER positive and HER2-amplified MBC. The addition of lapatinib did not result in significant benefit in HER2-negative patients, however, it did result in a 23% reduction in the risk of progression [164, 165]. There are currently 14 clinical trials on clinicaltrials.gov evaluating lapatinib and letrozole as a therapeutic intervention in ER positive breast cancer which is either HER2 positive or HER2 negative.

Lapatinib with trastuzumab

Preclinical data suggests that lapatinib has a synergistic effect with used in combination with trastuzumab [134, 143]. A Phase III study evaluated the effects of lapatinib alone versus lapatinib plus trastuzumab in patients with HER2-postitve breast cancer who had progressed on trastuzumab and reported increased PFS and clinical benefit in the combination group compared to lapatinib alone [166]. The NeoALTTO trial, an international, multicentre, randomised phase III study, evaluating the efficacy of lapatinib plus paclitaxel versus trastuzumab plus paclitaxel versus concomitant lapatinib and trastuzumab plus paclitaxel, when given as neoadjuvant therapy in patients with

HER2 positive breast cancer has completed recruitment. First reported results showed that pCR was significantly higher in the combination of lapatinib and trastuzumab plus paclitaxel arm (51.3%) compared to either trastuzumab and paclitaxel (29.5 % ($p < 0.01$)) or lapatinib and paclitaxel (24.7% ($p < 0.01$)) [167]. The ALTTO (Adjuvant Lapatinib and/or Trastuzumab Treatment Optimisation) trial was opened in April 2007 and is comparing the activity of lapatinib alone, trastuzumab alone, trastuzumab followed by lapatinib, and concomitant lapatinib and trastuzumab. The study has recruited 8,381 patients and first reports on results are expected in 2013. Recently, the lapatinib-alone arm has been discontinued, as lapatinib alone failed to meet the pre-specified criteria of non-inferiority to trastuzumab alone with respect to disease-free survival [168].

Lapatinib is also being examined in clinical trials with angiogenesis inhibitors, P13K/mTOR inhibitors, inhibitors of topoisomerase 1, and multiple cytotoxic agents including epirubicin, temozolamide, carboplatin, docetaxel, vinorelbine and gemcitabine [from www.clinicaltrials.gov].

1.7.2 Neratinib

Second-generation tyrosine kinase inhibitors include HKI-272 (neratinib) an irreversible inhibitor of EGFR and HER2. Neratinib inhibits HER2 with an IC_{50} of 59 nM and EGFR with an IC_{50} of 92 nM. Neratinib inhibits HER2 phosphorylation and removal of neratinib from the cells does not restore phosphorylation of HER2, thus the inhibition is irreversible [169]. In a phase II study, neratinib monotherapy showed clinical benefit among patients with HER2-positive breast cancer who were pre-treated with trastuzumab, the median PFS was 23 weeks and the objective response rate was 24 %. This study also evaluated neratinib as a monotherapy in HER2-positive breast cancer patients who had not been pre-treated with trastuzumab, interestingly the PFS doubled to 40 weeks and the objective response rate rose to 56 % [170]. Neratinib-monotherapy is being evaluated in a phase III trial in HER2 positive breast cancer following adjuvant trastuzumab therapy [171]. Neratinib is currently in multiple clinical trials including; a phase I/II study in combination with paclitaxel [172], in combination with trastuzumab [173], a phase II studying comparing neratinib and paclitaxel versus trastuzumab and paclitaxel (NEFERTT) [174] and a phase II study evaluating neratinib versus lapatinib and capecitabine in HER2 positive advanced breast cancer [175].

1.7.3 Afatinib

BIBW-2992 (afatinib) is also an irreversible inhibitor of EGFR, HER2 and HER4, with an IC_{50} of 14 nM for HER2 and 0.5 nM for EGFR [176, 177]. Afatinib is being examined extensively as a treatment for lung cancer in the LUX-Lung program, and early results indicate that afatinib significantly prolongs PFS compared with placebo in pretreated patients with clinically acquired resistance to gefitinib or erlotinib [178, 179]. Afatinib has also been shown to overcome acquired resistance to cetuximab, an EGFR monoclonal antibody [180]. Afatinib is also being investigated in several trials in HER2 positive patients including; alone and in combination with paclitaxel or vinorelbine in patients who have progressed on prior HER2-targeted therapy [181], as a single agent versus lapatinib or trastuzumab in HER2 positive treatment naïve patients [182] and also in HER2 positive IBC [183]. A phase III trial of afatinib in combination with vinorelbine compared to trastuzumab and vinorelbine is currently underway in trastuzumab refractory breast cancer [184].

1.7.4 Other novel HER-targeting agents in preclinical and clinical development

In addition to the HER2-targeting agents already described, there are several agents which target the HER family, which are currently in pre-clinical and clinical development. MM-111 is a bi-specific HER2/HER3 antibody which forms a trimeric complex with HER2 and HER3, effectively inhibiting HER3 signalling. MM-111 also inhibited the growth of cell line and xenograft models of HER2 positive breast cancer [185]. MM-111 is currently being investigated as a monotherapy for HER2-postive trastuzumab refractory breast cancer [186] and in combination with trastuzumab or lapatinib [187]. U3-1287 (AMG888) is a monoclonal antibody which targets HER3 and is currently in phase 1/11 trial in combination with trastuzumab and paclitaxel for the treatment of newly diagnosed HER2-positive MBC [188]. BMS-690514 is a reversible TKI inhibitor of EGFR, HER2, HER4 and VEGFR that has been shown to be effective in the treatment of erlotinib-resistant NSCLC cell lines [189]. BMS-690514 is currently being evaluated in combination with letrozole for the treatment of endocrine-resistant HER2 positive and negative breast cancer patients [188].

1.8 Resistance to HER2 targeted therapy

1.8.1 Mechanisms of resistance to trastuzumab

Although some patients with MBC respond to trastuzumab, most patients develop resistance to trastuzumab, while others fail to respond to trastuzumab at all [190]. The mechanisms of either the *de novo* or acquired resistance to trastuzumab are not fully understood but several potential mechanisms have been proposed.

1.8.1.1 Loss of PTEN / P13K mutation

Phosphatase and tensin homologue gene (PTEN) is a tumour suppressor which functions to prevent the activation of the P13K/AKT pathway, and loss of PTEN occurs in approximately 50 % of breast cancers [191]. Mutations in the P13KCA genes, which encode P13K, have been reported in approximately 30 % of breast cancers [192, 193]. The effect of PTEN loss or P13K mutation is the hyperactivation of the P13K/AKT pathway. Loss of PTEN has been implicated trastuzumab resistance *in vitro* and *in vivo,* and loss of PTEN is a predictive marker for trastuzumab resistance [82, 194]. *In vitro* expression of mutant P13KCA in HER2-amplified breast cancer cell lines confers resistance to trastuzumab [195], and PI3KCA mutations were associated with shorter time to progression in trastuzumab-treated breast cancer patients [193].

1.8.1.2 p95-HER2 expression

Truncation of HER2 is believed to be a prominent mechanism of trastuzumab resistance and truncated HER2 is commonly referred to as p95-HER2 [reviewed in [196]]. p95-HER2 can be generated in two ways; via cleavage or expression of splice variants. ADAM10, a disintergin and a metalloproteinase, mediates the cleavage of the extracellular domain (ECD) of HER2 leaving p95-HER2 bound to the membrane [197]. In addition, a role has been suggested for alternative mRNA splicing in the production of p95-HER2 [198]. p95-HER2 has been shown to be an independent prognostic factor in breast cancer, defining a subgroup of HER2 positive breast cancer patients with a significantly worse prognosis [199]. Retrospective studies have shown that p95-HER2 levels in breast cancer tumours correlate with trastuzumab resistance [200, 201]. Although these results suggest that the presence of p95-HER2 should be considered when determining the treatment of a HER2 positive patient however, the detection of p95-HER2 through current techniques is a controversial issue. The above mentioned studies use Western blotting [199], or immunofluorescence using two different

antibodies [200, 201] to detect p95-HER2. To date a clinically applicable assay for the detection of p95 has yet to be developed.

1.8.1.3 Ligand-dependant activation of HER3

HER2-HER3 heterodimers can be activated in a ligand-dependent or independent manner. Trastuzumab inhibits the ligand-independent activity of HER2-HER3 heterodimer but has no effect on ligand-stimulated HER2-HER3 heterodimer formation [202]. Ligand stimulation of breast cancer cells with heregulin can overcome the inhibitory effects of trastuzumab [203]. Knockdown of HER3 with shRNA resensitised trastuzumab-resistant cells to trastuzumab [204]. Increased expression of HER3 has been shown in a cell line model of trastuzumab resistance [205]. However, neither the expression nor phosphorylation of HER3 correlates with response to trastuzumab in a panel of breast cancer cell lines [194] or trastuzumab-treated breast cancer patients [206], suggesting that trastuzumab resistance may be mediated by lack of HER2-HER3 heterodimer inhibition rather than HER3 expression alone.

1.8.1.5 Crosstalk with IGF-IR

Increased expression of insulin-like growth factor receptor 1 (IGF-IR) correlated with diminished trastuzumab activity in HER2-amplified breast cancer cell lines [207]. HER2 heterodimerised with IGF-IR in trastuzumab-resistant cells, but the same effect was not seen in trastuzumab sensitive cells, and inhibition of IGF-IR activity increased the sensitivity of trastuzumab-resistant cells to trastuzumab [208]. A further study showed that heterodimerisation of HER2 with IGF-IR may not be limited to trastuzumab-resistant cells, and therefore may not be a causative factor in the development of trastuzumab resistance. In addition, the study showed increased expression of IGF-IR in a cell line model of acquired trastuzumab resistance and also shows enhanced activity of trastuzumab in combination with anti-IGF-IR therapy in trastuzumab sensitive cells [209]. A recent study implicates the formation of a heterotrimeric complex of HER2-HER3-IGF-IR in trastuzumab-resistant cells, and knockdown of HER3 or IGF-IR overcomes trastuzumab resistance [204]. Altered secretion of IGF-binding proteins has also been associated with trastuzumab resistance [210]. However, expression of IGF-IR does not predict response to trastuzumab therapy in patients with metastatic HER2 positive breast cancer [206, 211].

1.8.1.6 Other mechanisms implicated in trastuzumab resistance

Several other pathways and proteins have also been implicated in trastuzumab resistance. Briefly, these include; the inability of trastuzumab to inhibit EGFR signalling [212], the over-expression and/or amplification of cyclin E [213], Met receptor [214], EphA2 [215], the upregulation of miR-21[216], escape from ADCC [217], dysregulated glucose metabolism [218], and epitope masking via expression of mucin 4 (MUC4) [219], or CD44/hyaluronan complex [220, 221], both of which mask the HER2 binding site preventing trastuzumab binding to HER2.

1.8.2 Lapatinib overcomes trastuzumab resistance

As previously discussed, a synergistic interaction between trastuzumab and lapatinib has been seen in HER2-amplified cell lines [134, 143] and in clinical trials [167]. In addition, breast cancer cell lines exhibiting either *de novo* or acquired trastuzumab resistance remain sensitive to HER2 inhibition with lapatinib [134, 194], indicating that the mechanisms of lapatinib and trastuzumab resistance are non-overlapping. Several of the proposed mechanisms of trastuzumab resistance do not seem to apply to lapatinib, these include:

1.8.2.1 Loss of PTEN / mutations in PI3K

Loss of PTEN or PI3KCA mutations correlates with trastuzumab resistance. However, in preclinical studies, and clinical studies of women with HER2 positive breast cancer treated with lapatinib, the activity of lapatinib did not correlate with PTEN status [194, 222, 223]. In contrast to these studies, loss of PTEN and/or P13KCA mutations have been implicated in lapatinib resistance in cell line and xenograft models of HER2 positive breast cancer [224]. In addition, in HER2 positive patients treated with lapatinib and capecitabine, P13K activation, defined as loss of PTEN or PI3K mutation, was associated with lower clinical benefit and a lower ORR [224, 225]. Analysis of results from the NeoALTTO and ALTTO trials will hopefully determine the role of these alterations in trastuzumab and lapatinib resistance.

1.8.2.2 Lapatinib inhibits p95-HER2 activity

Trastuzumab does not inhibit p95-HER2. Cell line and xenograft models of p95-HER2 expression were resistant to trastuzumab however, they remain sensitive to lapatinib [200]. Lapatinib, as a monotherapy or in combination with capecitabine, was equally effective in patients with p95-HER2 positive and p95-HER2 negative HER2-positive breast tumours [226]. This is most likely due to the fact that p95-HER2 retains the

active kinase domain of HER2 and loss of the extracellular trastuzumab-binding domain does not inhibit the functionality or activity of the kinase domain [227].

1.8.2.3 Alterations in IGF-IR expression/activity

Alterations in IGF-IR have been implicated in trastuzumab resistance, however, treatment of trastuzumab-resistant cells with lapatinib resulted in inhibition of IGF-IR signalling and induction of apoptosis, even in the presence of IGF-1 [228].

1.8.3 Mechanisms of resistance to lapatinib

Since lapatinib gained FDA approval for the treatment of trastuzumab refractory HER2-positve breast cancer in 2007, there has been increased interest in determining its mechanisms of action, biomarkers of activity and also elucidating mechanisms of both *de novo* and acquired resistance. The mechanisms which have been proposed for lapatinib resistance are outlined below, and summarised in Table 1-3.

Table 1-3: Published cell line models of acquired lapatinib resistance, the method and concentration used to condition the cells and the proposed mechanism of lapatinib resistance. * denotes greater than peak plasma concentration (2.5 µM)

Cell line	Conditioning method	Lapatinib conc.	Profiling technique	Resistance mechanism	Ref.
BT474	single cell cloning	5 µM *	Affymetrix array	Upregulation of ER signalling	[229]
BT474, SKBR3	single cell cloning	5 µM *	Affymetrix array	Activation of RelA	[230]
SUM190	continuous exposure	(0.25 – 2.5 µM)	Immunoblotting	Overexpression of XIAP	[231]
BT474	single cell cloning	3 µM *	phospho-tyrosine immunoblotting	Overexpression of AXL	[232]
HCT116	continuous exposure	10 µM *	Immunoblotting	Increased expression of MCL-1	[233]
HCC1954 BT474	continuous exposure	(0.1 – 1 µM)	Immunoblotting	Increased expression of β1-integrin	[234]
SKBR3, MDA-MB-361, UACC893 BT474, HCC1954, SUM190	continuous exposure	increasing conc. up to: 1 µM or 2 µM	phospho-proteomic profiling	Increased SRC kinase activity	[235]
BT474, UACC812	continuous exposure	(0.1 – 1 µM)	Immunoblotting	Upregulation of ER signalling	[236]

1.8.3.1 Upregulation of ER signalling

Increased dependence on ER signalling has been described in an acquired model of lapatinib resistance [229]. ER signalling plays an essential role in breast cancer as over 60 % of breast cancers are ER positive [237]. FOXO3a is a member of the Forkhead family of transcription factors and it enhances ER transcriptional activity and its activation is regulated by AKT [238]. A comparison of the gene expression profiles of acquired lapatinib-resistant BT474 cells and sensitive BT474 cells revealed increased expression of several genes relating to ER signalling including FOXO3a, suggesting a switch from dependence on HER2 for signalling and survival to co-dependence on HER2 and ER. Combining lapatinib with ER inhibition prevented the emergence of lapatinib-resistant BT474 cells. Importantly, this study also reported increased ER signalling in tumour biopsies from lapatinib treated breast cancer patients [229]. Another study, which examined the effect of acquired lapatinib resistance on ER signalling, found that acquired lapatinib resistance was associated with increased ER or its downstream products in BT474 and UACC812, HER2-postive, ER positive cell lines with acquired lapatinib resistance. They also showed following ER upregulation that prolonged conditioning with lapatinib causes a switch from ER dependence back to HER2 dependence in a BT474 model of acquired lapatinib resistance [236]. In a different BT474 model of acquired lapatinib resistance, the resistant cells exhibited increased expression of ER and were sensitive to inhibition with a combination of lapatinib and fulvestrant [232]. In contrast to these studies, an ER-positive, HER2-postive SUM190 cell line model of acquired lapatinib resistance exhibited decreased expression of FOXO3a [231]. In a HCT116 colon cancer model of acquired lapatinib resistance, which is HER2-positive and ER-positive, resistance to lapatinib was not associated with increased ER expression nor was the resistance overcome by the addition of tamoxifen to lapatinib [233].

1.8.3.2 Overexpression of AXL

By examining a BT474 model of acquired lapatinib resistance, the overexpression of AXL protein was detected using phospho-tyrosine immunoblotting and identified using mass spectrometry and proposed as a mechanism of acquired lapatinib resistance [232]. AXL is a membrane-bound receptor tyrosine kinase containing a kinase domain closely related to MET and an extracellular domain resembling that of neural cell adhesion molecules. AXL activation is linked to several signal transduction pathways, including AKT, MAP kinases and NF-κB [Reviewed in [239, 240]]. AXL expression has been

reported in breast cancer cell lines [241] and also in human glioma carcinomas, where expression correlates with poorer prognosis [242]. Inhibition of AXL restored sensitivity to lapatinib in the lapatinib-resistant cells [232]. This study provides a mechanism by which HER2 positive, ER-positive breast cancer cells acquire resistance to lapatinib by increased expression of AXL.

1.8.3.3 Overexpression of MCL-1

Overexpression of myeloid cell factor-1 (MCL-1) has been reported in a HCT116 colon cancer cell line with acquired resistance to lapatinib [233]. The B-cell lymphoma-2 (BCL-2) family of proteins consists of 25 pro- and anti-apoptotic proteins that regulate the intrinsic/mitochondrial apoptosis pathway. Anti-apoptotic proteins, including MCL-1 associate with pro-apoptotic proteins, including BAX and BAK. When BAX and BAK are released from the complex with anti-apoptotic proteins they form pores in the mitochondrial membrane which allow for the release of cytochrome C and AIF leading to apoptosis. Tumour cells take advantage of this pathway to maintain survival via several mechanisms including: loss of expression of pro-apoptotic proteins (eg. BAX): and/or over-expression of anti-apoptotic proteins (eg. MCL-1) [reviewed in [243]]. The HCT116 colon cancer cell line with acquired lapatinib resistance had increased expression of MCL-1, decreased expression of BAX and decreased activation of BAX and BAK. Unlike sensitive cells, the lapatinib-resistant cells did not express activated BAX following either serum starvation or lapatinib treatment. Knockdown of MCL-1 in lapatinib-resistant cells enhanced lapatinib activity and this enhancement was abrogated by knockdown of BAX [233, 244]. Inhibition of MCL-1 has also been examined, in combination with lapatinib, in SKBR3 and BT474 breast cancer cell lines, whereby treatment with cyclin-dependent kinase (CDK) inhibitors resulted in reduced MCL-1 expression and enhanced lethality of lapatinib. Treatment of cells with the MCL-1 inhibitor, obatoclax, also enhanced the lethality of lapatinib in a synergistic fashion. Overexpression of MCL-1 or knockdown of BAX and BAK suppressed the enhanced lethality. This effect was also reproduced *in vivo* using xenograft models of BT474 cells [145]. Collectively, these studies suggest a mechanism whereby lapatinib resistance results in overexpression of MCL-1 rendering cells less susceptible to BAX/BAK-dependent apoptosis and tumour cell death.

1.8.3.4 Overexpression of XIAP

Acquired lapatinib resistance has been associated with overexpression of X inhibitor of apoptosis protein (XIAP) in a SUM190 model of HER2 positive IBC [231]. XIAP is an inhibitor of apoptosis protein (IAP) that binds to and inhibits the activation of procaspase-9, procaspase-7 and procaspase-3 leading to inhibition of both intrinsic and extrinsic apoptotic pathways. In addition to its caspase-binding function, XIAP regulates the activity of AKT, NF-κB and survivin. XIAP is overexpressed in tumour tissue compared to normal tissue including breast tumours and has been linked to therapeutic resistance in cervical, ovarian and prostate cancers [reviewed in [245]]. Expression of XIAP correlates with shorter overall survival and may act as an independent prognostic biomarker for invasive ductal carcinoma [246]. The SUM190 lapatinib-resistant cells had approx. 3-fold higher expression of XIAP compared to sensitive parental cells and stable expression of XIAP, using a lentiviral system, induced resistance to lapatinib in the parental SUM190 cells [231]. Downregulation of XIAP using embelin, a small molecule inhibitor which abrogates the XIAP/procaspase-9 interaction, resulted in decreased viability of SUM190 lapatinib-resistant cells. This suggests that XIAP is required for the survival of lapatinib-resistant cells and that XIAP represents a rational target for IBC patients with resistance to lapatinib [231].

1.8.3.5 Upregulation of SRC family kinases

Phospho-proteomic profiling of lapatinib-resistant cells suggested increased SRC (or a SRC family kinase) activity in a study of acquired lapatinib resistance [235]. The SRC family of tyrosine kinases has nine members including, YES, LYN and c-SRC (SRC). SRC has been implicated in pathways regulating proliferation, angiogensis, invasion and metastasis, and bone metabolism [reviewed in [247]]. Increased expression and activity of YES was observed in BT474 and UACC893 cell line models of acquired lapatinib resistance, and increased expression and activity of LYN was observed in a HCC1954 cell line model of acquired lapatinib resistance [235]. Treatment of the lapatinib-resistant cells with saracatinib (AZD0530) or dasatinib, both ATP competitive small molecule SRC inhibitors, resulted in inhibition of SRC phosphorylation, partial inhibition of AKT phosphorylation and inhibition of cell growth in both cell lines. Combined treatment of lapatinib sensitive breast cancer cell lines with lapatinib and saracatinib prevented the emergence of lapatinib-resistant cells. Importantly this study also showed that the expression of several SRC family members were upregulated in a small cohort of primary HER2 positive tumours following lapatinib treatment [235].

1.8.3.6 Activation of RelA

Using a BT474 cell line model of acquired lapatinib resistance, calcium-dependent activation of RelA has recently been associated with lapatinib resistance [230]. RelA is a subunit of NF-κB, which functions to protect cells from apoptosis. NF-κB functions to activate anti-apoptotic proteins which negate the pro-apoptotic effects of therapeutic agents [reviewed in [248]]. Lapatinib treatment triggered a cytoprotective stress response in SKBR3 and BT474 HER2-postive lapatinib-sensitive breast cancer cell lines, which was mediated by activation of RelA. Inhibition of RelA not only enhanced the apoptotic effects of lapatinib in BT474 and SKBR3 cells, but could overcome lapatinib resistance in a BT474 model of acquired lapatinib resistance [230]. There was also a small yet significant change in RelA expression between lapatinib responders and non-responders in lapatinib treated HER2-postive breast tumour samples [230].

1.8.3.7 Up-regulation of β1-integrin-mediated signalling

By examining HCC1954 and BT474 cell line models of acquired lapatinib resistance, the upregulation of several kinases which lie downstream of β1-integrin have been implicated in lapatinib resistance [234]. β1-intergrin is a critical mediator of breast cancer initiation and progression [249], has been associated with EGFR expression [250] and linked to therapeutic resistance in multiple cancer types. Notably, β1-integrin has been suggested as a predictive indicator for patients with *de novo* resistance to trastuzumab [251]. Acquired lapatinib resistance, in HCC1954 and BT474 lapatinib-resistant cells, was associated with increased expression of focal adhesion kinase (FAK) and SRC, downstream of β1-integrin [234]. In addition, inhibition of β1-integin significantly inhibited the growth of lapatinib-resistant HCC1954 and BT474 cells but did not significantly affect sensitive cells, suggesting a role of β1-integrin in acquired resistance to lapatinib.

1.8.3.8 Failure to downregulate survivin

Survivin is an IAP which when overexpressed can protect breast cancer cells from apoptotic stimuli [146]. One of the mechanisms of lapatinib action is the down-regulation of survivin. Failure to downregulate survivin was associated with lapatinib resistance in JIMT-1 cells, which represents a HER2-amplified cell line model of innate lapatinib resistance [148]. Thus, this suggests that constitutive activation of survivin protects the cells from lapatinib-mediated apoptosis. Knockdown of survivin in combination with HER2 inhibition suppressed proliferation and colony formation of the lapatinib-resistant cells [148].

1.8.3.9 Induction of autophagy

Induction of autophagy in response to lapatinib treatment has been proposed as a potential mechanism for lapatinib resistance [252]. Interestingly induction of autophagy has also been suggested as a mechanism of action for lapatinib in lapatinib sensitive breast cancer cells [154]. The role of autophagy in lapatinib resistance has yet to be fully explored or confirmed.

1.8.3.10 Upregulation of Grb7

Growth factor receptor-bound 7 (Grb7) is an adaptor protein which is frequently co-amplified with HER2 [253]. Lapatinib induces upregulation of Grb7 in cancer cells *in vitro* and *in vivo.* P13K signalling normally represses Grb7. Inhibition of AKT by lapatinib leads to Grb7 de-repression, and thus increased Grb7 expression. Knockdown of Grb7 reduces breast cancer cell viability and increases the activity of lapatinib [254]. This study suggests that Grb7 upregulation is a potentially adverse consequence of HER2 inhibition and that preventing Grb7 accumulation and or/its interaction with RTKs may increase the benefit of lapatinib.

1.8.3.10 Decreased phosphorylation of eEF2

Unpublished data from our laboratory identified eukaryotic elongation factor 2 (eEF2) as a protein whose phosphorylation is significantly altered in a model of acquired lapatinib resistance [255]. eEF2 is a monomeric GTPase that plays an essential role in regulating protein synthesis. Phosphorylation of eEF2 which results in its inactivation can occur through various different pathways, including the mTOR pathway [reviewed in [60, 256]]. A number of phosphorylated forms of eEF2 were significantly decreased in lapatinib-resistance SKBR3 cells compared to lapatinib-sensitive SKBR3 cells [255]. This suggests that altered phosphorylation of eEF2 may play a role in lapatinib resistance.

1.9 Quantitative methods used to identify alterations in lapatinib-resistant models

Various different techniques were utilised to identify the alterations discussed above, including; either unbiased pathway [233, 244] or selective [231] immunoblotting analysis; immunoblotting coupled with mass-spectrometry-based peptide sequencing [232]; phospho-tyrosine proteomics [235] and human affymetrix oligonucleotide array platform [229]. Below, the quantitative methods utilised in this study to identify alterations in models of acquired lapatinib resistance are discussed.

1.9.1 Array Comparative Genome Hybridisation analysis (aCGH)

aCGH analysis, also known as molecular karyotyping, is a technique used to identify copy number variations (CNV) in a genomic-wide screen [reviewed in [257]]. This technique utilises genomic DNA probes, known as oligos, which are robotically spotted and immobilised onto glass microscope slides, known as arrays. DNA from the test material (e.g. resistant cell line), is labelled with a green fluorescent dye (Cy3) and combined with the control material (e.g. sensitive cell line), which has been labelled with red fluorescent dye (Cy5). The 2 samples are co-hybridised to the array and the resulting ratio of fluorescence intensities is proportional to the copy numbers of DNA sequences in the test and control genomes. The areas on the slide that appear green indicate extra chromosomal material (duplication) in the test sample at that particular region. Areas on the slide that appear red indicate relatively less test DNA (deletion) in the sample at that specific spot [Figure 1-8]. aCGH analysis has been used as a tool to identify alterations in a broad spectrum of different cancer types including; ovarian cancer [258, 259], prostate cancer [260], melanoma [261], lung cancer [262], lymphoma [263] and breast cancer [264, 265]. It has also been used to identify alterations in newly developed models of trastuzumab resistance [266, 267]. To date aCGH technology has not been used to identify genomic alterations in a model of acquired lapatinib resistance.

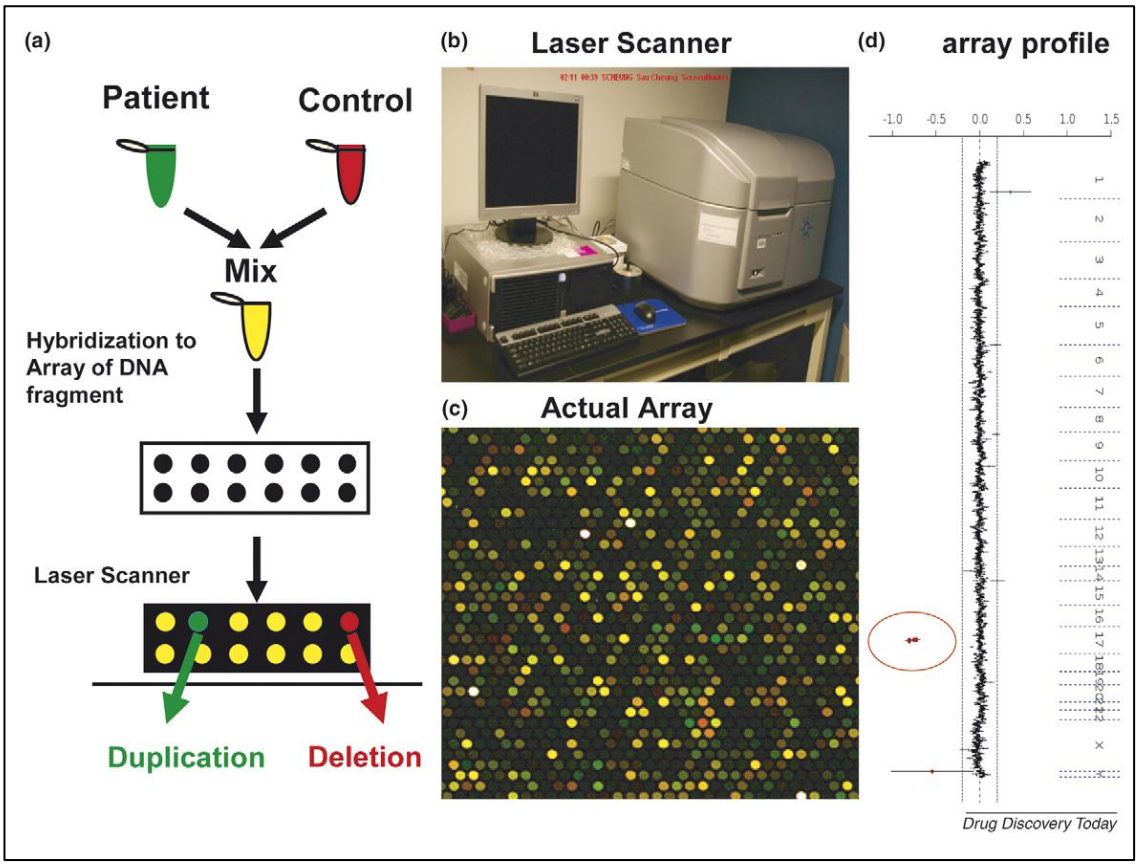

Figure 1-8: Principles of the aCGH technology. (a) DNA from the sample to be tested is Cy3 labelled and the control sample is Cy5 labelled. The samples are mixed and co-hybridised to the array. (b) The slides are scanned into image files using a specific microarray scanner (c). An output of scanning depicts hundreds of spots with different ratios of the fluorescence intensities. (d). Sample output of aCGH analysis showing alterations on a specific chromosome. [Image and legend reproduced from [257]].

1.9.2 SILAC proteomic based technology

Stable Isotope Labelling of Amino acids in Cell culture (SILAC) is a proteomic labelling strategy which utilises the metabolic machinery of cells to incorporate isotope labelled amino acids into the proteins of the cells [for review and protocol [268]]. With SILAC, the entire proteome of a given cell population is metabolically labelled with "heavy", non-radioactive isotopic variants of amino acids, usually [U-$^{13}C^{6}$]-L-Lysine, which alters the weight of the peptide fragments by 6 Daltons, thus making it distinguishable from a second non-labelled cell line by mass spectrometry (MS). Therefore two or more distinctly SILAC-labelled cell-populations can be mixed and analysed in one MS experiment which allows for accurate quantitation of proteins from different cellular states. A conventional SILAC workflow involves culturing one population of cells in media containing the heavy amino acid, and the second population

of cells in media containing non-isotope labelled lysine [Figure 1-9]. The cells are grown in their respective media for a minimum of 6 doublings to allow for full incorporation (≥ 95 %) of the heavy lysine, after which time the two populations are combined, analysed by mass-spectroscopy (MS). The signal intensities from the heavy labelled and non-labelled samples provide a quantitative comparison of their abundance in the mixed population [268].

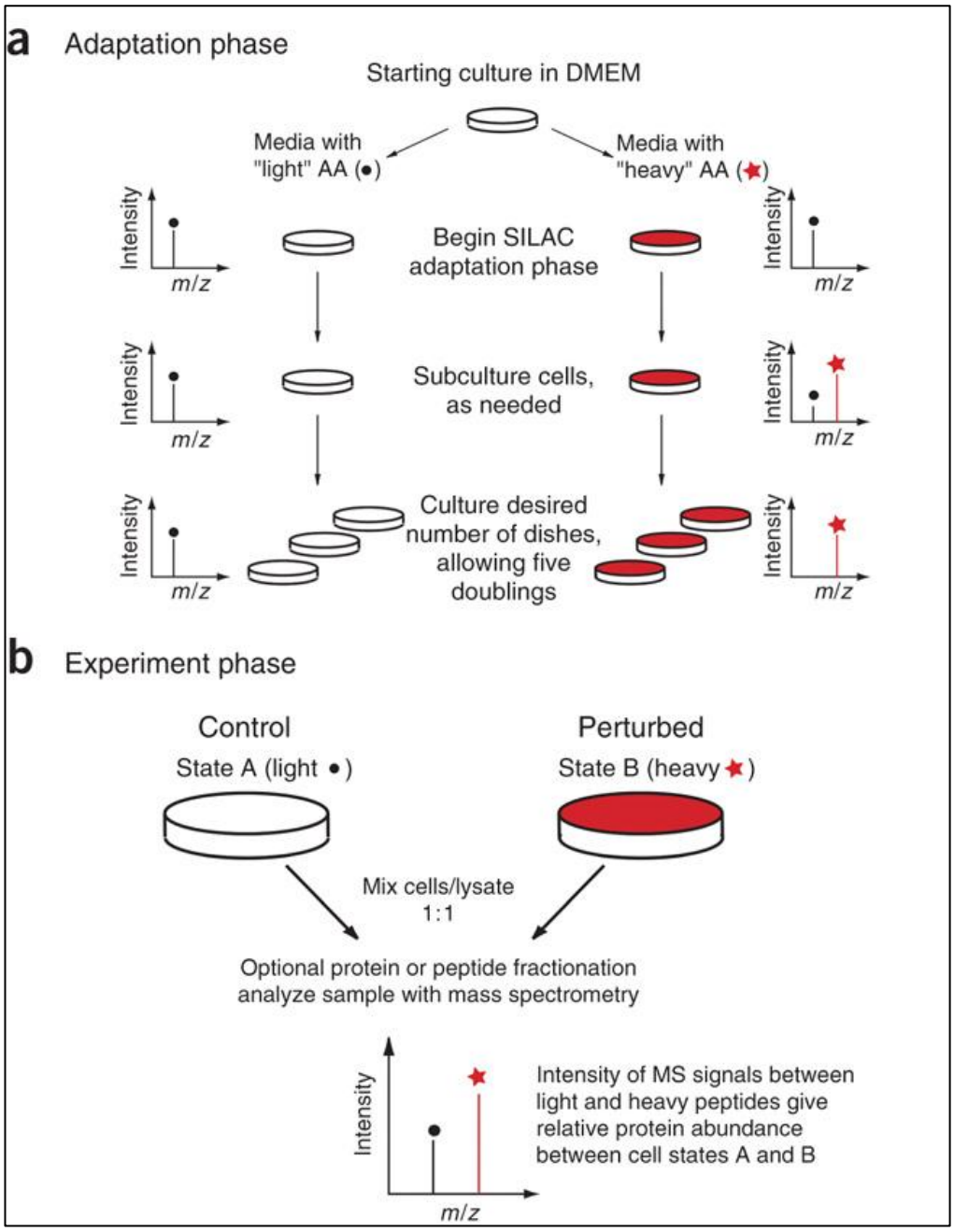

Figure 1-9: Overview of SILAC protocol. The SILAC experiment consists of two distinct phases - (a) an adaptation and (b) an experimental phase. (a) During the adaptation phase, cells are grown in light and heavy SILAC media until the heavy cells have fully incorporated the heavy amino acids (red star). This allows the two SILAC cell pools to be fully distinguishable by MS (black dot and red star, indicating light and heavy SILAC peptides, respectively) and can then be mixed and processed as a single sample. The adaptation phase can include the expansion of cells to reach the required number of dishes for the experiment. (b) In the second phase, the two cell populations are mixed, digested to peptides as a single pool and analysed by MS for protein identification and quantification [Image and legend reproduced from [268]].

1.9.2.1 Advantages of SILAC labelling over traditional methods

SILAC is advantageous over traditional gel based proteomic methods such as Difference In-Gel Electrophoresis (DIGE) for several reasons. DIGE allows samples to be mixed and separated on a two dimensional gel for the identification of alterations in the expression levels of proteins, however, this technique is associated with greater run-to-run variability compared to SILAC. The lower variability associated with SILAC allows smaller statistically significant differences in protein abundance to be detected and requires fewer repetitions making the technique more high throughput [269]. One of the main differences between the capabilities of DIGE and SILAC is that DIGE is incapable of identifying co-migrating proteins. DIGE image software assumes a spot on a gel is homogeneous but it has been shown that some spots may contain multiple proteins. As there is a limit on the maximum number of spots that can be observed on a typical DIGE gel, many proteins will inevitably co-migrate to the same spot position, thus confounding their accurate quantitation and mass spectrometric identification [270]. A major limitation of DIGE is inefficient detection of low abundant proteins, proteins with high or low molecular weights and hydrophobic proteins. Proteins with these characteristics are important in receptor tyrosine kinase signalling pathways and are therefore of particular interest in cancer cell models.

1.9.2.2 SILAC labelling coupled with phospho-tyrosine enrichment

Post-translational modification events, such as phosphorylation, account for approximately 10 % of total protein in the cell, which results in a large number of non-phosphorylated peptides being present with a smaller population of phosphorylation peptides. This adds unwanted complexity to the MS analysis which can mask signals from the low abundant phospho-peptides behind the higher abundant non-phosphorylated peptides. Therefore robust separation and enrichment strategies for purification of phosphorylated peptides from non-phosphorylated peptides are highly beneficial. There are several enrichment techniques that can be coupled with SILAC analysis to yield more specific results [reviewed in [271]]. Antibody based purification methods utilise specific targeted antibodies to immunoprecipitate proteins of interest. By utilising either a protein specific or phospho-site specific antibody information about other phospho-sites on the protein of interest can be obtained and it can also give information about the binding partners of the phospho-protein of interest. One antibody based approach for the enrichment of phospho-peptides is to examine tyrosine phosphorylation sites. Phosphoproteomic approaches generally reveal only small

numbers of tyrosine phosphorylation sites, due to the low level of phospho-tyrosine sites compared to phospho-serine and phospho-threonine residues. Using immunoaffinity purification and reverse-phase chromatography, this technique allows the investigator to obtain a global overview of tyrosine phosphorylation in the cell, covering many classes of proteins without preconceived biases about where tyrosine phosphorylation sites will be found [272].

1.9.2.3 SILAC proteomics - a cancer research tool

SILAC proteomic based techniques have been used to identify alterations at the protein level in various different cancer types including; lung [273], melanoma [274], ovarian [269], prostate [275], and breast cancer [276-278]. SILAC labelling has been used to compare normal breast epithelial cells to HER2 positive amplified cells extracted from HER2 transfected mice [278]. SILAC proteomic techniques have also been used to identify alterations in cell lines models of lapatinib resistance [235].

1.9.2.4 Limitations of SILAC proteomics

There are several limitations to SILAC-based proteomics; 1) SILAC is an unsuitable method for performing proteomic analysis on clinical samples due to the requirement for metabolic labelling, 2) Incorporation of the metabolic label is dependent on the rate of intracellular protein turn-over requiring optimisation on a cell line to cell line basis, 3) and the cost of media containing isotopically-labelled amino acids is high which is a deterrent to performing multiple comparisons with additional replicates.

1.10 Summary

Lapatinib is approved for the treatment of metastatic HER2 positive breast cancer and although it provides effective treatment for some patients, many patients fail to respond to lapatinib or develop resistant after an initial period of response. Thus, resistance to lapatinib is a significant clinical issue and identifying mechanism of how tumours become resistant to lapatinib would aid in the development of therapeutic strategies to prevent the onset of resistance. In this study, we developed a number of cell line models of HER2-positive lapatinib-resistant breast cancer and applied genomic and proteomic profiling techniques to investigate mechanism of lapatinib resistance.

1.11 Study Aims

The aims of this study were as follows:

1. To develop new cell line models of acquired lapatinib resistance – developing additional models of lapatinib resistance may help identify mechanisms of resistance that are present in a subset of HER2 positive breast cancers, thus helping to predict the subset of patients likely to present with the same mechanism of resistance. There are very few published cell line models of acquired lapatinib resistance and many of these cell lines were conditioned with lapatinib concentrations in excess of the peak plasma concentration of lapatinib achievable in patients.

2. To characterise the resistant phenotype of acquired lapatinib resistance cells – extensive characterisation in the form of growth assays, drug sensitivity assays and immunoblotting for members of key signalling pathways provides a context additional alterations to be examined and allows for the comparison of newly developed cell lines to previously published models

3. To utilise aCGH and SILAC proteomic based technology to identify alterations in acquired lapatinib-resistant cells – global profiling techniques suggest alterations at the genomic and proteomic level which may predict lapatinib resistance for provide a target for the treatment of lapatinib-resistant breast cancer

4. To examine the role of eEF2 phosphorylation in lapatinib resistance – previous phospho-proteomic work in our laboratory identified that the phosphorylation of eEF2 was decreased in acquired lapatinib-resistant cells, thus identifying the mechanism(s) responsible for the decreased phosphorylation of eEF2 may provide a target for the treatment of lapatinib-resistant breast cancer

5. To explore alterations in HER2 signalling innate lapatinib-resistant cells - many patients exhibit innate resistance to lapatinib and by examining alterations in the key signalling pathways using a panel of HER2-positive breast cancer cells lines, some of which exhibit innate lapatinib resistance, biomarkers which may

predict or correlate with response could be found which could improve the outcome for these patients.

Chapter 2

Materials and Methods

2.1 Cell lines, cell culture and reagents

Nineteen human breast cancer cell lines were used in this study, including 17 established cell lines, a lapatinib-conditioned HER2 overexpressing breast cancer cell line (SKBR3-L), which was selected for long-term growth in drug-containing medium and its parent cell line (SKBR3-par). The cell lines BT474, HCC1419, HCC1954 and SKBR3 were obtained from the American Type Culture Collection (ATCC). UACC812, HCC202, HCC2218, HCC1569, EFM-192A, SUM225, SUM190, ZR-75, UACC893, UACC732, MDA-MB-361 and MDA-MB-453 and were obtained from the University of California Los Angeles, USA. JIMT-1 cells were purchased from the German Collection of Microorganisms and Cell Cultures (DSMZ). The growth conditions for each cell line are described in Table 2-1. SKBR3-L cells were generated by Dr Brigid Browne through continuous culturing of SKBR3 cells in RPMI supplemented with 250 nM lapatinib for 6 months [255]. All cell lines were routinely tested for the presence of mycoplasma, and found to be negative. Lapatinib (Tykerb ®) was obtained from GlaxoSmithKline, NVP-AEW541 from Novartis, BMS-536924 from Bristol-Myers Squibb, gefitinib was purchased from Sequoia Research Products, LY294002 from Merck, and U0126 and NH125 from Calbiochem. Unless otherwise specified, all reagents were of laboratory or electrophoresis grade. All cell culture procedures were performed as per the guidelines set out in NICB SOPs [#001-01, #002-02 and #003-01]. In addition, mitochondrial DNA from all cell lines, including newly developed lapatinib-resistant cell lines, was sequenced to confirm their correct identify [this was performed in collaboration with Dr. Neil O'Brien and Dr. Charles Ginther in UCLA].

Table 2-1: Growth media, foetal calf serum (FCS) and supplements for each of the cell lines used in this study

Cell line	Media	FCS	Supplements
BT474	RPMI 1640	10%	None
EFM-192A	RPMI 1640	10%	None
SKBR3	RPMI 1640	10%	None
HCC1419	RPMI 1640	10%	None
MDA-MB-453	RPMI 1640	10%	None
HCC1954	RPMI 1640	10%	None
JIMT-1	DMEM	10%	glutamine [1]
UACC812	L-15	15%	glutamine
MDA-MB-361	L-15	15%	glutamine
SUM190	DMEM-F12	10%	10 μg/mL insulin, 1 μg/mL hydrocortisone
SUM225	DMEM-F12	10%	10 μg/mL insulin, 1 μg/mL hydrocortisone
HCC1569	RPMI 1640	10%	glutamine, D-glucose [2], sodium pyruvate [3]
ZR75-30	RPMI 1640	10%	glutamine, D-glucose, sodium pyruvate
HCC202	RPMI 1640	10%	glutamine, D-glucose, sodium pyruvate
HCC2218	RPMI 1640	10%	glutamine, D-glucose, sodium pyruvate
UACC732	MEM	10%	glutamine, 1% MEM nonessential amino acids, sodium pyruvate
UACC893	L-15	15%	glutamine, 20ng/ml EGF, 10 μg/ml insulin, 10 μg/ml glutathione

[1] 2 mmol/L glutamine

[2] 1 μmol/L sodium pyruvate

[3] 4.5 g/L D-glucose

2.2 Preparation of cell lysates

Cells were grown in duplicate wells in 6-well plates and whole cell lysates were prepared as follows: cells were washed twice with cold phosphate buffered saline solution (PBS) and 150 µl/well RIPA buffer ((Sigma, R0278) 5 mM Tris-HCl pH 7.4, 1% NP-40, 0.1% SDS, 150 mM NaCl, 1% Triton x-100) containing 1x Protease Inhibitor cocktail (Calbiochem, 539131), 2 mM PMSF (Sigma, P7626), and 1 mM sodium orthovanadate (Sigma, 6508), was added and cells were incubated on ice for 20 minutes. Cells were scraped into lysis buffer. The lysis buffer was collected and centrifuged at 16,100 x g for 10 minutes at 4 ^{o}C. The pellets were discarded and the supernatants collected and stored at -80^{o}C. Protein quantification was performed using the BCA quantitation kit (Pierce, 23227).

2.3 Immunoblotting

Protein (30 µg) was electrophoretically resolved on 7.5 % (Lonza, 59501) or 10 % (Lonza, 59502) denaturing polyacrylamide gels. The resolved proteins were then transferred to nitrocellulose membranes (Invitrogen, IB3010-01) using the iBlot transfer system (Invitrogen, IB1001). Protein transfer was visually confirmed using Ponceau S staining (Sigma, P7170). Membranes were blocked with skimmed-milk powder (Bio-Rad, 170-6404) in PBS-tween (Sigma, P1379) (0.1%), and incubated overnight at 4 ^{o}C with primary antibodies. The blotting conditions for each antibody used in this study are described in Table 2-2. Proteins were visualised using horseradish peroxidase-conjugated anti-mouse, anti-goat or anti-rabbit antibodies (Sigma – see Table 2-2 for full details) and ECL plus reagent (GE Healthcare, RPN2132). Membranes were washed with 0.1 % PBS-tween 3 times for 10 minutes each, both prior to and following incubation with secondary antibodies. Protein bands were detected using the Typhoon 9400 (Amersham Biosciences) system. Densitometry was performed using the ImageQuant software ((version 5.2), (Amersham Biosciences)) on biological triplicate immunoblots and the results were normalised using α-tubulin as a loading control.

Table 2-2: List of antibodies, blotting conditions, secondary antibodies, companies and catalogue numbers for all antibodies used in the study; where PBS-T is PBS-Tween, PTG is ProteinTech Group, SCB is Santa Cruz Biotechnology and CST is Cell Signalling Technology. MDA-MB-468 positive control lysate was provided by Dr. Brendan Corkery, and Hela cell lysate was purchased from BD transduction laboratories, (611449).

Antibody	Phospho-site	dilution	blotting conditions	Secondary	+ ve control	company	Cat no.
anti-Rabbit secondary		1:1000	2.5 % milk / 0.1 % PBS-T			Sigma	A6154
anti-mouse secondary		1:1000	2.5 % milk / 0.1 % PBS-T			Sigma	A6782
anti-goat secondary		1:500	2.5 % milk / 0.1 % PBS-T			Sigma	A5420
α-tubulin		1:1000	2.5 % milk / 0.1 % PBS-T	Mouse		Sigma	T6199
anti-HER2		1:1000	5 % milk / 0.1 % PBS-T	Mouse	BT474	Calbiochem	OP15
anti-phospho-HER2	Tyr1221/1222	1:1000	2.5 % milk / 0.1 % PBS-T	Rabbit	BT474	CST	#2249
anti-EGFR		1:250	2.5 % milk / 0.1 % PBS-T	Mouse	MDA-MB-468	Neomarkers	MS-665-P
anti-phospho-EGFR	Tyr1173	1:1000	2.5 % milk / 0.1 % PBS-T	Rabbit	MDA-MB-468	CST	#4407
anti-HER3		1:1000	2.5 % milk / 0.1 % PBS-T	Rabbit	BT474	CST	#4754
anti-phospho-HER3	Tyr1289	1:1000	2.5 % milk / 0.1 % PBS-T	Rabbit	BT474	CST	#4791
anti-HER4		1:500	1 % milk / 0.1 % PBS-T	Rabbit	MCF7	CST	#4795
anti-AKT		1:1000	2.5 % milk / 0.1 % PBS-T	Rabbit	SKBR3	CST	#9272
anti-phospho-AKT	Ser473	1:1000	2.5 % milk / 0.1 % PBS-T	Rabbit	SKBR3	CST	#9271

Table 2-2: Continued

Antibody	Phospho-site	dilution	blotting conditions	Secondary	+ ve control	company	Cat no.
anti-ERK		1:1000	2.5 % milk / 0.1 % PBS-T	Rabbit	SKBR3	CST	#9102
anti-phospho-ERK	Thr202/Tyr204	1:1000	2.5 % milk / 0.1 % PBS-T	Rabbit	SKBR3	CST	#9101
anti-XIAP		1:1000	2.5 % milk / 0.1 % PBS-T	Mouse	SUM190	BD Biosciences	610717
anti-ER		1:200	3 % milk / 0.1 % PBS-T	Mouse	MCF7	SCB	sc-8002
anti-SRC		1:1000	2.5 % milk / 0.1 % PBS-T	Rabbit	MCF7	CST	#2108
anti-phospho-SRC	Tyr416	1:500	1 % milk / 0.1 % PBS-T	Rabbit	MCF7	Millipore	05-677
anti-MCL-1		1:1000	2.5 % milk / 0.1 % PBS-T	Rabbit	A549	CST	#4572
anti-IGF1R		1:500	5 % milk / 0.1 % PBS-T	Rabbit	BT474	SCB	sc-713
anti-phospho-IGF1R	Thr1131	1:1000	2.5 % milk / 0.1 % PBS-T	Rabbit	BT474	CST	#3021
anti-eEF2		1:1000	2.5 % milk / 0.1 % PBS-T	Rabbit	MDA-MB-453	CST	#2332
anti-phospho-eEF2	Thr56	1:1000	2.5 % milk / 0.1 % PBS-T	Rabbit	MDA-MB-453	CST	#2331
anti-p70S6K		1:1000	2.5 % milk / 0.1 % PBS-T	Rabbit	UACC732	CST	#2708
anti-phospho-p70S6K	Thr389	1:1000	2.5 % milk / 0.1 % PBS-T	Rabbit	UACC732	CST	#9234
anti-eEF2k		1:1000	2.5 % milk / 0.1 % PBS-T	Rabbit	HELA	CST	#3692
anti-phospho-eEF2k	Ser366	1:1000	2.5 % milk / 0.1 % PBS-T	Rabbit	HELA	CST	#3691

Table 2-2: Continued

Antibody	Phospho-site	dilution	blotting conditions	Secondary	+ ve control	company	Cat no.
anti-phospho-eEF2k	Ser359	1:200	2.5 % milk / 0.1 % PBS-T	Rabbit	HELA	SCB	sc-21644
anti-phospho-eEF2k	Ser396	1:200	2.5 % milk / 0.1 % PBS-T	Rabbit	HELA	SCB	sc-21646
anti-mTOR		1:500	1 % milk / 0.1 % PBS-T	Rabbit	MDA-MB-453	CST	#2983
anti-phospho-mTOR	Ser2448	1:500	1 % milk / 0.1 % PBS-T	Rabbit	MDA-MB-453	CST	#2971
anti-EPB1		1:1000	2.5 % milk / 0.1 % PBS-T	Goat	HELA	SCB	sc-68478
anti-CDKI		1:500	2.5 % milk / 0.1 % PBS-T	Rabbit	MCF7	CST	#9112
anti-phospho-CDK1	Tyr15	1:500	2.5 % milk / 0.1 % PBS-T	Rabbit	MCF7	CST	#4539
anti-GAPDH		1:1000	2.5 % milk / 0.1 % PBS-T	Mouse	MCF7	R&D systems	mab5718
anti-SELENBP1		1:1000	2.5 % milk / 0.1 % PBS-T	Goat	MCF7	SCB	sc-160788
anti-SET protein		1:1000	2.5 % milk / 0.1 % PBS-T	Goat	HELA	SCB	sc-5655
anti-STARD3		1:1000	2.5 % milk / 0.1 % PBS-T	Rabbit	MCF7	PTG	20292-1-AP

2.4 Proliferation Assays

Cells were seeded into 96-well plates at the following densities, 3000 cells/well SKBR3 cells, 2000 cells/well HCC1954 cells and 5000 cells/well HCC1419 cells. After 24 hours, cells were treated with the appropriate media supplemented with 10 % FCS with or without serial dilutions of lapatinib, NVPAEW541, BMS-536924, gefitinib, NH125 or rapamycin. Proliferation was measured after five days using the acid phosphatase assay. For the acid phosphatase assay, media was removed and each well rinsed with PBS; 100 µl of acid phosphatase substrate (10 mM p-nitrophenol phosphate (Sigma, 1040) in 0.1 M sodium acetate (Sigma, S2899), 0.1% triton X-100 (BDH, 9002-93-1), pH 5.5) was then added to each well followed by incubation at 37^{o}C for 60 minutes, at which time 50 µl of NaOH (Sigma, S5881) was added to each well and the absorbance was read at 405 nm with 620 nm as a reference. Proliferation or inhibition of proliferation was calculated relative to untreated controls. Each assay was carried out in triplicate.

2.5 Growth inhibition – cell count method

HCC1954 and HCC1419 cells were seeded into 24-well plates. Once the cells reached approx. 40% confluence, cells were treated with a range of lapatinib concentrations: 100, 200 and 300 nM for HCC1419 cells and 750, 1000 and 1250 nM for HCC1954 cells. Following 4 days of treatment, the media was removed from the cells, they were washed with PBS and 100 µL of trypsin was added to each well. Once the cells had detached, 100 µL of media containing 10 % FCS was added to each well. In a round-bottom 96-well plate, 100 µL of cell suspension was added to 100 µL of ViaCount reagent (Millipore, 4000-040). Cell counts were performed using the Guava EasyCyte ((version 5.3), (Millipore)) in triplicate and proliferation or inhibition of proliferation was calculated relative to untreated controls.

2.6 Lapatinib conditioning of cell lines

HCC1419 and HCC1954 cells were conditioned with lapatinib. Four day growth assays (described in section 2.5) were performed to determine the concentration of lapatinib to condition cells with. Each cell line was grown in duplicate T75 flasks containing either control media or conditioned media, and media was replaced twice weekly for 6 months. HCC1419 cells were conditioned with 250 nM lapatinib and HCC1954 cells with 1000 nM lapatinib. The effects of lapatinib conditioning on the cells were

examined by monitoring cell morphology and sensitivity to lapatinib at 4-weekly intervals during the conditioning process.

2.7 Doubling time assays

Doubling time assays were performed by seeding 3000 cells into each well of a 24 well plate. After 24 hours, cells were treated with and without 100 nM trastuzumab or 100 nM lapatinib. Cell counts were performed at day 0, 3, 5 and 7 as follows: the media was removed from the cells, they were washed with PBS and 100 µL of trypsin was added to each well. Once the cells had detached 100 µL of media, containing 10 % FCS was added to each well. In a round-bottom 96-well plate, 100 µL of cell suspension was added to 100 µL of ViaCount reagent (Millipore, 4000-040). Cell counts were performed using the Guava EasyCyte ((version 5.2) (Millipore)) in both technical and biological triplicate. Doubling times were calculated between days 5 and 7, while the cells were growing exponentially, using the formula;

$$\text{Doubling time} = \frac{(T_t - T_0)(Log\ 2)}{(Log\ T_t - Log\ T_0)}$$

where T_t is the end time point and T_0 is the beginning time point (days), which in this case were 7 and 5, respectively.

2.8 Drug withdrawal assays

Drug withdrawal assays were performed by culturing lapatinib-conditioned cells for an extended period of time (up to 4 months) in the absence of lapatinib. Proliferation assays, to assess the sensitivity of the cells to lapatinib, were performed at 4 week intervals using the acid phosphatase method, as described in section 2.4.

2.9 HER2 fluorescent *in situ* hybridisation analysis

2.9.1 Preparation of cell donor paraffin blocks

Cells (5 x 10^6) were re-suspended in 10 ml of a 10 % (v/v) neutral-buffered formalin solution, containing formaldehyde solution (Sigma, 252549), sodium dihydrogen phosphate (Fisher Scientific, 7558-79-4) and disodium hydrogen phosphate (Fisher Scientific, 7558-80-7), and incubated overnight at room temperature. Cells were pelleted by centrifugation at 500 x g for 10 minutes, washed with PBS and re-pelleted. Cells were re-suspended in a 0.8 % agarose (Sigma, A9539) solution and transferred to a 1.5 ml microcentrifuge tube, from which the tapered end had been removed. The

agarose plug was left to solidify within the tube, removed via the cap end and transferred to an embedding cassette (Fisher Scientific, 15-200-402E). The cassettes were placed in a slide bath and were washed for 1 hour each in the following solutions: ultra-high purity (UHP) water, 50 % ethanol (Merck, 100983), 70 % ethanol, 90 % ethanol, 100 % ethanol. This was followed by 2x 1 hour washes in 100 % xylene (Applichem, A0663), before being placed into melted paraffin (McCormick Scientific, 561006) for 2 hours. Using the Leica EG1150H machine the cassettes were placed in plastic moulds (SKS Science, M475), embedded with paraffin and left to cool. Once the paraffin was set the cell culture blocks were stored at 4 °C prior to sectioning.

2.9.1 Sectioning and de-paraffinisation of slides

Sectioning of cell culture blocks and subsequent FISH analysis were carried out by Ms. Alison Prendergast (St. Vincent's University Hospital, Dublin). An overview of the procedure is outlined below. Sections (4 µm) were cut from the cell blocks, mounted on silanised slides and incubated overnight at 56 °C. Slides were de-paraffinised using a Paraffin pre-treatment kit (Abbott, 32-801200). All buffers were supplied with the kit unless otherwise specified. Briefly, slides were immersed in 0.2 M hydrochloric acid (HCL) (Fluka, 382887) for 20 minutes at room temperature and then washed with wash buffer with agitation for 5 minutes. Slides were immersed in pre-treatment solution at 80 °C for 30 minutes, washed in wash buffer with agitation for 5 minutes, then incubated with protease solution at 37 °C for 30 minutes before repeating wash step. Slides were immersed in 4 % neutral buffered formalin solution (containing formaldehyde solution (Sigma, 252549), sodium dihydrogen phosphate (Fisher Scientific, 7558-79-4) and disodium hydrogen phosphate (Fisher Scientific, 7558-80-7)), at room temperature for 10 minutes and the wash step was repeated. Slides were dehydrated by consecutive 1 minute washes in 70 %, 85 % and 100 % ethanol (Merck, 100983) and air dried at 37 °C.

2.9.2 PathVysion HER-2 DNA Probe Hybridisation

All subsequent steps were performed using the PathVysion HER-2 DNA Probe Kit (Abbott, 02-J01-030), and all reagents were supplied with the kit unless otherwise specified. LSI HER-2/neu SpectrumOrange/CEP 17 SpectrumGreen DNA Probe mixture (10 µl) was applied to each slide and covered with a coverslip, sealed and placed in a humidified hybridisation chamber (HYBrite) overnight. Slides were then immersed in post-hybridisation wash buffer at room temperature to remove the coverslip and then immersed in post-hybridisation wash buffer, which had been pre-

heated to 74 °C, for 2 minutes with gentle agitation, transferred to a 70 % ethanol (Merck, 100983) solution for 20 seconds and air dried at 37 °C. DAPI counterstain (10 µl) was applied to the slides. Slides were covered with a coverslip, sealed and stored at 4 °C prior to signal enumeration.

2.9.3 HER2/CEP17 ratio enumeration

Signal enumeration was performed using a fluorescence microscope equipped with appropriate excitation and emission filters allowing visualisation of the intense orange and green fluorescent signals. The filters required for signal enumeration are DAPI, FITC and TRITC. Normal and amplified Vysis ProbeChek HER-2/neu control slides were included and they met the acceptable range for HER2/CEP17 ratio (Normal 0.75-1.25; Amplified 1.60-2.00) (Abbott, 02-J05-030, 02-J04-030). Enumeration was performed on 60 interphase nuclei giving a HER2/CEP17 ratio for each nucleus, yielding a ratio of the HER-2/neu gene to chromosome 17 copy number. Images of the FITC stain, TRITC stain and DAPI stain were taken and overlaid to create a composite image using the fluorescence microscope.

2.10 Senescence associated β-galactosidase activity assay

The activity of β-galactosidase was measured using a β-galactosidase staining kit (Cell Signalling Technology, #9860). Briefly, media was removed from the cells, followed by 2 washes with PBS and cells were then incubated with fixative solution (containing 2 % formaldehyde and 0.2 % glutaraldehyde in UHP water) for 15 minutes at room temperature. Following 2 washes with PBS, staining solution is added. The staining solution contains 40 mM citric acid/sodium phosphate (pH 6.0) , 0.15 M NaCl, 2 mM MgCl, to which 10 µl/ml of both 500 nM potassium ferrocyanide solution, 500 nM potassium ferricyanide solution and 50 µl/ml of 20 mg/ml X-gal (5-bromo-4-chloro-3-indolyl-βD-galactopyranoside powder) dissolved in N-N-dimethylformamide (DMF) was added. Note, all reagents for fixative and staining solutions were supplied with the kit. The volumes of each fixative solution and staining solution required per well and per flask are described in Table 2-3. The cells were incubated in staining solution at 37 °C overnight. After incubation cells were washed twice with PBS and then examined for the presence of blue staining within cells, indicating activity of β-galactosidase. Triplicate representative images were taken of each treatment condition using unbiased cell selection and all experiments were repeated in biological triplicate. Treatment of

cells with 50 µM bromodeoxyuridine (BrdU) (Sigma, B5002) was used as a positive control for β-galactosidase activity.

Table 2-3: Volumes of fixative and staining solutions required for each different cell culture vessel used for experiments involving β-galactosidase staining.

Cell culture vessel	Volume of solution required
24-well plate	500 µl / well
6-well plate	1 ml / well
T25 flask	2.5 ml / flask
T75 flask	4 ml / flask

2.11 RNA extraction

RNA was extracted from HCC1419 and SKBR3 cells using the following method. Media was removed from the cells and they were washed twice with PBS. Tri-reagent (Sigma, 93289) was added to the flask (1 ml / T75), cells were scraped into the Tri-reagent using cell scrapers, and the RNA lysates was stored at -80 °C until required. To extract RNA from the lysate, lysates were thawed on ice and 200 µl/ml of chloroform (Lab-Scan Analytical Systems, AR1027E) was added. Samples were mixed by inversion (5 times) and left to sit at room temperature for 15 minutes. Samples were then centrifuged at 15,700 x g for 15 minutes at 4 °C, resulting in the separation of the sample into 3 distinct layers. The top, clear layer of the sample was removed to a new eppendorf to which 500 µL of ice-cold isopropanol (Fluka, 34965) was added. Samples were mixed by inversion (5 times) and left to sit at room temperature for 10 minutes. The samples were then centrifuged at 13,400 x g for 30 minutes at 4 °C and the supernatant then removed. Following this, 750 µl of 75 % ethanol (Merck, 100983) was added to the samples, samples were vortexed to detach the pellet and centrifuged at 16,100 x g for 5 minutes at 4 °C. The supernatant was removed and discarded and the ethanol wash step repeated. The pellet was then re-suspended in 20 µl of RNase-free water (Ambion, 9932) and left to sit at room temperature for 20 minutes. Samples were then stored at -80 °C or on ice for immediate use.

2.12 Reverse transcription polymerase chain reaction (RT-PCR)

The concentration of total RNA in extracted samples was determined using the Nano-Drop Spectrophotometer (Thermo Scientific). Stock solutions of 2 µg /10 µl were made by diluting RNA-extracts with RNase-free water (Ambion, 9932). Using a high capacity cDNA Reverse Transcription Kit (Applied Biosystems, 4368814), a 2X master mix solution was prepared as per Table 2-4. For each reaction, 10 µl of RNA sample and 10 µL of master mix were combined in PCR tubes, briefly centrifuged to spin down contents and loaded into the thermo-cycler (G-STORM) and the reverse transcription run as per Table 2-5. The samples were then stored at 4 °C, for immediate use, or at -80 °C until required. Controls were included at this point; non-target control (NTC) which was prepared without the RNA template, and a minus reverse transcriptase control (-RTC) which was prepared without the reverse transcriptase enzyme.

Table 2-4: Components of master mix for RT-PCR experiments

Component	**Volume / Reaction (µl)**
10X RT buffer	2.0
25X dNTP Mix (100 mM)	0.8
MultiScribe ^{TM} Reverse transcriptase	1.0
RNase-free water	4.2
10X RT random primers	2.0
Total per reaction	**10.0**

Table 2-5: Thermo-cycler steps, indicating the temperature and duration, for RT-PCR experiment

Step	**Temperature (°C)**	**Time (minutes)**
1	25	10
2	37	120
3	85	5
4	4	hold

2.13 Quantitative real-time polymerase chain reaction (qrt-PCR)

Using cDNA obtained from the RT-PCR step, qrt-PCR for the following assays was performed; p15 (Applied Biosystems, HS00793225_m1), p16 (Applied Biosystems, HS04189686_m1), p21 (Applied Biosystems, HS00355782_m1) and p27 (Applied Biosystems, HS00153277_m1), with GADPH (Applied Biosystems, HS02758991_g1) as an endogenous control. Briefly, the cDNA samples were diluted with 30 µl of RNase-free water (Ambion, 9932) and 2 µl of this stock was added to a 96-well PCR reaction plate (Applied Biosystems, 4346906) and combined with 18 µl of assay master mix. The assay master mix consisted of 10 µl of Taqman Universal PCR Master Mix (Applied Biosystems, 4364340), 7 µl of RNase-free water (Ambion, 9932) and 1 µl of the specific assay (primer), per reaction. The PCR plate was then sealed using Optical Adhesive film strips (Applied Biosystems, 4360954). The qrt-PCR reaction was performed on the ABI7900HT fast system using Sequence Detection System (SDS) automated controller software (version 2.2) (Applied Biosystems). The procedure for qrt-PCR was 10 minutes at 95 °C followed by 40 cycles of 15 seconds at 95 °C and then 1 minute at 60 °C. Once complete the cycle threshold (Ct) values were exported to Excel and relative RNA expression levels calculated using the DeltaCt method where ΔCt was the Ct value of the sample minus the Ct value of the endogenous control. The ΔΔCt values were calculated as the ΔCt of the test sample minus the ΔCt of the calibration sample (e.g. treated minus control). The relative quantity ratios (RQ) of each sample were calculated using the equation:

$$RQ = 2^{\Delta\Delta Ct} = 2^{\Delta Ct_{control} - \Delta Ct_{test}} = 2^{(Ct,X-Ct,R)_{control} - (Ct,X-Ct,R)_{test}}$$

Where, Ct,X is the cycle threshold of the gene of interest and Ct,R is the cycle threshold of the endogenous reference gene.

2.14 Array Comparative Genome Hybridisation analysis (aCGH)

The following aCGH experimental protocol was used, and supplied, by Dr. Lee Anderson (UCLA) who carried out the aCGH experiments described in this study.

Genomic DNA was extracted from cell lines using the DNeasy Kit (Qiagen) with the following modifications: 70 % ethanol was substituted for Buffer AW2 in the final wash, and DNA was eluted in 50 µl of sterile water (Invitrogen). The concentration and quality of the DNA were measured by NanoDrop and by electrophoresis in 1 % agarose. Labelling and hybridisation of Agilent 105K oligonucleotide CGH arrays was

performed according to the manufacturer's protocol for Human Genome CGH 105A Oligo Microarray Kit, Version 5.0 (Agilent Technologies). Briefly, 1 µg of test cell line and 1 µg of the control cell line were digested with Alu I and Rsa I restriction enzymes (Promega) for 2 hours, then labelled with Cy5-dUTP (test cell line) and Cy3-dUTP (control cell line) using the Agilent Genomic DNA Enzymatic Labelling Kit for 2 hours at 37 ºC followed by 14-18 hours at room temperature. Unincorporated nucleotides were removed using Amicon spin filter units (Millipore), and incorporation and yield were measured with the NanoDrop Spectrophotometer. Labelled test and control cell line DNAs were combined, annealed with COT-1 DNA (Invitrogen) and 10X Blocking Agent (Agilent Technologies) for 30 minutes at 37 ºC after boiling, then hybridised to Agilent 105A arrays for 40 hours at 65 ºC according to the manufacturer's instructions. After hybridisation, arrays were washed according to Procedure B (which includes an ozone blocking wash), and scanned using an Agilent Scanner (G2565BA). Files were extracted using Agilent Feature Extraction software (version 9.5) with the default CGH protocol. Extracted arrays with a DRL Spread < 0.3 were included in the analysis. CGH Analytics software (version 4.0.85) (Agilent Technologies) was used for copy number analysis, employing the ADM2 algorithm (Threshold 5), with Fuzzy Zero and Centralization corrections to minimise background noise. All map positions were based on the March 2006 NCBI36/hg18 genome assembly. A minimum of 3 consecutive probes was required to define a region as amplified or deleted. The data was also filtered by requiring a minimum absolute average $\log^2$ ratio of 0.58. All data was inspected visually using the interactive view. Log^2 ratios larger than 1 were considered amplified and $\log^2$ ratios larger than 2 highly amplified, $\log^2$ ratios smaller than -1 were considered hemizygous deletions and $\log^2$ ratios smaller than -2 were considered homozygous deletions.

2.15 Stable Isotope Labelling with Amino acids in Cell culture (SILAC) – based proteomic profiling of cell lines

Labelling of cells with [U-$^{13}C^6$]-L-Lysine (heavy) amino acid was performed using SILAC RPMI 1640-Flex media (Invitrogen, MS10031) and media were made up using the kit components, as per Table 2-6. L-Arginine, L-Lysine HCL and [U-$^{13}C^6$]-L-Lysine were re-suspended in 1 ml of basal un-supplemented media prior to addition.

Table 2-6: Media components of heavy and light SILAC RPMI 1640-Flex media

Reagent	**Volume (ml)**	
	Heavy SILAC media	Light SILAC media
RPMI 1640-Flex	877.5 ml	877.5 ml
Glucose solution (200 g/L)	10 ml	10 ml
L-Glutamine 200mM (100X)	10 ml	10 ml
Phenol Red solution (10 g/L)	0.5 ml	0.5 ml
Dialysed Fetal Calf Serum (ml/L)	100 ml	100 ml
L-Arginine (100 mg)	1 ml	1 ml
L-Lysine HCL (100 mg)	-	1 ml
[U-$^{13}C^{6}$]-L-Lysine (100 mg)	1 ml	-
Total volume	**1000 ml**	**1000 ml**

2.15.1 SILAC labelling and protein extraction

SKBR3-par cells were cultured in heavy SILAC media and SKBR3-L cells cultured in light SILAC media. Three biologically different passages of SKBR3-par and SKBR3-L cells were grown independently of each other and termed replicates 1, 2 and 3. Each biological replicate for each cell line consisted of twelve T175 cm^2 flasks of cells, which was calculated to give an approx. total cell number per replicate of 2 x 10^8 cells. The cells were grown for approx. 15 days in the SILAC media which allowed for maximum labelled amino acid incorporation and enabled the cells to reach 80% confluence. At this stage each of the 3 replicates for each cell line was split in half; 6 of the flasks were fed with the appropriate SILAC media while the other 6 flasks were treated with SILAC media containing 1 µM lapatinib. After exactly 24 hours, the cells in 6 of the flasks were lysed using RIPA buffer and stored at -80 °C for protein validation. The remaining 60 flasks were lysed using cell lysis buffer supplied as a component of the downstream purification kit, Phospho-Scan (Cell-Signaling Technology, #7900). Note, unless otherwise specified all reagents for downstream purification were supplied in this kit. This lysis buffer consisted of: 1 ml of 10X lysis buffer mix ((20 mM HEPES (pH 8.0), 9M urea, 1 mM sodium orthovanadate, 2.5 mM sodium pyrophosphate, 1 mM b-glcerophosphate)), 5.4 g urea and 0.2 ml of sodium vanadate in 10 ml of mass spectrometry (MS) grade water (Fisher Scientific,

W/0112/15). To lyse the cells, 5 ml of lysis buffer solution was added to one flask and cells scraped into buffer, the same buffer solution containing lysed cells was added to the second flask (of the same biological replicate) the second flask of cells was scraped into the lyse buffer and so on – until the cells from all 5 flasks were contained in the same 5 ml of lysis buffer. All samples were prepared in this manner. The lysates were then cooled on ice for 15 minutes and sonicated at 15W output with 2 bursts of 30 seconds each. The samples were cooled on ice between bursts. The samples were then cleared by centrifugation at 20,000 x g for 15 minutes and the supernatant collected and stored at -80 °C.

2.15.2 Phospho-tyrosine enrichment of SILAC labelled samples

Protein concentration was determined using the BCA assay (Pierce, 23227), and comparison samples were mixed at a 1:1 ratio based on protein concentration to yield 6 samples with a total of 30 mg of protein each. The downstream processing of one such sample is outlined below. Carboxamidomethylation of proteins was performed to inactivate enzymatic activity, by adding 1/10 volume of 45 mM dithiothreitol (DTT) to the supernatant and incubating at 60 °C for 20 minutes. The solution was then cooled to room temperature and then 100 mM idoacetamide, at an equal volume to that of DTT, was added and the solution was incubated in the dark at room temperature for 15 minutes. Lysates were then diluted 4-fold (e.g. a 10 ml lysate was diluted with 1 ml DTT, 1 ml iodoacetamine, 3 ml of 10X lysis buffer mix and 25 ml of MS grade water (Fisher Scientific, W/0112/15) – yielding a 40 ml lysate). A small aliquot (100 µl) of the solution was removed and stored at -80 °C. After dilution, 400 µl of a 1 mg/ml trypsin-TPCK solution was added to each sample and digested overnight at room temperature. The digestion was assessed by resolving 20 µl of digested and undigested sample on 10 % gels and staining with colloidal Comassie blue reagent (Pierce, 24590) – undigested samples yield multiple protein bands whereas digested samples do not. The peptide solution was then acidified to contain 1 % trifluoracetic acid (TFA) (Pierce, 28904), left to stand at room temperature for 10 minutes, centrifuged for 5 minutes at 1,800 x g and decanted into a new tube. The solution was then purified using Sek-Pak C_{18} columns; the column was connected to a 10 cc syringe, pre-wet with 5 mls of 100 % Acetonitrile (ACN) (Sigma, 34967), washed with 7 ml of 0.1 % TFA, loaded with the lysate, washed with 12 ml of 0.1 % TFA and peptides were eluted using 6 ml (3 x 2 ml) of a 0.1% TFA, 40% ACN solution. The eluted peptides were stored at -80 °C overnight and then lyophilised for 2 days, to remove all traces of TFA. The lyophilised peptides were re-

suspended in 1.4 ml of IAP buffer ((50 mM MOPS (pH 7.2), 10 mM sodium phosphate, 50 mM NaCl)), and left to stand for 5 minutes at room temperature followed by 30 minutes of gentle shaking. The re-suspended peptides were then sonicated at 15W output with 2 bursts of 10 seconds each. The pH of the re-suspended peptides was checked using pH indicator strips (Santa Cruz, sc-3667), and if found to be acidic, the pH was adjusted to pH 7.0 using a concentrated Tris (Sigma, 93352) solution, which had not been adjusted for pH. The neutral re-suspended peptide solution was cleared by centrifugation for 5 minutes at 1,800 x g at room temperature and transferred to a micro-centrifuge tube containing 80 µl of phopsho-tyrosine mouse monoclonal antibody (P-Tyr-100) beads. The mixture was incubated for 2 hours, on a rotator at 4 °C and then centrifuged at 1,500 x g for 1 minute at 4 °C and the supernatant was discarded. All subsequent steps were performed on ice. A wash step was performed; IAP buffer (1 ml) was added to the beads, mixed by inversion (5 times), centrifuged at 1,500 x g for 1 minute at 4 °C and the supernatant removed and discarded. The IAP wash step was repeated a further 2 times followed by 2 washes (as above) with MS-grade water. The peptides were eluted from the beads using a two-step process; using first 55 µL of 0.15 % TFA was added to the beads, mixed by gentle tapping, left to stand for 10 minutes at room temperature, centrifuged at 1,500 x g for 1 minute and the supernatant removed to a new micro-centrifuge tube. The above step was repeated with 45 µl of 0.15 % TFA and the supernatant combined with the first eluate and mixed. The eluate was divided into 7 aliquots of 14 µl each. A ZipTip (included with kit) was pre-wet with 10 µl of 40 % ACN, 0.1% TFA twice, equilibrated by washing the tip with 4 x 10 µl washes of 0.1 TFA and pipettes were bound to the tip by drawing each of the 7 aliquots fully into the tip and pipetting each aliquot 10 times. The tip was washed 4 times with 10 µl each of 0.1 % TFA and peptides eluted with 20 µl of 40% ACN, 0.1 % TFA by pipetting 4 times up and down and transferring to a new micro-centrifuge tube. The eluted samples were then dried to completion under vacuum and transferred to the Mass Spectrometry Facility (UCLA Pasarow Mass Spectrometry Laboratory), where they were stored at -80 °C prior to analysis.

2.15.3 Analysis of total protein from SILAC-labelled samples

A comparison of the expression of total protein between cell lines was performed by mixing 10 µg of sample from each cell line and resolving the mixed samples on a 10 % gel (Lonza, 59501). The gel was stained with colloidal Comassie blue reagent (Pierce, 24590) for 1 hour, and destained with a 40 % methanol (Sigma, 34860), 5 % acetic acid

(Sigma, 45754) solution overnight. Each lane on the gel was cut into 32 gel bands with a fresh disposable scalpel blade, and each band was further cut into 6 pieces. The gel pieces were transferred to a MS format 96-well plate, washed with MS-grade water (Fisher Scientific, W/0112/15), suspended in 70 µl of 200 mM ammonium bicarbonate (NH_4HCO_3) (Sigma, 09830) and incubated for 10 minutes at 37 °C in a thermoshaker (Thermo-Scientific) at 400 x g. This was followed by a series of wash steps each carried out for 10 minutes at 400 x g at 37 °C; 100 µl of 200 mM NH_4HCO_3, ACN (2:3); followed by 100 µl of 50 mM NH_4HCO_3 and then 100 µl of 100 % ACN. The gel pieces were incubated in 50 µl of 10 mM DTT (Sigma, 43817) in 100 mM NH_4HCO_3 for 60 minutes at 400 x g at 56 °C, liquid removed and replaced with 50 µl of 50 mM iodoacetamide (Sigma, L1149) in 100 mM NH_4HCO_3 at 400 x g for 30 minutes at room temperature in the dark. This was followed by; a 15 minute incubation with 150 µl of 100mM NH_4HCO_3 at 400 x g and 37 °C; a 15 minute incubation with 150 µl of 100mM NH_4HCO_3/ACN (1:1) at 400 x g and 37 °C and then a 10 minute incubation with 100 µl of 100 % ACN at 400 x g and 37 °C. Following removal of ACN the samples were incubated with 30 µl of gold grade trypsin (12.5 ng/µl) (Promega, V5280) at 37°C overnight. The liquid was transferred to a new plate and the gel pieces were incubated with 100 µL of extraction buffer (5 % formic acid (Sigma, 06440))/ACN 1:2) for 10 minutes at 400 x g and 37 °C. The liquid from each was added to the new plate and this extraction step was repeated and extracts were pooled. The plate was transferred to a vacuum centrifuge and dried down. The dried down samples were then transferred to the Mass Spectrometry Department (DCU) where they were stored at -20 °C prior to analysis.

2.15.4 Mass Spectrometry

The phospho-enriched samples were analysed by Dr. Julian Whitelegge (UCLA) and the total protein samples by Mr. Michael Henry (DCU) using the below method. Digested samples were re-suspended in 0.1% TFA, 2% ACN and analysed by nanoLC-MS/MS using an Ultimate 3000 system (Dionex) coupled to a nanospray LTQ Orbitrap mass spectrometer (Thermo Fisher Scientific), using a linear acetonitrile gradient from 0% to 65% ACN over 45 minutes. Buffers used for nano LC separation contained 0.1% Formic acid as the ion pairing reagent. The flow rate was 300 nL/minute. The LTQ Orbitrap was operated in data-dependent acquisition mode with Xcalibur software. Survey scan MS data were acquired in the Orbitrap on the 300–2000 *m*/*z* mass range with the resolution set to a value of 60,000 at 400 *m*/*z* . The five most intense ions per

survey scan were selected for MS/MS fragmentation and the resulting fragments were analysed in the linear trap. Collision energy was set to 35%. Dynamic exclusion was employed within 60 seconds. Full scan mass spectra were recorded in profile mode and tandem mass spectra in centroid mode.

2.15.5 Peptide/Protein Identification

The resulting RAW files of MS data from both the phospho- and total protein experiments were analysed using TurboSEQUEST software (Bioworks Browser (version 3.3.1), Thermo Fisher Scientific)) using the UniProt_SwissProt_Human database (downloaded in March 2011). The following filters were applied: for charge state 1, $X_{Corr} > 1.5$; for charge state 2, $X_{Corr} > 2.0$; for charge state 3, $X_{Corr} > 2.5$; for charge state 4, $X_{Corr} > 3.0$. Modification of peptides: carbamidomethylation of cysteines and SILAC modification of +6.0204 Daltons on Lysine, were set. Peptide probability was set as $p \leq 0.05$ giving 95 % confidence of peptide identification. Protein identifications were accepted if they had at least 2 unique identified peptides. SILAC ratios of heavy to light (H/L) amino acid were calculated using the in-built SILAC search function. For each protein identified with a SILAC ratio a manual examination of MS and MS/MS data was performed to ensure accurate identification of both heavy and light lysine containing peptides. Lists of identified phospho- and total proteins and their corresponding SILAC ratios were exported to Excel.

2.15.6 Statistical cut-off for identified proteins

For an identified protein to be considered significant and subject to further analysis, it had to meet the following criteria: i) only proteins which were identified in all three biological comparisons were considered for inclusion; ii) proteins had to have a corresponding SILAC ratio (and have manually verified heavy and light peptide identifications); iii) deviation of the ratio across the 3 biological replicates ≤ 20 %; iv) SILAC ratios indicating a fold change ≥ 1.2-fold. A shortlist of proteins which met these statistical requirements were then generated and subjected to bioinformatical analysis.

2.15.6.1 Panther

Shortlisted proteins were analysed using PANTHER Classification System [available from www.pantherdb.org]. The PANTHER (**P**rotein **AN**alysis **TH**rough **E**volutionary **R**elationships) Classification System is a unique resource that classifies genes by their functions, using published scientific experimental evidence and evolutionary

relationships to predict function even in the absence of direct experimental evidence [279]. The shortlisted proteins were analysed for; Molecular Pathways, Molecular function, Biological Processes, Protein Class and Cellular Component.

2.17.6.2 Pathway studio

Protein function, regulation and interaction were investigated by analysing shortlisted proteins in Pathway Studio 8.0 (Ariadne Genomics). This software was used to build protein networks based on *in silico* literature mining. When features of interest were identified the literature for that node was assessed.

2.16 Statistics

Drug IC_{50} values were calculated using CalcuSyn (version 1.1.0.0) software. Analysis of the difference of comparisons in protein levels and response to treatment was performed using the Student t-test (two-tailed with unequal variance). Bi-variant scattergraphs and Spearman rank correlations were performed using StatView (version 5.0.1) (SAS institute Inc.). The cut-off for statistical significance was set as $p \leq 0.05$.

Chapter 3

Development of HCC1954-L, a HER2 positive cell line model of acquired lapatinib resistance

3.1 Introduction

Lapatinib, the dual EGFR and HER2 tyrosine kinase inhibitor has shown promising results in clinical trials. However, resistance to lapatinib is an emerging clinical problem. Patients can exhibit either *de novo* (innate) or acquired resistance to lapatinib, the mechanisms of which are currently poorly understood and the number of cell line models of resistance available is limited. To investigate mechanisms of acquired resistance to lapatinib, a cell line model of acquired lapatinib resistance was developed using the HER2 amplified breast cancer cell line HCC1954, which is sensitive to lapatinib. The development and characterisation of the resistant cell line is detailed in this chapter.

3.2 Development of a cell line model of acquired lapatinib resistance

3.2.1 Lapatinib-conditioning of HCC1954 cells

HCC1954 cells overexpress HER2 and thus represent a cell line model of HER2 positive breast cancer. HCC1954 cells are resistant to trastuzumab but are moderately sensitive to lapatinib with an IC_{50} of 0.430 ± 0.027 µM [Figure 3-1]. A lapatinib dose response assay was performed in order to select the concentration of lapatinib which would result in 70 % growth inhibition over a 4 day treatment. Treatment of HCC1954 cells with 1 µM lapatinib inhibited the growth of the cells by 71.5 ± 1.2 % compared to untreated controls ($p = 0.004$) [Figure 3-2]. Therefore, lapatinib conditioning of HCC1954 cells was initiated with twice weekly treatments of 1 µM lapatinib.

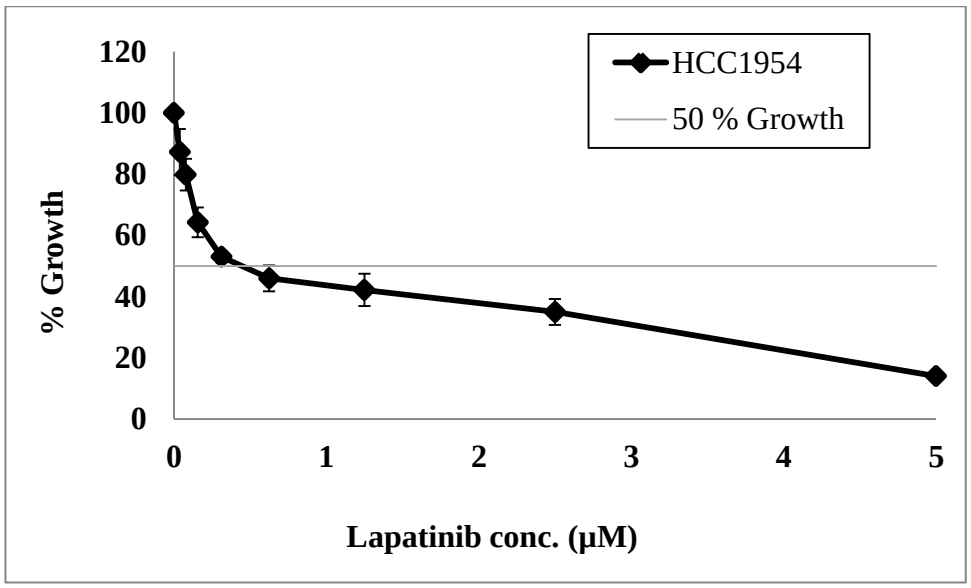

Figure 3-1: Proliferation of HCC1954 cells following a 5-day treatment with lapatinib (0 – 5 µM). Growth is expressed relative to untreated control cells. Error bars represent the standard deviation of triplicate experiments.

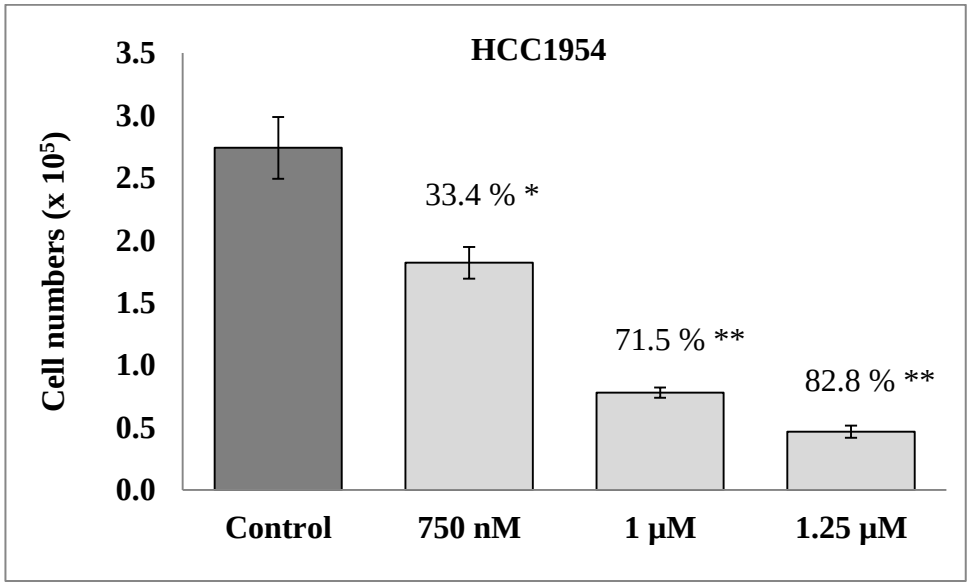

Figure 3-2: HCC1954 cells treated with varying concentrations of lapatinib over a four day period. Cell counts were performed using ViaCount reagent and Guava Software and expressed relative to control untreated cells. Error bars denote the standard deviation of triplicate cell counts from triplicate experiments. Percentages shown on graph represent the percentage of growth inhibition compared to control cells across three independent experiments. Student's t-test was performed to determine significant differences between treatments and control: * denotes $p < 0.05$; ** denotes $p < 0.01$.

3.2.2 Lapatinib-conditioning: 3 months

HCC1954 cells were seeded into two flasks, one flask was left untreated but was passaged alongside the treatment flask, and these cells were named HCC1954-par cells. The other flask of cells was treated with 1 μM twice weekly and throughout the conditioning process and characterisation these cells were referred to as HCC1954-L. During the conditioning process, the morphology of both cell lines and the sensitivity of the cell lines to lapatinib was monitored. The morphology of HCC1954-L cells did not alter during the first 3 months of lapatinib conditioning [Figure 3-3]. After 3 months of conditioning, the sensitivity of the cells to lapatinib was tested. The lapatinib IC_{50} for HCC1954-par cells was 0.42 ± 0.01 μM, which is similar to the original HCC1954 cells. The lapatinib IC_{50} for HCC1954-L cells was 0.75 ± 0.07 μM [Figure 3-4]. This represents 1.8-fold change decrease in sensitivity to lapatinib. At this stage of the conditioning process the lapatinib IC_{50} of HCC1954-L cells had not yet reached the critical threshold for resistance (1 μM), however they had begun to actively proliferate in the presence of lapatinib. The concentration of lapatinib was therefore increased from 1 μM to 1.25 μM and conditioning continued with this concentration for a further 3 months.

HCC1954-par (3 months) **HCC1954-L (3 months)**

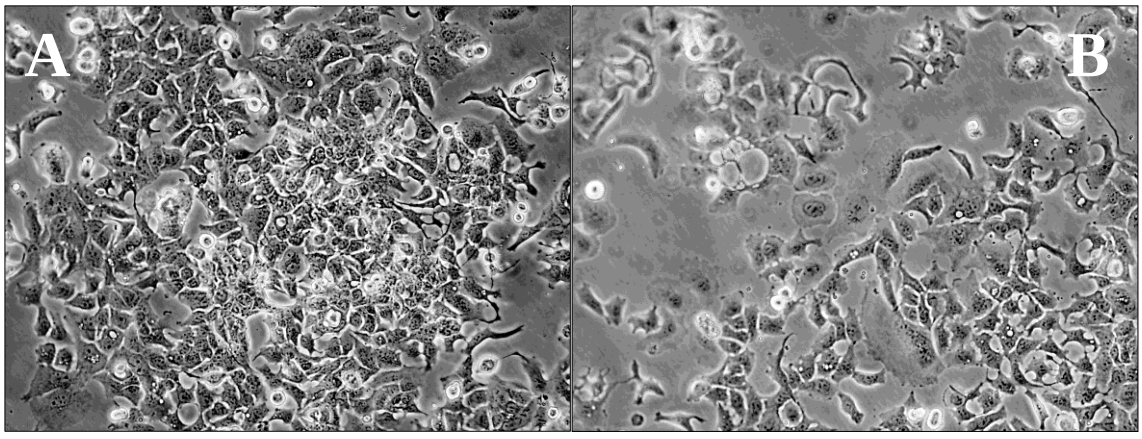

Figure 3-3: Images of (A) HCC1954-par and (B) HCC1954-L cells after 3 months of lapatinib conditioning at 100X magnification.

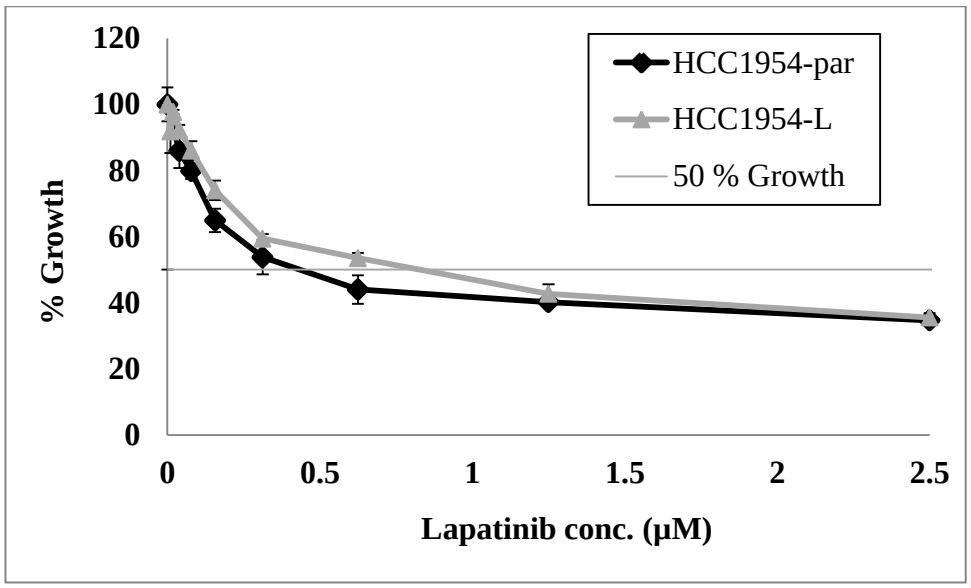

Figure 3-4: After 3 months conditioning with 1 µM lapatinib the proliferation of HCC1954-par and HCC1954-L cells following a 5-day treatment with lapatinib (0 – 2.5 µM) was measured. Growth is expressed relative to untreated control cells. Error bars represent the standard deviation of triplicate experiments.

3.3 Characterisation of HCC1954-L cells

3.3.1 HCC1954-L cells are resistant to lapatinib

After 6 months of lapatinib conditioning, the sensitivity of the cells was again tested. The lapatinib IC_{50} for HCC1954-par was 0.42 ± 0.02 µM whereas the lapatinib IC_{50} for HCC1954-L cells was 2.67 ± 0.08 µM ($p = 0.01$) [Figure 3-5]. This represents 6.1-fold decrease in sensitivity to lapatinib. HCC1954-L cells were deemed to be resistant to lapatinib as the lapatinib IC_{50} was above the 1 µM threshold for sensitivity [194]. The resistant cells also exhibited distinct morphological alterations compared to the parental cell line. These differences were indicated by more distinct colony boundaries and a flatter cell shape [Figure 3-6].

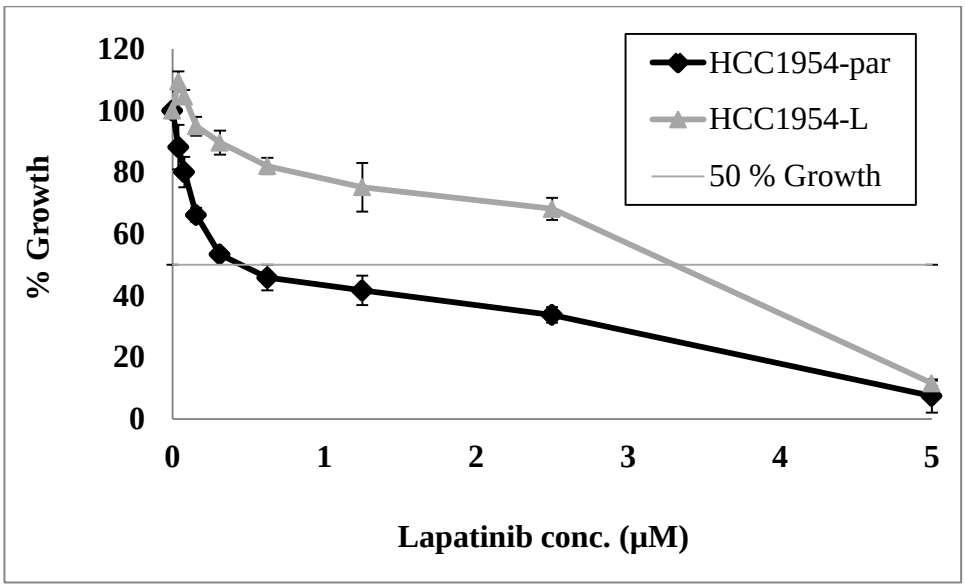

Figure 3-5: After 6 months conditioning with lapatinib the proliferation of HCC1954-par and HCC1954-L cells following a 5 day treatment with lapatinib (0 – 5 µM) was measured. Growth is expressed relative to untreated control cells. Error bars represent the standard deviation of triplicate experiments.

HCC1954-par (6 months) **HCC1954-L (6 months)**

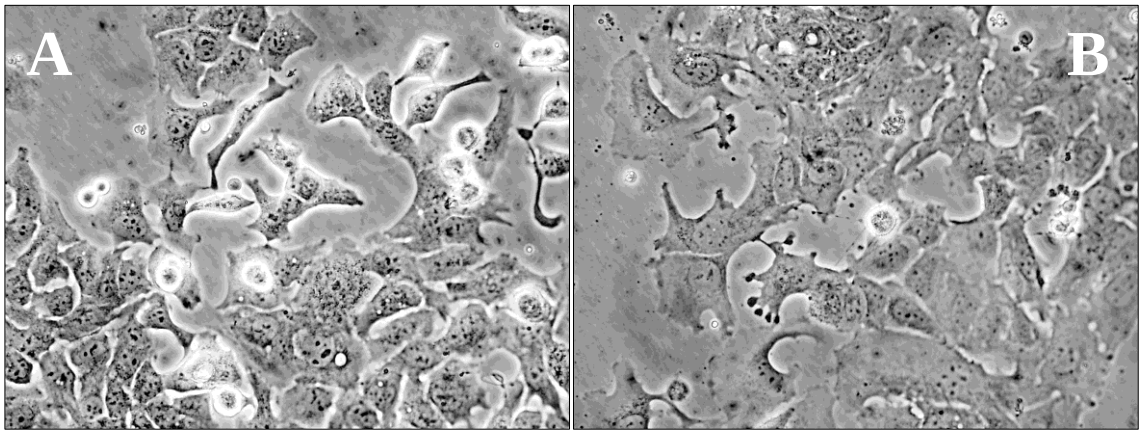

Figure 3-6: Images of (A) HCC1954-par and (B) HCC1954-L cells after 6 months of lapatinib conditioning at 200X magnification.

3.3.2 Assessing the stability of acquired lapatinib resistance

To establish a reliable cell line model of lapatinib resistance, the phenotype must be stable when the cell line is frozen and re-thawed. To asses this, frozen stocks of the HCC1954 par and HCC1954-L cells were prepared in foetal calf serum containing 5 % DMSO. After a minimum of 48 hours in liquid nitrogen, the frozen stocks were thawed

and the viability of the stocks assessed by microscopy. The cells were then passaged a minimum of 3 times before lapatinib sensitivity assays were repeated [Figure 3-7]. The lapatinib IC_{50} was 0.44 ± 0.02 µM in the parental cells while the lapatinib IC_{50} in HCC1954-L cells was 2.73 ± 0.05 µM. This indicates that the HCC1954-L cells retain their resistant phenotype following a freeze/thaw cycle.

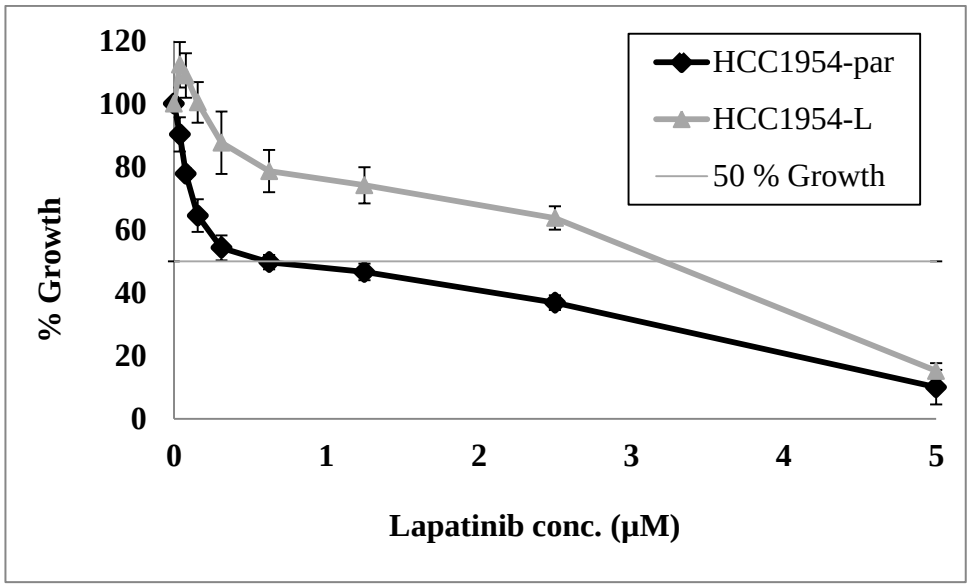

Figure 3-7: Sensitivity of HCC1954-par and HCC1954-L cells to lapatinib following a freeze-thaw cycle. Proliferation of cells was assessed following 5 days treatment with lapatinib (0 – 5 µM). Growth is expressed relative to untreated control cells. Error bars represent the standard deviation of triplicate experiments.

In order to assess the long-term stability of the resistant phenotype, drug withdrawal assays were performed. Lapatinib was removed from the HCC1954-L cells and the sensitivity of the cells to lapatinib was tested at 4 week intervals for a period of 12 weeks, the results at each interval are illustrated in Figure 3-8. Following 12 weeks growth in the absence of lapatinib the lapatinib IC_{50} of the parental cells was 0.43 ± 0.05 µM while the lapatinib IC_{50} of HCC1954-L cells was 2.63 ± 0.16 µM. There was no significant difference between the initial lapatinib IC_{50} for either the parental or resistant cell line and the lapatinib IC_{50} for the cell lines after 12 weeks growth in the absence of lapatinib [Table 3-1].

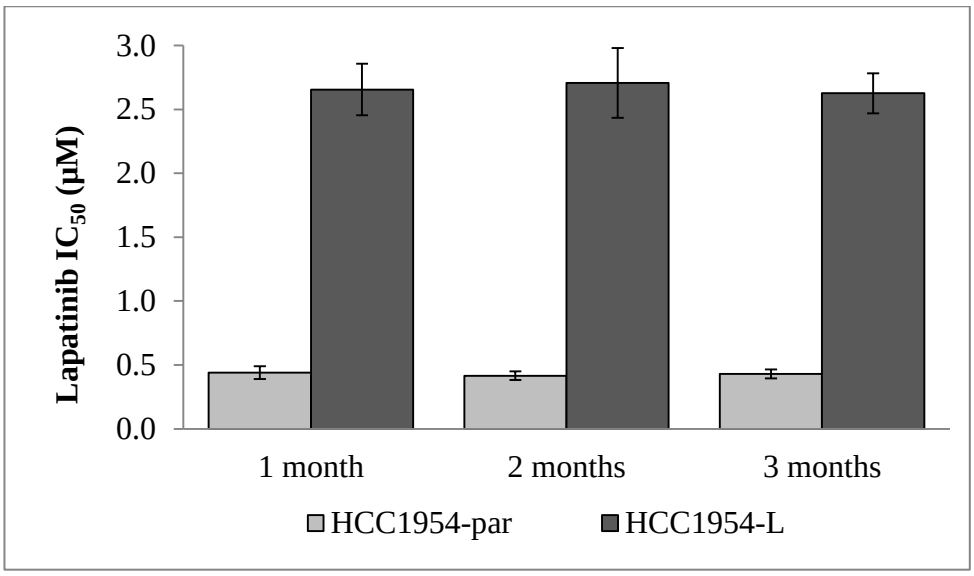

Figure 3-8: Lapatinib IC_{50} values for HCC1954-par and HCC1954-L cells following 1, 2 and 3 months growth in the absence of lapatinib. IC_{50}s were calculated following a 5 day lapatinib treatment (0 – 5 µM). Error bars represent the standard deviation of triplicate experiments.

Table 3-1: IC_{50} values (± standard deviation of triplicate experiments) for lapatinib in HCC1954 par and HCC1954-L cells after 1 month, 2 months and 3 months growth in the absence of lapatinib.

IC50 (µM)	**HCC1954-par**	**HCC1954-L**
Initial	0.424 ± 0.018	2.674 ± 0.083
1 month	0.440 ± 0.051	2.655 ± 0.202
2 months	0.416 ± 0.035	2.706 ± 0.273
3 months	0.430 ± 0.045	2.626 ± 0.157

3.3.3 Effect of HER2 inhibition on doubling time of HCC1954-par and HCC1954-L cells

The effect of lapatinib and trastuzumab on the growth rate of HCC1954-par and HCC1954-L cells was investigated used cell counting. Cells were counted at days 0, 3, 5, and 7 using ViaCount Reagent and the Guava system. Treatment of both cell lines with lapatinib or trastuzumab resulted in lower cell counts compared to untreated control cells [Figure 3-9].

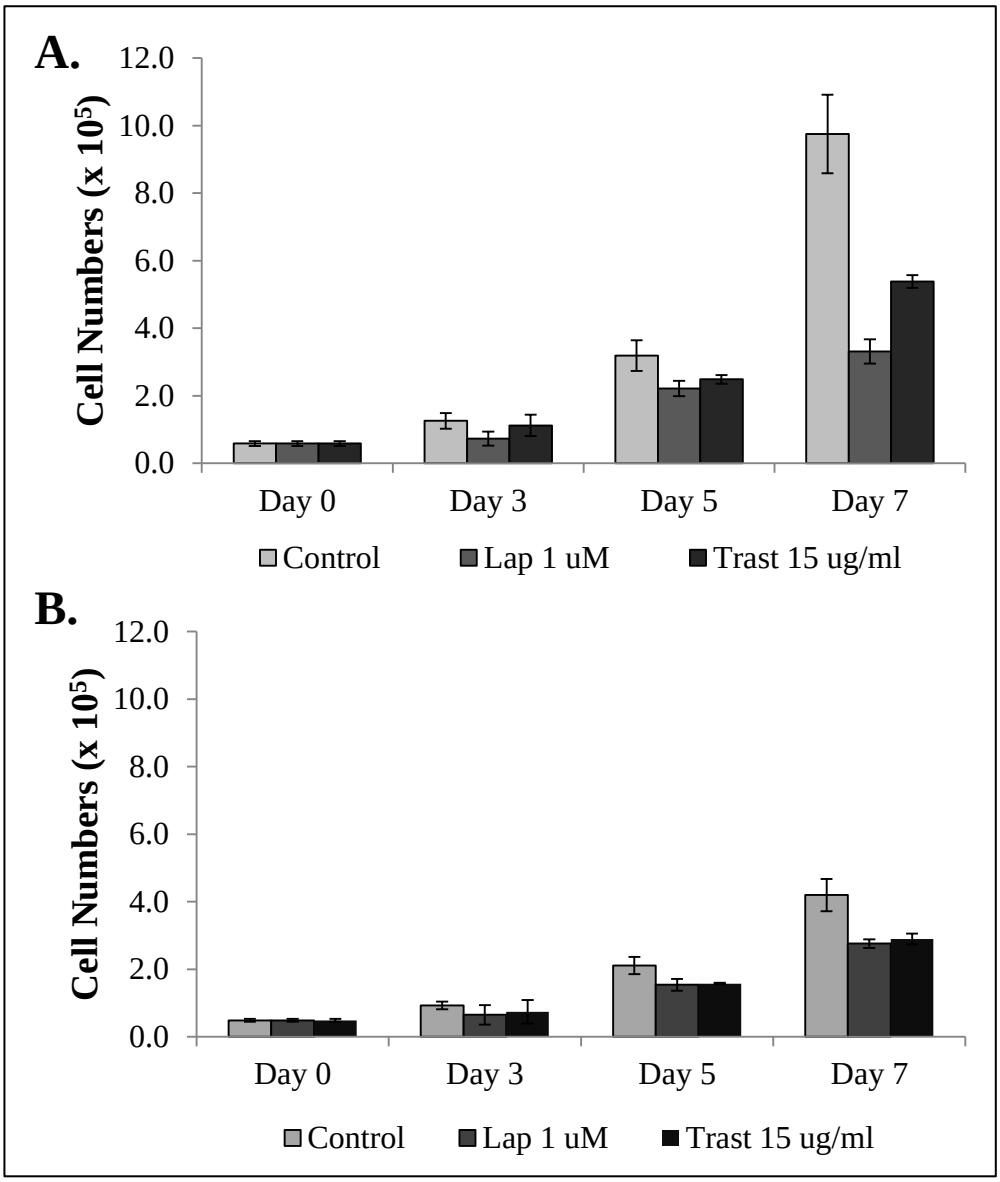

Figure 3-9: Proliferation of (A) HCC1954-par and (B) HCC1954-L cells treated with 1 µM lapatinib or 15 µg/ml trastuzumab for 7 days. Cells were plated in 24-well plates and proliferation was measured at days 0, 3, 5 and 7 by cell counting. Error bars represent standard deviation of triplicate experiments.

These cell counts were used to calculate the doubling times of each cell line, under each treatment condition using the formula detailed in [section 2.7]. HCC1954-par cells have a doubling time of 29.8 ± 1.0 hours. Compared to this the doubling time of HCC1954-L cells, 48.5 ± 2.6 hours, was significantly increased ($p = 0.0026$). Lapatinib treatment increased the doubling time of both cells lines, in HCC1954-par cells the doubling time significantly increased from 29.8 ± 1.0 hours in the control to 83.0 ± 3.6 hours ($p = 0.0007$) in the lapatinib treated cells. In HCC1954-L cells, lapatinib did not significantly

increase the doubling time (48.5 ± 2.6 hours in the control to 57.2 ± 7.1 hours in the lapatinib treated cells, p = 0.1544). Trastuzumab treatment also increased the doubling time of both cells lines, in HCC1954-par cells the doubling time significantly increased from 29.8 ± 1.0 hours in the control to 43.2 ± 3.9 hours (p = 0.0213) in the trastuzumab treated cells. In HCC1954-L cells, the doubling time increased from 48.5 ± 2.6 hours in the control to 55.1 ± 5.1 hours in the lapatinib treated cells, however this increase was not statistically significant (p = 0.1381) [Table 3-2].

Table 3-2: Doubling times (hours) of conditioned HCC1954 cells with and without lapatinib (Lap) (1 μM) or trastuzumab (Trast) (15 μg/ml) treatment (± standard deviation of triplicate experiments). The fold change in cell growth in response to treatment is expressed relative to the control untreated cells for each cell line.

Cell line		**Control**	**Lap**	**Trast**
HCC1954-par	Doubling time (hrs)	29.8 ± 1.0	83.0 ± 3.6	43.2 ± 3.9
	Fold change relative to control		*2.8*	*1.5*
HCC1954-L	Doubling time (hrs)	48.5 ± 2.6	57.2 ± 7.1	55.1 ± 5.1
	Fold change relative to control		*1.2*	*1.1*

3.4 Array Comparative Genomic Hybridisation (CGH) analysis of HCC1954-L cells

Array CGH analysis is used to examine alterations, either amplifications or deletions of genes at the chromosome level. HCC1954-L cells were compared to the parental cell line using array CGH technology. This work was carried out in collaboration with Dr. Lee Anderson, UCLA. Briefly, DNA is fragmented and fluorescently labelled and hybridised to Agilent arrays, fluorescent signals are detected by a microarray scanner and results are viewed as a common karyogram revealing copy number changes. HCC1954-L cells displayed 14 unique aberrations compared to HCC1954-par cells; these aberrations are listed in Table 3-3, and the gene descriptions are listed in Table 3-4.

Table 3-3: List of aberrations, chromosome and cytoband position, number of annealed probes, degree of amplification of deletion, p-value and corresponding gene names for HCC1954-L cells compared with HCC1954-par

Aberr No.	Chr	Cytoband	Start	Stop	#Probes	Amp.	Del.	pval	Gene Names
1	chr1	p12	1.18E+08	1.18E+08	25	0.523	0.000	4.30E-70	MAN1A2, FAM46C, GDAP2, WDR3, SPAG17
2	chr4	q22.3	9.80E+07	9.82E+07	3	0.996	0.000	1.02E-10	
3	chr4	q26	1.15E+08	1.16E+08	28	0.738	0.000	9.25E-25	ARSJ, UGT8, NDST4
4	chr4	q27	1.21E+08	1.23E+08	51	0.609	0.000	2.37E-14	MAD2L1, PRDM5, C4orf31, TNIP3, GPR103, ANXA5, TMEM155
5	chr11	p14.3	2.37E+07	2.58E+07	42	0.525	0.000	3.98E-42	LUZP2
6	chr12	p12.2-p12.1	2.01E+07	2.25E+07	94	0.777	0.000	0.00E+00	PDE3A, SLCO1C1, SLCO1B3, LST-3TM12, SLCO1B1, SLCO1A2, IAPP, PYROXD1, RECQL, GOLT1B, C12orf39, GYS2, LDHB, KCNJ8, ABCC9, CMAS, ST8SIA1, KIAA0528
7	chr12	q23.1	9.88E+07	9.91E+07	10	0.747	0.000	6.01E-24	ANKS1B, UHRF1BP1L
8	chr13	q12.11	1.84E+07	1.85E+07	3	0.504	0.000	1.93E-09	
9	chr17	q12	3.43E+07	3.45E+07	11	0.000	-0.52	7.04E-09	LASP1, FBXO47, PLXDC1
10	chr17	q12	3.49E+07	3.54E+07	33	0.720	0.000	1.47E-248	CRKRS, NEUROD2, PPP1R1B, STARD3, TCAP, PNMT, PERLD1, ERBB2, C17orf37, GRB7, IKZF3, ZPBP2, GSDML, ORMDL3, GSDM1

11	chr18	q12.3-q21.1	4.17E+07	4.25E+07	39	0.000	-0.52	3.01E-11	KIAA1632, PSTPIP2, ATP5A1, CCDC5, C18orf25, RNF165
12	chr20	q11.22	3.17E+07	3.18E+07	5	0.580	0.000	9.51E-19	PXMP4, ZNF341
13	chr20	q11.22	3.30E+07	3.32E+07	11	0.547	0.000	8.21E-35	MYH7B, TRPC4AP, EDEM2, PROCR
14	chr20	q11.22	3.34E+07	3.35E+07	6	0.518	0.000	5.36E-18	UQCC, GDF5, CEP250
15	chr22	q13.32-q13.33	4.77E+07	4.83E+07	20	0.605	0.000	1.04E-08	

Table 3-4: List of names and descriptions of genes altered in HCC1954-L compared to HCC1954-par.

Gene Name	Description of Gene
MAN1A2	mannosidase, alpha, class 1A, member 2
FAM46C	family with sequence similarity 46, member C
GDAP2	ganglioside induced differentiation associated protein 2
WDR3	WD repeat domain 3
SPAG17	sperm associated antigen 17
ARSJ	arylsulfatase family, member J
UGT8	UDP glycosyltransferase 8
DST4	STE20 family protein kinase
MAD2L1	MAD2 mitotic arrest deficient-like 1 (yeast)
PRDM5	PR domain containing 5
C4orf31	neuron-derived neurotrophic factor
TNIP3	TNFAIP3 interacting protein 3
GPR103	pyroglutamylated RFamide peptide receptor
ANXA5	annexin A5
TMEM155	transmembrane protein 155
LUZP2	leucine zipper protein 2
PDE3A	phosphodiesterase 3A, cGMP-inhibited
SLCO1C1	solute carrier organic anion transporter family, member 1C1
SLCO1B3	solute carrier organic anion transporter family, member 1B3
LST-3TM12	organic anion transporter LST-3b
SLCO1B1	solute carrier organic anion transporter family, member 1B1
SLCO1A2	solute carrier organic anion transporter family, member 1A2
IAPP	islet amyloid polypeptide
PYROXD1	pyridine nucleotide-disulphide oxidoreductase domain 1
RECQL	RecQ protein-like (DNA helicase Q1-like)
GOLT1B	golgi transport 1B
C12orf39	chromosome 12 open reading frame 39

Table 3-5: Continued

Gene Name	Description of Gene
GYS2	glycogen synthase 2 (liver)
LDHB	lactate dehydrogenase B
KCNJ8	potassium inwardly-rectifying channel, subfamily J, member 8
ABCC9	ATP-binding cassette, sub-family C (CFTR/MRP), member 9
CMAS	cytidine monophosphate N-acetylneuraminic acid synthetase
ST8SIA1	ST8 alpha-N-acetyl-neuraminide alpha-2,8-sialyltransferase 1
KIAA0528	novel C2 domain containing protein
ANKS1B	ankyrin repeat and sterile alpha motif domain containing 1B
UHRF1BP1L	UHRF1 binding protein 1-like
LASP1	LIM and SH3 protein 1
FBXO47	F-box protein 47
PLXDC1	plexin domain containing 1
CRKRS	cyclin-dependent kinase 12
NEUROD2	neurogenic differentiation 2
PPP1R1B	protein phosphatase 1, regulatory (inhibitor) subunit 1B
STARD3	StAR-related lipid transfer (START) domain containing 3
TCAP	titin-cap (telethonin)
PNMT	phenylethanolamine N-methyltransferase
PERLD1	post-GPI attachment to proteins 3
ERBB2	Epidermal growth factor receptor 2
C17orf37	migration and invasion enhancer 1
GRB7	growth factor receptor-bound protein 7
IKZF3	IKAROS family zinc finger 3
ZPBP2	zona pellucida binding protein 2
GSDML	gasdermin B
ORMDL3	ORM1-like 3 (S. cerevisiae)
GSDM1	gasdermin A

Table 3-6: Continued

Gene Name	Description of Gene
KIAA1632	ectopic P-granules autophagy protein 5 homolog (C. elegans)
PSTPIP2	proline-serine-threonine phosphatase interacting protein 2
ATP5A1	ATP synthase, H+ transporting, mitochondrial F1 complex, alpha subunit 1, cardiac muscle
CCDC5	HAUS augmin-like complex, subunit 1
C18orf25	chromosome 18 open reading frame 25
RNF165	ring finger protein 165
PXMP4	peroxisomal membrane protein 4, 24kDa
ZNF341	zinc finger protein 341
MYH7B	myosin, heavy chain 7B, cardiac muscle, beta
TRPC4AP	transient receptor potential cation channel, subfamily C, member 4 associated protein
EDEM2	ER degradation enhancer, mannosidase alpha-like 2
PROCR	protein C receptor, endothelial
UQCC	ubiquinol-cytochrome c reductase complex chaperone
GDF5	growth differentiation factor 5
CEP250	centrosomal protein 250kDa

3.4.1 Increased amplification of chr17q12

HCC1954-L cells have increased amplification of chr17q12 compared to HCC1954-L cells [Figure 3-10]. Amplification of this region is associated with the amplification of several genes including HER2, STARD3, Grb7 and gasdermin. The expression levels of HER2 and STARD3 was used to determine whether amplification of this region corresponded with increased protein expression.

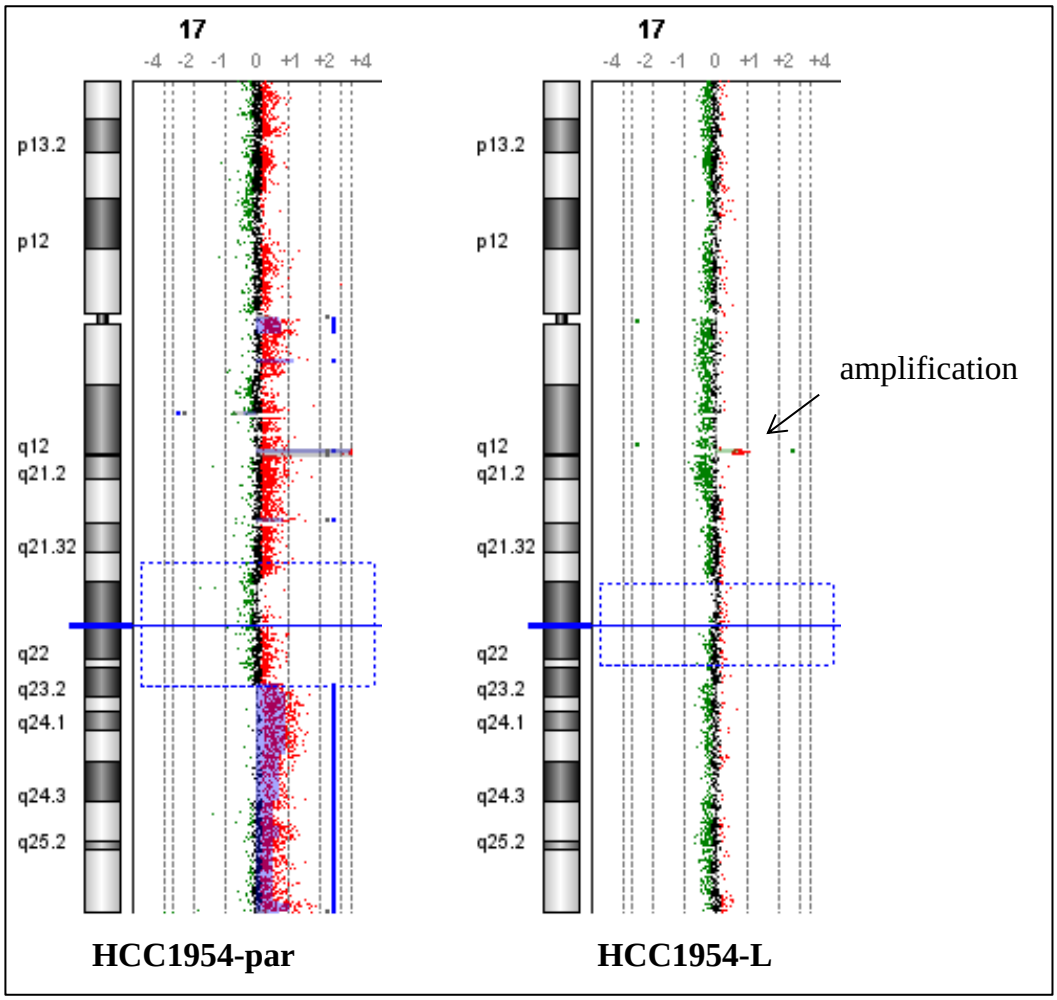

Figure 3-10: Representation of increased amplification of chr17q12 in HCC1954-L cells compared to HCC1954-par cells.

3.4.2 Validation of increased HER2 amplification

The increased amplification of HER2 in HCC1954-L cells compared to HCC1954-par cells was confirmed using Western blotting. HCC1954-L cells exhibit a small but significant 1.2-fold (p=0.02) increase in HER2 expression compared to parental cells [Figure 3-11]. The increased amplification of HER2 was also examined using Fluorescent *In-situ* Hybridisation (FISH) analysis, carried out in collaboration with Alison Prendergast, St. Vincent's University Hospital. Briefly paraffin blocks of HCC1954-par and HCC1954-L cells were sectioned and analysed for HER2 using the PathVysion HER-2 DNA Probe Kit. The HER2 FISH ratio (HER2/CEP17) for HCC1954-par cells was 3.80 while HCC1954-L cells have a HER2 FISH ratio of 4.04.

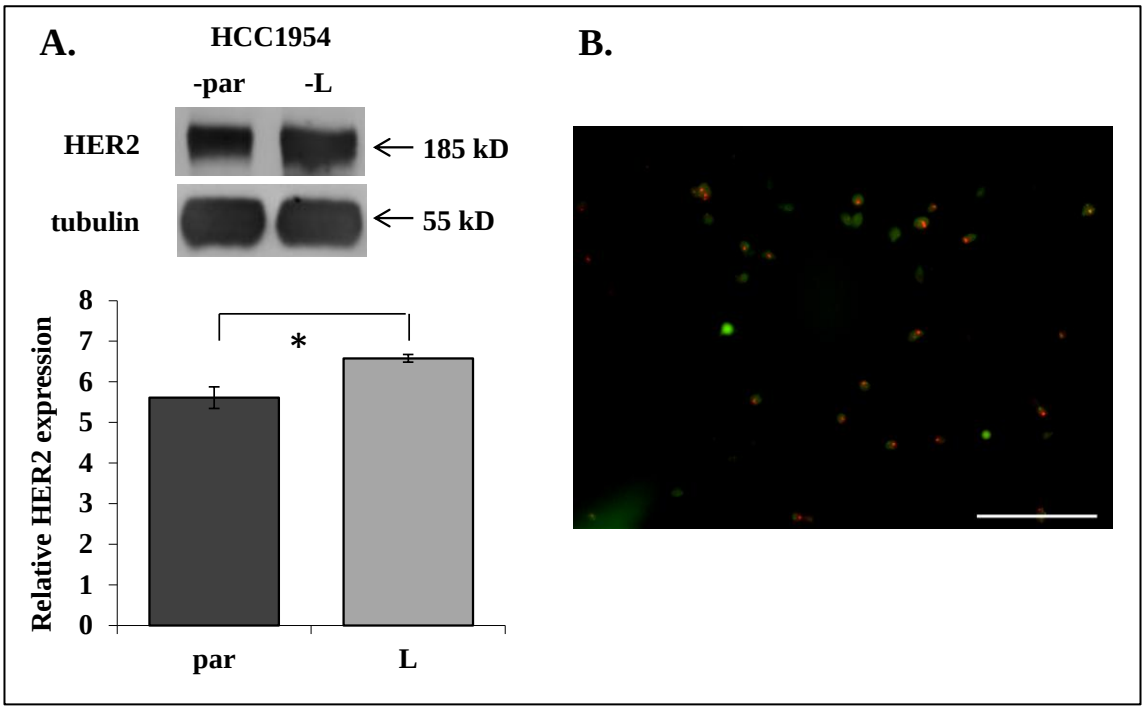

Figure 3-11: (A) Immunoblotting for HER2 in HCC1954-par and HCC1954-L cells. α-tubulin was used as a loading control. Images are representative of triplicate experiments. Densitometry analysis of triplicate immunoblots was performed using ImageQuant software. * denotes $p \leq 0.05$ (B) Image of HCC1954-par cells stained for HER2 using the PathVysion HER-2 DNA Probe Kit.

3.4.3 Validation of increased STARD3 amplification

STARD3 (StAR-related lipid transfer (START) domain containing 3) was also associated with a dramatic increase in STARD3 protein expression. STARD3, often referred to as MLN64 (metastatic lymph node 64), was initially identified from a breast-cancer-derived metastatic lymph node cDNA library as a gene that was overexpressed and amplified in breast cancer [280]. Immunoblotting for STARD3 was performed to examine whether the increased amplification of STARD3 in HCC1954-L cells compared to HCC1954-par cells corresponded with increased expression at the protein level. STARD3 expression was 29.7-fold higher in HCC1954-L cells compared to HCC1954-par cells, in which expression of STARD3 was barely detectable [Figure 3-12].

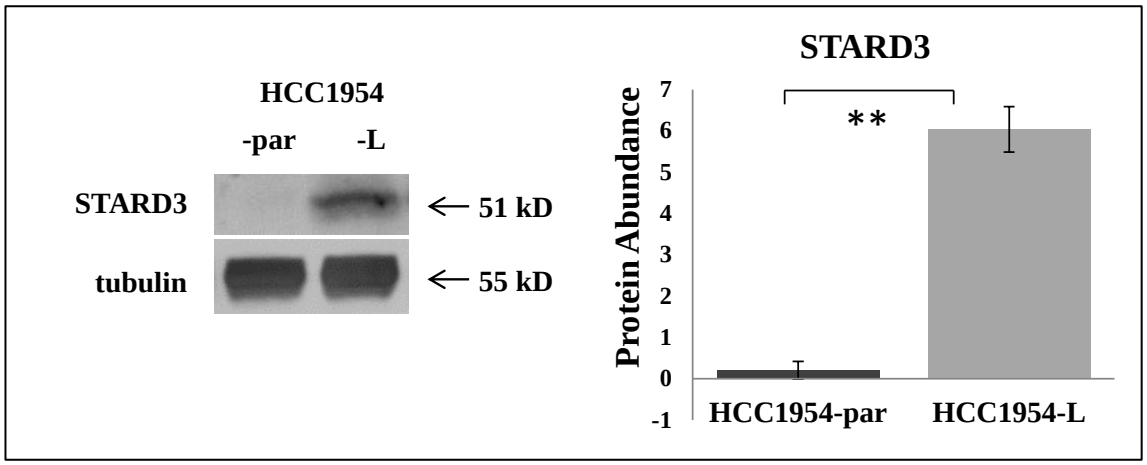

Figure 3-12: Immunoblotting for STARD3 in HCC1954-par and HCC1954-L cells. α-tubulin was used as a loading control. Images are representative of triplicate experiments. Densitometry analysis of triplicate immunoblots was performed using ImageQuant software. * denotes $p \leq 0.05$.

3.5 Analysis of signalling pathways downstream of HER2

To determine if the increased amplification of HER2 in HCC1954-L cells compared to HCC1954-par cells contributes to lapatinib resistance in these cells, the phosphorylation of HER2 and other key HER signalling molecules were examined.

3.5.1 Expression of HER family members

HCC1954-L cells express higher levels of HER2 compared to HCC1954-par cells ($p = 0.008$) [Figure 3-13]. Treatment of HCC1954-par cells with 1 µM lapatinib for 24 hours results in a slight, yet statistically significant increase in HER2 ($p = 0.04$), and a significant decrease in phospho-HER2 levels ($p = 0.03$). Treatment of HCC1954-L cells with 1 µM lapatinib resulted in a significant decrease in phospho-HER2 levels ($p = 0.04$) and a small increase in HER2 which failed to reach statistical significance ($p = 0.05$). There was a small decrease in phospho-HER2 in HCC1954-L cells compared to HCC1954-par cells, however, when the levels of phospho-HER2 were normalised to total HER2 this decrease failed to reach statistical significance ($p = 0.42$).

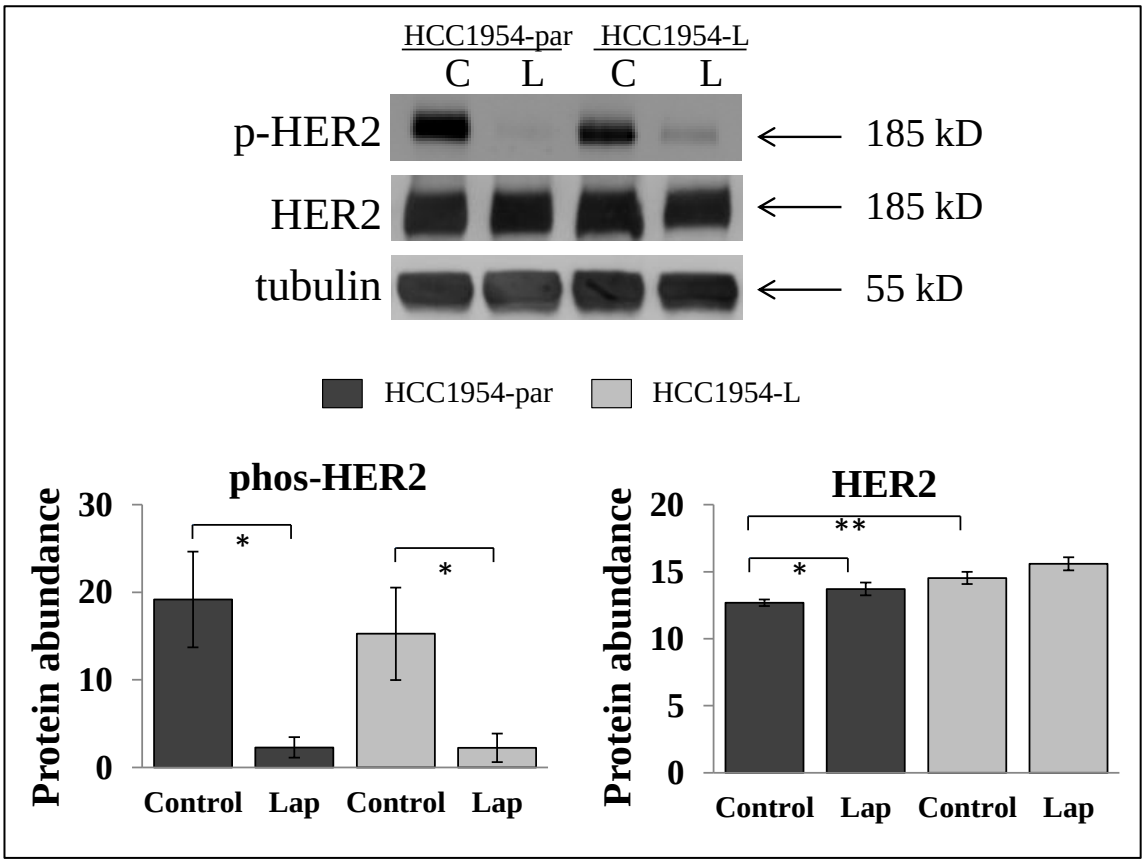

Figure 3-13: Immunoblotting for phospho- (Tyr1221/1222) and total HER2 in HCC1954-par and HCC1954-L cells treated with 1 μM lapatinib for 24 hours. α-tubulin was used as a loading control on each gel. Images are representative of triplicate experiments. Densitometry analysis of triplicate immunoblots was performed using ImageQuant software. * denotes $p \leq 0.05$, ** denotes $p \leq 0.001$.

There was no significant difference in the levels of EGFR or HER3 between HCC1954-par and HCC1954-L cells. Treatment of HCC1954-par cells with 1 μM lapatinib did not significantly alter the levels of HER3 or EGFR [Figure 3-14]. However, treatment of HCC1954-L cells with 1 μM lapatinib resulted in a significant increase in HER3 levels ($p = 0.0248$). Phospho-HER3 levels were barely detectable and phospho-EGFR levels were undetectable by Western blot, in HCC1954-par and HCC1954-L cells. Positive controls for phospho-HER3 (BT474 cells) and phospho-EGFR (MDA-MB-468 cells) were detected (not shown).

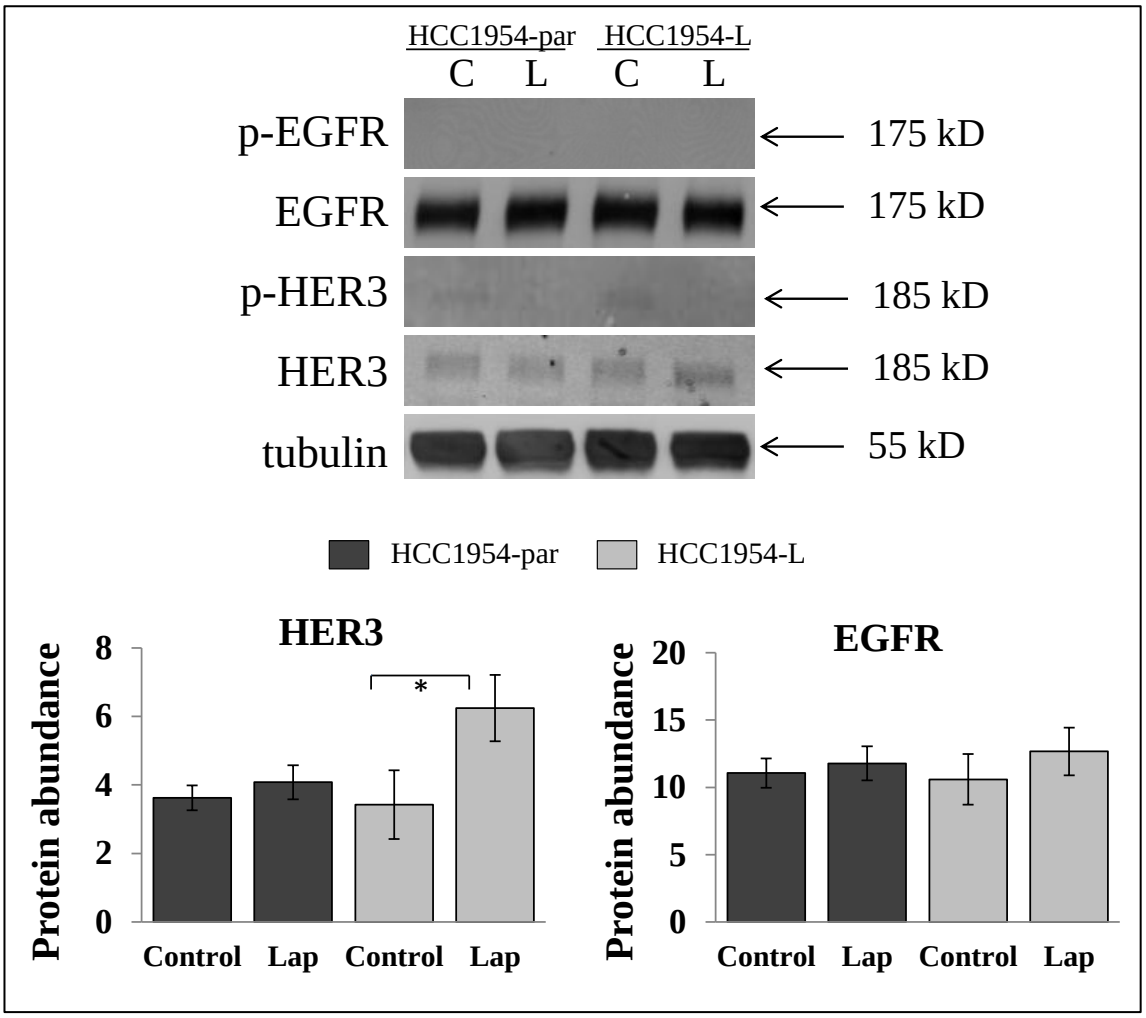

Figure 3-14: Immunoblotting for phospho- and total HER3, and phospho- and total EGFR in HCC1954-par and HCC1954-L cells treated with 1 μM lapatinib for 24 hours. α-tubulin was used as a loading control on each gel. Images are representative of triplicate experiments. Densitometry analysis of triplicate immunoblots was performed using ImageQuant software. * denotes $p \leq 0.05$.

3.5.2 Alterations in P13K/AKT and MAPK signalling pathways

Phospho-AKT levels were significantly decreased in HCC1954-par ($p = 0.01$) and HCC1954-L ($p = 0.04$) cells following 24 hour treatment with 1 μM lapatinib [Figure 3-15]. Lapatinib treatment resulted in a similar decrease in the levels of phospho-ERK in HCC1954-par ($p = 0.0001$) and HCC1954-L ($p = 0.003$) cells. HCC1954-L cells had higher levels of both phospho-AKT ($p = 0.04$) and phospho-ERK ($p = 0.01$) compared to HCC1954-par cells, with no significant change in the levels of total AKT or ERK.

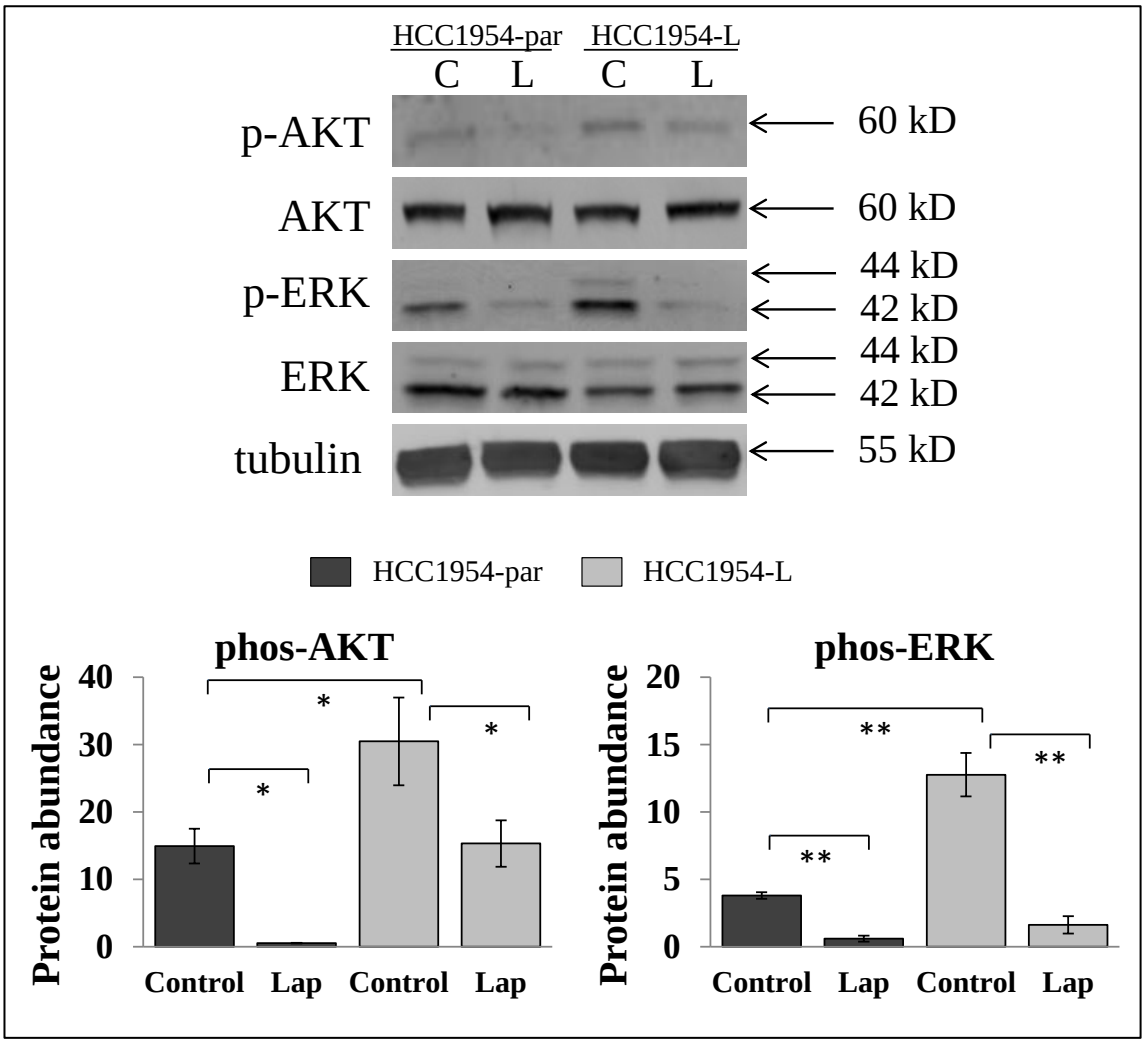

Figure 3-15: Immunoblotting for phospho- (Ser473) and total AKT, and phospho- (Thr202/Tyr204) and total ERK in HCC1954-par and HCC1954-L cells treated with 1 μM lapatinib for 24 hours. α-tubulin was used as a loading control on each gel. Images are representative of triplicate experiments. Densitometry analysis of triplicate immunoblots was performed using ImageQuant software. * denotes $p \leq 0.05$, ** denotes $p \leq 0.001$.

3.5.2 Examination of previously published mechanisms of acquired lapatinib resistance

The overexpression and/or upregulation of the following proteins have been shown in previously published cell line models of acquired lapatinib resistance; ER, MCL-1, SRC and XIAP. ER and phospho-SRC were undetectable in HCC1954-par and HCC1954-L cells. Controls for ER (BT474 cells) and phospho-SRC (MCF-7) were positive (not shown). HCC1954-L cells had higher levels of SRC ($p = 0.01$), and lower levels of XIAP ($p = 0.0005$) and MCL-1 ($p = 0.01$) compared to HCC1954-par cells [Figure 3-

16]. Treatment with 1 μM lapatinib resulted in a decrease in XIAP levels in HCC1954-par cells ($p = 0.01$) and an increase in XIAP levels in HCC1954-L cells ($p = 0.02$). The treatment also resulted in a decrease in MCL-1 levels in HCC1954-par cells ($p = 0.03$) but not in HCC1954-L cells, nor did the treatment have an effect on the levels of SRC in either cell line.

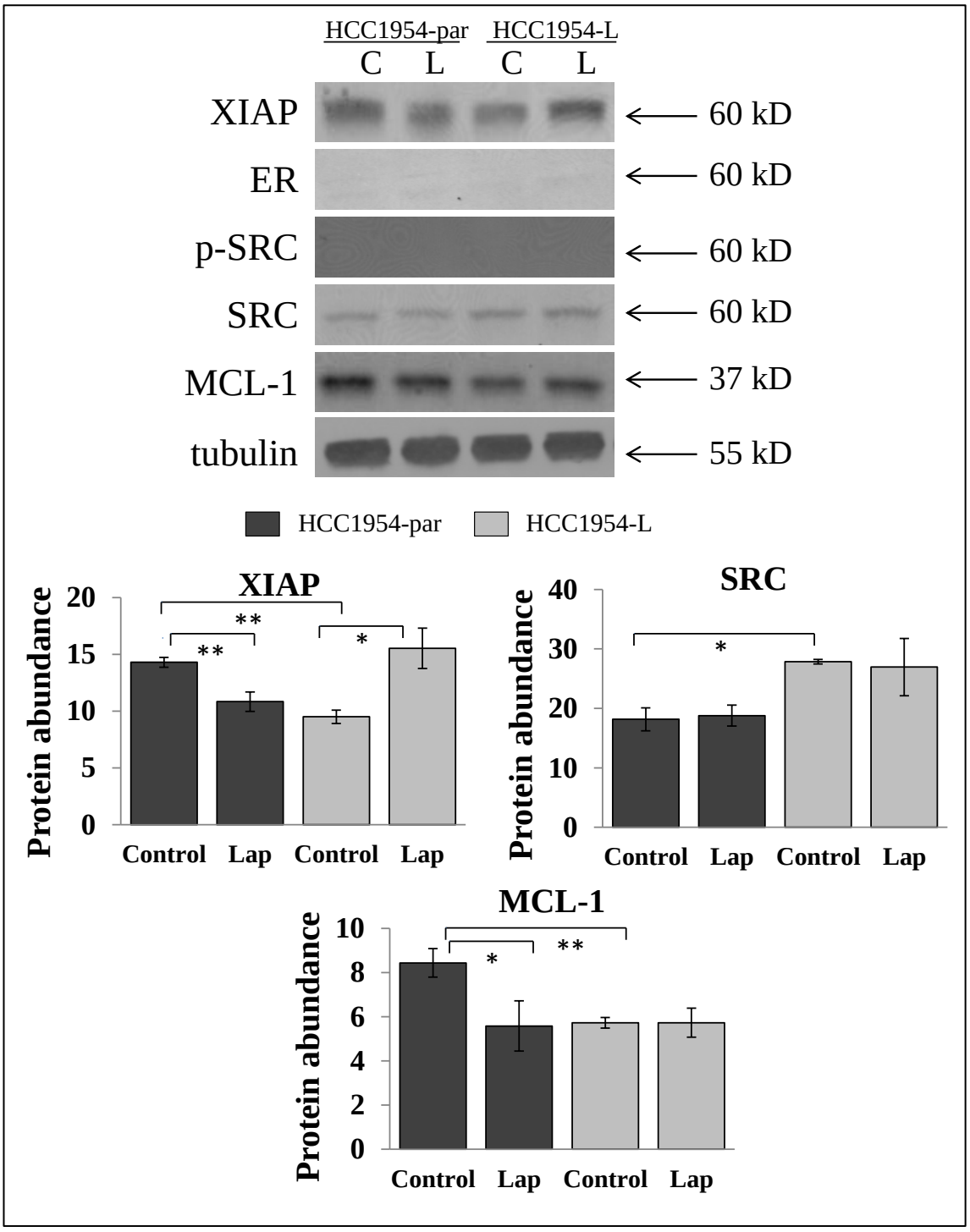

Figure 3-16: Immunoblotting for XIAP, ER, phospho- (Tyr416) and total SRC, and MCL-1 in HCC1954-par and HCC1954-L cells treated with 1 μM lapatinib for 24 hours. α-tubulin was used as a loading control on each gel. Images are representative of triplicate experiments. Densitometry analysis of triplicate immunoblots was performed using ImageQuant software. * denotes $p \leq 0.05$, ** denotes $p \leq 0.001$

3.6 Summary

A novel cell line model of acquired lapatinib resistance, HCC1954-L, was developed by continuously culturing HCC1954 cells in the presence of lapatinib for 6 months. The HCC1954-L cells were resistant to lapatinib and the resistant phenotype was stable following a freeze-thaw cycle and 3 months growth in the absence of lapatinib. Array CGH analysis of HCC1954-L cells revealed increased gene amplification of HER2 compared to HCC1954-par cells. This increased amplification was confirmed using immunoblotting and FISH analysis. However, phospho-HER2 levels were not increased in the HCC1954-L cells, and phospho-HER2 levels were decreased in both the parental and resistant cells following treatment with lapatinib. Immunoblotting also revealed alterations in phospho-AKT, phospho-ERK, XIAP, MCL-1 and SRC in the resistant cells.

Chapter 4

Senescence – a novel mechanism of acquired lapatinib resistance

4.1 Introduction

In addition to developing HCC1954-L, the model of acquired lapatinib resistance described in Chapter 3, HCC1419 cells were also conditioned with lapatinib. However, in contrast to the HCC1954-L cells which became resistant to lapatinib, HCC1419 cells did not continue to grow in the presence of lapatinib. Previous data generated in our lab has shown that HCC1419 cells treated with 250 nM lapatinib ceased proliferation and after 6 months of treatment, very few treated cells remained and these cells neither proliferated nor died in the presence of lapatinib. When lapatinib was removed from the media the cells slowly began proliferating again, after 3 months of growth the cells were tested and found to exhibit the same sensitivity to lapatinib as lapatinib-naïve cells. In this chapter, the effects of lapatinib treatment on HCC1419 cells are examined and the mechanism which enables the cells to survive long-term lapatinib treatment without active proliferation is investigated.

4.2 Lapatinib conditioning of HCC1419 cells

HCC1419 cells overexpress HER2 and thus represent a cell line model of HER2 positive breast cancer. HCC1419 cells are resistant to trastuzumab, but are sensitive to lapatinib with an IC_{50} of 0.08 ± 0.01 µM [Figure 4-1]. This cell line was chosen to be conditioned in lapatinib-containing media. A lapatinib dose response assay was performed in order to select the concentration of lapatinib which would result in 70 % growth inhibition over a 4 day treatment. Treatment of HCC1419 cells with 200 nM lapatinib inhibited the growth of the cells by 67.5 ± 1.1 % compared to untreated controls (p = 0.0001), while 300 nM lapatinib inhibited 79.0 ± 2.3 % compared to untreated controls (p = 0.0005) [Figure 4-2]. Therefore lapatinib conditioning of HCC1419 cells began with twice weekly treatments of 250 nM lapatinib, as this concentration should result in approximately 70 % inhibition of cell growth.

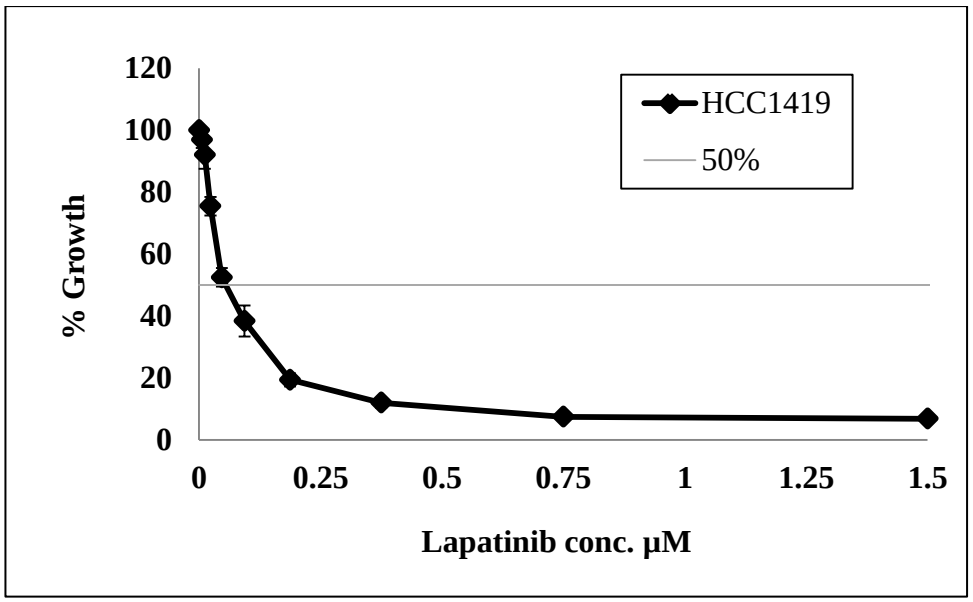

Figure 4-1: Proliferation of HCC1419 cells following a 5-day treatment with lapatinib (0 – 1.5 µM). Growth is expressed relative to untreated control cells. Error bars represent the standard deviation of triplicate experiments.

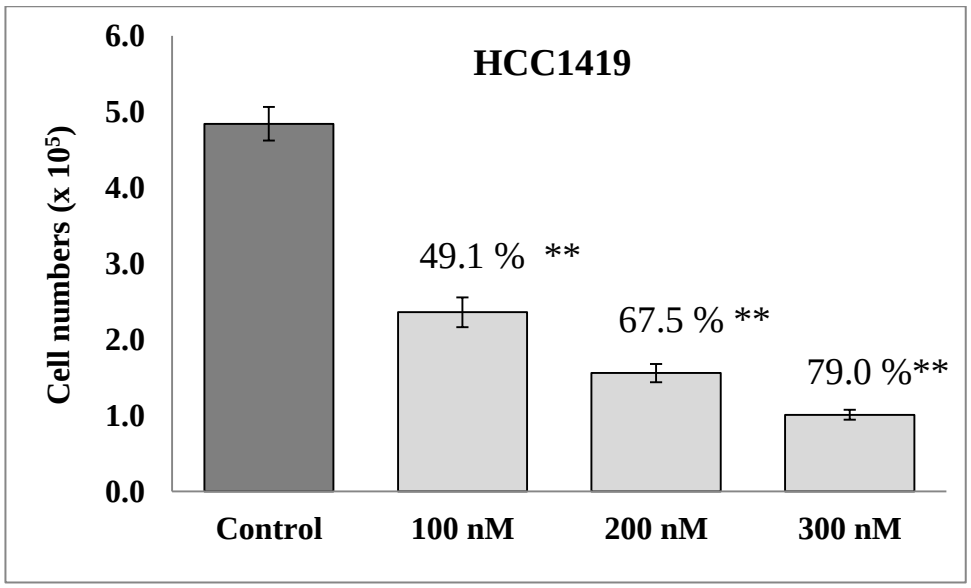

Figure 4-2: HCC1419 cells treated with varying concentrations of lapatinib over a four day period. Cell counts were performed using ViaCount reagent and Guava Software and expressed relative to control untreated cells. Error bars denote the standard deviation of triplicate cell counts from triplicate experiments. Percentages shown on graph represent the percentage of growth inhibition compared to control cells across three independent experiments. Student's t-test was performed to determine significant differences: * denotes $p < 0.05$; ** denotes $p < 0.01$

4.3 The lapatinib conditioning process

HCC1419 cells were seeded into 2 flasks; one flask was left untreated but was passaged alongside the treated cells for the duration of the treatment process. These are referred to as control untreated cells. The other flask was treated twice weekly with 250 nM lapatinib and these cells are referred to as lapatinib conditioned cells. During the conditioning process the morphology and sensitivity of the cell lines to lapatinib was monitored. In contrast to HCC1954-L cells, HCC1419 lapatinib conditioned cells ceased active proliferation in the presence of lapatinib during the conditioning process. The growth of HCC1419 lapatinib conditioned cells completely ceased within 3 months of treatment, and the remaining cells displayed a visibly altered morphology; the conditioned cells exhibited a flatter and enlarged cell shape compared to control cells [Figure 4-3].

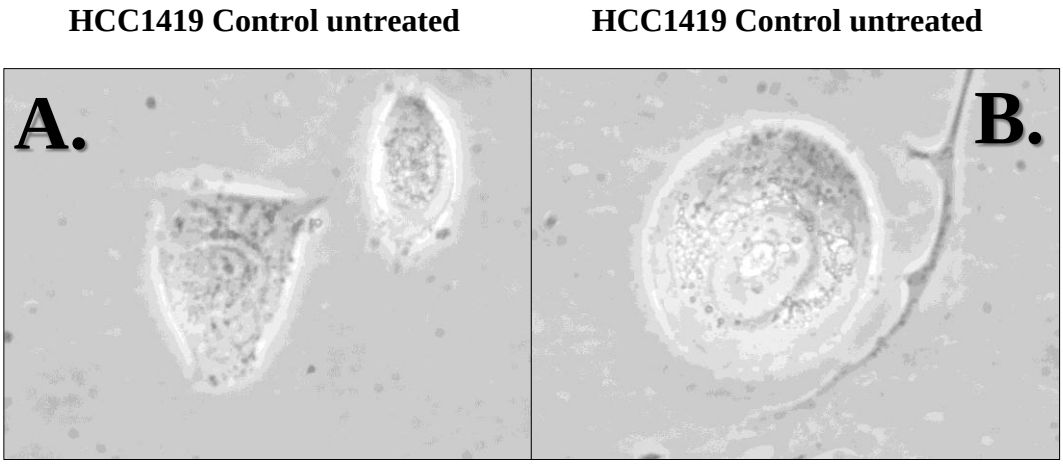

Figure 4-3: Images of (A) HCC1419 control untreated and (B) HCC1419 lapatinib (250 nM) conditioned cells after 3 months of lapatinib conditioning at 400X magnification.

The cells were conditioned for a further 3 months, as this was the length of time taken for HCC1954-L cells to become fully resistant to lapatinib. At this stage HCC1419 lapatinib conditioned cells still appeared growth arrested and displaying morphological alterations compared to the control cells. Whether this arrested growth and the associated morphological changes were the result of lapatinib-induced cellular senescence was then investigated. Senescence is characterised most typically by specific morphological alterations, to flattened and enlarged cell shape, and the induction of senescence markers such as senescence-associated β-galactosidase (β-gal). β-gal is the most widely accepted marker of senescence [281] and two weeks of treatment with 50 μM bromodeoxyuridine (BrdU) has been shown to induce senescence in mammalian cells regardless of cell type or species [282]. Treatment of HCC1419 cells with 50 μM BrdU for 2 weeks induced β-gal activity [Figure 4-4] and was therefore used a positive control for the β-gal assay.

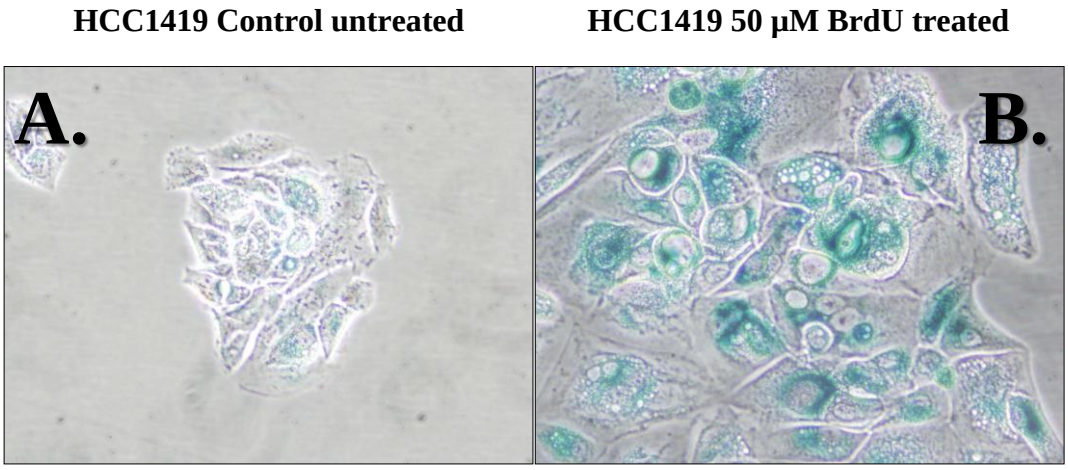

Figure 4-4: Staining for senescence-associated β-galactosidase activity in (A) HCC1419 control untreated, and (B) HCC1419 cells treated for 2 weeks with BrdU (50 µM) Images are at 200X magnification.

4.4 Lapatinib-conditioning induces senescence in HCC1419 cells

Following confirmation that the β-gal assay could detect BrdU-induced senescence in HCC1419 cells, β-gal activity was examined in HCC1419 cells which had been conditioned with lapatinib for 6 months. HCC1419 lapatinib conditioned cells exhibit a senescent-like phenotype, as indicated by an increase in β-gal activity compared to control untreated cells [Figure 4-5]. During the conditioning process the cells appeared to display arrested growth and showed morphological changes within 12 weeks of treatment. Therefore, the length of time required for lapatinib to induce β-gal activity in HCC1419 cells was investigated. Cells were conditioned with 250 nM lapatinib, and the cells were tested for β-gal activity compared to untreated controls, at weekly intervals for a period of 6 weeks. One week of treatment with 250 nM lapatinib was sufficient to induce a senescent-like phenotype in HCC1419 cells [Figure 4-6], and this phenotype remained stable throughout the 6 week treatment period.

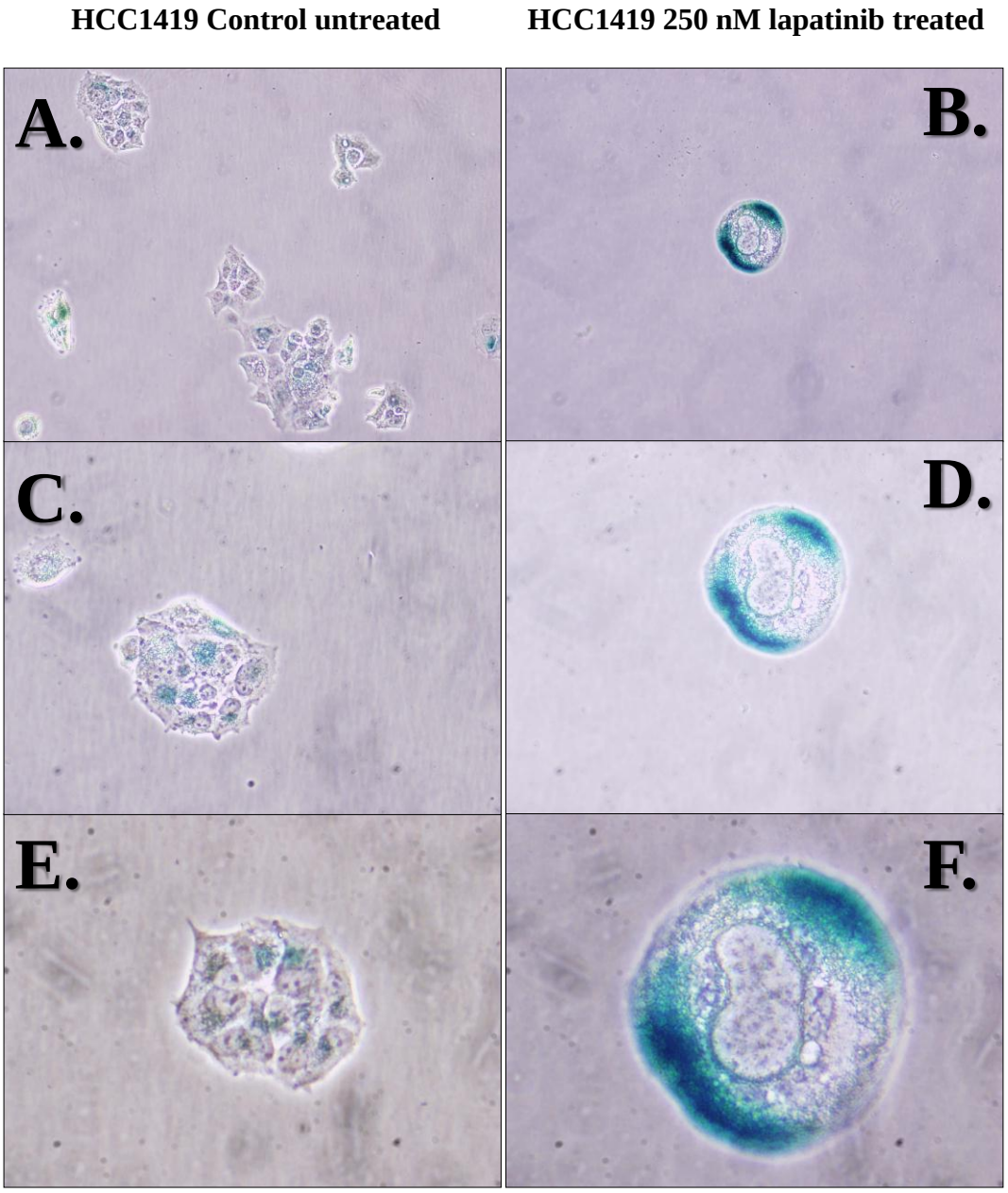

Figure 4-5: Staining for senescence-associated β-galactosidase activity in (A, B and C) HCC1419 control untreated cells and (D, E and F) HCC1419 cells following 6 month treatment with 250 nM lapatinib. Images are represented at (A, B) 100X, (C, D) 200X and (E, F) 400X magnifications respectively.

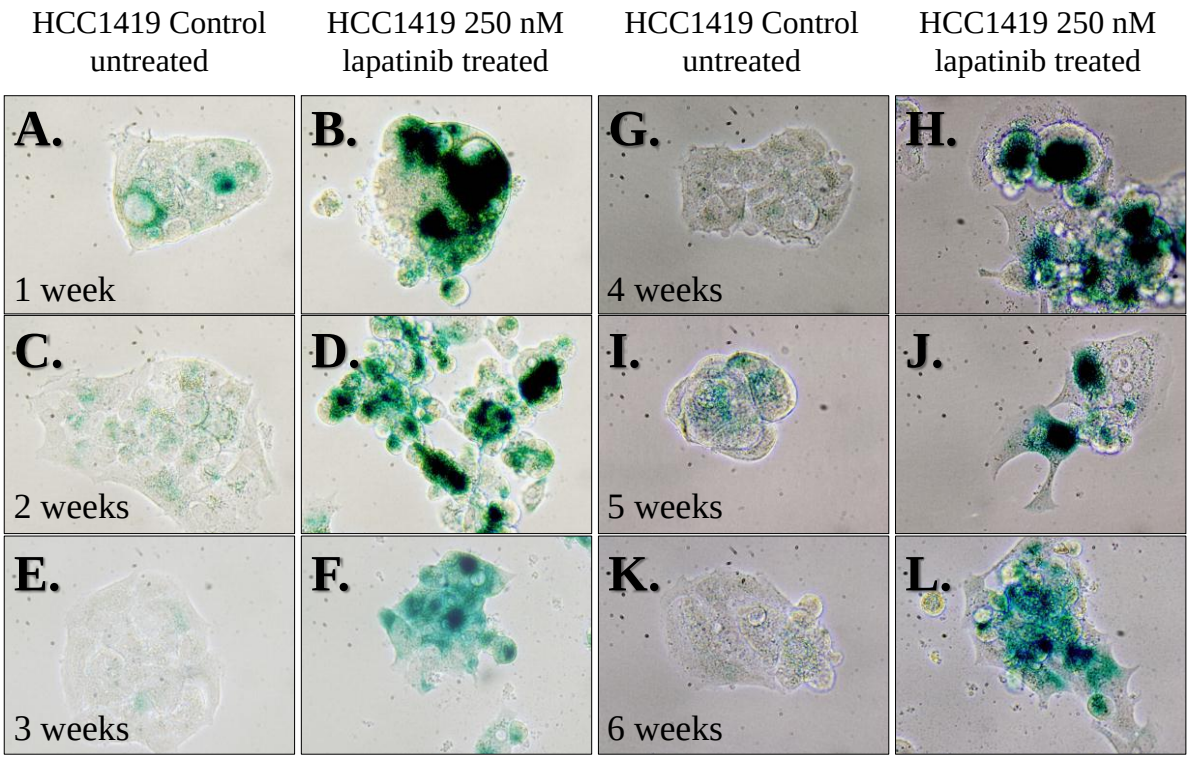

Figure 4-6: Staining for senescence-induced β-galactosidase activity in (A, C, E, G, I and K) HCC1419 untreated control cells and (B, D, F, H, J and L) HCC1419 cells treated with lapatinib 250 nM for 1 – 6 weeks. All images taken at 400X magnification.

4.6 Examining other putative markers of senescence

To further investigate the senescent-like phenotype induced by lapatinib treatment in HCC1419 cells, the expression of other putative markers of senescence were examined. While 1 week of 250 nM lapatinib treatment induced a senescent-like phenotype in HCC1419 cells, it did not induce a senescent-like phenotype in SKBR3 cells [Figure 4-7]. Thus, SKBR3 cells were used as a control for this experiment.

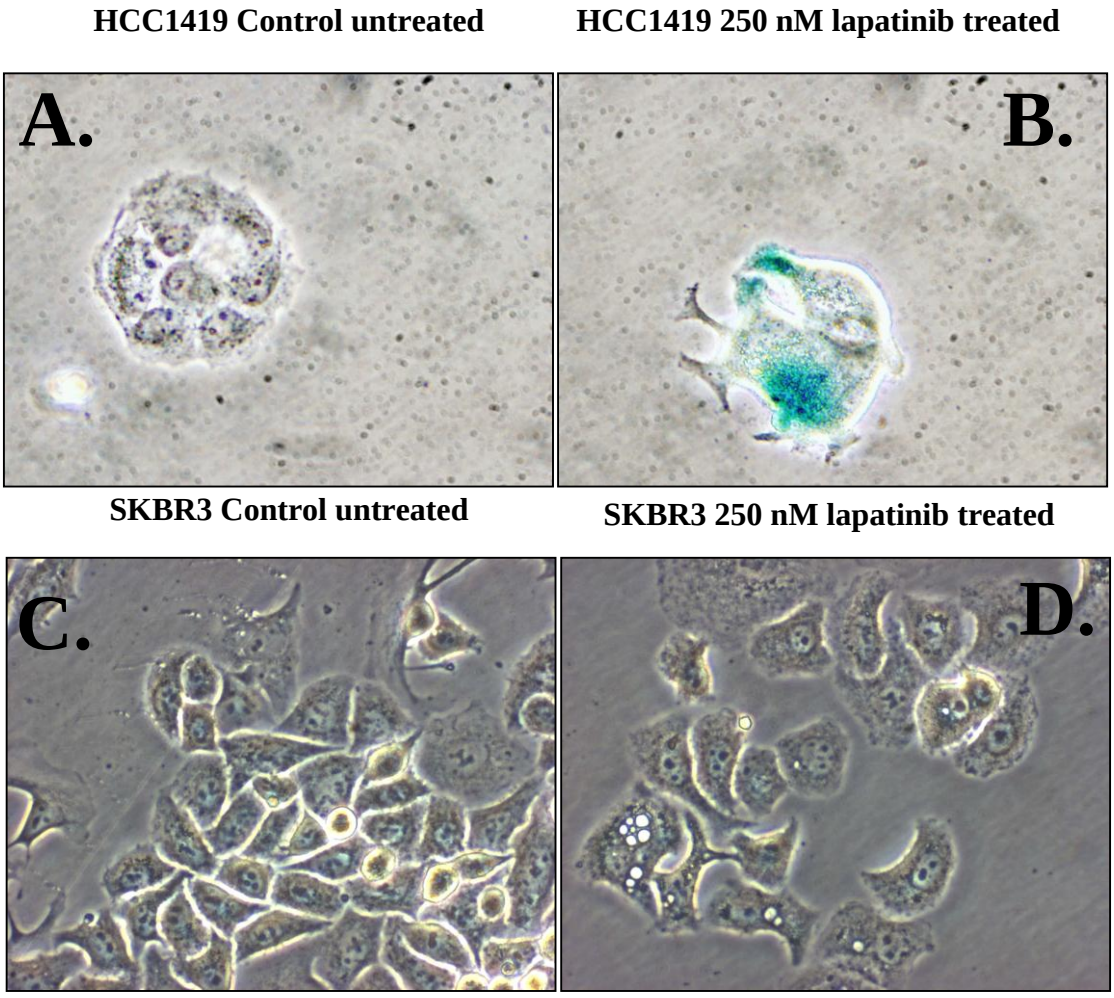

Figure 4-7: Staining for senescence-associated β-galactosidase activity in (A) HCC1419 control untreated cells, (B) HCC1419 250nM lapatinib treated cells, (C) SKBR3 control untreated cells and (D) SKBR3 250 nM lapatinib treated cells following 1 week of lapatinib treatment. Images taken at 400X magnification.

4.6.1 Expression of p15, p16, p21 and p27 by qRT-PCR

Increased expression of specific cyclin-dependent kinase inhibitors (CDKIs), including p15 (CDKN), p16 ^{Ink4a} (CDKN2A), p21^{Waf1} (CDKN1A), and p27^{Kip1} (CDKN1B) are associated with the induction of senescence [283]. The expression of these targets was examined using quantitative reverse-transcriptase PCR in HCC1419 and SKBR3 cells. HCC1419 have 3.7-fold higher levels of p15 ($p = 0.04$), 7.7-fold higher levels of p21 ($p = 0.01$) and 17.5-fold higher levels of p27 ($p = 0.01$) [Table 4-1], compared to SKBR3 cells. Treatment of HCC1419 cells with 250 nM lapatinib for 1 week resulted in a 12.1-fold increase in p15 expression ($p = 0.01$), and a 6.8-fold increase in p27 expression (p

= 0.01). Similarly, treatment of SKBR3 cells with 250 nM lapatinib for 1 week resulted in a 25.3-fold increase in p15 (p = 0.0005), and a 3.1-fold increase in p27 expression, which failed to reach statistical significance (p = 0.07). There was no change in the expression of p21 in either cell line. As lapatinib treatment had the same effect on the expression of p15, p21 and p27 in both SKBR3 and HCC1419 cells, this suggests that higher expression of p15, p21 and p27 in untreated cells may predict whether lapatinib treatment induces a senescent-like phenotype. p16 mRNA was not detected in any of the samples tested.

Table 4-1: Expression of p15, p21 and p27 in HCC1419 and SKBR3 cells quantified using qRT-PCR. Data is representative of triplicate technical replicates of triplicate biological replicates and presented as averages ± the standard deviation of the triplicate ΔΔCts, where RQ is the fold change increase in mRNA levels in HCC1419 compared to SKBR3 cells.

Assay	ΔCt HCC1419 CTRL	ΔCt SKBR3 CTRL	ΔΔCt (HCC1419-SKBR3)	RQ
p15	14.41343	16.1632	- 1.7497 ± 0.2262	3.7
p21	7.932068	10.87824	- 2.9462 ± 0.6587	7.7
p27	7.63037	11.75963	- 4.1292 ± 0.3266	17.5

4.7 Lapatinib-induced senescence is reversible

Previous data generated in our laboratory showed that HCC1419 cells conditioned with 250 nM lapatinib for 6 months resumed active proliferation 3 months after lapatinib was removed from the media [255]. HCC1419 cells were treated with 250 nM lapatinib for 1 week and then tested for β-gal activity. The cells were confirmed as positive for senescence. Lapatinib was then removed from the media and cells were cultured for a further week, after which time they were again tested for β-gal activity. Removing lapatinib from the media of senescent HCC1419 cells reverses the senescent phenotype as indicated by the conditioned cells exhibiting a similar level of β-gal activity compared to control untreated cells [Figure 4-8].

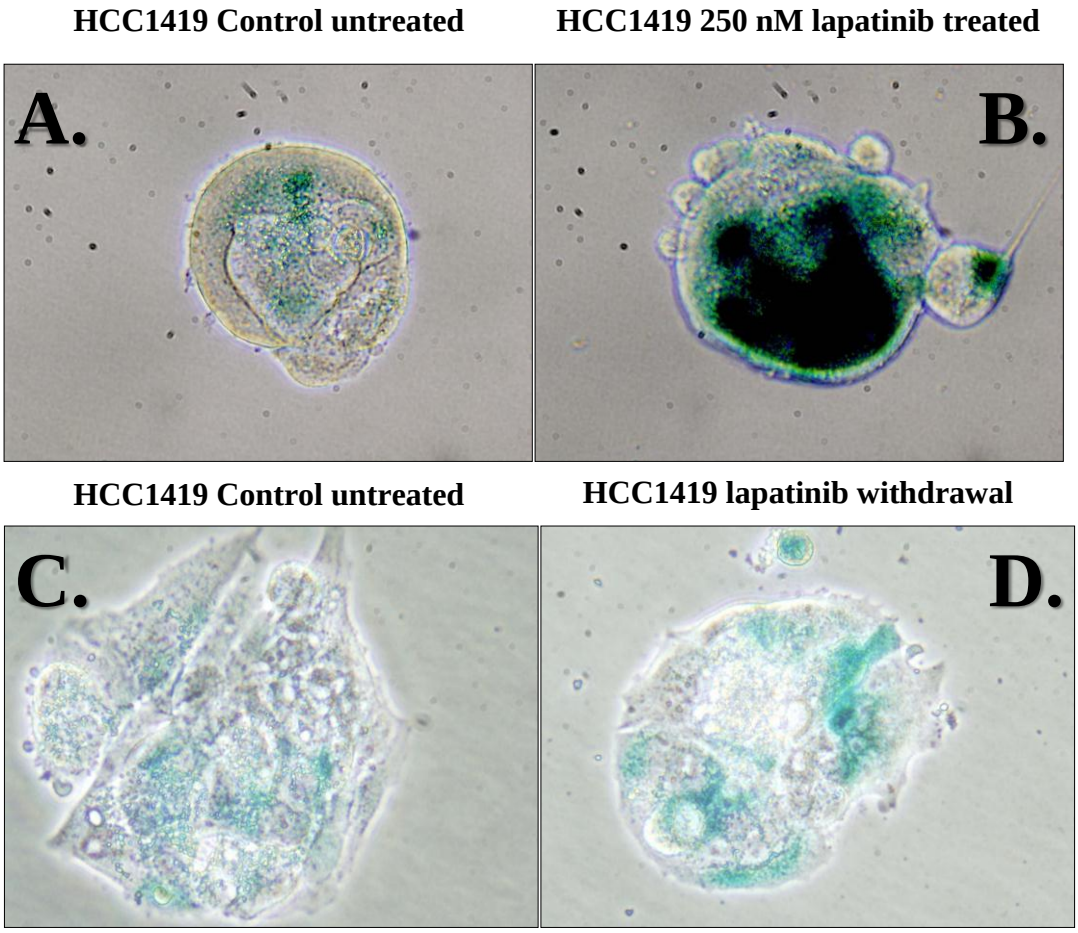

Figure 4-8: Staining for senescence-induced β-galactosidase activity in (A) HCC1419 control untreated cells and (B) HCC1419 250 nM lapatinib treated cells following 1 week treated with lapatinib. Lapatinib was removed from the media for one week and cells were tested again, (C) HCC1419 control untreated cells and (D) HCC1419 cells from which lapatinib had been removed. Images taken at 400X magnification.

4.8 AKT versus ERK-mediated senescence induction

The MAPK and PI3K/AKT pathways are activated by HER signalling. Inhibition of HER2 signalling with lapatinib inhibits both MAPK and AKT signalling. It is therefore possible that lapatinib-induced senescence may be mediated either by inhibition of MAPK signalling or PI3K signalling or may require inhibition of both signalling pathways. HCC1419 cells were treated with an ERK inhibitor, U0126, (MAPK pathway) and an AKT inhibitor, LY294002, (PI3K/AKT pathway) as single agents and in combination at a range of concentrations [Figure 4-9]. Treatment of HCC1419 cells with 250 nM LY294002 did not result in strong β-gal activity compared to control

untreated cells but treatment with 500 nM and 1 μM resulted in strong β-gal activity. Treatment of HCC1419 cells with 500 nM, 1 μM or 2 μM U0126 resulted in strong β-gal activity in each case. All tested combinations of LY294002 and U0126 resulted in β-gal activity indicating that inhibition of either MAPK and/or PI3K/AKT signalling pathways results in induction of senescence in HCC1419 cells.

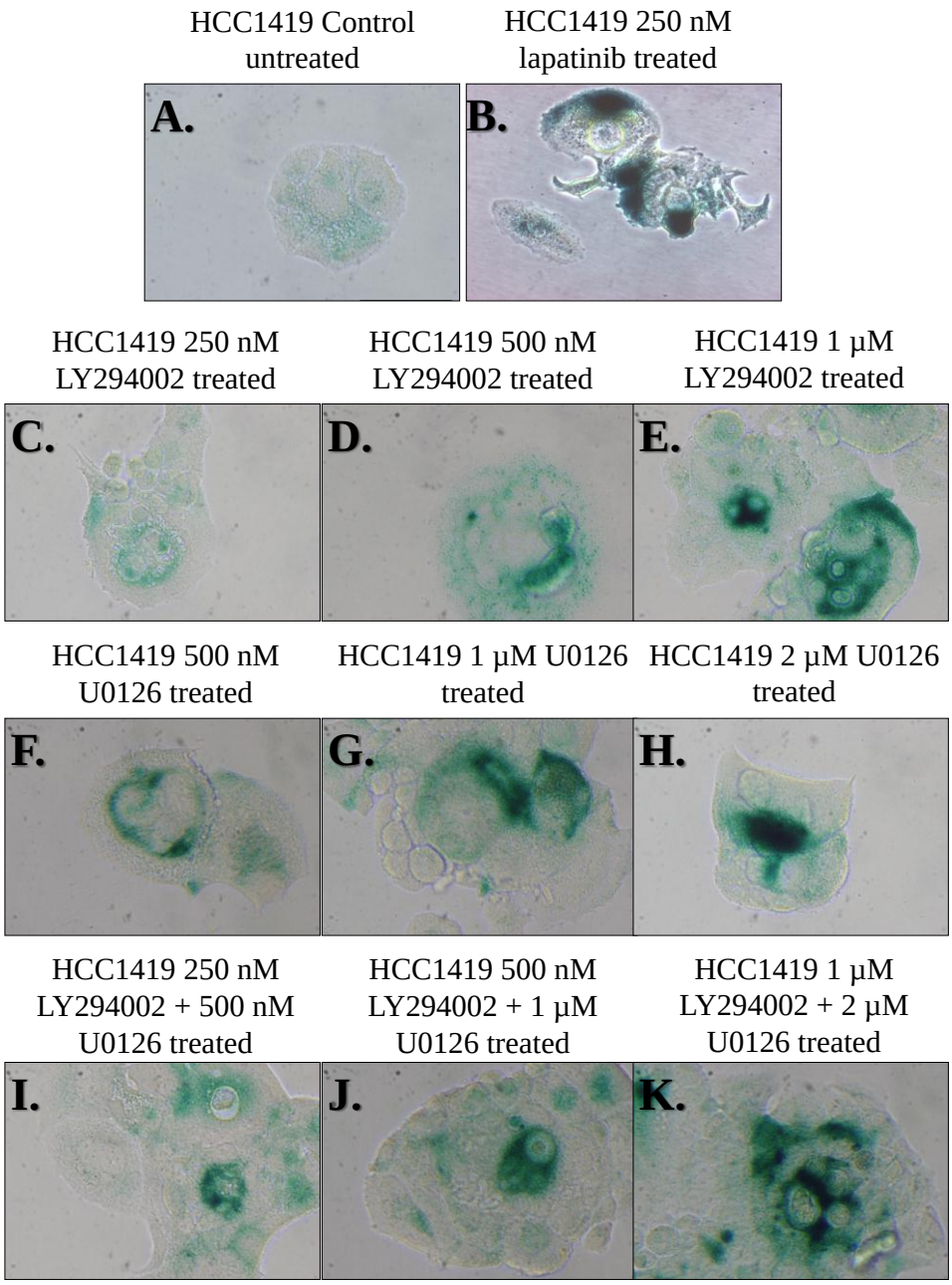

Figure 4-9: Staining for senescence-associated β-galactosidase activity in (A) HCC1419 control untreated cells, and (B) HCC1419 treated with 250 nM lapatinib, (C) 250 nM LY294002, (D) 500 nM LY294002, (E) 1 µM LY294002, (F) 500 nM U0126, (G) 1 µM U0126, (H) 2 µM U0126, (I) 250 nM LY294002 and 500 nM U0126, (J) 500 nM LY294002 and 1 µM U0126, and (K) 1 µM LY294002 and 2 µM U0126 following 1 week of treatment. Images taken at 400X magnification.

4.9 Lapatinib and trastuzumab-induced senescence

HCC1419 cells were treated with a range of lapatinib concentrations (0.05 – 1 μM), 15 μg/ml trastuzumab and a combination of lapatinib and trastuzumab for 1 week and the activity of β-gal was examined. Concentrations of 50 – 500 nM lapatinib induced strong β-gal activity compared to control cells. Although concentrations of lapatinib in excess of 500 nM (750 nM and 1 μM) induced some β-gal activity it appeared to be at a much lower intensity than that induced by lower concentrations, suggesting that lower concentrations of lapatinib resulted in stronger induction of the senescent-like phenotype in HCC1419 cells. Treatment of HCC1419 cells with trastuzumab did not induce senescence whereas trastuzumab combined with 250 nM lapatinib induced senescence, although the intensity of β-gal staining appears lower than that induced by 250 nM lapatinib alone [Figure 4-10].

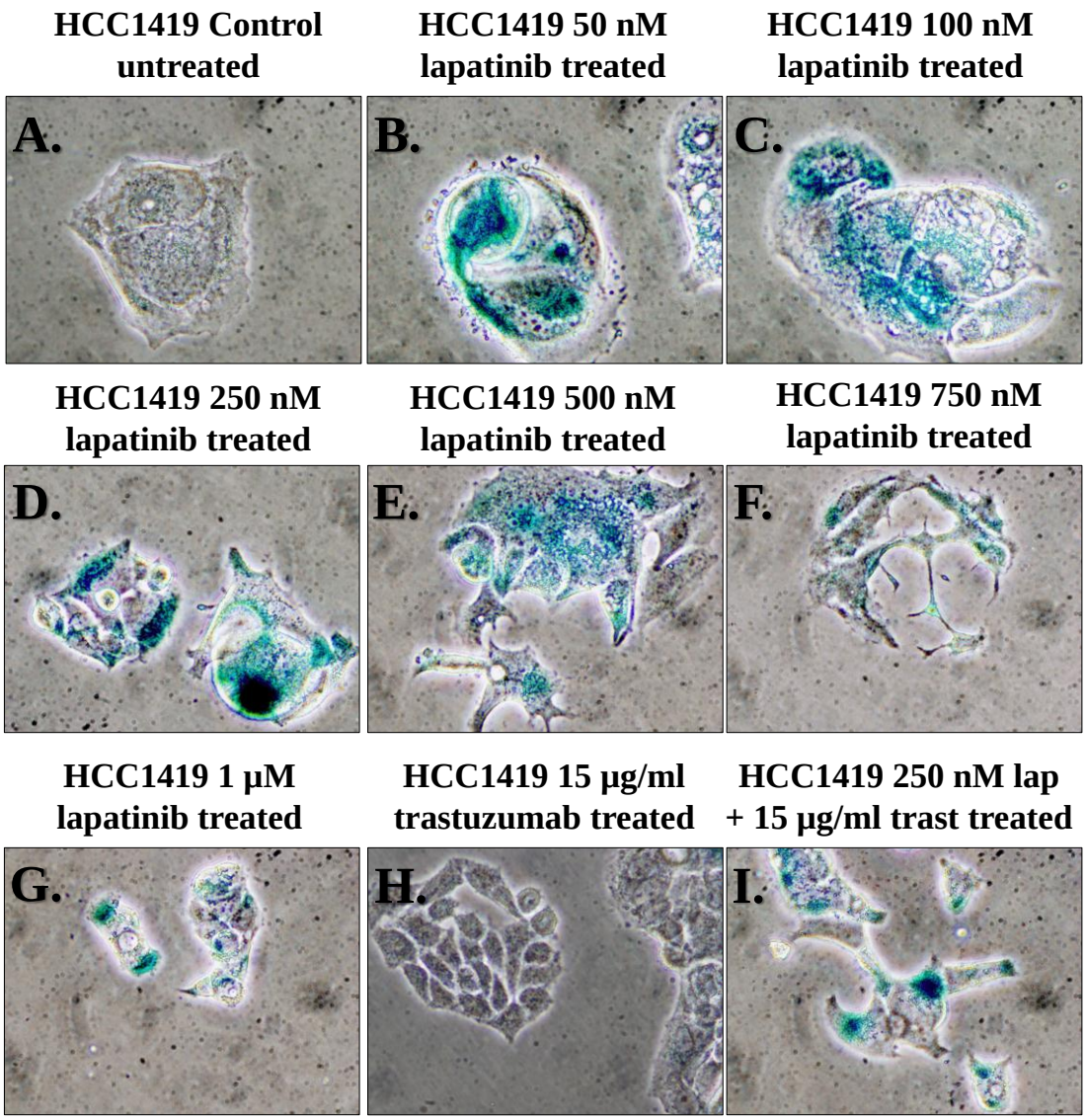

Figure 4-10: Staining for senescence-associated β-galactosidase activity in (A) HCC1419 control untreated cells and (B) HCC1419 treated with 50 nM lapatinib, (C) 100 nM lapatinib, (D) 250 nM lapatinib, (E) 500 nM lapatinib, (F) 750 nM lapatinib, (G) 1 µM lapatinib, (H) 15 µg/ml trastuzumab, and (I) a combination of 15 µg/ml trastuzumab and 250 nM lapatinib following 1 week of treatment. Images taken at 400X magnification.

4.10 Lapatinib induced senescence in a panel of HER2 positive cell lines

The induction of senescence was tested in a panel of HER2 cell lines which are sensitive to lapatinib [194]. Cells were treated with 250 nM lapatinib for 1 week and β-gal activity was compared to control untreated cells. HCC1419 cells treated with lapatinib were included as a positive control for induction of β-gal activity. Although UACC812 and HCC2218 cells exhibit β-gal activity, there is no increase in activity compared to control untreated cells. Also, HCC2218 cells are an anchorage-independent cell line and the β-gal assay is designed for anchorage-dependent cells, therefore it is possible that the assay conditions were not optimal for that cell line. No other cell lines showed an alteration in β-gal activity following lapatinib treatment [Figure 4-11]. This suggests that lapatinib induced senescence may be specific to HCC1419 cells.

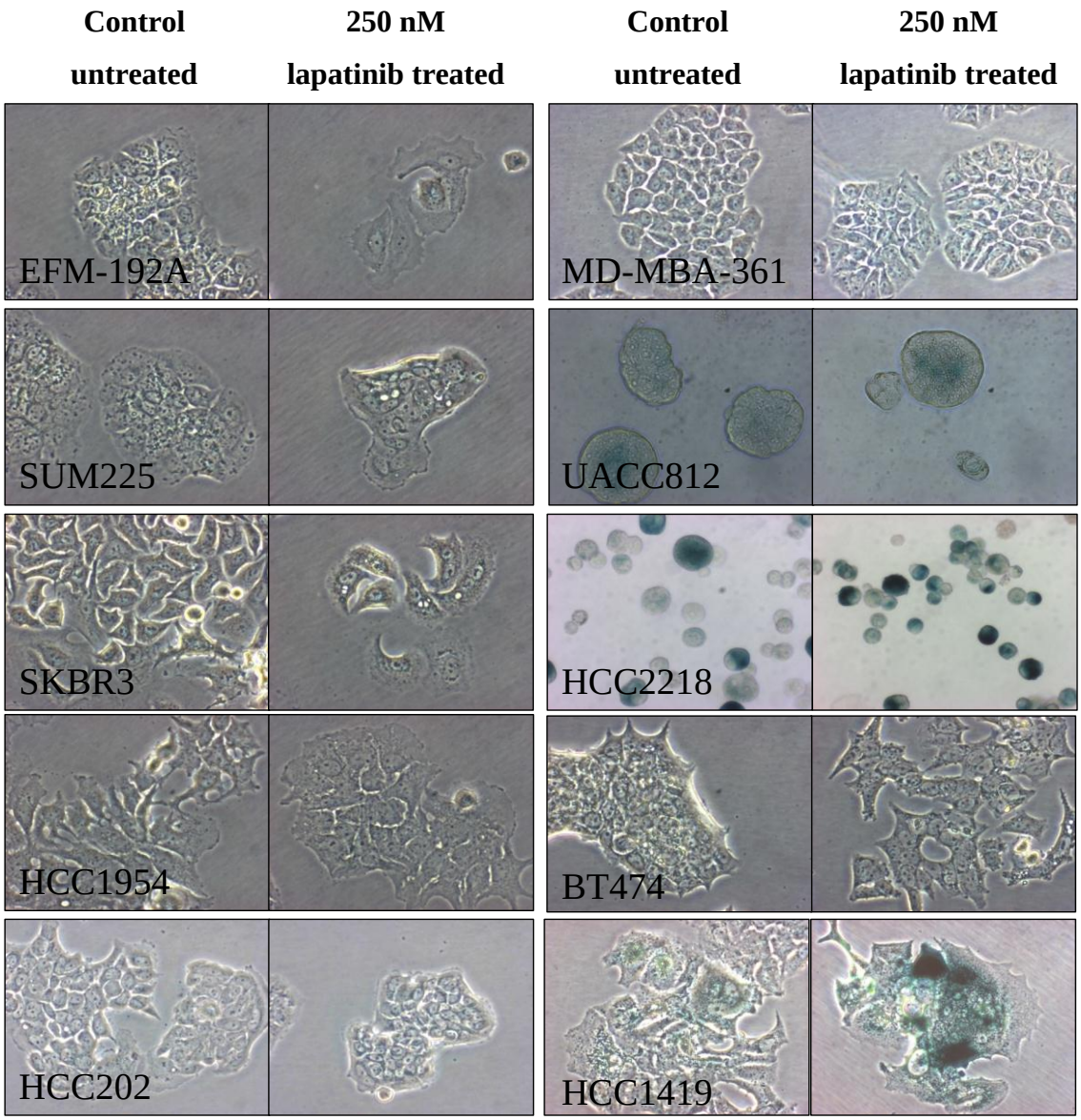

Figure 4-11: Staining for senescence-induced β-galactosidase activity in EFM-192A, MD-MBA-361, SUM225, UACC812, SKBR3, HCC2218, HCC1954, BT474, HCC202 and HCC1419 cells treated with 250 nM lapatinib for 1 week. Images are representative of duplicate experiments and are taken at 400X magnification.

4.11 Summary

HCC1419 cells did not proliferate in the presence of 250 nM lapatinib, instead the lapatinib treatment induced a senescent-like phenotype in the cells, determined using an assay which detects activity of β-galactosidase. Lapatinib induced this phenotype in HCC1419 cells following short-term (1 week) and long term (6 months) treatment. Treatment of HCC1419 cells with 250 nM lapatinib for one week resulted in an increase

in the expression of p15 and p27, two other putative markers of senescence. SKBR3 cells when treated with 250 nM lapatinib for 1 week also exhibited an increase in the expression of p15 and p27 but did not display β-galactosidase activity. The lapatinib-induced senescent-like phenotype in HCC1419 cells was reversed when lapatinib was removed from the media. Inhibition of MAPK and/or PI3K/AKT signalling induced a senescent-like phenotype in HCC1419 cells. Different concentrations of lapatinib induced β-galactosidase activity to varying degrees with a trend towards higher activity occurring at lower concentration of lapatinib treatment. Treatment of HCC1419 cells with trastuzumab did not result in a β-galactosidase activity. Combined treatment with trastuzumab and lapatinib resulted in β-galactosidase activity but at a lower level than treatment with lapatinib alone. A panel of HER2-amplified cell lines were treated with 250 nM lapatinib for one week but lapatinib did not induce β-galactosidase activity in any cell line other than HCC1419 cells.

Chapter 5

SKBR3-L – a cell line model of acquired lapatinib resistance

5.1 Introduction

Previous work in our laboratory resulted in the generation of SKBR3-L cells, a cell line model of lapatinib resistance [255]. Briefly, SKBR3-par cells were conditioned with 250 nM lapatinib for 6 months after which time the resulting cell line was resistant to lapatinib. Two-dimensional differential in-gel electrophoresis analysis was used to examine alterations in the levels of phospho-proteins in SKBR3-L compared to SKBR3 parental cells (SKBR3-par). Further characterisation of the SKBR3-L cell line and validation of one of the most interesting targets from the phospho-proteomic analysis are described in this chapter.

5.2 Characterisation of SKBR3-L cells

5.2.1 SKBR3-L cells are resistant to lapatinib

Characterisation of SKBR3-L cells was performed. The IC_{50} for lapatinib in the conditioned cell line was 6.5 ± 0.4 µM lapatinib compared to 0.1 ± 0.01 µM lapatinib in parental SKBR3 (SKBR3-par) cells ($p = 0.0014$) [Figure 5-1], consistent with previous results [255].

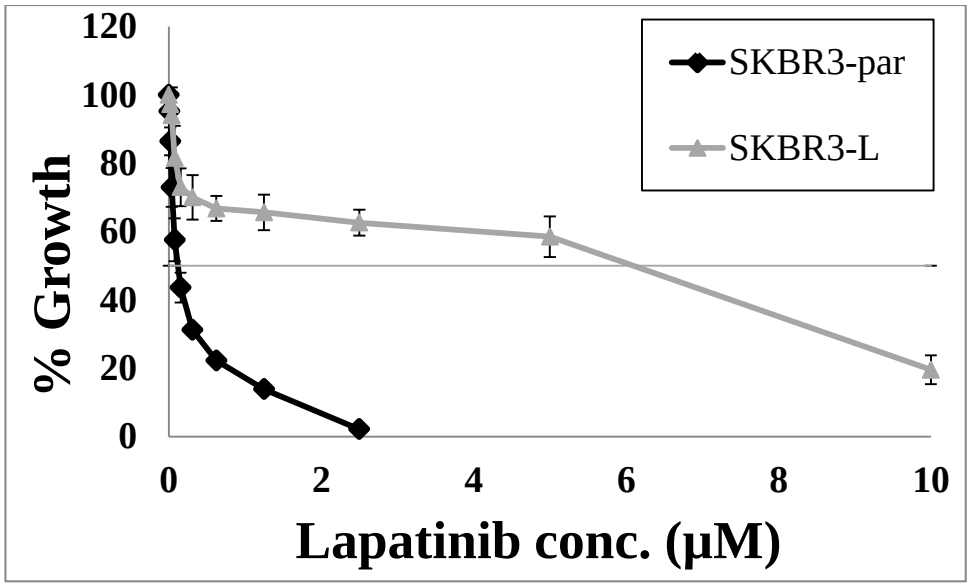

Figure 5-1: Proliferation of SKBR3-par and SKBR3-L cells following a 5 day treatment with lapatinib (0 – 10 µM). Growth is expressed relative to untreated control cells. Error bars represent the standard deviation of triplicate experiments.

5.2.2 Assessing the stability of lapatinib resistance

In order to assess the long-term stability of the resistant phenotype, drug withdrawal assays were performed. Lapatinib was removed from the media of SKBR3-L cells and the cells were cultured without lapatinib for approx. 4 months. The sensitivity of SKBR3-L cells to lapatinib was tested at 1 month intervals and the sensitivity of the SKBR3-par cells was measured concurrently with the SKBR3-L cells to ensure that there was no adverse effect of long-term culture on lapatinib sensitivity. After 1 month of growth in the absence of lapatinib, the lapatinib IC_{50} in SKBR3-L cells was 4.4 ± 1.5 µM lapatinib compared to 0.1 ± 0.0 µM in SKBR3-par cells ($p = 0.0372$) [Figure 5-2]. After 2 months of growth in the absence of lapatinib, the lapatinib IC_{50} in SKBR3-L cells was 3.8 ± 1.1 µM compared to 0.09 ± 0.01 µM in SKBR3-par cells ($p = 0.0130$). Although the lapatinib IC_{50} in SKBR3-L cells remained above 1 µM after both 1 and 2 months growth in the absence of lapatinib the IC_{50} values were lower than the initial lapatinib IC_{50} of 6.5 ± 0.4 µM and there was a high standard deviation between the replicates suggesting the lapatinib IC_{50} was varying over the course of the 3 replicates. This suggests that SKBR3-L cells are slower regaining sensitivity to lapatinib the longer they are grown in the absence of lapatinib.

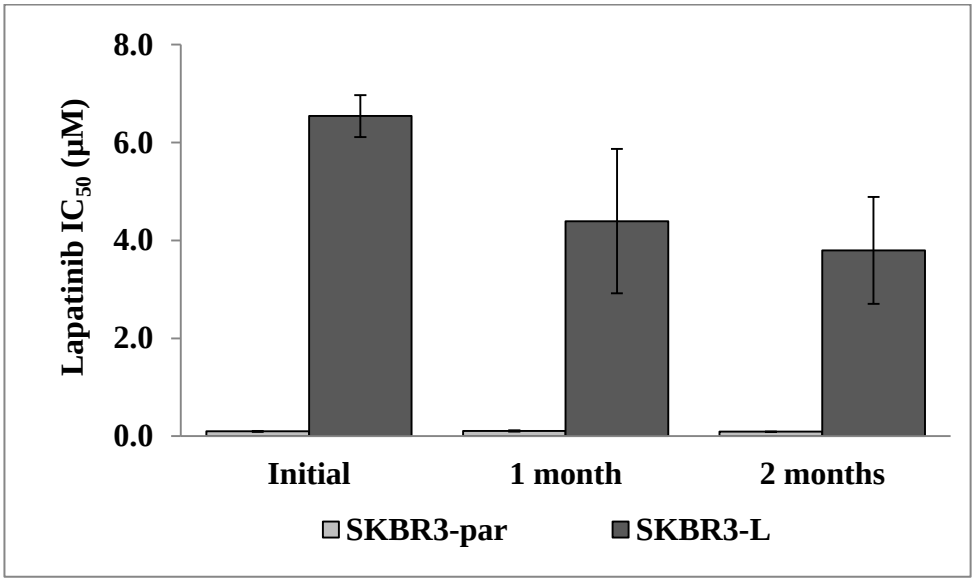

Figure 5-2: Lapatinib IC_{50} values for SKBR3-par and SKBR3-L cells following 1 and 2 months growth in the absence of lapatinib. IC_{50} values were calculated following a 5 day lapatinib treatment (0 – 2.5 µM). Error bars represent the standard deviation of triplicate experiments.

The sensitivity of both cell lines to lapatinib was tested again at the 3 month interval. However, it was not possible to get reproducible replicates at this time point as the IC_{50} values in SKBR3-L cells varied significantly. Over 2 weeks, and 4 independent replicates the lapatinib IC_{50} in SKBR3-L cells decreased from 4.6 µM to 0.2 µM lapatinib [Figure 5-3]. As a result accurate IC_{50} values with standard deviations could not be calculated at this time point. This data combined with the IC_{50} data generated after 1 month and 2 months of lapatinib withdrawal suggests that SKBR3-L cells slowly regain sensitivity to lapatinib over a 3-4 month period [Table 5-1].

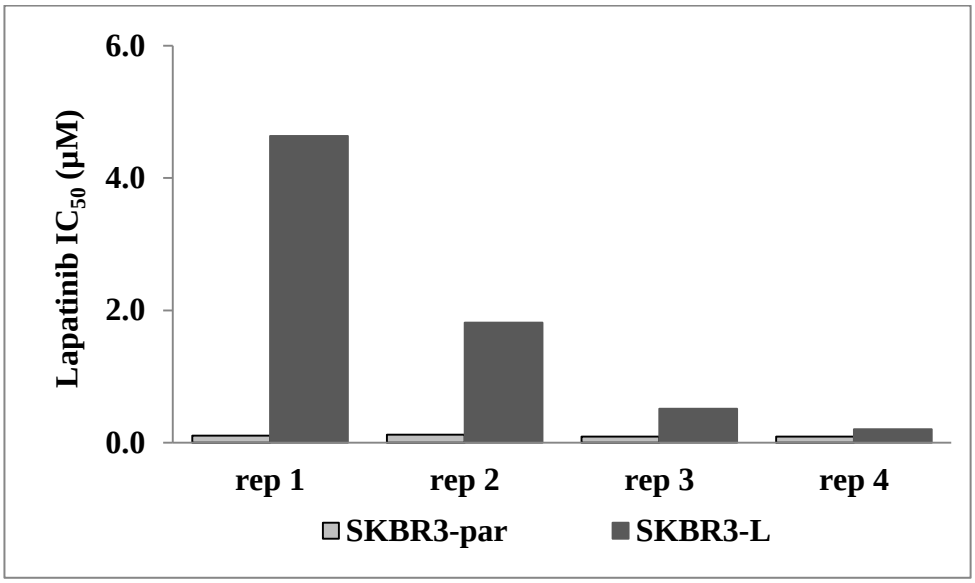

Figure 5-3: Lapatinib IC_{50} values for SKBR3-par and SKBR3-L cells following 12, 13, 14 and 15 weeks growth in the absence of lapatinib. IC_{50} values were calculated following a 5 day lapatinib treatment (0 – 2.5 µM). Each replicate is an independent experiment.

Table 5-1: Lapatinib IC_{50} values for SKBR3-par and SKBR3-L cells over the course of the lapatinib withdrawal experiment. Where indicated standard deviations are expressed for triplicate replicates.

IC_{50} (µM)	**SKBR3-par**	**SKBR3-L**
Initial	0.100 ± 0.011	6.540 ± 0.427
1 month	0.108 ± 0.015	4.392 ± 1.474
2 months	0.093 ± 0.002	3.794 ± 1.093
12 weeks (rep 1)	0.095	4.634
13 weeks (rep 2)	0.108	1.814
14 weeks (rep 3)	0.103	0.512
15 weeks (rep 4)	0.098	0.205

5.2.3 Analysis of HER2 signalling pathways

As lapatinib is a specific HER2/EGFR tyrosine kinase inhibitor, alterations in the phosphorylation and expression of HER2, EGFR, HER3 and HER4 between SKBR3-par and SKBR3-L were examined. The effect of lapatinib treatment on the phosphorylation and expression of these proteins was also examined.

5.2.3.1 Expression of HER2

There was no significant difference in the levels of HER2 between SKBR3-par and SKBR3-L cells ($p = 0.55$) [Figure 5-4]. However, SKBR3-L cells have significantly higher levels of phospho-HER2 compared to SKBR3-par cells ($p = 0.016$). Treatment of SKBR3-par cells with 1 µM lapatinib resulted in a decrease in phospho-HER2 levels ($p = 0.004$), but no change in total HER2 levels ($p = 0.452$). Treatment of SKBR3-L cells with 1 µM lapatinib also resulted in a significant decrease in phospho-HER2 levels ($p = 0.0007$) with no alteration in total HER2 levels ($p = 0.772$).

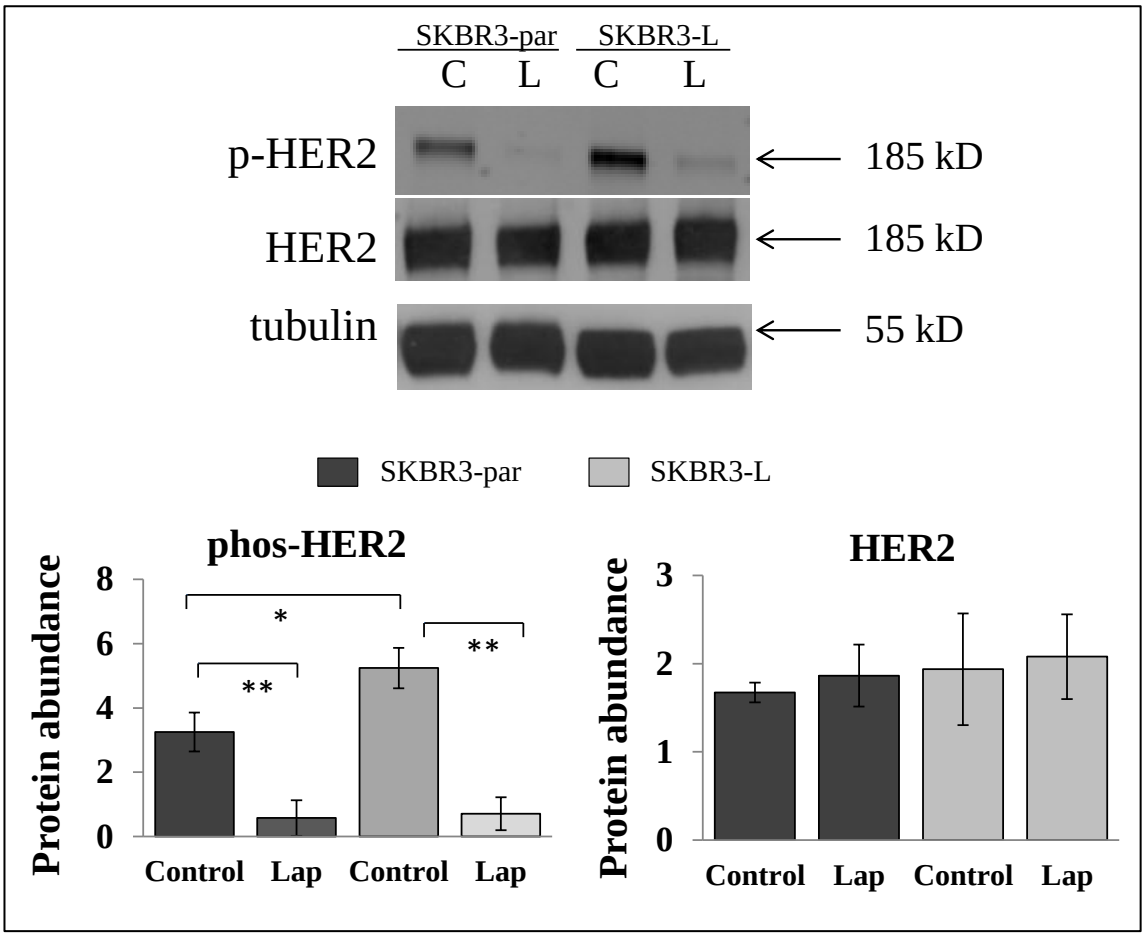

Figure 5-4: Immunoblotting for phospho-HER2 (Tyr1221/1222) and total HER2 in SKBR3-par and SKBR3-L cells following 24 hours treatment with 1μM lapatinib. α-tubulin was used as a loading control. Images are representative of triplicate experiments. Densitometry analysis of triplicate immunoblots was performed using ImageQuant software. * denotes $p \leq 0.05$, ** denotes $p \leq 0.001$.

5.2.3.2 Expression of EGFR

SKBR3-L cells express higher levels of EGFR ($p = 0.004$) and have higher levels of phospho-EGFR ($p = 0.024$) compared to SKBR3-par cells. Treatment of SKBR3-par cells with 1 μM lapatinib for 24 hours results in a non-significant decrease in phospho-EGFR ($p = 0.83$) and no change in total EGFR levels ($p = 0.48$) compared to untreated cells [Figure 5-5]. Treatment of SKBR3-L cells with 1 μM lapatinib for 24 hours results in a significant decrease in phospho-EGFR levels ($p = 0.009$) with no change in total EGFR levels ($p = 0.303$) compared to untreated cells.

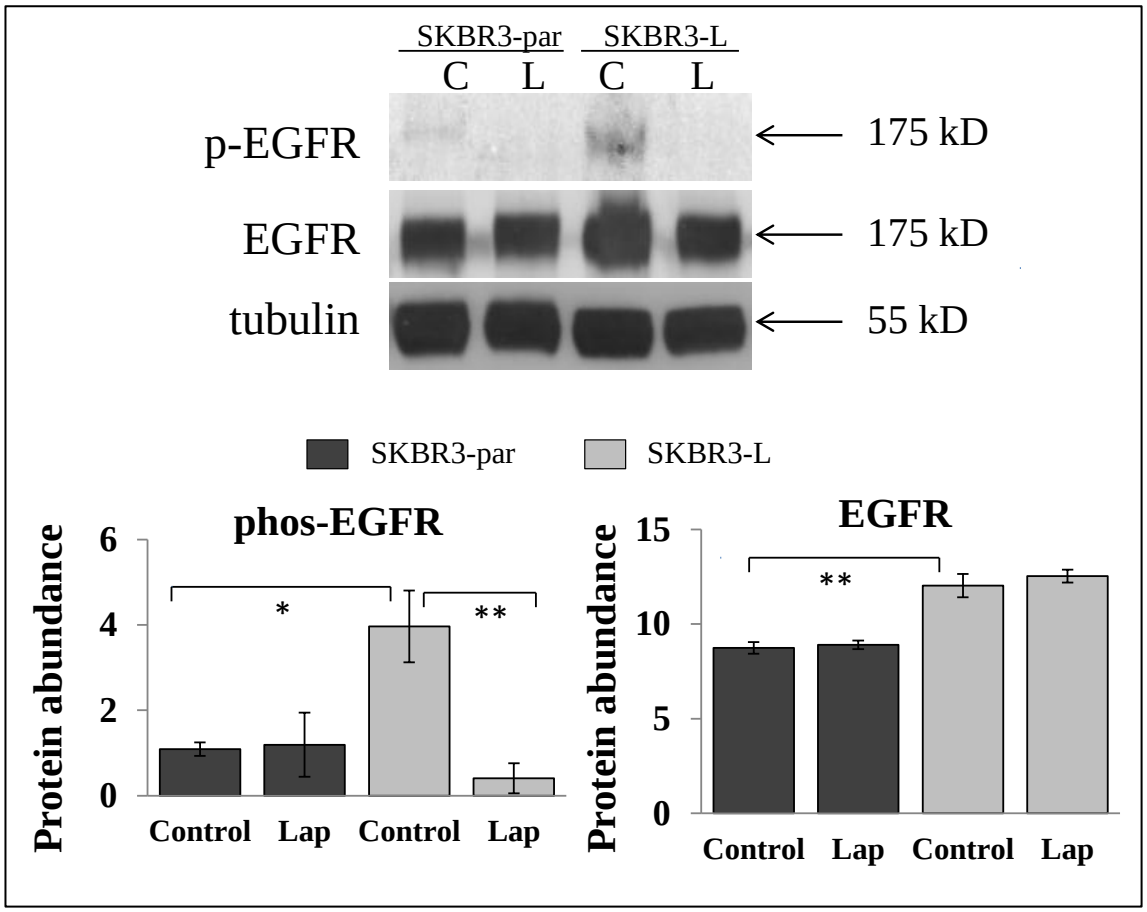

Figure 5-5: Immunoblotting for phospho-EGFR (Thr1173) and total EGFR in SKBR3-par and SKBR3-L cells following 24 hours treatment with 1μM lapatinib. α-tubulin was used as a loading control. Images are representative of triplicate experiments. Densitometry analysis of triplicate immunoblots was performed using ImageQuant software. * denotes $p \leq 0.05$, ** denotes $p \leq 0.001$.

5.2.3.3 Expression of HER3

There was no significant difference in the levels of phospho-HER3 ($p = 0.14$) between SKBR3-par and SKBR3-L cells. SKBR3-L cells have higher levels of total HER3 compared to SKBR3-par cells however, the difference failed to reached statistical significance ($p = 0.09$) [Figure 5-6]. Treatment of SKBR3-par cells with 1 μM lapatinib resulted in a significant decrease in phospho-HER3 levels ($p = 0.02$) and a significant increase in total HER3 levels ($p = 0.03$). Treatment of SKBR3-L cells with 1 μM lapatinib resulted in a significant decrease in phospho-HER3 levels ($p = 0.03$). There was also a 2.7-fold increase in total HER3 levels in SKBR3-L cells following lapatinib treatment ($p = 0.01$).

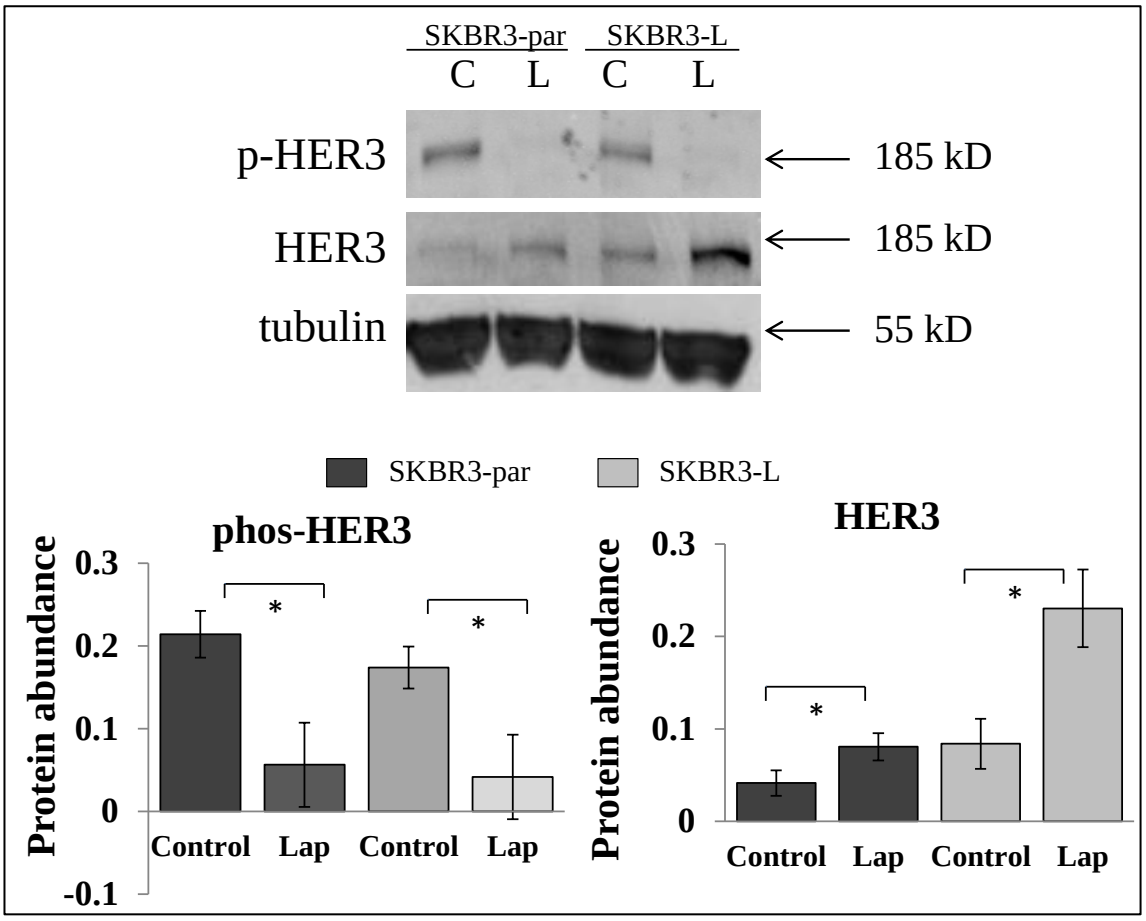

Figure 5-6: Immunoblotting for phospho-HER3 (Tyr1289) and total HER3 in SKBR3-par and SKBR3-L cells following 24 hours treatment with 1μM lapatinib. α-tubulin was used as a loading control. Images are representative of triplicate experiments. Densitometry analysis of triplicate immunoblots was performed using ImageQuant software. * denotes $p \leq 0.05$, ** denotes $p \leq 0.001$.

5.2.3.1 Expression of HER4

SKBR3-par cells express significantly higher levels of HER4 compared to SKBR3-L cells ($p = 0.04$) [Figure 5-7]. Treatment with 1 μM lapatinib did not affect the levels of HER4 in either SKBR3-par ($p = 0.93$) or SKBR3-L cells ($p = 0.21$).

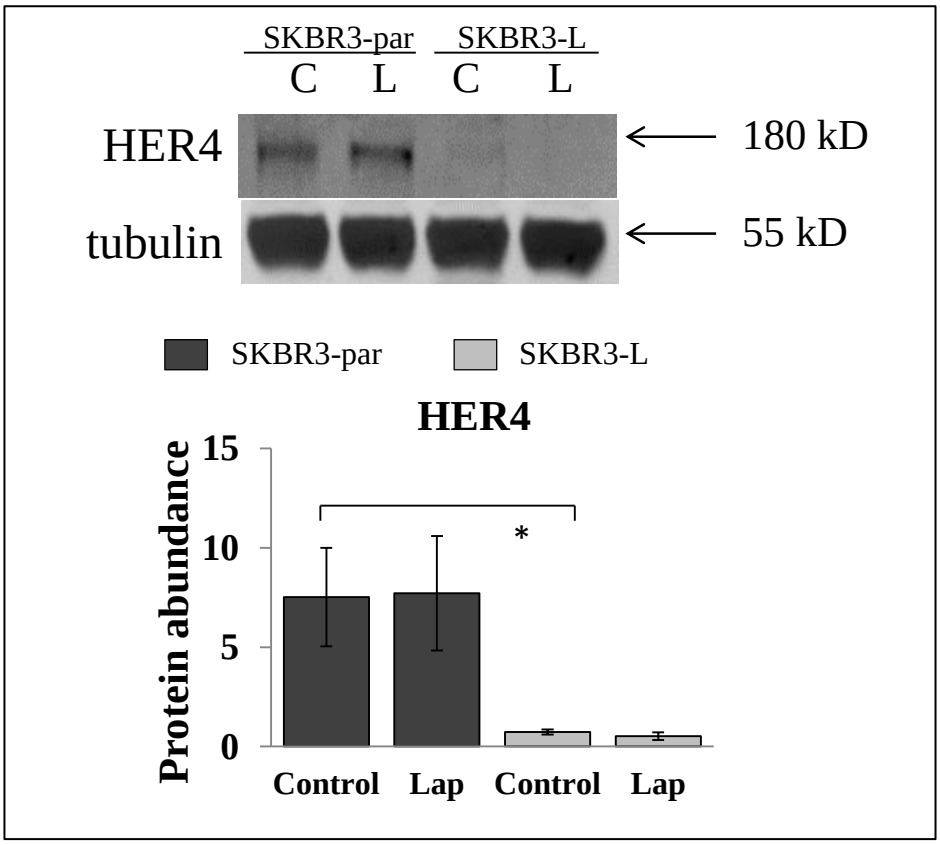

Figure 5-7: Immunoblotting for HER4 in SKBR3-par and SKBR3-L cells following 24 hours treatment with 1μM lapatinib. α-tubulin was used as a loading control. Images are representative of triplicate experiments. Densitometry analysis of triplicate immunoblots was performed using ImageQuant software. * denotes $p \leq 0.05$, ** denotes $p \leq 0.001$.

5.2.4 Alterations in MAPK and P13K/AKT signalling pathways

SKBR3-L cells have significantly lower levels of phospho-AKT compared to SKBR3-par cells ($p = 0.0009$), in fact levels of phospho-AKT are barely detectable in SKBR3-L cells [Figure 5-8]. Levels of phospho-ERK are also decreased in SKBR3-L cells compared to SKBR3-par ($p = 0.009$), while there are no significant differences in the expression of total AKT ($p = 0.18$) or total ERK ($p = 0.21$) between the 2 cell lines. Treatment of SKBR3-par cells with 1 μM lapatinib for 24 hours resulted in a significant decrease in phospho-AKT ($p = 0.0008$) and phospho-ERK ($p = 0.003$) without any changes in the levels of total AKT ($p = 0.39$) or total ERK ($p = 0.93$). Treatment of SKBR3-L cells with 1 μM lapatinib for 24 hours resulted in no significant changes in the levels of phospho-AKT ($p = 0.45$), AKT ($p = 0.22$), phospho-ERK ($p = 0.39$) or ERK ($p = 0.93$).

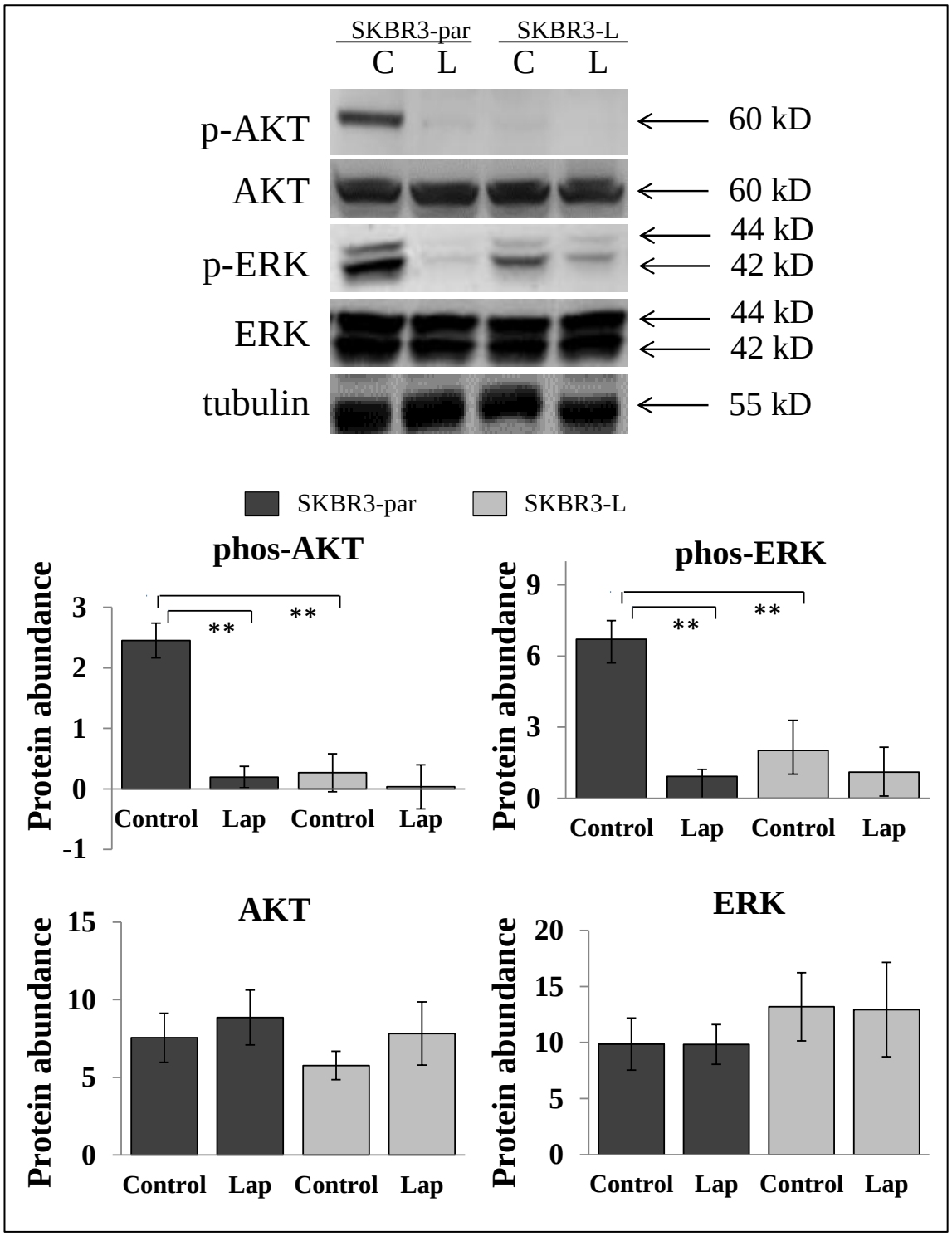

Figure 5-8: Immunoblotting for phospho- (Ser473) and total AKT, and phospho- (Thr202/Tyr204) and total ERK in SKBR3-par and SKBR3-L cells treated with 1 µM lapatinib for 24 hours. α-tubulin was used as a loading control on each gel. Images are representative of triplicate experiments. Densitometry analysis of triplicate immunoblots was performed using ImageQuant software. * denotes $p \leq 0.05$, ** denotes $p \leq 0.001$.

5.2.5 Sensitivity of SKBR3-L cells to EGFR inhibition

As previously shown in Figure 5-5, SKBR3-L cells express higher levels of EGFR ($p = 0.004$) and have higher levels of phospho-EGFR ($p = 0.024$) compared to SKBR3-par cells. Therefore, the sensitivity of both cell lines to the EGFR inhibitor gefitinib was examined. SKBR3-L cells are significantly less sensitive to gefitinib with an IC_{50} of 4.9 ± 1.1 µM compared to 0.8 ± 0.2 µM in SKBR3-par cells ($p = 0.02$) [Figure 5-9]. This suggests that SKBR3-L cells are resistant to both HER2 and EGFR inhibition.

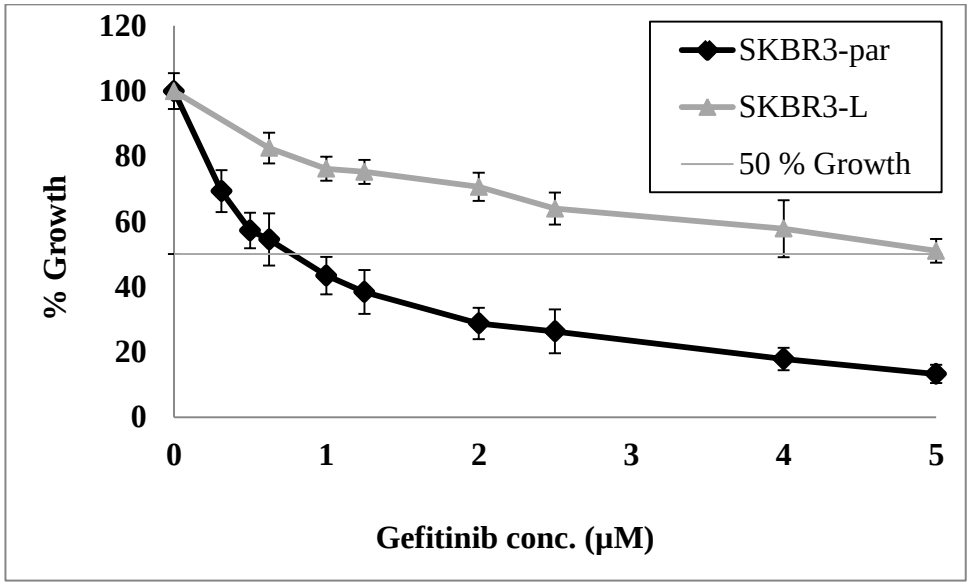

Figure 5-9: Proliferation of SKBR3-par and SKBR3-L cells following a 5 day treatment with gefitinib (0 – 5 µM). Growth is expressed relative to untreated control cells. Error bars represent the standard deviation of triplicate experiments.

5.2.6 Sensitivity of SKBR3-L cells to IGF-IR inhibition

Increased IGF-IR signalling has been associated with resistance to trastuzumab. Therefore, the expression of IGF-IR was examined in SKBR3-L cells to determine whether altered IGF-1R signalling is specific to trastuzumab resistance or more broadly relevant to resistance to HER2 inhibitors. SKBR3-L cells express significantly higher levels of IGF-IR ($p = 0.02$) and have higher levels of phospho-IGF-1R ($p = 0.01$) compared to SKBR3-par cells [Figure 5-10].

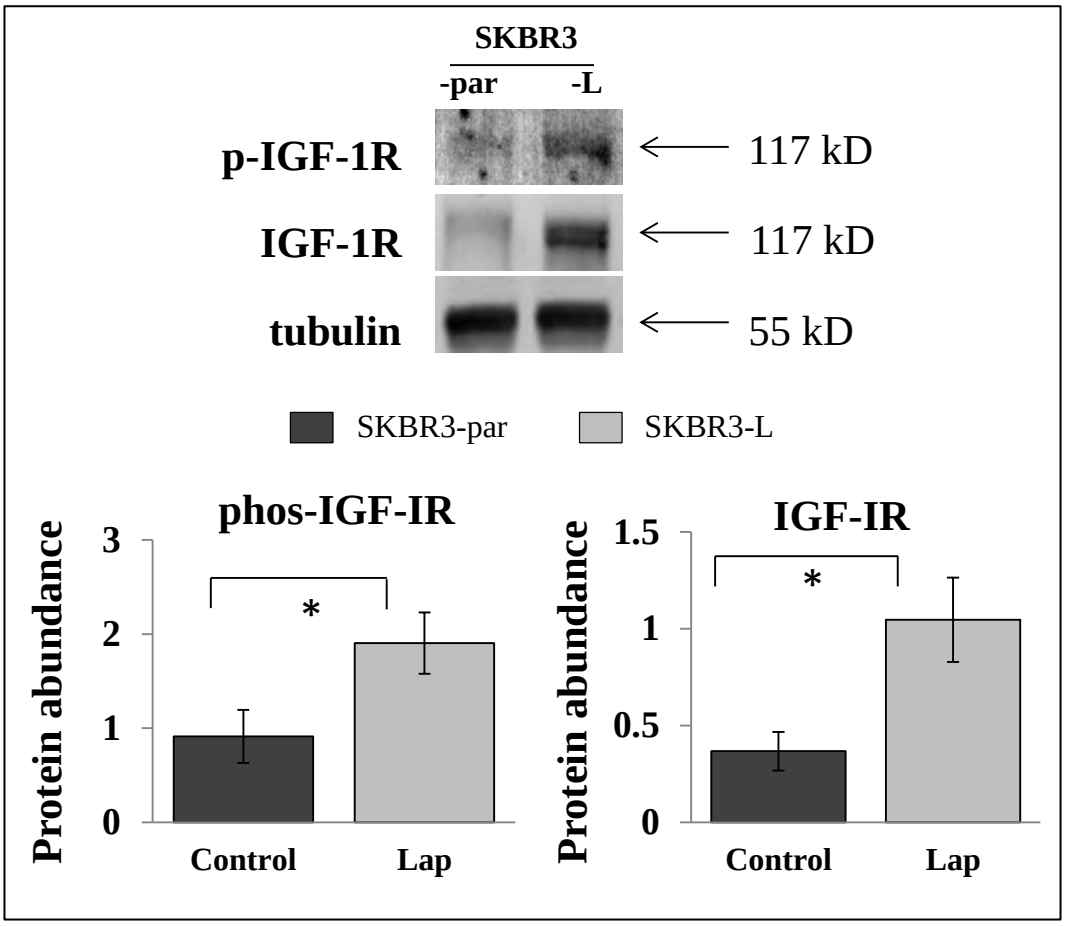

Figure 5-10: Immunoblotting for phospho-IGF-1R (Thr1131) and total IGF-1R in SKBR3-par and SKBR3-L cells. α-tubulin was used as a loading control. Images are representative of triplicate experiments. Densitometry analysis of triplicate immunoblots was performed using ImageQuant software. * denotes $p \leq 0.05$

To examine whether the increased phosphorylation and expression of IGF-1R resulted in an alteration in sensitivity to IGF-1R inhibition, the cells were treated with two anti-IGF-IR TKIs; NVP-AEW541 and BMS-536924. The NVP-AEW541 IC_{50} in SKBR3-L cells was 8.4 ± 0.6 μM compared to 6.3 ± 0.1 μM in SKBR3-par cells, making SKBR3-L cells slightly less sensitive to NVP-AEW541 than SKBR3-par ($p = 0.03$) [Figure 5-11]. The BMS-536924 IC_{50} in SKBR3-L cells was 6.4 ± 0.3 μM compared to 7.6 ± 0.3 μM in SKBR3-par cells. In contrast to the NVP-AEW541 results SKBR3-L cells were slightly more sensitive to BMS-536924 than SKBR3-par cells ($p = 0.01$) [Figure 5-12].

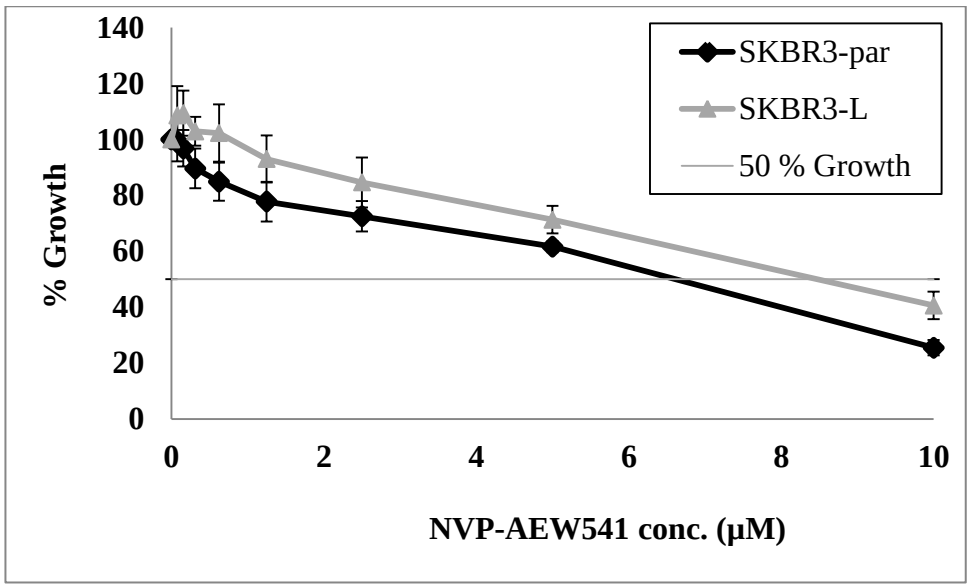

Figure 5-11: Proliferation of SKBR3-par and SKBR3-L cells following a 5 day treatment with NVP-AEW541 (0 – 10 µM). Growth is expressed relative to untreated control cells. Error bars represent the standard deviation of triplicate experiments.

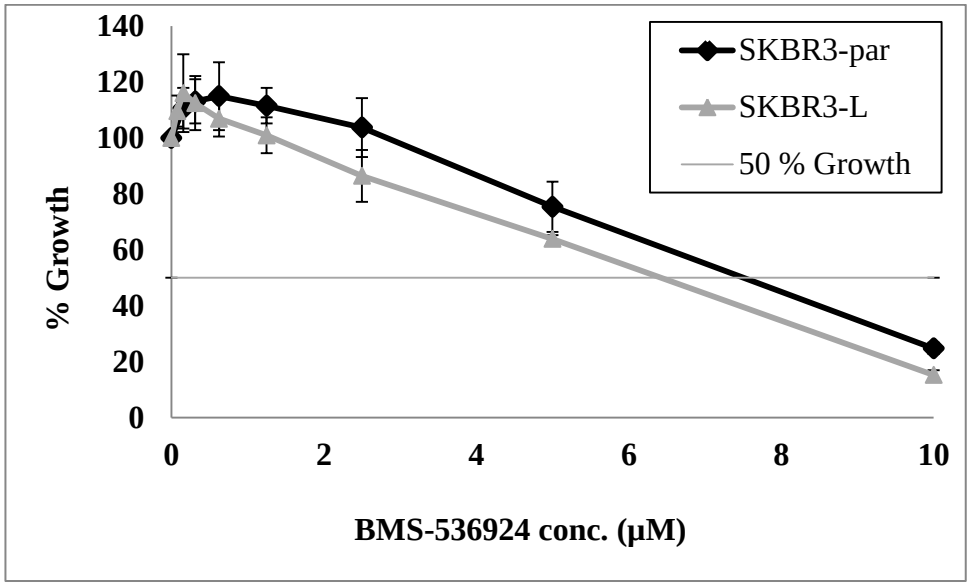

Figure 5-12: Proliferation of SKBR3-par and SKBR3-L cells following a 5 day treatment with BMS-536924 (0 – 10 µM). Growth is expressed relative to untreated control cells. Error bars represent the standard deviation of triplicate experiments.

5.2.7 Examination of previously published mechanisms of acquired lapatinib resistance

The overexpression and/or upregulation of the following proteins have been shown in previously published cell line models of acquired lapatinib resistance; ER, MCL-1, SRC, and XIAP. Levels of ER were undetectable in SKBR3-par and SKBR3-L cells [Figure 5-13] (a positive control for ER (BT474 cells) was included on each replicate blot and was detected (not shown)). There were no significant changes in the levels of XIAP or phospho-SRC between SKBR3-par and SKBR3-L cells, and treatment of either cell line with 1 μM lapatinib for 24 hours did not affect the levels of these proteins in either cell line. Expression of MCL-1 was increased in SKBR3-L cells compared to SKBR3-par ($p = 0.04$), while treatment with lapatinib did not affect the expression of MCL-1 in either cell line.

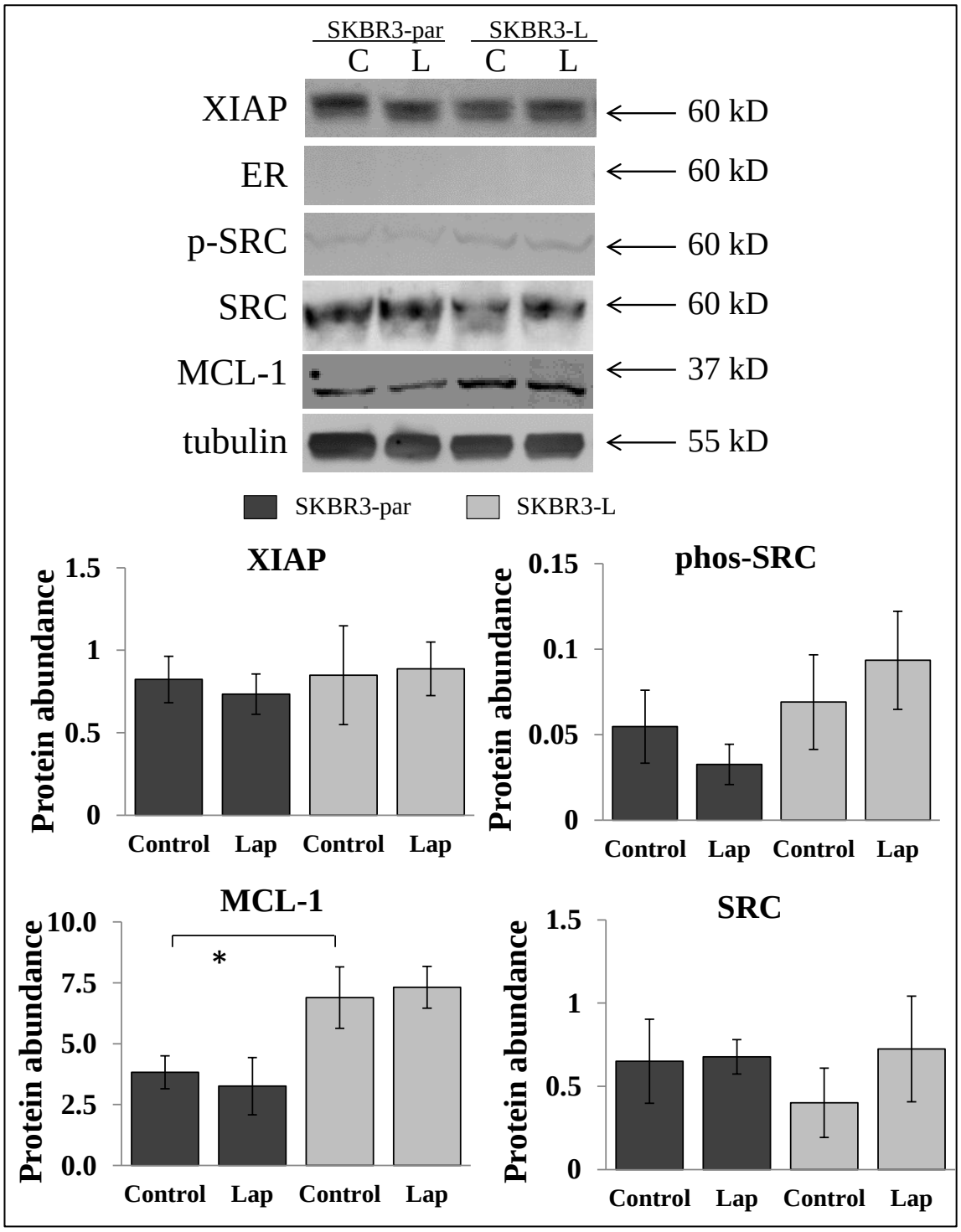

Figure 5-13: Immunoblotting for XIAP, ER, phospho- (Tyr416) and total SRC, and MCL-1 in SKBR3-par and SKBR3-L cells treated with 1 μM lapatinib for 24 hours. α-tubulin was used as a loading control on each gel. Images are representative of triplicate experiments. Densitometry analysis of triplicate immunoblots was performed using ImageQuant software. * denotes $p \leq 0.05$

5.3 Validation of eEF2, a phospho-protein down-regulated in SKBR3-L cells

A phospho-proteomic comparison of the SKBR3-par and SKBR3-L cell lines was previously performed using 2D-DIGE and MALDI-ToF/ToF MS [255]. Protein lysates were prepared, enriched for phospho-proteins, separated by 2D-gel electrophoresis and identified using MS analysis. Forty-one differentially regulated phospho-proteins were identified, 20 were significantly higher and 21 were significantly lower in abundance in SKBR3-L compared to SKBR3-par. Proteins identified included heat shock proteins, translation, degradation and metabolism-related proteins. Several phosphorylated forms of eukaryotic elongation factor 2 (eEF2) were identified. One form of phospho-eEF2 was up-regulated and 6 forms were down-regulated in SKBR3-L compared to SKBR3-par.

5.3.1 Decrease in phospho-eEF2 in SKBR3-L cells

Phosphorylation of eEF2 at Thr56 inhibits the activity of eEF2 which in turn causes a decrease in protein synthesis. In order to confirm the 2D-DIGE results, immunoblotting for phospho-eEF2 was performed on SKBR3-par and SKBR3-L cells. SKBR3-L cells have significantly lower levels of phospho-eEF2 compared to SKBR3-par cells ($p = 0.0001$). There is no significant difference in the levels of total eEF2 between the 2 cell lines ($p = 0.55$) [Figure 5-14].

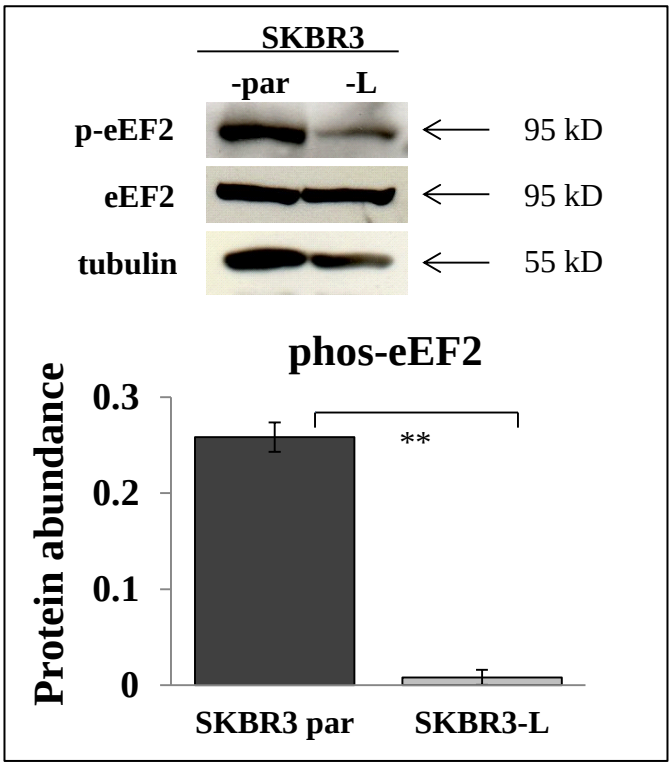

Figure 5-14: Immunoblotting for phospho-eEF2 (Thr56) and total eEF2 in SKBR3-par and SKBR3-L cells. α-tubulin was used as a loading control on each gel. Images are representative of triplicate experiments. Densitometry analysis of triplicate immunoblots was performed using ImageQuant software. * denotes $p \leq 0.05$, ** denotes $p \leq 0.001$.

5.3.2 Effect of lapatinib treatment on levels of phospho-eEF2

Treatment of SKBR3-par cells with 1 μM lapatinib for 24 hours results in a significant increase in the levels of phospho-eEF2 compared to untreated cells ($p = 0.0008$) [Figure 5-15]. Treatment of SKBR3-L cells with 1 μM lapatinib for 24 hours has no effect on the levels of phospho-eEF2 compared to untreated cells ($p = 0.373$).

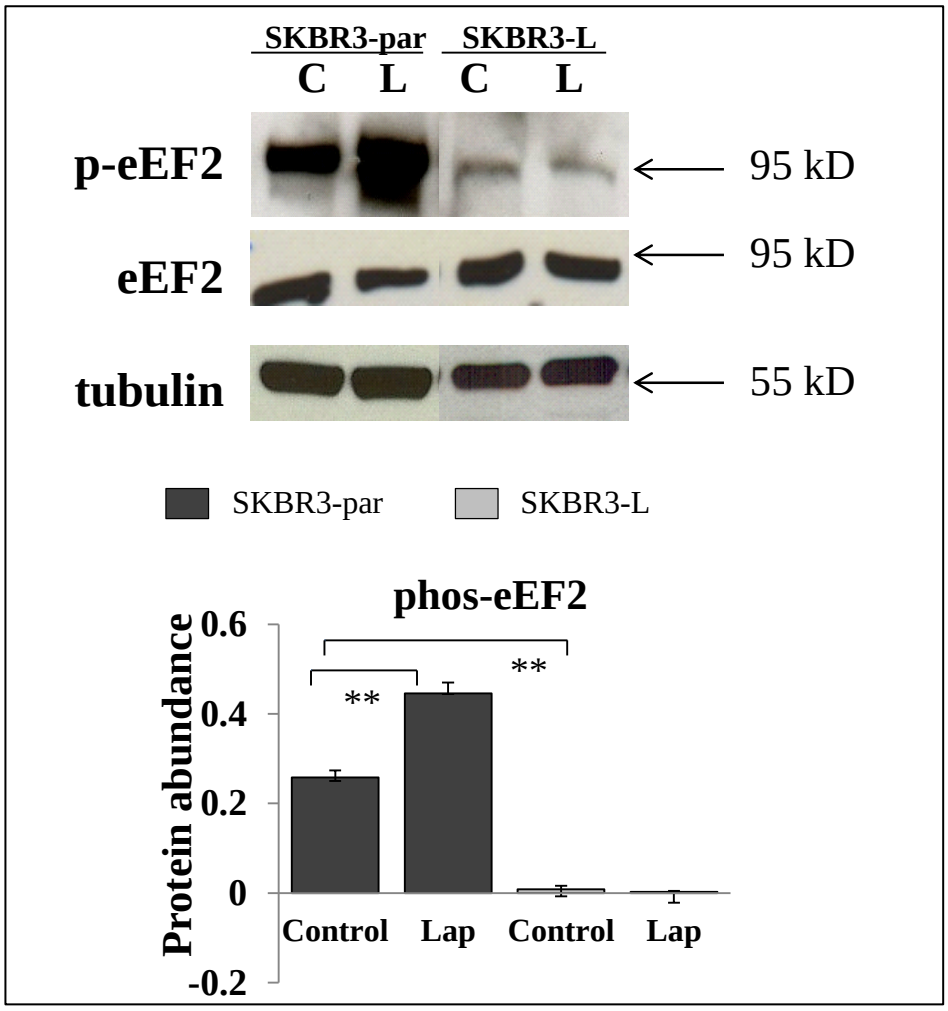

Figure 5-15: Immunoblotting for phospho-eEF2 (Thr56) and total eEF2 in SKBR3-par and SKBR3-L cells treated with 1 μM lapatinib for 24 hours. α-tubulin was used as a loading control on each gel. Images are representative of triplicate experiments. Densitometry analysis of triplicate immunoblots was performed using ImageQuant software. * denotes $p \leq 0.05$, ** denotes $p \leq 0.001$.

5.3.3 Role of eEF2k in regulation of eEF2 phosphorylation

eEF2k phosphorylates eEF2 at Thr56 leading to its inactivation. The activity of eEF2k is also negatively regulated by phosphorylation. Thus, we examined the expression and phosphorylation of eEF2k in SKBR3-par and SKBR3-L cells. SKBR3-L cells have higher levels of total eEF2k compared to SKBR3-par cells ($p = 0.017$), and treatment of either cell line with 1 μM lapatinib had no effect on the expression of eEF2k [Figure 5-16]. eEF2k is phosphorylated at Ser366 via mTOR signalling, thus, we examined the mTOR-mediated phosphorylation of eEF2k. SKBR3-L cells have higher levels of Ser366 phosphorylation of eEF2k compared to SKBR3-par cells ($p = 0.042$). However,

lapatinib treatment of SKBR3-par cells caused a significant increase in eEF2k phosphorylation at Ser366 ($p = 0.033$), which would suggest decreased activity of eEF2k leading to decreased phosphorylation of eEF2, however, as previously seen in Figure 5-15 treatment of SKBR3-par cells with lapatinib results increased phosphorylation of eEF2. This result suggests that the phosphorylation of eEF2 is not regulated by mTOR signalling in SKBR3-par cells. The phosphorylation of eEF2k at another site, Ser359 was then examined. SKBR3-L cells have higher levels of Ser359 phosphorylation of eEF2k compared to SKBR3-par cells ($p = 0.003$) [Figure 5-16]. Importantly, treatment of SKBR3-par cells with 1 μM lapatinib results in decreased phosphorylation of Ser359 of eEF2k ($p = 0.047$) which correlates with the increased phosphorylation of eEF2 following lapatinib treatment. While there was a small decrease in phosphorylation eEF2k at Ser359 in SKBR3-par cells following lapatinib treatment, the decrease was not significant ($p = 0.239$). Taken together these results suggest that the phosphorylation of eEF2 is regulated by phosphorylation of Ser359 of eEF2k in SKBR3 cells.

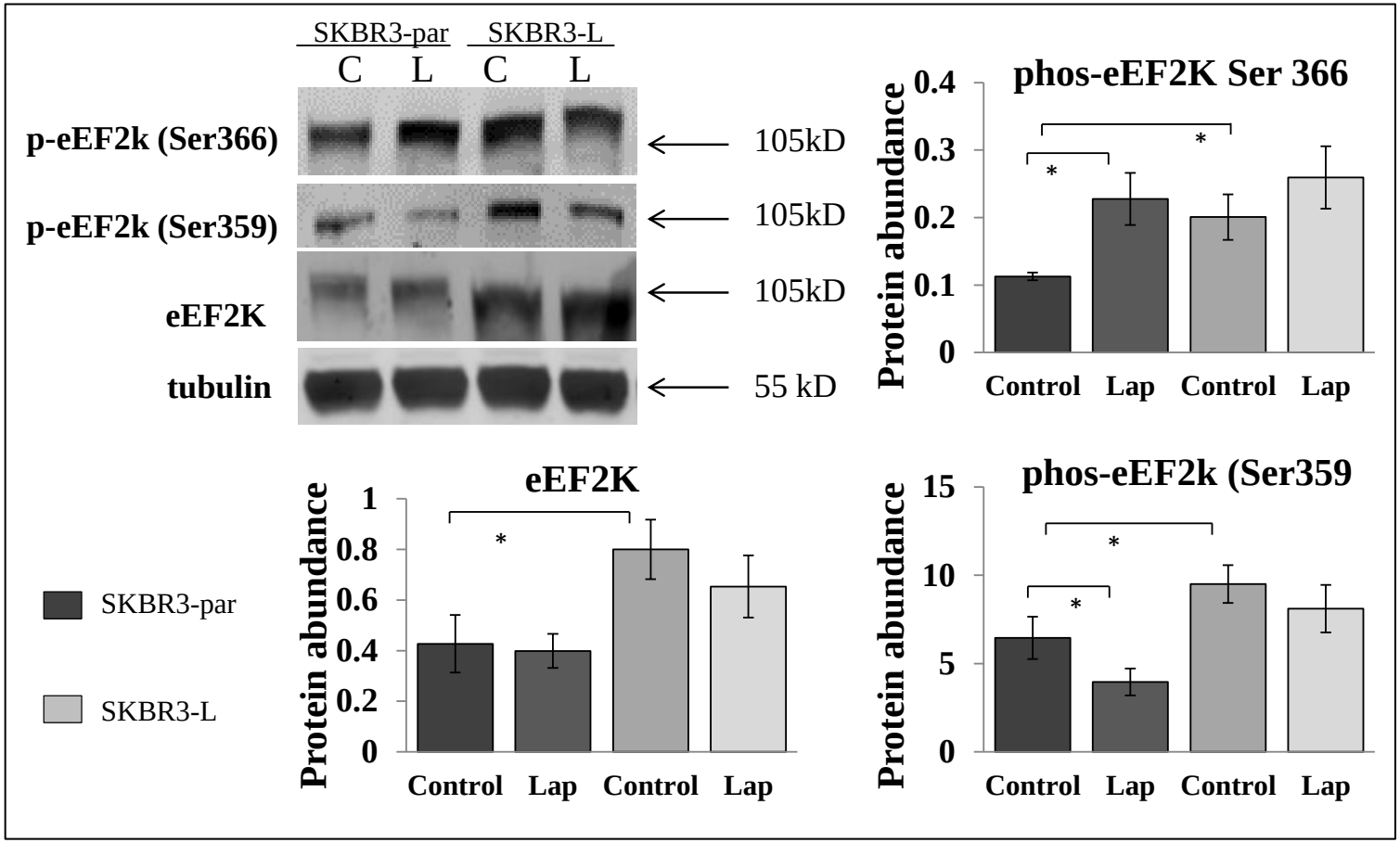

Figure 5-16: Immunoblotting for phospho-eEF2k (Ser366 and Ser359), and total eEF2k in SKBR3-par and SKBR3-L cells treated with 1 μM lapatinib for 24 hours. α-tubulin was used as a loading control on each gel. Images are representative of triplicate experiments. Densitometry analysis of triplicate immunoblots was performed using ImageQuant software. * denotes $p \leq 0.05$, ** denotes $p \leq 0.001$.

5.3.4 mTOR and phosphorylation of eEF2

The above results have indicated that phosphorylation of Ser366 of eEF2k does not regulate the phosphorylation of eEF2, suggesting that eEF2 phosphorylation is mTOR-independent. To determine whether or not mTOR signalling plays a role in eEF2 regulation, the expression and phosphorylation of mTOR in SKBR3-par and SKBR3-L cells was examined. There was no significant difference in the expression of mTOR between the two cell lines and treatment of either cell line with lapatinib had no effect on the expression of mTOR [Figure 5-17]. The levels of phosphorylated mTOR (Ser2448) were significantly lower in SKBR3-L cells compared to SKBR3-par cells ($p = 0.01$) and interestingly, treatment of either cell line with 1 µM lapatinib significantly decreased the phosphorylation of mTOR ((SKBR3-par ($p = 0.005$), SKBR3-L ($p = 0.028$)), indicating that lapatinib inhibits mTOR signalling in both cell lines. Examining whether inhibition of mTOR with rapamycin, lapatinib or a combination of lapatinib and rapamycin would affect the phosphorylation of eEF2 in SKBR3-par and SKBR3-L revealed that SKBR3-par cells exhibit a similar increase in phosphorylation of eEF2 in response to rapamycin, lapatinib or lapatinib and rapamycin combined. However, there was no change in the phosphorylation of eEF2 in SKBR3-L cells in response to any of the treatments. Taken together, these results suggest that the regulation of eEF2 in SKBR3-L cells is mTOR-independent.

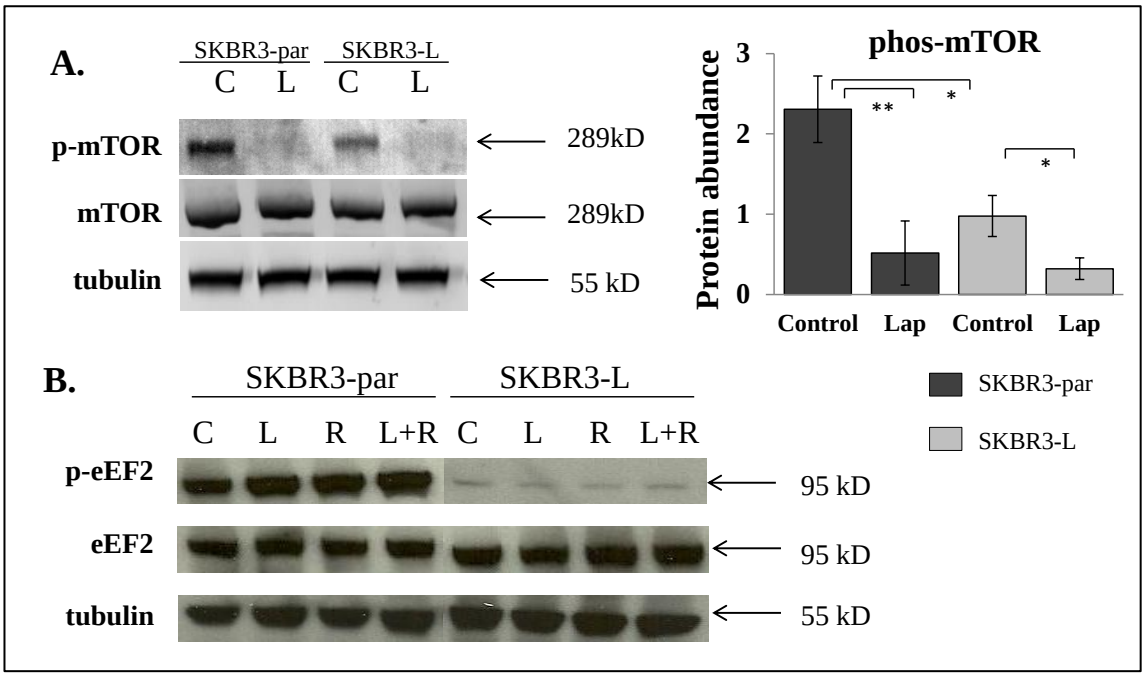

Figure 5-17: (A) Immunoblotting for phospho-mTOR (Ser2448), and total mTOR in SKBR3-par and SKBR3-L cells treated with 1 μM lapatinib for 24 hours. α-tubulin was used as a loading control on each gel. Images are representative of triplicate experiments. Densitometry analysis of triplicate immunoblots was performed using ImageQuant software. * denotes $p \leq 0.05$, ** denotes $p \leq 0.001$, (B) Immunoblotting for phospho-eEF2 (Thr56), and total eEF2 in SKBR3-par and SKBR3-L cells treated with 100 nM lapatinib (L), 1 nM rapamycin (R), or a combination of 100 nM lapatinib and 1 nM rapamycin (L+R) for 24 hours. α-tubulin was used as a loading control on each gel. Images are representative of duplicate experiments.

5.3.5 Altered phosphorylation of p70S6k in acquired lapatinib resistance

p70S6k lies downstream of mTOR and upstream of eEF2k. There was no difference in the levels of total p70S6k between SKBR3-par and SKBR3-L cells, nor was there a difference in the level of phosphorylation of p70S6k between SKBR3-par and SKBR3-L cells [Figure 5-18]. However, when SKBR3-par cells were treated with lapatinib there was a significant decrease in phospho-p70S6k levels ($p = 0.006$). In contrast, there was no change in the phosphorylation of p70S6k in response to lapatinib treatment in SKBR3-L cells ($p = 0.408$).

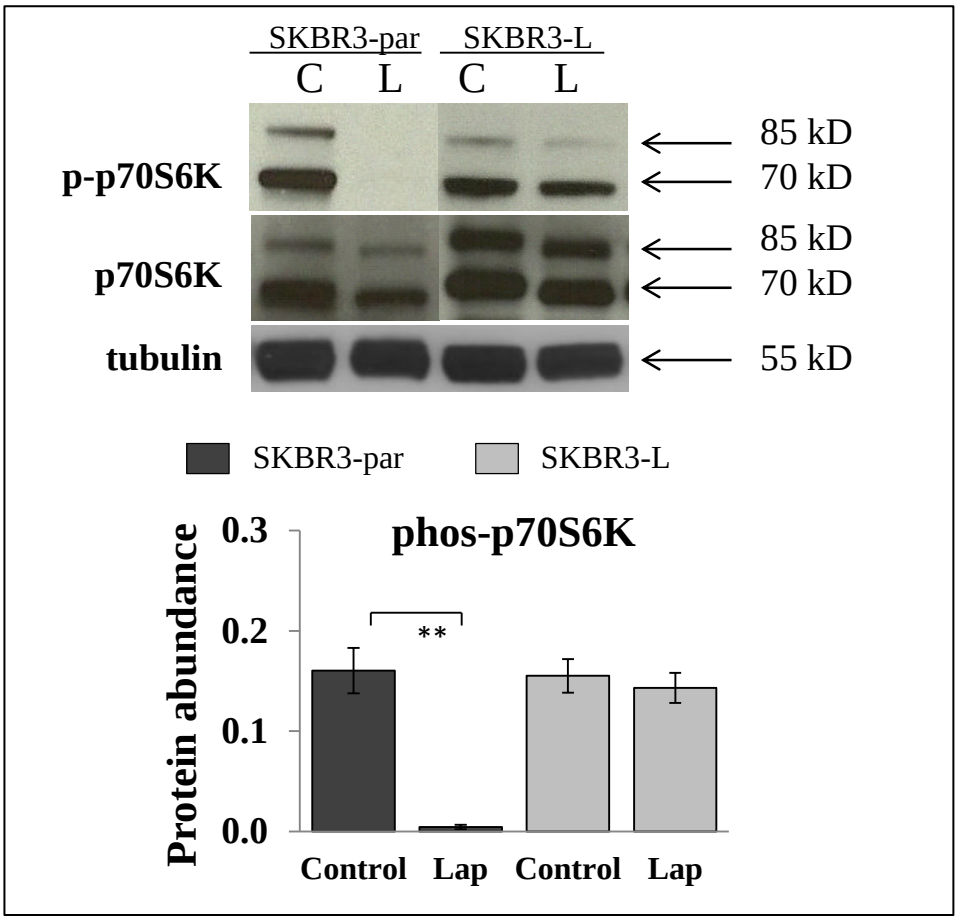

Figure 5-18: Immunoblotting for phospho-p70S6k (Thr389), and total p70S6k in SKBR3-par and SKBR3-L cells treated with 1 μM lapatinib for 24 hours. α-tubulin was used as a loading control on each gel. Images are representative of triplicate experiments. Densitometry analysis of triplicate immunoblots was performed using ImageQuant software. * denotes $p \leq 0.05$, ** denotes $p \leq 0.001$.

5.3.4 eEF2k in acquired lapatinib resistance

There is increased phosphorylation and expression of eEF2k in SKBR3-L cells compared to SKBR3-par cells. In addition there is decreased phosphorylation of Ser359 of eEF2k in SKBR3-par cells, resulting in increased activity, in response to lapatinib which correlates with increased phosphorylation of eEF2. These results suggest a role for altered eEF2k activity in lapatinib resistance. Thus, inhibition of eEF2k activity may result in decreased sensitivity to lapatinib in SKBR3-par cells. NH125 is a tyrosine kinase inhibitor of eEF2k, and inhibition of eEF2k with NH125 results in the dephosphorylation of eEF2. The effect of eEF2k inhibition on the levels of phospho-eEF2, was examined at varying concentrations. Treatment of SKBR3-par cells with 100

nM (p = 0.009), 250 nM (p = 0.025) or 500 nM (p = 0.019) significantly reduced the levels of phospho-eEF2 [Figure 5-19]. Treatment of SKBR3-par cells with the eEF2k inhibitor did not alter the levels of phospho-AKT or phospho-ERK at any of the concentrations tested suggesting specificity for eEF2k at the concentrations tested.

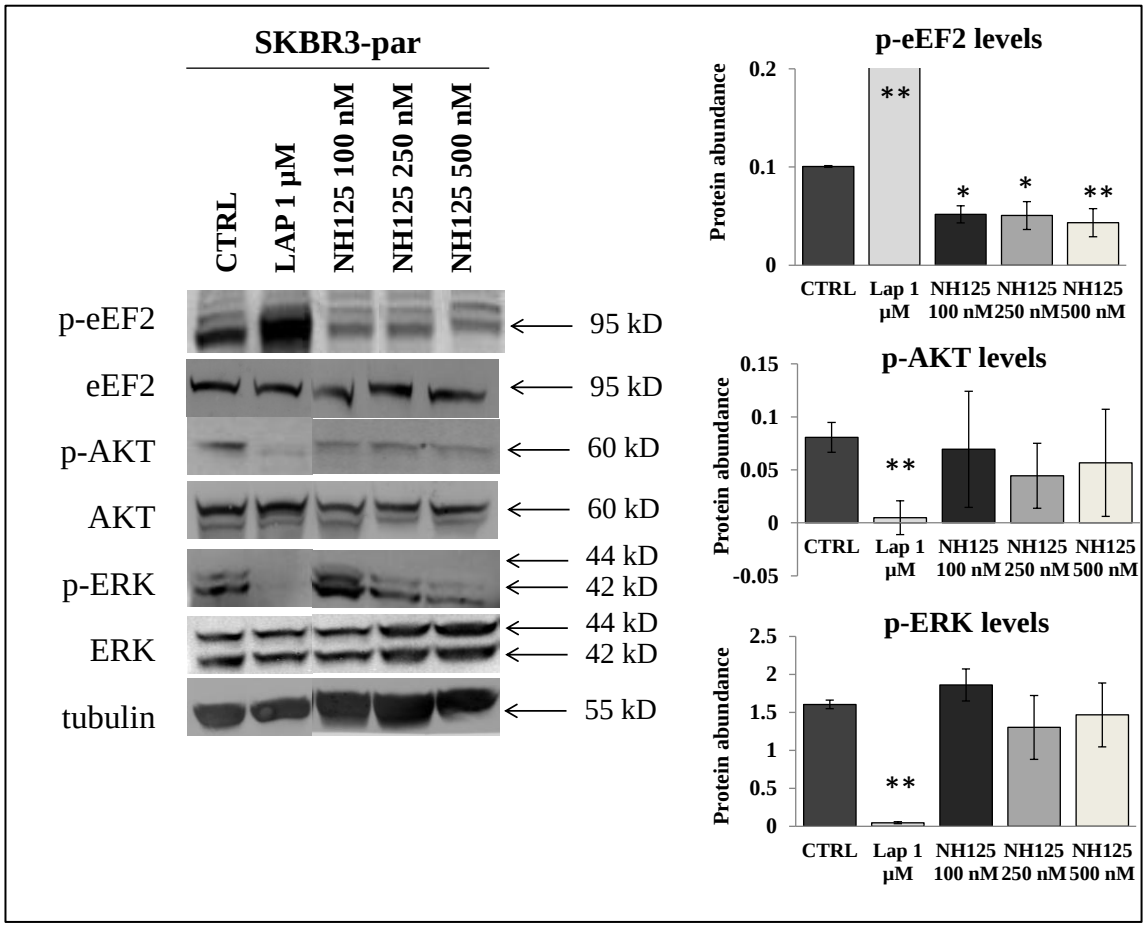

Figure 5-19: Immunoblotting for phospho-eEF2 (Thr56), phospho-AKT (Ser473), phospho-ERK (Thr202/Tyr204) and total eEF2, AKT and ERK in SKBR3-par cells treated with lapatinib (1 µM) or eEF2k inhibitor NH125 at 100, 250 and 500 nM for 24 hours. α-tubulin was used as a loading control. Images are representative of triplicate experiments. Densitometry analysis of triplicate immunoblots was performed using ImageQuant software. * denotes $p \leq 0.05$, ** denotes $p \leq 0.001$.

After confirming that inhibition of eEF2k with NH125 reduced the phosphorylation of eEF2 in SKBR3-par cells, the effect of NH125 in combination with lapatinib on the growth of SKBR3-par cells was examined. SKBR3-par cells were pre-treated with 100 nM NH125; a concentration that effectively inhibits the phosphorylation of eEF2 without significantly affecting cell growth. After 24 hours, NH125 was removed from the media and the cells were treated with 250 nM lapatinib for 5 days. The combination of NH125 pre-treatment and lapatinib resulted in 70.8 % inhibition of growth compared to 77.4 % in cells treated with lapatinib alone ($p = 0.03$) [Figure 5-20]. This suggests the NH125 pre-treatment decreases the sensitivity of SKBR3-par cells to lapatinib. However, when 24 hour NH125 (100 nM) pre-treatment was performed prior to assessing the lapatinib IC_{50} in SKBR3-par cells, the NH125 pre-treatment did not decrease lapatinib sensitivity in SKBR3-par cells [Figure 5-21]. In fact, NH125 pre-treatment resulted in a small increase the sensitivity of SKBR3-par cells to lapatinib; 0.1 µM lapatinib alone compared to 0.08 µM in pre-treated cells. NH125 failed to decrease the sensitivity of SKBR3-par cells to lapatinib in a range of different concentrations and combinations [see appendix Figures 9-1 – 9-3]. These results suggest that inhibition of eEF2k with NH125 can decrease the sensitivity of SKBR3-par cells to lapatinib but only under very specific conditions.

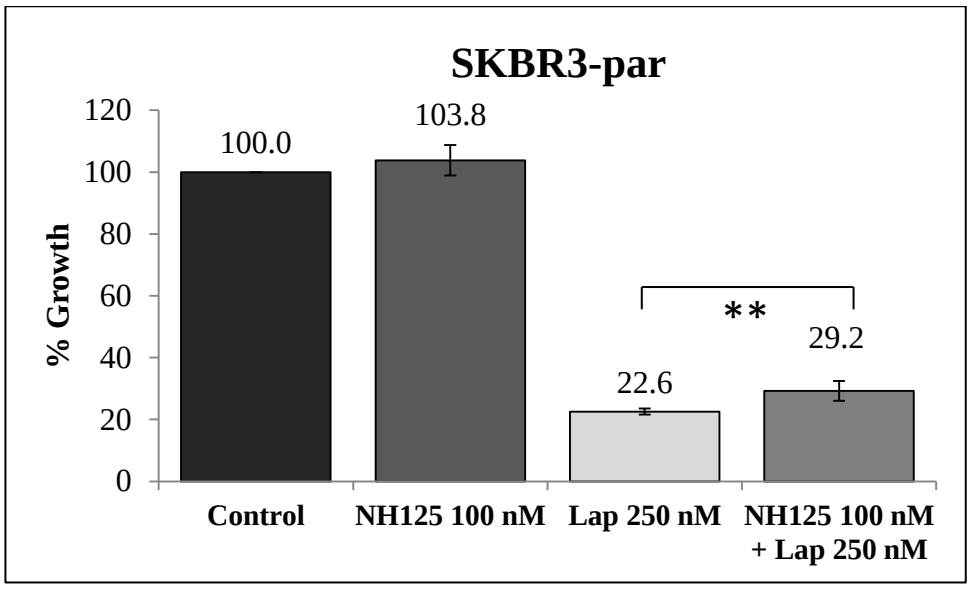

Figure 5-20: Proliferation of SKBR3-par cells treated with NH125 and lapatinib. Cells were pre-treated with 100 nM NH125 for 24 hours, NH125 was removed from the media and the cells were treated with 250 nM lapatinib. NH125 100 nM alone and lapatinib 250 nM alone were used as comparative controls. Results are expressed as percentage growth relative to untreated control cells. Error bars represent the standard deviation of triplicate biological experiments. * denotes $p \leq 0.05$, ** denotes $p \leq 0.01$

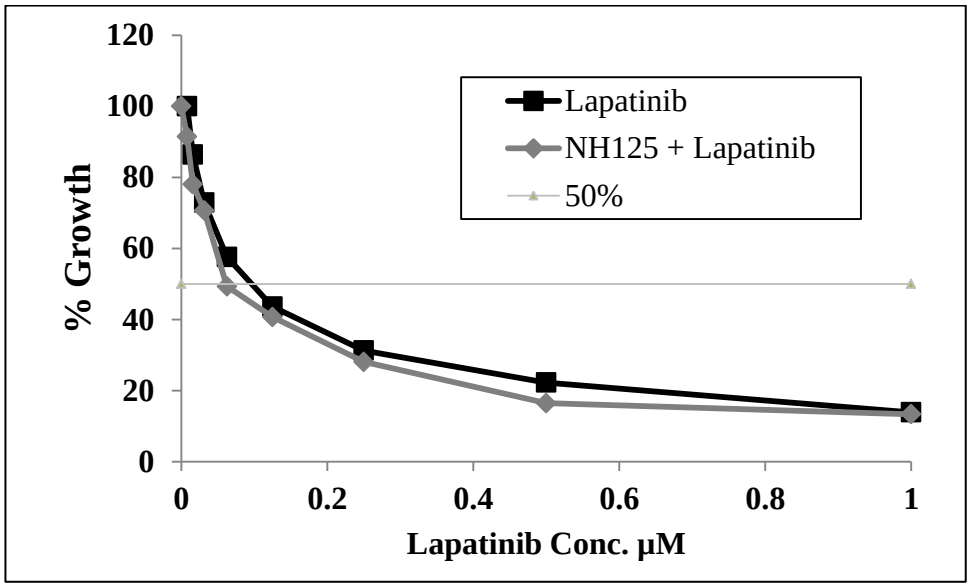

Figure 5-21: Proliferation of SKBR3-par cells following pre-treatment with 100 nM NH125 for 24 hours after which time NH125 was removed from the media and cells were treated with lapatinib (0 – 1 µM) for 5 days. Growth is expressed relative to untreated control cells. Represented here are the results of biological duplicate experiments.

5.4 Summary

SKBR3-L is a cell line model of acquired lapatinib resistance. In the absence of lapatinib, the resistant phenotype is stable for 8 weeks; however, after this point the cells begin to regain sensitivity to lapatinib. Analysis of HER family members and other downstream pathways resulted in the detection of several significantly altered proteins in comparison with parental cells, including phospho-AKT and phospho-ERK and HER4, which were significantly lower in SKBR3-L cells, and phospho-HER2 which was higher in SKBR3-L cells compared to SKBR3-par. Both cell lines exhibit decreased levels of phospho-HER3, in response to lapatinib treatment, despite having increased expression of total HER3. Although SKBR3-L cells exhibited increased levels of phospho and total EGFR they were less sensitive to EGFR inhibition than SKBR3-par cells. Increased levels of phospho- and total IGF-IR in SKBR3-L cells compared to SKBR3-par cells resulted in SKBR3-L cells being more sensitive to IGF-IR inhibition with BMS-536924, while being less sensitive to IGF-IR inhibition with NVP-AEW541.

Phospho-proteomic analysis revealed decreased phosphorylation of eEF2 in SKBR3-L cells compared to SKBR3-par cells, which was confirmed using immunoblotting. The regulation of eEF2 phosphorylation in SKBR3-L cells was mTOR independent; i) phosphorylation of Ser359 rather than Ser366 correlated with alterations in eEF2 phosphorylation in SKBR3-par cells, ii) lapatinib treatment inhibited phospho-mTOR in both cell lines, iii) mTOR inhibition with rapamycin did not alter the phosphorylation of eEF2 in SKBR3-L cells. Inhibition of eEF2k with NH125 prevented the phosphorylation of SKBR3-par cells but had limited effects on the sensitivity of the cells to lapatinib.

Chapter 6

SILAC proteomic comparison of SKBR3-par and SKBR3-L cells

6.1 Introduction

To overcome some of the limitations of traditional 2D-DIGE and to gain a more comprehensive overview of the proteins and phosphorylated proteins which may play a role in acquired resistance to lapatinib a phospho-protein screen was performed on the SKBR3-par and SKBR3-L cells (with and without 24 hour treatment with 1 µM lapatinib), using stable-isotope labelling with amino acids in cell culture (SILAC). SILAC is one of the most effective methods for the simultaneous detection of diverse changes in protein expression. With SILAC, the entire proteome of a given cell population is metabolically labelled by heavy, non-radioactive isotopic variants of amino acids, thus making it distinguishable by mass spectrometry (MS) analysis. Thereafter, two or more distinctly SILAC-labelled cell populations can be mixed and analysed in one MS experiment which allows accurate quantitation of proteins from the different cellular states.

6.2 Optimisation of purification procedure

There are various methods that can be used to enrich for phospho-proteins. This study utilised the PhosphoScan ® Kit from Cell Signalling Technology which allows for the purification and identification of tyrosine phosphorylation sites in cellular proteins when coupled with liquid chromatography (LC) tandem mass spectroscopy. The assay is based on the specific enrichment of phospho-tyrosine-containing peptides using an antibody against phospho-tyrosine depicted in Figure 6-1.

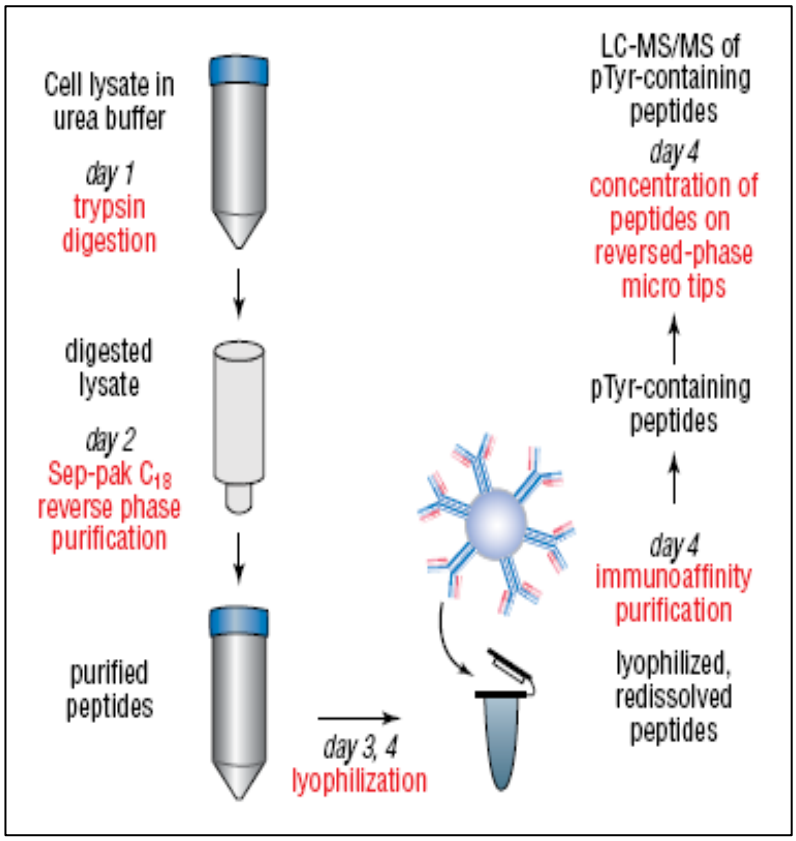

Figure 6-1: Phospho-peptide purification procedure: protein lysate is digested with trypsin, cleared through a C18 column, lyophilized for 2 days, immunoaffinity purified using phospho-tyrosine beads, concentrated using Zip-tips and analysed using LC-MS/MS. Image from PhosphoScan kit insert (Cell Signalling Technology #7900)

6.2.1 Protein yield

In order to assess and optimise the purification procedure an optimisation sample consisting of unlabelled SKBR3-par cells was prepared. A total of 1.5 x 10^8 cells yielded a total of 32 mg of protein, which was the optimal quantity required for downstream purification.

6.2.2 Protein digestion

Following the protocol outlined in [section 2.15.2], the protein lysate was digested using trypsin overnight. The efficiency of the tryptic digestion was assessed by running 10 – 50 µg of undigested and digested protein on a one dimensional gel and staining with Comassie Blue [Figure 6-2]. After 24 hours of digestion with trypsin the protein bands

were no longer visible suggesting that the proteins were successfully cleaved into peptides.

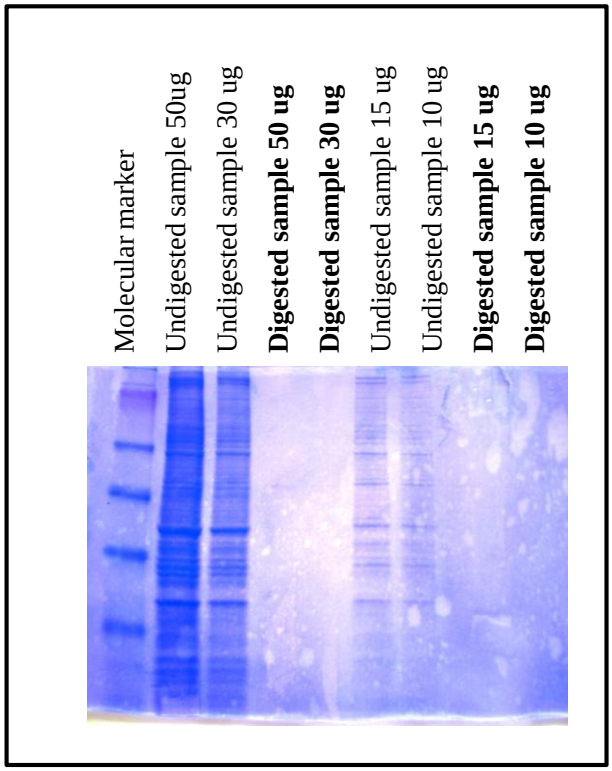

Figure 6-2: Comassie-blue stained gel depicting undigested and digested SKBR3-par samples. 10 – 50 µg protein samples were run on a one dimensional gel and stained overnight with Comassie blue. Image was taken following de-staining procedure.

6.2.3 Purification of control peptides

The PhosphoScan ® kit supplies control peptides to act as a control for the immunoaffinity purification and LC-MS/MS analysis steps. The control sample consists of peptides purified from 2 x 10^8 Jurkat cells, an immortalised line of T-lymphocytes, treated with pervandate and calculin A. A list of the top 40 phospho-tyrosine containing peptides identified in the Jurkat cells is supplied with the kit and acts as a reference. In optimisation experiments Jurkat peptides were included as a control for the immunoaffinity and LC-MS/MS stages. Thirty five of the top 40 phospho-peptides were identified which, according to the kit, is deemed to be a successful enrichment of phospho-tyrosine peptides. For example, analysis of the Jurkat cells is expected to reveal the phospho-peptide sequence ALGADDSY*Y*TAR for the protein ZAP70

(where the * indicates a phospho-tyrosine site at Y492 and Y493). When the Jurkat peptides were purfied, 22 peptides for ZAP70 were identified, including 6 identified copies of the phospho-peptide sequence ALGADDSY*Y*TAR, with phospho-tyrosine sites at Y492 and/or Y493 [Table 6-1]. Including this control in the experimental procedure indicated that the purification and LC-MS/MS was optimised.

Table 6-1: Phospho-tyrosine containing peptides for ZAP70 protein in Jurkat control cells. Peptide and protein identification performed using MASCOT software. The phosphotryosine-containing peptides are indicated by a Phospho (Y) after the peptide sequence. Highlighted in red is the phospho-peptide sequence ALGADDSY*Y*TAR; identification of which serves as a control for phospho-tyrosine enrichment. Score refers to the ion score where ≥ 42 indicates identity or extensive homology ($p < 0.05$). If there are duplicate matches to the same peptide, then only the highest scoring match is counted, lower scoring matches are shown in brackets, peptides are ranked 1-10 with 1 being the best possible match.

Query	Mol. Weight	Score	Rank	Peptide sequence
103	465.2946	15	9	K.FLLRPRK.E
176	566.7582	(21)	1	K.ADGLIYCLK.E + Phospho (Y)
177	566.7596	(25)	1	K.ADGLIYCLK.E + Phospho (Y)
178	566.7596	35	1	K.ADGLIYCLK.E + Phospho (Y)
179	566.7596	(20)	2	K.ADGLIYCLK.E + Phospho (Y)
318	458.5683	(24)	1	K.LKADGLIYCLK.E + Phospho (Y)
319	687.3493	(35)	1	K.LKADGLIYCLK.E + Phospho (Y)
320	687.3495	45	1	K.LKADGLIYCLK.E + Phospho (Y)
321	687.3495	(44)	1	K.LKADGLIYCLK.E + Phospho (Y)
322	687.3495	(43)	1	K.LKADGLIYCLK.E + Phospho (Y)
326	691.7857	(61)	1	K.ALGADDSYYTAR.S + Phospho (Y)
327	691.7859	(64)	1	K.ALGADDSYYTAR.S + Phospho (Y)
328	691.7862	69	1	K.ALGADDSYYTAR.S + Phospho (Y)
343	731.7691	(56)	1	K.ALGADDSYYTAR.S + 2 Phospho (Y)
344	731.7695	(56)	1	K.ALGADDSYYTAR.S + 2 Phospho (Y)
345	731.7696	(57)	1	K.ALGADDSYYTAR.S + 2 Phospho (Y)
408	864.8789	(54)	1	R.IDTLNSDGYTPEPAR.I + Phospho (Y)
409	864.8789	(57)	1	R.IDTLNSDGYTPEPAR.I + Phospho (Y)
410	864.8800	58	1	R.IDTLNSDGYTPEPAR.I + Phospho (Y)
475	628.9551	(36)	1	R.RIDTLNSDGYTPEPAR.I + Phospho (Y)
476	628.9553	(42)	1	R.RIDTLNSDGYTPEPAR.I + Phospho (Y)
477	942.9301	45	1	R.RIDTLNSDGYTPEPAR.I + Phospho (Y)

6.2.4 Purification of SKBR3-par peptides

The Jurkat control peptides indicated that the purification procedure was optimised therefore the peptides obtained from SKBR3-par cells were purfied using the same procedure. Purification of SKBR3-par cells resulted in the identification of proteins containing multiple phospho-tyrosine containing peptide sequences. One such identification was tyrosine-phosphorylated HER2. HER2 has many phospho-tyrosine sites including those which regulate its kinase activity at Y1221 and Y1222. Nine copies of a sequence containing 1 phospho-tyrosine and 1 copy of a different sequence containing a phospho-tyrosine [Table 6-2] were identified. Based on these results the purification procedure was considered to be optimised.

Table 6-2: Phospho-tyrosine containing peptides for HER2 protein in SKBR3-par control cells. Peptide and protein identification performed using MASCOT software. The phospho-tryosine-containing peptides are indicated by a Phospho (Y) after the peptide sequence. Score refers to the ion score where ≥ 42 indicates identity or extensive homology ($p < 0.05$). If there are duplicate matches to the same peptide, then only the highest scoring match is counted, lower scoring matches are shown in brackets, peptides are ranked 1-10 with 1 being the best possible match.

Query	**Mol. weight**	**Score**	**Rank**	**Peptide**
12	378.2060	13	5	R.ENTSPK.A + Phospho (ST)
440	926.4242	(45)	1	K.GTPTAENPEYLGLDVPV.- + Phospho (Y)
441	926.4242	(45)	1	K.GTPTAENPEYLGLDVPV.- + Phospho (Y)
442	926.4246	85	1	K.GTPTAENPEYLGLDVPV.- + Phospho (Y)
443	926.4247	(60)	1	K.GTPTAENPEYLGLDVPV.- + Phospho (Y)
444	926.4247	(71)	1	K.GTPTAENPEYLGLDVPV.- + Phospho (Y)
445	926.4253	(37)	1	K.GTPTAENPEYLGLDVPV.- + Phospho (Y)
446	926.4253	(70)	1	K.GTPTAENPEYLGLDVPV.- + Phospho (Y)
447	926.4256	(50)	1	K.GTPTAENPEYLGLDVPV.- + Phospho (Y)
448	926.4259	(34)	1	K.GTPTAENPEYLGLDVPV.- + Phospho (Y)
519	816.7215	36	1	R.FVVIQNEDLGPASPLDSTFYR.S + Phospho (Y)

6.3 Optimisation of labelling procedure

Optimisation experiments, as described below, were performed in order to ascertain the following:

- the length of time required to obtain 95% incorporation of the heavy lysine
- the growth rate of the cells in the media following incorporation
- the viability of the cells in the media following incorporation
- the lapatinib resistance status of SKBR3-L cells in the media following incorporation.

6.3.1 Incorporation of labelled amino acid

An amino-acid incorporation experiment was performed over the course of 15 days. SKBR3-par and SKBR3-L cells were cultured in SILAC media containing with [U-$^{13}C^{6}$]-L-Lysine, known as heavy SILAC media. Incorporation of [U-$^{13}C^{6}$]-L-Lysine is reported to take approximately 6 cell doublings, and SKBR3-par cells complete 6 doublings in approximately 9 days and SKBR3-L cells in approximately 11 days [255], therefore the incorporation experiment was performed over 15 days with protein samples taken at day 6, 9, 12 and 15. The percentage of incorporation of heavy lysine was estimated using the top 5 protein hits from each cell line at each time point. Optimal incorporation of heavy lysine, defined as > 95 % incorporation, was achieved after 9 days for SKBR3-par cells [Table 6-3], and after 12 days for SKBR3-L cells [Table 6-4]. Therefore prior to all further experiments, SKBR3-par cells were treated with heavy SILAC media for 9 days to ensure full incorporation and SKBR3-L cells were treated for 12 days to ensure full incorporation.

Table 6-3: Incorporation of [U-$^{13}C^{6}$]-L-Lysine in glyceraldehyde-3-phosphate dehydrogenase, one of the top 5 proteins identified in SKBR3-par cells, following 9 days growth in heavy SILAC media. [U-$^{13}C^{6}$]-L-Lysine is indicated by a red # symbol within the peptides below. * indicates carboxymethylation

Scan	Peptide
Glyceraldehyde-3-phosphate dehydrogenase [MASS=36053]	
446	K.AGAHLQGGAK#.R
1407	R.VVDLM*AHM*ASK#E.-
1549	R.LEK#PAK#YDDIK#.K
2253	K.VGVNGFGR.I
3450	R.VVDLMAHMASK#.E
3533	R.VVDLMAHMASK#E.-
3555	R.VVDLMAHMASKE.-
3609	R.GALQNIIPASTGAAK.A
3648	R.GALQNIIPASTGAAK#.A
3731	R.VPTANVSVVDLTCR.L
3926	K.RVIISAPSADAPMFVM*GVNHEK#.Y
3926	K.RVIISAPSADAPM*FVMGVNHEK#.Y
4668	K.RVIISAPSADAPMFVMGVNHEK#.Y
4749	K.RVIISAPSADAPMFVMGVNHEK#YDNSLK#.I
5038	R.VIISAPSADAPMFVMGVNHEK#.Y
5179	K.LVINGNPITIFQERDPSK#.I
5197	K.GILGYTEHQVVSSDFNSDTHSSTFDAGAGIALNDHFVK#.L
5207	K.LVINGNPITIFQERDPSK.I
5362	K.LISWYDNEFGYSNR.V
6115	K.IK#WGDAGAEYVVESTGVFTTMEK#.A
6155	K.WGDAGAEYVVESTGVFTTMEK#.A
6185	K.WGDAGAEYVVESTGVFTTMEK.A
6389	K.VIHDNFGIVEGLM*TTVHAITATQK#.T

Table 6-4: Incorporation of [U-$^{13}C^{6}$]-L-Lysine in glyceraldehyde-3-phosphate dehydrogenase, one of the top 5 proteins identified in SKBR3-L cells, following 12 days growth in heavy SILAC media. [U-$^{13}C^{6}$]-L-Lysine is indicated by a red # symbol within the peptides below. * indicates carboxymethylation

Scan	Peptide
Glyceraldehyde-3-phosphate dehydrogenase [MASS=36053]	
478	K.AGAHLQGGAK#R.V
532	K.AGAHLQGGAK#.R
1553	R.LEK#PAK#YDDIK#.K
2272	K.VGVNGFGR.I
3495	R.VVDLMAHMASK#.E
3607	R.VVDLMAHMASK#E.-
3608	R.VVDLMAHMASKE.-
3659	R.GALQNIIPASTGAAK.A
3662	R.GALQNIIPASTGAAK#.A
4690	K.RVIISAPSADAPMFVMGVNHEK#.Y
4727	K.RVIISAPSADAPMFVMGVNHEK#YDNSLK#.I
5060	R.VIISAPSADAPMFVMGVNHEK#.Y
5074	R.VIISAPSADAPMFVMGVNHEK#YDNSLK#.I
5182	K.GILGYTEHQVVSSDFNSDTHSSTFDAGAGIALNDHFVK#.L
5185	K.LVINGNPITIFQERDPSK#.I
5369	K.LISWYDNEFGYSNR.V
5873	K.LVINGNPITIFQER.D
6153	K.IK#WGDAGAEYVVESTGVFTTMEK#.A
6164	K.WGDAGAEYVVESTGVFTTMEK#.A
6391	K.VIHDNFGIVEGLM*TTVHAITATQK#.T

6.3.2 Effect of heavy lysine incorporation on cell viability and growth rate

To ensure that incorporation of the heavy amino acid had no impact on the growth rate of SKBR3-par and SKBR3-L cells, the growth rate of both cell lines was monitored. Both cell lines were cultured in SILAC media containing either heavy lysine or light lysine and the incorporation of the heavy amino acid had no apparent effect on the viability of either cell line [Figure 6-3].

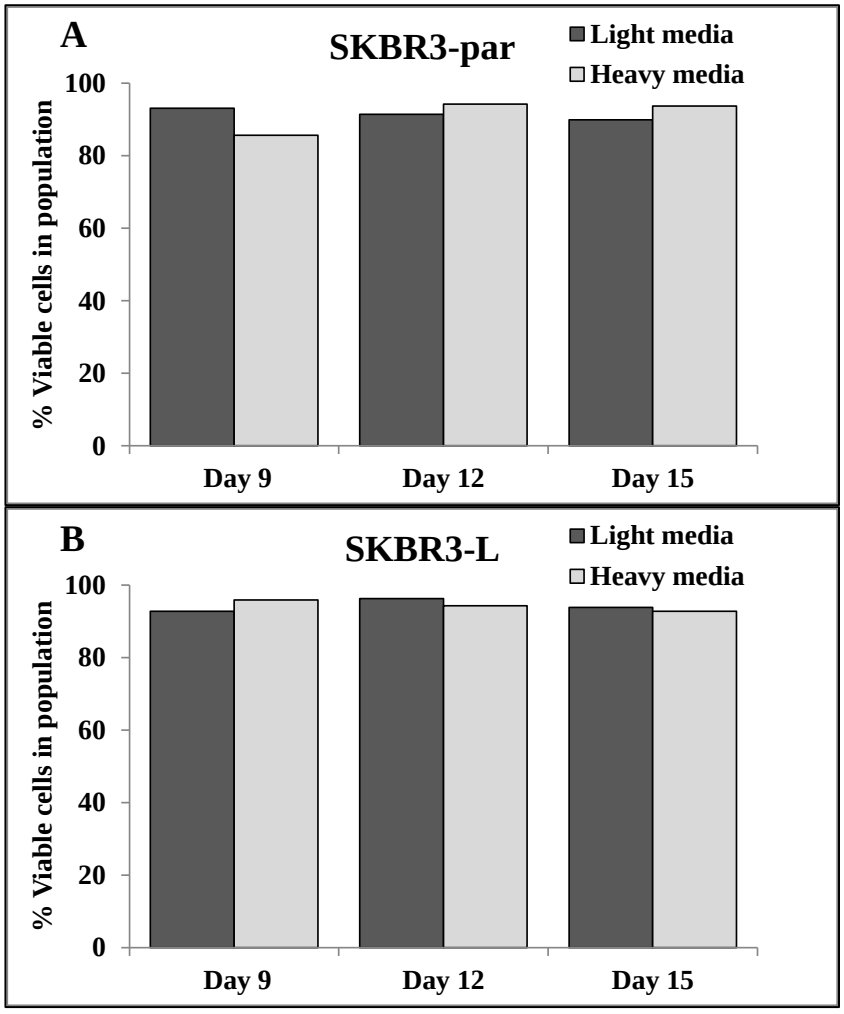

Figure 6-3: The viability of (A) SKBR3-par and (B) SKBR3-L cells was measured following 9, 12 and 15 days growth in heavy and light SILAC media. The percentage viability was measured and calculated using ViaCount reagent and Guava Software. These are the results of a single biological experiment.

There was an increase in the estimated doubling time (φ) of both cell lines cultured in the heavy media. To minimise the effects on cell growth SKBR3-par cells were cultured in the heavy media, as these cells exhibited a smaller change in estimated doubling time compared to the SBKR3-L cells [Table 6-5].

Table 6-5: Cell counts and estimated doubling time of SKBR3-par and SKBR3-L cells cultured for 15 days in heavy and light SILAC media. These results are from a single biological experiment.

Cell line	Condition	Cell count Day 12	Cell count Day 15	Doubling time (hours)
SKBR3-par	Light	2.06E+06	6.27E+06	44.9
	Heavy	1.72E+06	5.18E+06	49.2
SKBR3-L	Light	1.43E+06	3.83E+06	50.6
	Heavy	1.63E+06	3.83E+06	58.3

6.3.4 Effect of heavy lysine incorporation on lapatinib sensitivity

In order to assess whether incorporation of heavy lysine into SKBR3-par and SKBR3-L cells affected the sensitivity of the cells to lapatinib, sensitivity was measured both prior to and following heavy amino acid incorporation. There was no significant change in the sensitivity of SKBR3-par cells or SKBR3-L cells to lapatinib following incorporation [Figure 6-4]. This experiment was only performed once as the results were consistent with our previous experiments measuring lapatinib sensitivity in these cells lines [Chapter 5].

[φ] Cells were split on days 9, 12 and 15 and one third of the cells reseeded at each passage. The doubling time is estimated between days 12 and 15. This experiment was performed once.

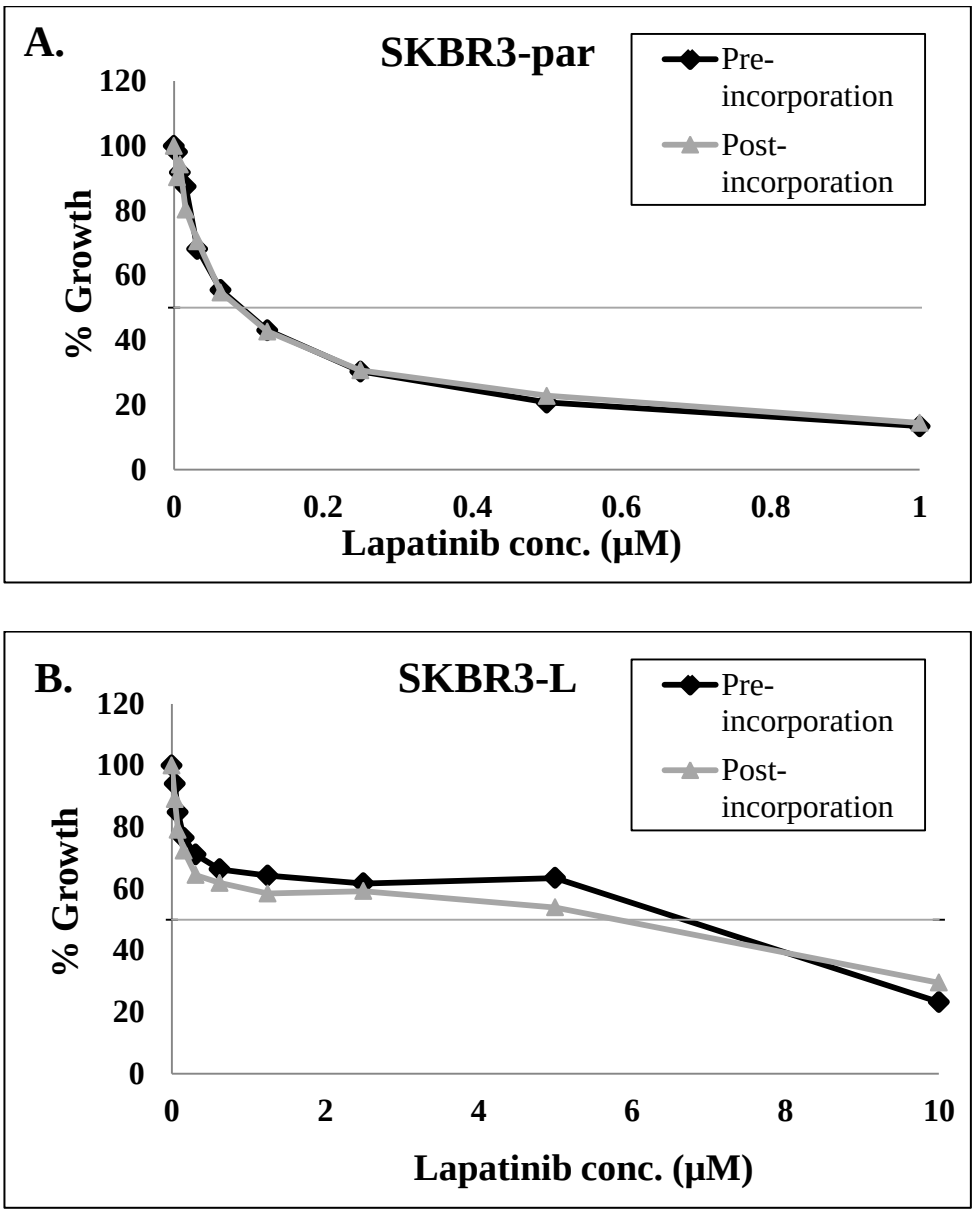

Figure 6-4: Proliferation of (A) SKBR3-par and (B) SKBR3-L cells prior to and following incorporation with heavy amino acid, following a 5-day treatment with lapatinib (0 – 10 µM). Growth is expressed relative to untreated control cells.

6.4 Outline of SILAC protocol

Based on the results of the optimisation experiments, which showed that it took 9 days for SKBR3-par cells to incorporate the SILAC label compared to 12 days in SKBR3-L cells, SKBR3-par cells were chosen as the cell line to be labelled with the heavy amino acid for the full experimental protocol. The SILAC experiment consists of 2 separate comparisons performed in triplicate; SKBR3-par control untreated versus SKBR3-L control untreated and the second comparison of SKBR3-par 1 µM lapatinib treated

versus SKBR3-L 1 µM lapatinib treated. The experimental flowchart for the SILAC experiment is depicted in [Figure 6-5].

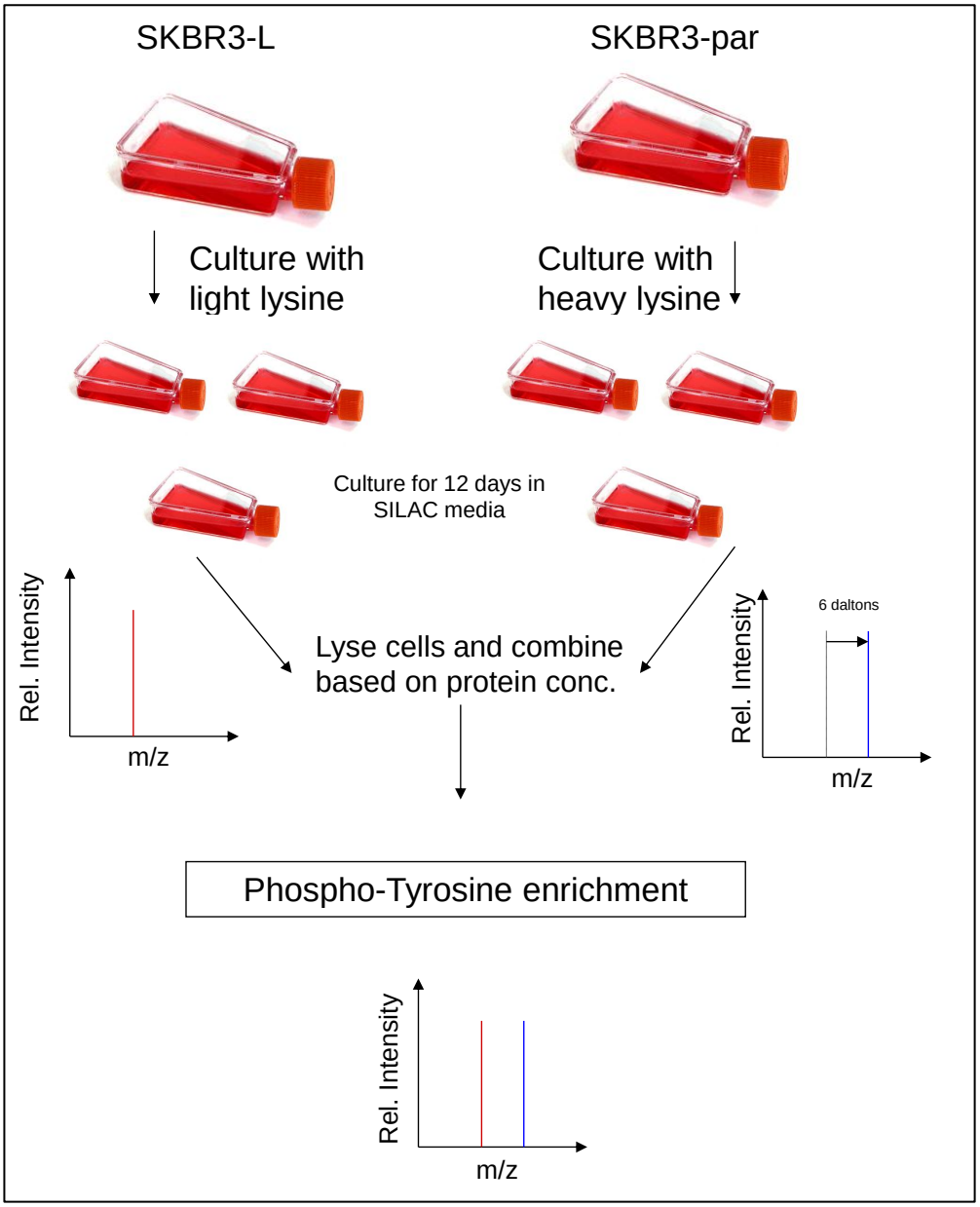

Figure 6-5: Schematic depiction of SILAC experiment. The two populations of cells were grown, one in light SILAC media and the other in heavy SILAC media. All peptides and/or proteins in the heavy population are 6 Daltons heavier than the corresponding peptide/protein in the light population. This enables the samples to be mixed and a direct comparison to be made of altered peptides/proteins between the two populations.

The experiment was set-up as depicted in [Figure 6-5], with SKBR3-par cells cultured in heavy SILAC media and SKBR3-L cells cultured in light SILAC media. Three biologically different passages of SKBR3-par and SKBR3-L cells were grown independently of each other and termed replicates 1, 2 and 3. Each biological replicate for each cell line consisted of twelve T175 cm^2 flasks of cells, which was calculated to give an approx. total cell number per replicate of 2×10^8 cells. The cells were grown for approx. 15 days in the SILAC media which allowed for optimal labelled amino acid incorporation and enabled the cells to reach 80% confluent. At this stage each of the 3 replicates for each cell line was split in two; 6 of the flasks were fed with the appropriate SILAC media while the other 6 flasks were treated with SILAC media containing 1 µM lapatinib. After exactly 24 hours the cells in 60 of the flasks were lysed and the Phospho-Scan procedure was followed as described in [sections 2.15.1 and 2.15.2]. The remaining 12 flasks, corresponding to one flask per replicate per cell line was lysed using RIPA buffer and stored to use for protein validation purposes. The protein yield of each biological replicate is listed in [Table 6-6]. The samples were combined at a 1:1 ratio based on protein concentration to compare SKBR3-par untreated with SKBR3-L untreated and both cell lines treated with lapatinib. Following phospho-purification the samples were analysed by LC-MS/MS by Dr. Julian Whitelegge and Mr. Punett Souda in UCLA.

Table 6-6: Total protein yield from each sample following growth in SILAC media and protein extraction.

Cell line	Treatment	Rep	mg/ml	total protein (mg)
SKBR3-par	Control	1	5.8	29.2
		2	7.3	36.7
		3	7.3	36.6
SKBR3-par	Lap 1 µM	1	5.0	25.1
		2	5.8	29.0
		3	6.0	30.0
SKBR3-L	Control	1	4.5	22.3
		2	3.7	18.3
		3	3.6	18.1
SKBR3-L	Lap 1 µM	1	3.6	17.8
		2	4.8	24.2
		3	4.2	21.0

6.5 Results of SILAC phospho-proteomic analysis

The purified, phospho-tyrosine enriched peptides were analysed using LC-MS/MS. The first analysis consisted of SKBR3-par untreated cells compared to SKBR3-L untreated cells in triplicate followed by a second analysis of SKBR3-par cells treated with 1 µM lapatinib compared to SKBR3-L cells treated with 1 µM lapatinib. The results of these two analyses are outlined below.

6.5.1 Comparison of SKBR3-par and SKBR3-L control untreated samples.

Proteins were identified for the SKBR3-par and SKBR3-L control untreated samples; 33 in replicate 1, 67 in replicate 2 and 51 in replicate 3. Of the proteins identified, only 5 proteins were phosphorylated and common to all 3 reps [Table 6-7]. However, only one of the phosphorylated proteins, cyclin-dependent kinase 1 (CDK1), had SILAC quantification data. The identification of phospho-Glycogen synthase kinase-3 alpha (GSK3A) is depicted in Figure 6-6, where a light peptide for phospho-GSK3A was detected, however, there was no matching heavy peptide identified. Thus, there is no quantification data available for GSK3A. The identification of phospho-CDK1 is

depicted in Figure 6-7, where both heavy and light peptides for phospho-CDK1 were identified. Levels of phosphorylated CDK1 were 6.4-fold higher in SKBR3-L cells compared to SKBR3-par cells. However, the SILAC ratios ranged from 1:1.66 to 1:15.95, across the 3 replicates giving a deviation of 129 %, indicating very high variability between replicates.

Table 6-7: Identified phospho-proteins in SKBR3-par compared to SKBR3-L control untreated cells.

		SILAC Ratio	
Protein Identification	**Phospho-Ty**	**Heavy/Light**	**% Dev**
Serine/threonine-protein kinase PRP4 homolog	Yes		
Mitogen-activated protein kinase 1	Yes		
Glycogen synthase kinase-3 alpha	Yes		
Cyclin-dependent kinase 1	Yes	1:6.40	129.11
Dual specificity tyrosine-phosphorylation-regulated kinase 1A	Yes		

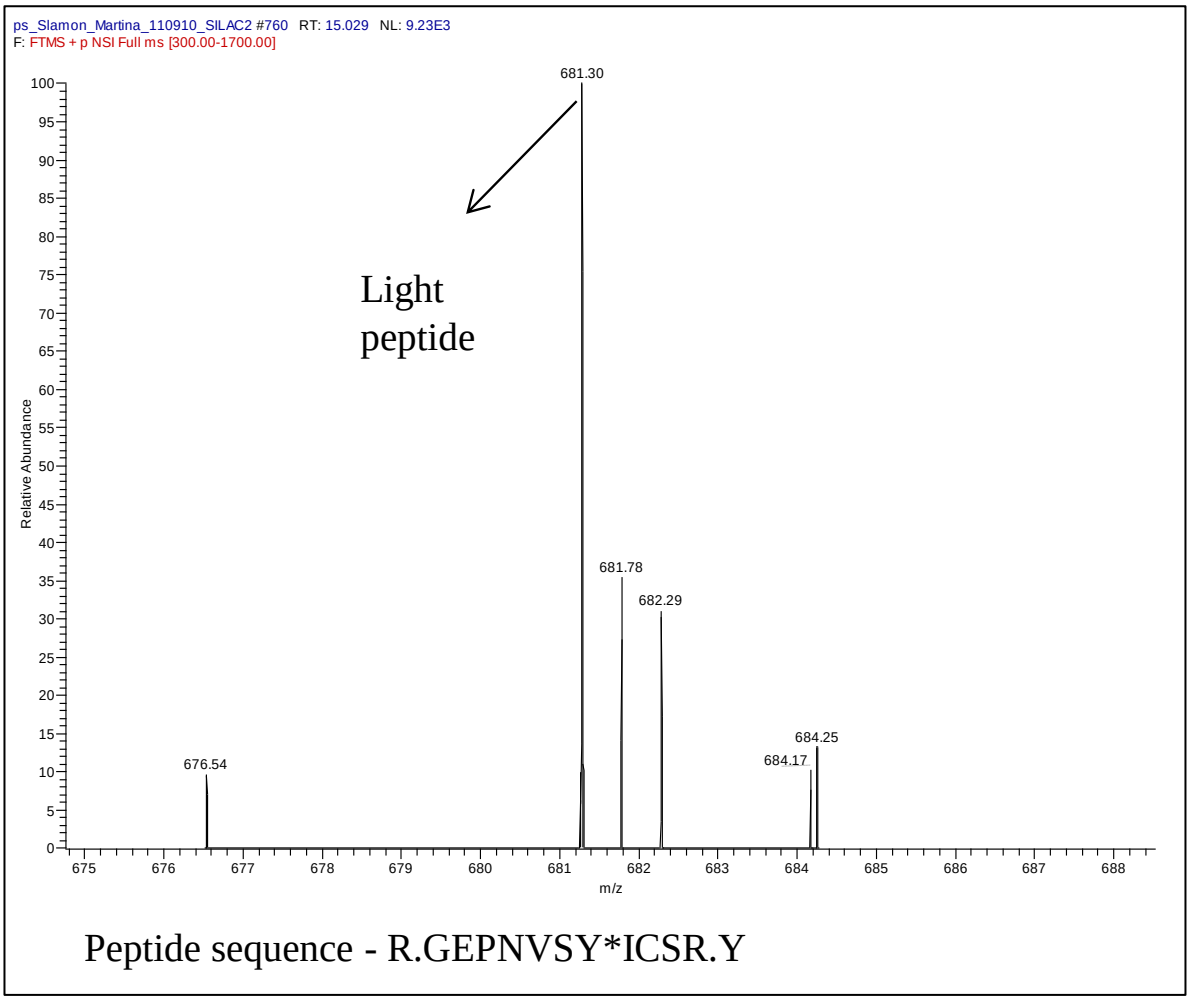

Figure 6-6: Full-MS scan (Bioworks) depicting the identification of a light phospho-peptide only for GSK3A. No matched heavy phospho-peptide was identified.

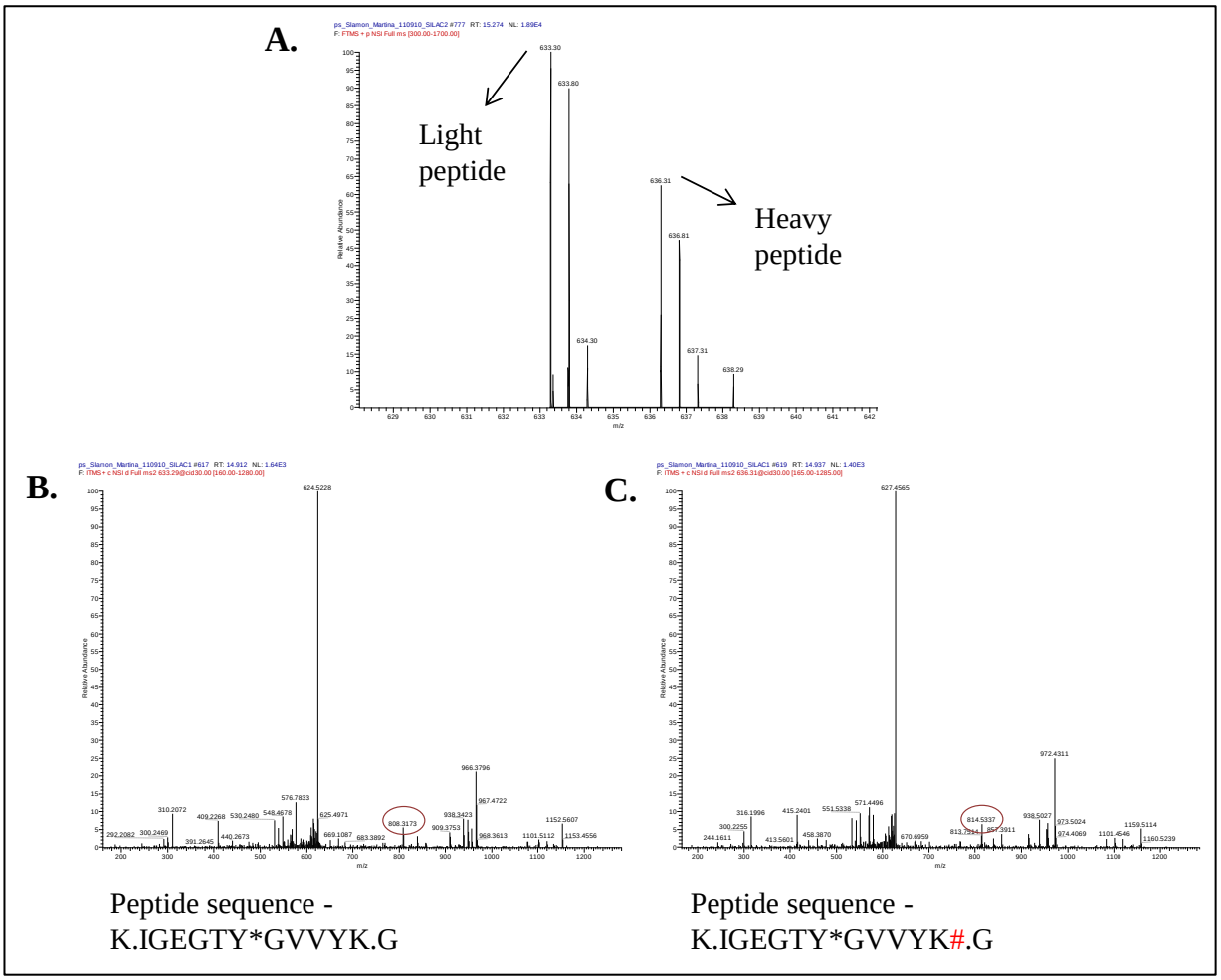

Figure 6-7: Identification of phospho-CDK1 using Bioworks. (A.) Full-MS scan depicting the light and heavy peptides of phospho-CDK1. (B) Identification of a light phospho-CDK1 peptide and (C) identification of a heavy phospho-CDK1 peptide. Phosphorylated tyrosine is highlighted with a red circle.

6.5.2 Comparison of SKBR3-par and SKBR3-L cells treated with 1 µM lapatinib

Proteins were identified for the SKBR3-par and SKBR3-L lapatinib treated samples; 43 in replicate 1, 43 in replicate 2 and 25 in replicate 3. Of these identified proteins there were 3 phosphorylated proteins which were common to all 3 replicates; serine/threonine-protein kinase PRP4 homolog; glycogen synthase kinase-3 alpha; and dual specificity tyrosine-phosphorylation-regulated kinase 1A. However, matched peptides for these phospho-proteins were not detected thus SILAC quantification data is unavailable.

6.5.3 Analysis of phospho-proteomic results.

The phospho-proteomic analysis was not as efficient as expected. Only 5 phospho-tyrosine containing proteins were identified in the control untreated comparison experiment and of these 5 phospho-proteins, the SILAC H/L ratio could only be calculated for one protein, CDK1. For all other identified phospho-proteins the differences were not readily quantitated. The extremely low yield of protein identifications suggests that optimum purification of the phospho-tyrosine peptides was not achieved. However, the remaining labelled total protein (not phospho-enriched) was then used to examine alterations in total proteins between the two cell lines.

6.6 Alterations in total protein levels

6.6.1 Outline of SILAC proteomic experiment

The experimental design comparing the levels of total protein between SKBR3-par and SKBR3-L cells is outlined in Figure 6-8. Comparisons between SKBR3-par and SKBR3-L control samples, and SKBR3-par and SKBR3-L 1 µM lapatinib treated were both performed in triplicate. Briefly, 10 µg of sample from each cell line was mixed and resolved on a 10 % gel. The gel was then stained with Comassie Blue to visualise protein bands. Each lane on the gel was cut into 32 pieces, known as gel plugs. These gel plugs were trypsinised and dehydrated to give digested peptides. The digested peptides were re-suspended in elution buffer and analysed using LC-MS/MS, this step was performed by Mr Michael Henry in DCU. The data was then analysed using Bioworks to assign protein identifications and SILAC ratio information.

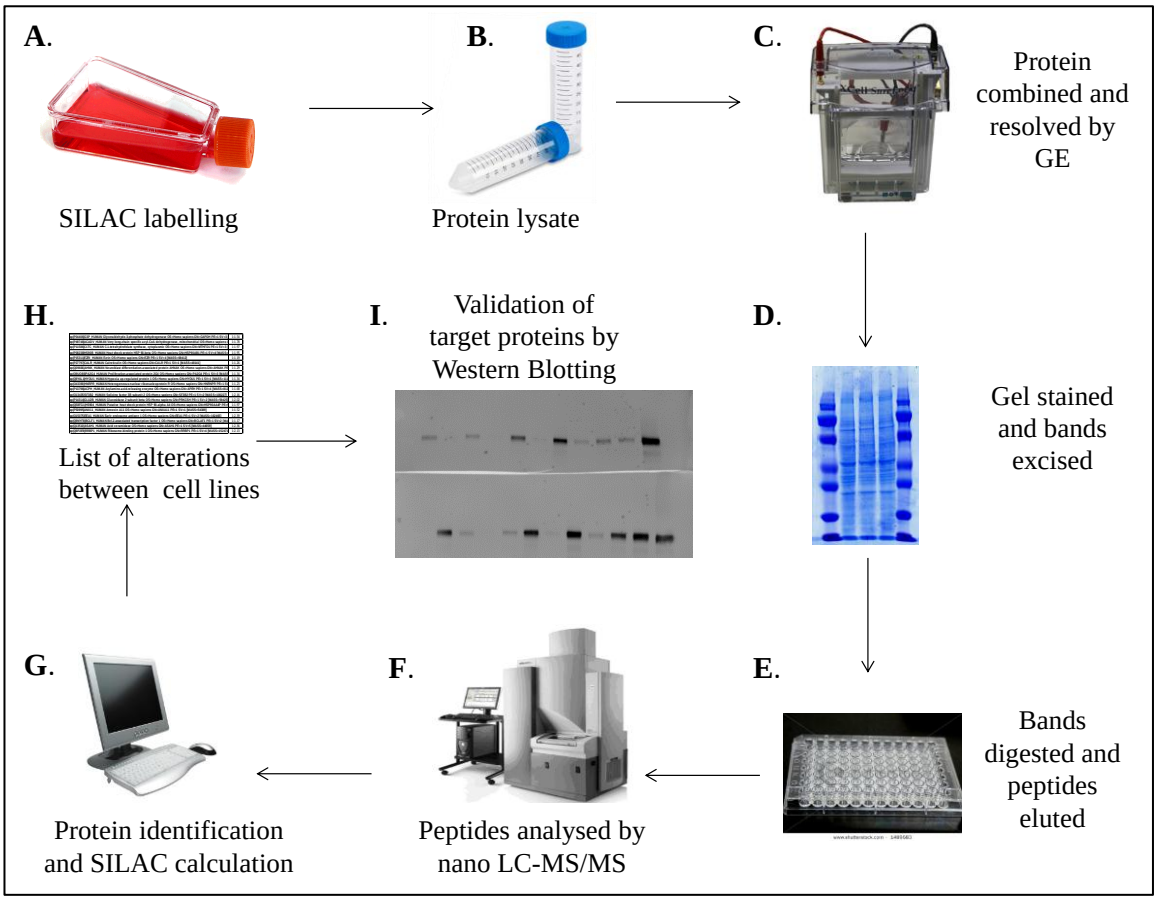

Figure 6-8: Schematic representation of total protein SILAC experimental protocol. (A) Cells are metabolically labelled using SILAC media, (B) Cells are lysed, (C) Lysates are combined at a 1:1 ratio based on protein concentration and resolved on a 10 % gel, (D) Gel is stained with Comassie blue and each is split into 32 separate gel plugs, (E) Gel plugs are digested with trypsin and peptides are eluted from the plugs, (F) Peptides are quantified using nano-LC-MS/MS technology, (G) Proteins are identified and SILAC ratios calculated using Bioworks software, (H) A list of proteins which are altered between the two cell lines is established and then (I) target proteins are validated using western blotting.

6.6.2 Comparison of SKBR3-par and SKBR3-L control untreated cells

SKBR3-par control untreated cells were compared to SKBR3-L control untreated cells. Triplicate biological samples were prepared by combining replicate 1 of untreated parental lysate with an equal amount of replicate 1 of untreated SKBR3-L lysate, and so forth for the other 2 replicates [Table 6-8].

Table 6-8: Combining biological replicates of SKBR3-par and SKBR3-L control untreated samples to yield the 3 comparative samples analysed by LC-MS/MS.

Replicate	Sample 1	Sample 2	Combined sample
1	SKBR3-par CTRL 1	SKBR3-L CTRL 1	CTRL V CTRL 1
2	SKBR3-par CTRL 2	SKBR3-L CTRL 2	CTRL V CTRL 2
3	SKBR3-par CTRL 3	SKBR3-L CTRL 3	CTRL V CTRL 3

6.6.2.1 Protein identification and global protein profiling

There were 306 proteins identified in replicate 1, 359 proteins in replicate 2 and 335 proteins in replicate 3. There were 236 proteins common to replicates 1 and 2, 262 proteins common to replicates 2 and 3, and 239 proteins common to replicates 1 and 3. Of these proteins, 208 were identified in all 3 biological comparisons of SKBR3-par untreated control cells and SKBR3-L untreated control cells [Figure 6-9]. Panther software was used to analyse the list of common proteins for molecular function, biological processes, cellular component, pathways and protein class [Figure 6-10]. This analysis indicates that the identified proteins encompass a vast range of different processes, functions and pathways. The SILAC ratios for these 208 common proteins were then calculated.

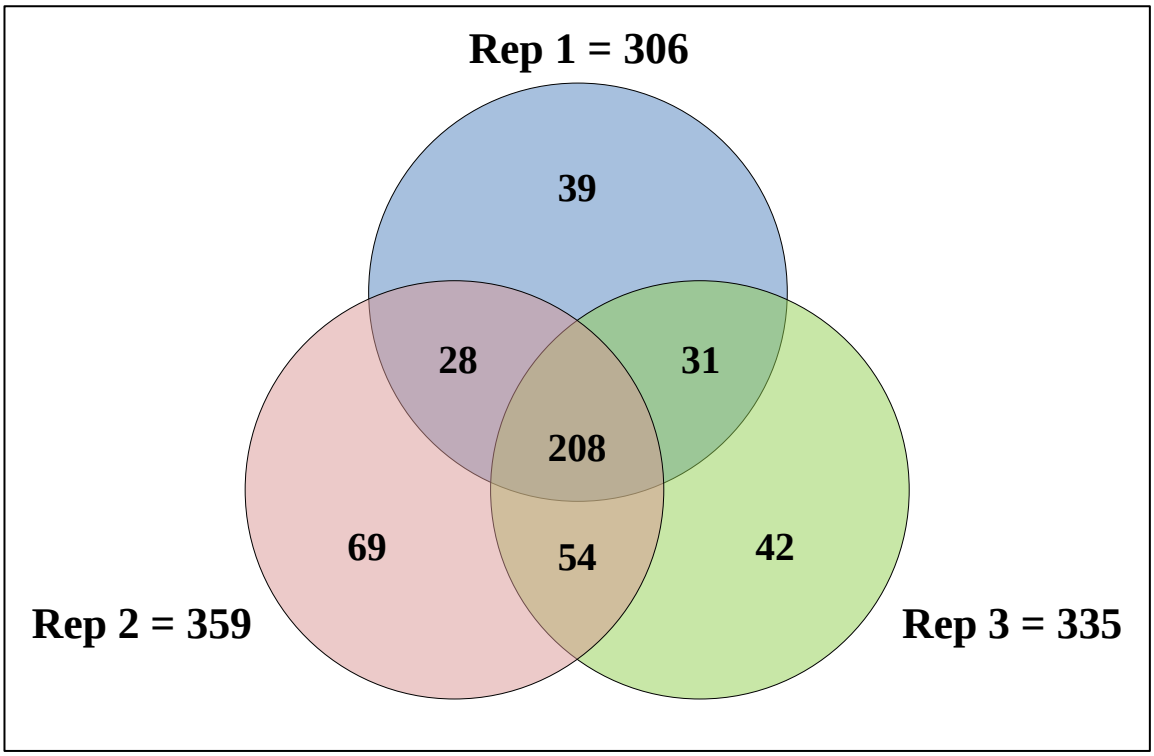

Figure 6-9: Venn diagram illustrating the overlap of identified proteins between the different biological replicates of SKBR3-par and SKBR3-L control untreated samples.

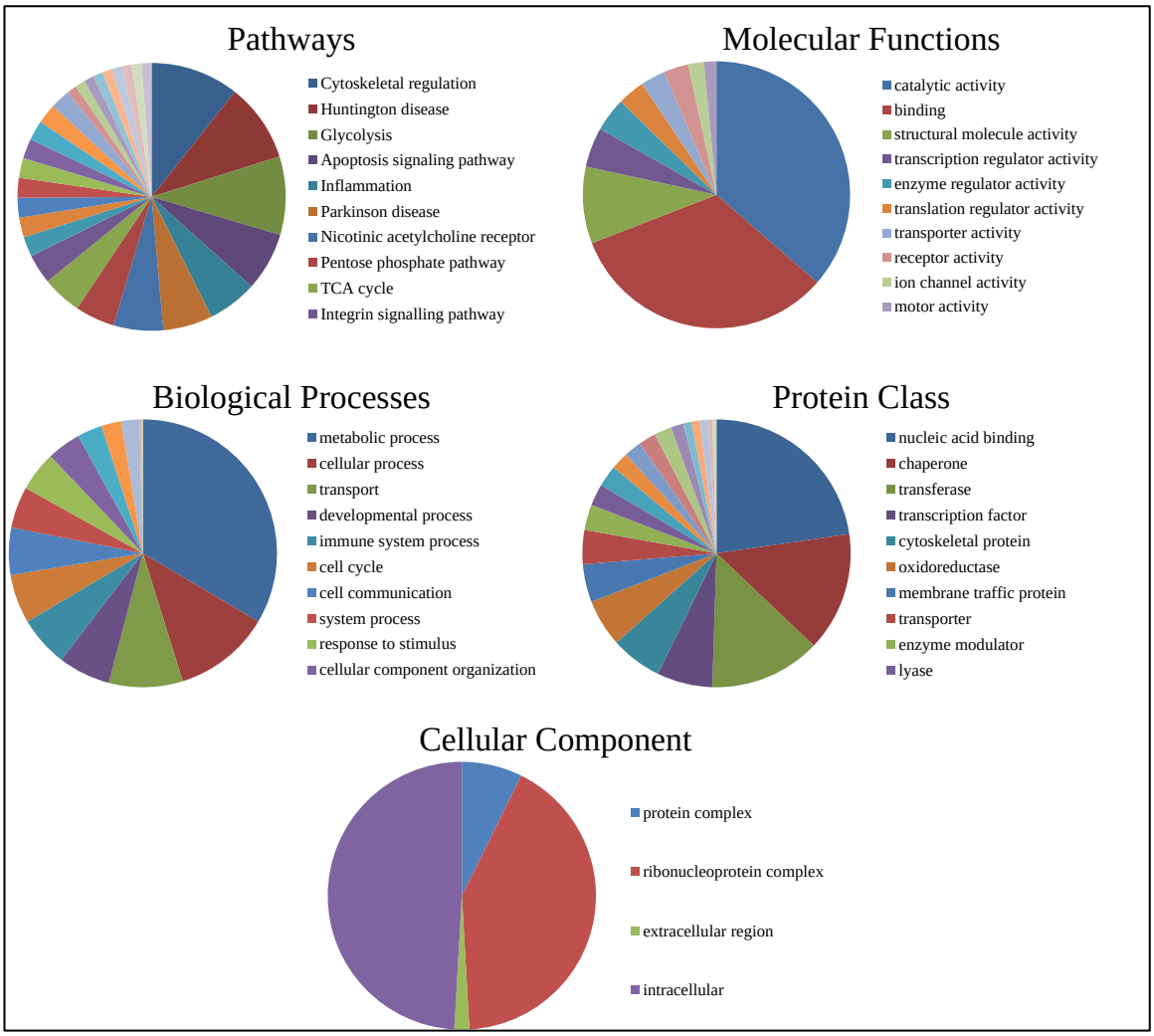

Figure 6-10: Analysis of Pathways, Molecular function, Biological Processes, Protein Class and Cellular Component on the 208 proteins that were common to all 3 reps of control SKBR3-par versus control SKBR3-L using Panther software. Pie-charts were constructed in Excel using percentages with the only the 10 largest percentages forming the legend for each pie chart to aid visibility.

6.6.2.2 Generation of list of significantly altered proteins

SILAC ratios were calculated for the 208 proteins which were common to all 3 replicates of the SKBR3-par compared to SKBR3-L. Each of the 208 proteins had SILAC ratios calculated for each biological replicate. Of these 208 proteins, 39 showed the same trend in SILAC ratios across the 3 reps, (e.g., some proteins had SILAC ratios which showed an increase in one cell line in 2 reps but a decrease in the same cell line in the third rep – these proteins were omitted from further study). The SILAC ratios of the remaining 39 proteins were averaged and standard deviations were calculated.

Proteins with a standard deviation 20 % or less and a fold change greater than or equal to 1.2-fold were considered significant. Of the 39 proteins, 26 proteins had a standard deviation of 20 % or less, and 20 of those had a fold change greater than or equal to 1.2-fold and were considered to be the significantly altered proteins between SKBR3-par and SKBR3-L control untreated cells. The expression of 8 proteins was higher in SKBR3-par compared to SKBR3-L cells [Table 6-9], while the expression of 12 proteins was higher in SKBR3-L cells compared to SKBR3-par cells [Table 6-10].

Table 6-9: List of identified proteins whose expression was ≥ 1.2-fold higher in SKBR3-par cells compared to SKBR3-L cells. SILAC heavy/light (H/L) ratios are represented as the average ratio of triplicate biological experiments where the percentage standard deviation between replicate ratios is ≤ 20 %. The deviations of the proteins in red suggest further validation is required to confirm a significant alteration in expression.

Protein Identification	SILAC Ratio H/L	St. Dev	% Dev
Glucose-6-phosphate 1-dehydrogenase	2.0:1	0.4	20.3
Heterogeneous nuclear ribonucleoprotein Q	1.9:1	0.3	16.2
Dihydrolipoyllysine-residue succinyltransferase component of 2-oxoglutarate dehydrogenase complex	1.3:1	0.2	16.2
Heterogeneous nuclear ribonucleoprotein F	1.3:1	0.2	16.3
Heterogeneous nuclear ribonucleoprotein K	1.3:1	0.2	12.0
Polyadenylate-binding protein 1	1.2:1	0.1	10.8
Heterogeneous nuclear ribonucleoprotein A3	1.2:1	0.1	8.3
Heterogeneous nuclear ribonucleoprotein D0	1.2:1	0.2	14.3

Table 6-10: List of identified proteins whose expression was ≥ 1.2-fold higher in SKBR3-L cells compared to SKBR3-par cells. SILAC heavy/light (H/L) ratios are represented as the average ratio of triplicate biological experiments where the percentage standard deviation between replicate ratios is ≤ 20 %. The deviations of the proteins in red suggest further validation is required to confirm a significant alteration in expression.

Protein Identification	SILAC Ratio H/L	St. Dev	% Dev
Early endosome antigen 1	1:2.4	0.2	9.2
Acid ceramidase	1:2.4	0.3	10.7
Ribosome-binding protein 1	1:2.1	0.4	16.7
C-1-tetrahydrofolate synthase	1:2.0	0.3	16.5
Very long-chain specific acyl-CoA dehydrogenase	1:1.8	0.3	15.9
Acylamino-acid-releasing enzyme	1:1.7	0.1	4.4
Glyceraldehyde-3-phosphate dehydrogenase	1:1.5	0.2	14.3
Annexin A11	1:1.5	0.2	13.5
PDZ and LIM domain protein 5	1:1.4	0.3	20.3
Neuroblast differentiation-associated protein AHNAK	1:1.3	0.1	6.8
Calreticulin	1:1.3	0.1	1.8
Heterogeneous nuclear ribonucleoprotein R	1:1.2	0.2	16.9

6.6.2.3 Pathway Analysis of altered proteins

The 20 proteins showing altered expression between SKBR3-par and SKBR3-L were analysed using Pathway Studio 8.0. Nine of the 20 proteins had direct interactions with each other; either by direct protein binding (purple lines) or direct regulation of expression (blue arrows) [Figure 6-11]. Analysis of the common regulators of expression of the differentially expressed proteins suggests that insulin, IGF1, EGF and TGFβ1, among others, may play a role in regulating the expression of the differentially expressed proteins [Figure 6-12]. Analysis of the common targets of the differentially expressed proteins revealed a huge array of different proteins involved in multiple processes and signalling pathways, in particular several proteins were implicated in AKT signalling including glucose-6-phosphate 1-dehydrogenase and calreticulin [Figure 6-13].

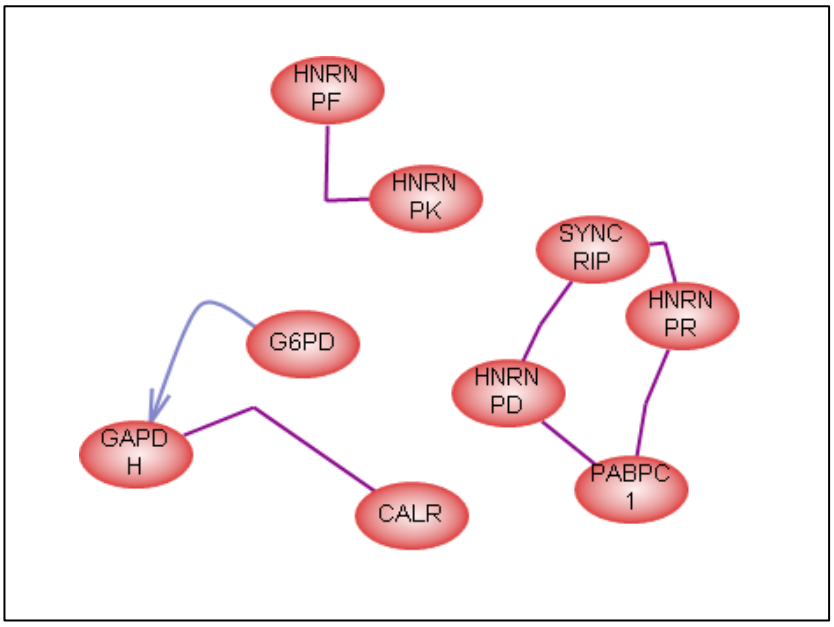

Figure 6-11: Analysis of direct protein interactions using Pathway Studio 8.0. Direct protein binding is shown by purple lines and direct regulation of protein expression is shown by blue arrows.

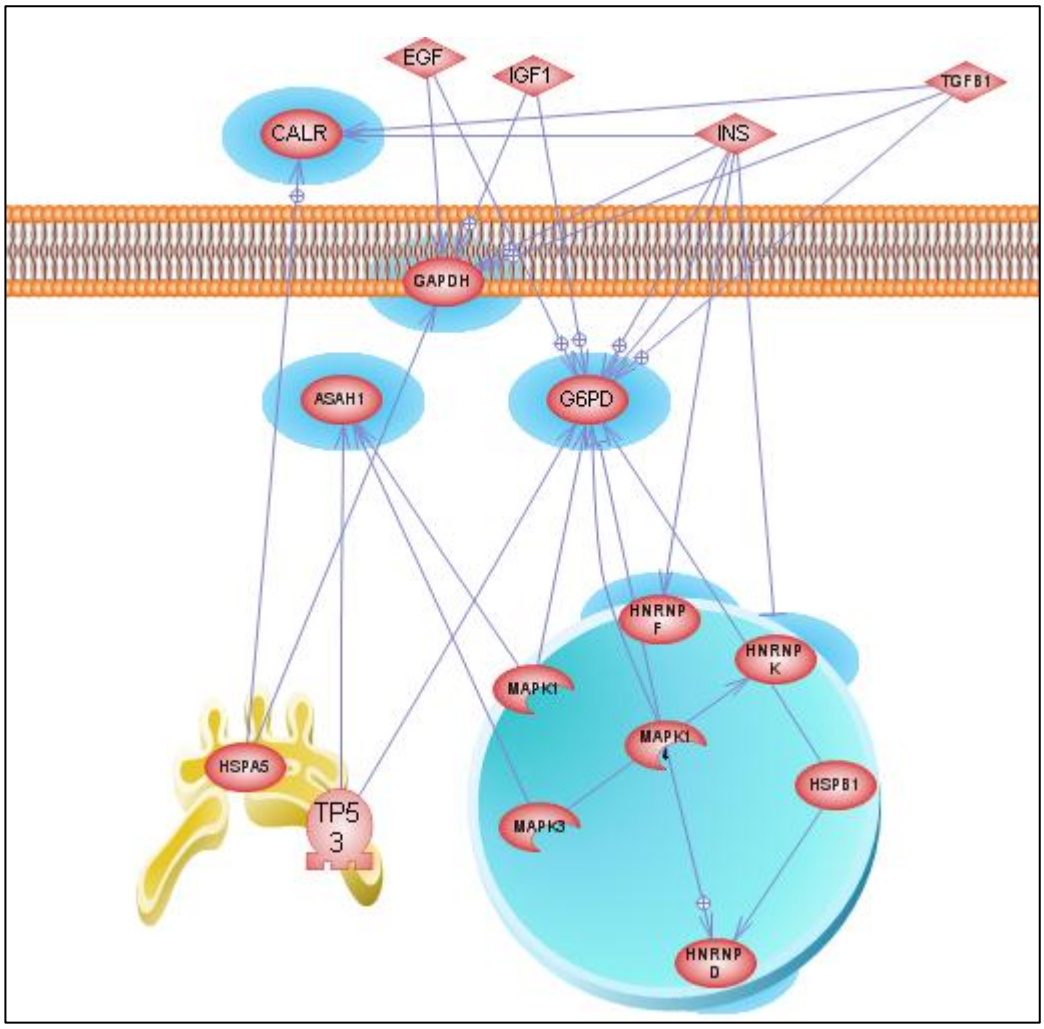

Figure 6-12: Analysis of common regulators of expression of the 20 proteins differentially expressed in SKBR3-par and SKBR3-L cells. Analysis performed using Pathway Studio 8.0. Proteins highlighted in blue are from the list of altered proteins.

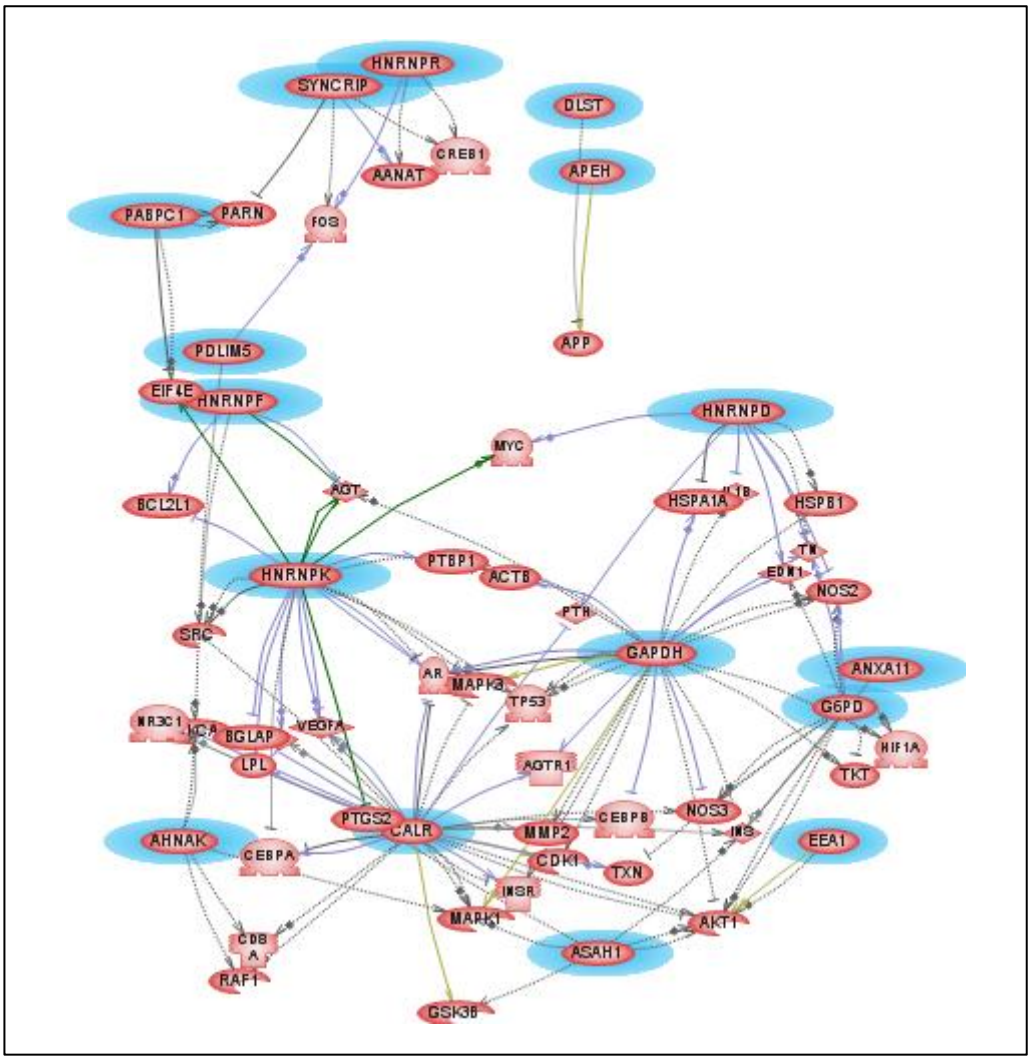

Figure 6-13: Analysis of common targets for the 20 differentially expressed proteins. Analysis performed using Pathway Studio 8.0. Proteins highlighted in blue are from the list of altered proteins.

6.6.3 Comparison of SKBR3-par and SKBR3-L cells treated with 1 µM lapatinib

In addition to examining alterations in the levels of total protein between SKBR3-par control untreated cells and SKBR3-L control untreated cells; the effect of 24 hour treatment with 1 µM lapatinib on each cell line was compared. Samples were combined as per [Table 6-11].

Table 6-11: Combining biological replicates of SKBR3-par and SKBR3-L 1 µM lapatinib treated samples to yield the 3 comparative samples analysed by LC-MS/MS.

Replicate	Sample 1	Sample 2	Combined sample
1	SKBR3-par LAP 1	SKBR3-L LAP 1	LAP V LAP 1
2	SKBR3-par LAP 2	SKBR3-L LAP 2	LAP V LAP 2
3	SKBR3-par LAP 3	SKBR3-L LAP 3	LAP V LAP 3

6.6.3.1 Protein identification and global protein profiling

There were 215 proteins identified in replicate 1, 335 proteins in replicate 2 and 352 proteins in replicate 3. There were 175 proteins common to replicates 1 and 2, 263 proteins common to replicates 2 and 3, and 184 proteins common to replicates 1 and 3. Of these proteins, 163 were identified in all 3 biological comparisons of SKBR3-par 1 µM lapatinib treated cells compared to SKBR3-L 1 µM lapatinib treated cells [Figure 6-14]. Panther analysis again showed that the identified proteins encompass a vast range of different processes, functions and pathways [Figure 6-15], similar to the results of the analysis for the proteins identified in the untreated cells. This again indicates that there is no bias in the type of proteins detected by this identification method.

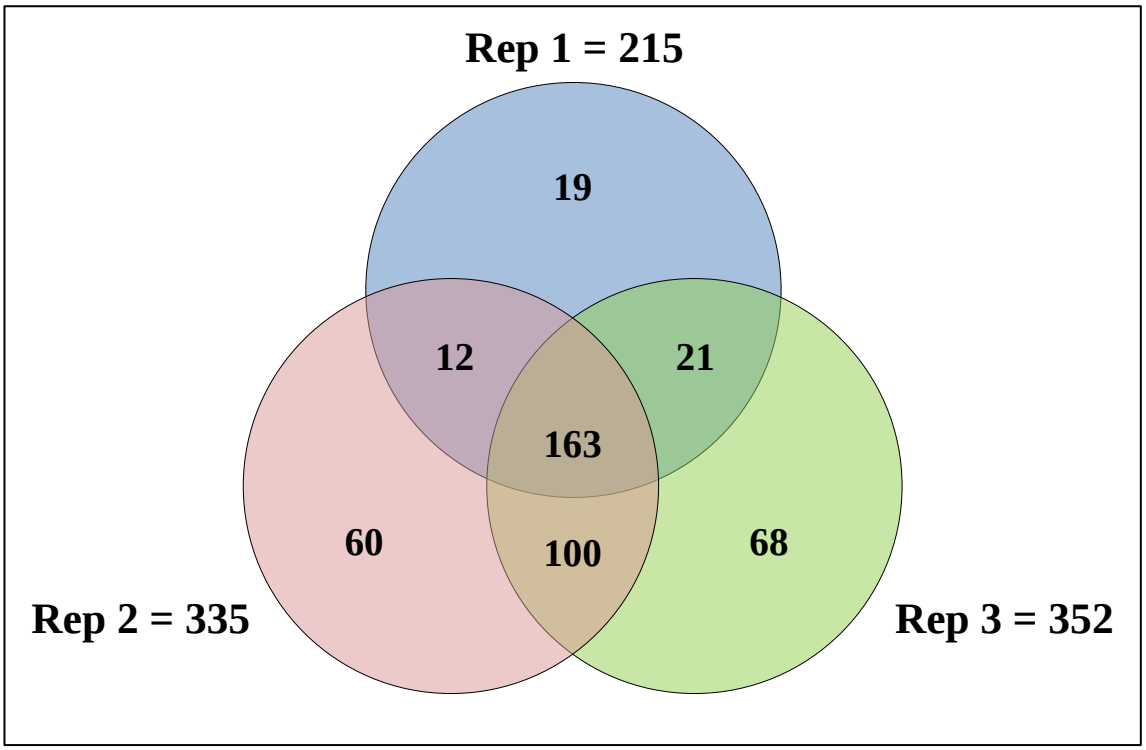

Figure 6-14: Venn diagram illustrating the overlap of identified proteins between the different biological replicates of SKBR3-par and SKBR3-L lapatinib treated samples.

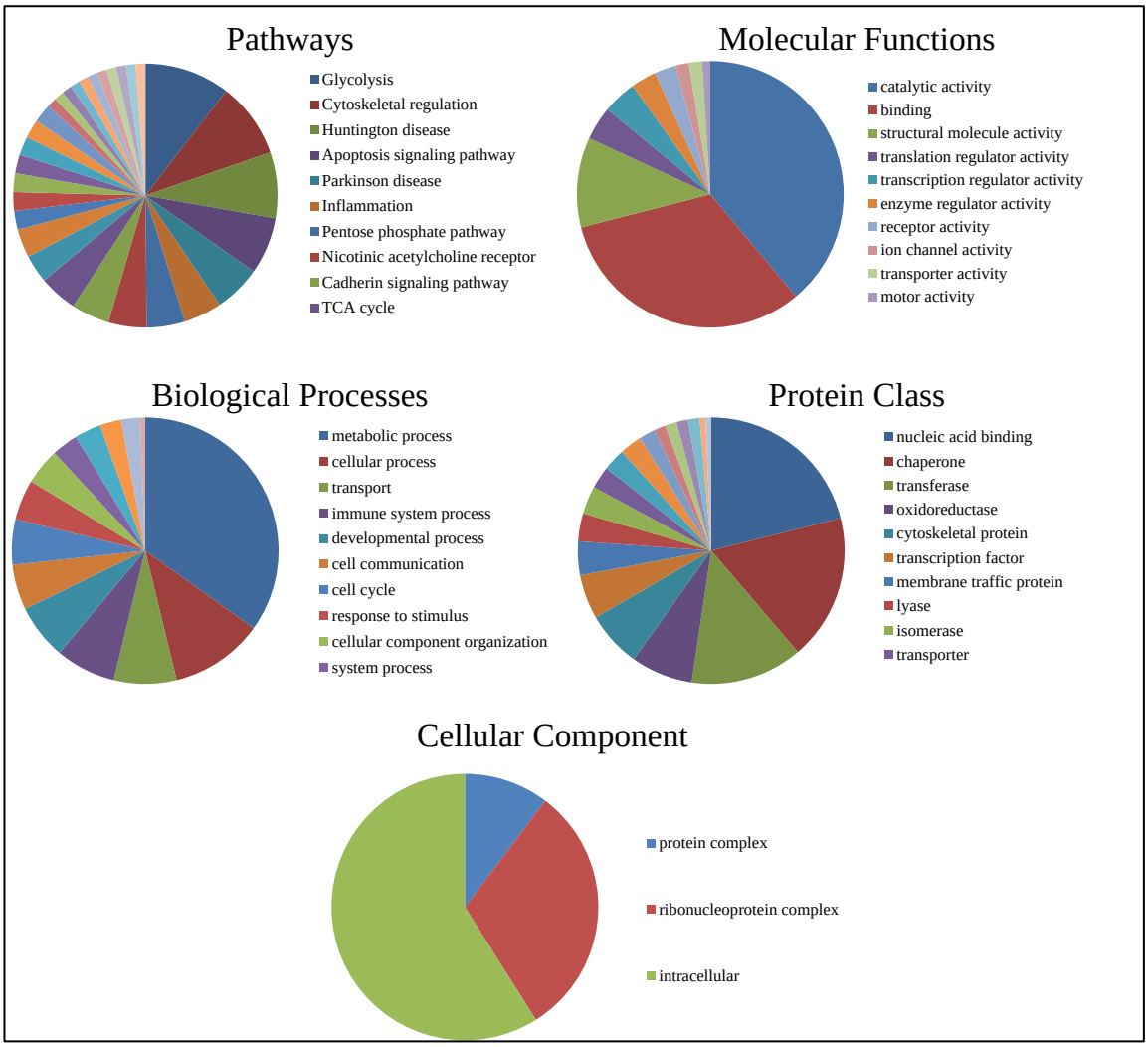

Figure 6-15: Analysis of Pathways, Molecular function, Biological Processes, Protein Class and Cellular Component on the 163 proteins that were common to all 3 reps of SKBR3-par lapatinib treated versus SKBR3-L lapatinib treated cells using Panther software. Pie-charts were constructed in Excel using percentages with the only the 10 largest percentages forming the legend for each pie chart to aid visibility.

6.6.3.2 Generation of list of significantly altered proteins

SILAC ratios were calculated for the 163 proteins which were common to all 3 replicates of the SKBR3-par 1 µM lapatinib treated compared to SKBR3-L 1 µM lapatinib treated. Of the 163 common proteins, 157 proteins had SILAC ratios calculated for each biological replicate. Of these 157 proteins, 50 showed the same trend in SILAC ratios across the 3 reps. The SILAC ratios of the 50 proteins were averaged and standard deviations were calculated. Of the 50 proteins, 18 had a standard deviation of 20 % or less and 15 proteins of those showed a fold change greater than or

equal to 1.2-fold and were considered to be the significantly altered proteins between SKBR3-par and SKBR3- L lapatinib treated cells. The expression of 13 proteins was higher in SKBR3-par compared to SKBR3-L cells while the expression of 2 proteins was higher in SKBR3-L cells compared to SKBR3-par cells [Table 6-12].

Table 6-12: List of identified proteins whose expression was ≥ 1.2-fold higher or ≥ 1.2-fold lower in SKBR3-par cells compared to SKBR3-L cells following 24 hour treatment with 1 µM lapatinib. SILAC heavy/light (H/L) ratios are represented as the average ratio of triplicate biological experiments where the percentage standard deviation between replicate ratios is ≤ 20 %. The deviations of the proteins in red suggest further validation is required to confirm a significant alteration in expression.

Protein Identification	SILAC Ratio H/L	St. Dev	% Dev
Protein SET	1.9:1	0.3	14.2
Receptor tyrosine-protein kinase erbB-2	1.6:1	0.2	14.5
Putative pre-mRNA-splicing factor ATP-dependent- RNA helicase DHX15	1.5:1	0.2	13.0
Elongation factor 1-gamma	1.5:1	0.1	8.9
Selenium-binding protein 1	1.5:1	0.3	16.7
Programmed cell death 6-interacting protein	1.4:1	0.3	20.4
Splicing factor, proline- and glutamine-rich	1.3:1	0.2	16.1
Heterogeneous nuclear ribonucleoprotein D0	1.3:1	0.2	13.5
Transaldolase	1.3:1	0.1	10.9
Heterogeneous nuclear ribonucleoprotein C-like 1	1.3:1	0.1	7.7
Desmin	1.3:1	0.1	9.9
Transformer-2 protein homolog beta	1.2:1	0.2	12.7
Neutral alpha-glucosidase AB	1.2:1	0.1	3.9
Proliferation-associated protein 2G4	1:1.6	0.3	18.6
Elongation factor 1-delta	1:1.2	0.2	12.9

6.6.3.3 Pathway analysis of altered proteins

The 15 proteins which showed altered expression between SKBR3-par and SKBR3-L were analysed using Pathway Studio 8.0. Five of the 15 proteins had direct interactions with each other; either by direct protein binding (purple lines) or direct regulation of expression (blue lines and arrows) [Figure 6-16]. This analysis suggests a link between PA2G4 (also known as EBP1) and HER2. Analysis of common regulators of expression suggests the androgen receptor, FAS, TGF1β and IGF1 as possible regulators of interest for this data set [Figure 6-17]. Analysis of the common targets for the 15 proteins identified, revealed a huge array of different proteins involved in multiple processes and signalling pathways [Figure 6-18], however of particular note, the targets appear to centralise around HER2 and protein SET.

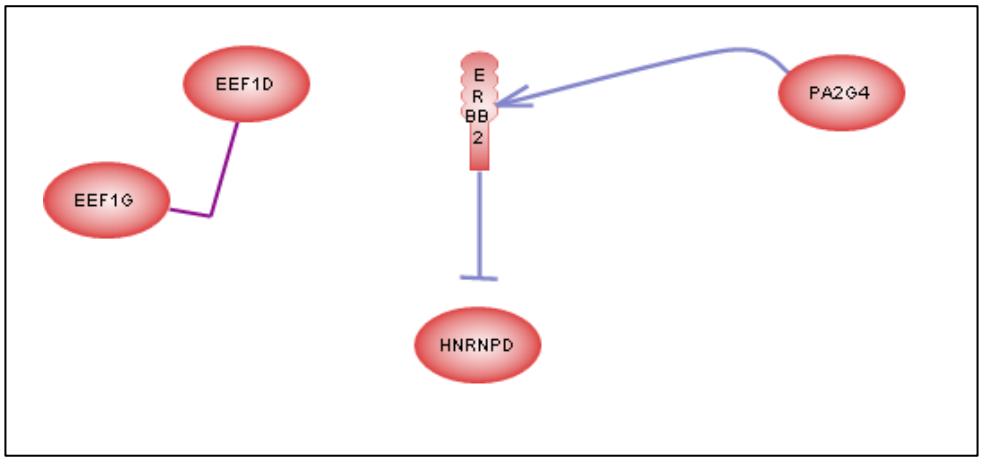

Figure 6-16: Analysis of direct protein interactions using Pathway Studio 8.0. Direct protein binding is shown by purple lines and direct regulation of protein expression is shown by blue arrows or lines.

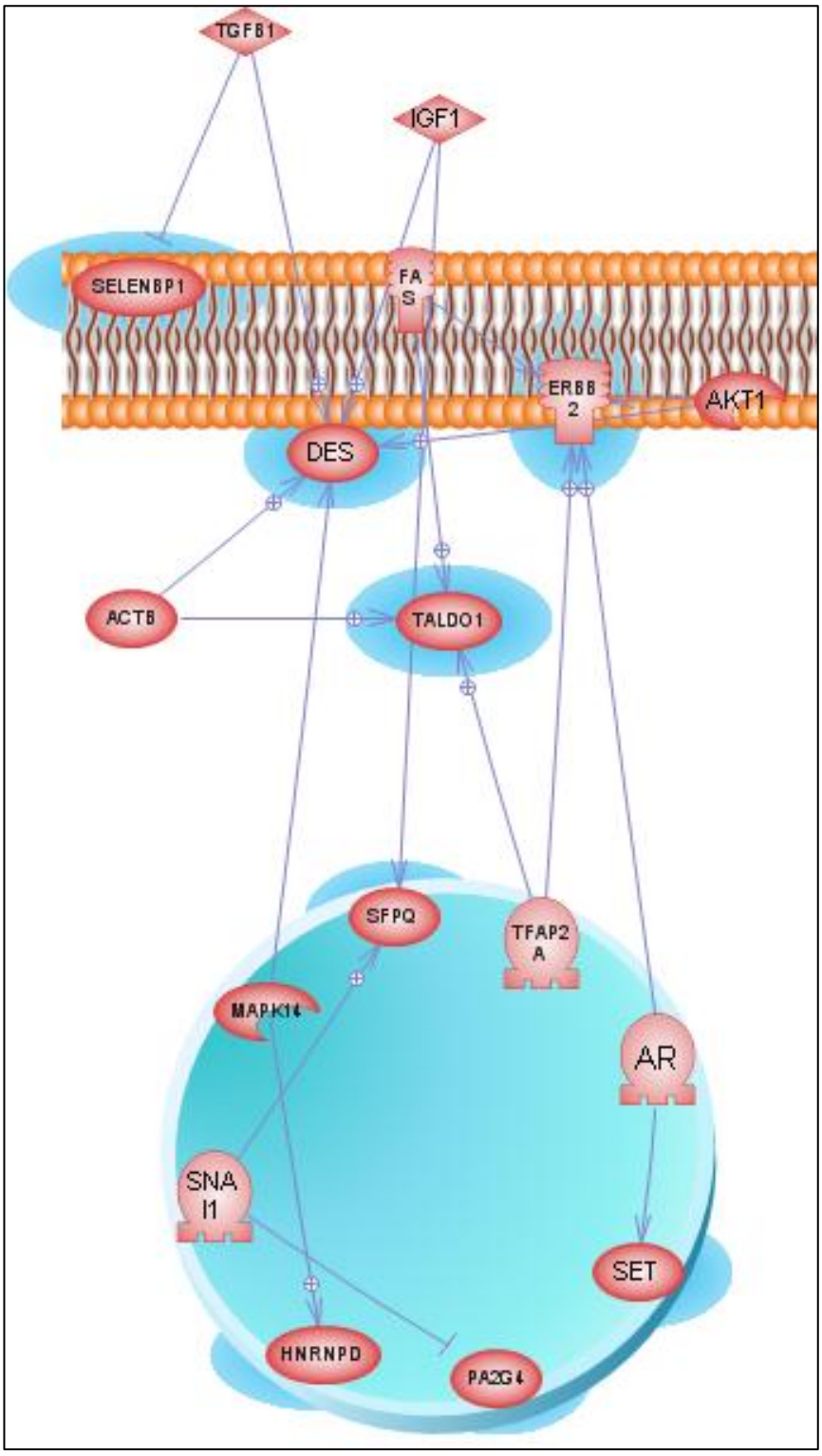

Figure 6-17: Analysis of common regulators of expression of the 15 proteins differentially expressed in SKBR3-par and SKBR3-L cells. Analysis performed using Pathway Studio 8.0. Proteins highlighted in blue are from the list of altered proteins.

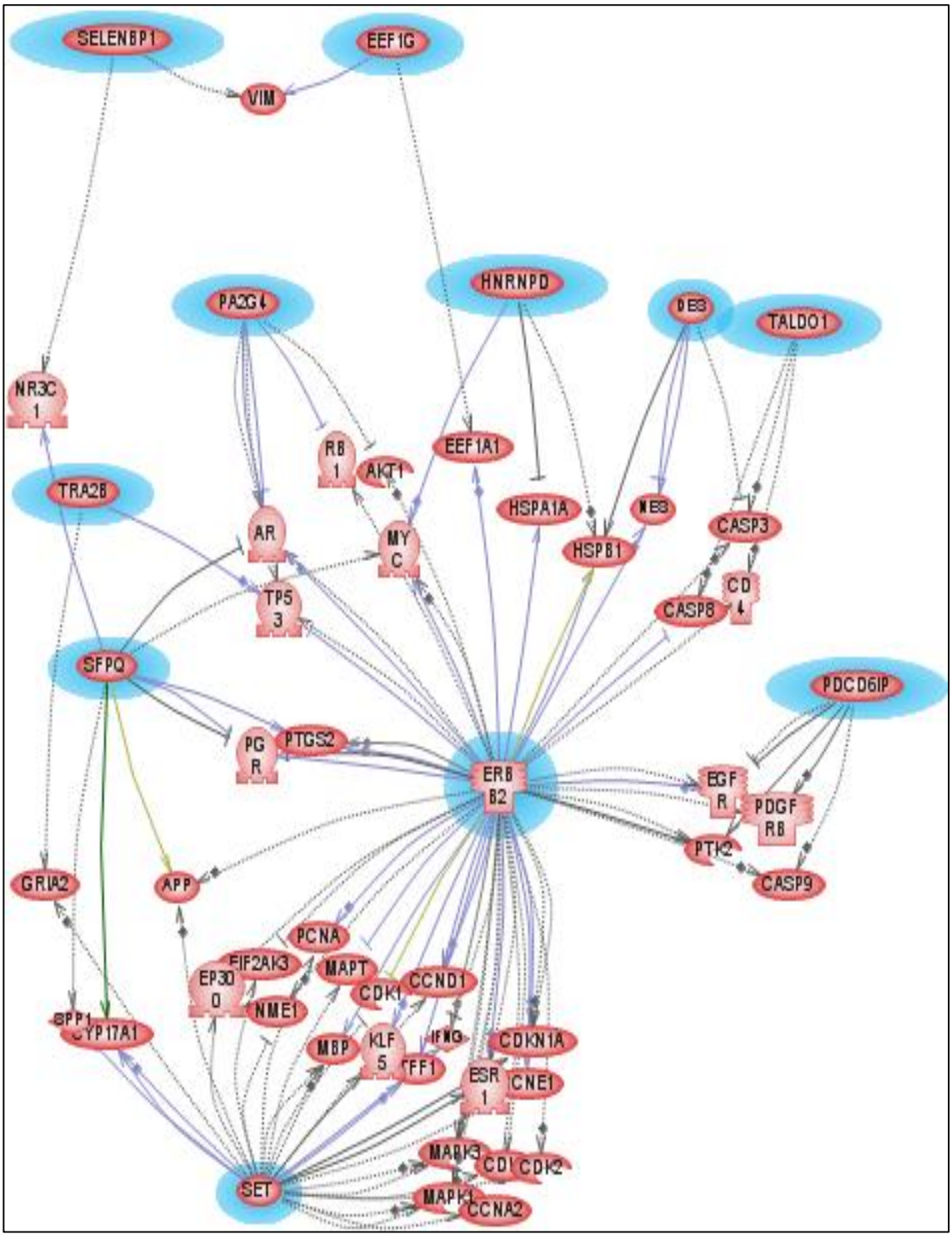

Figure 6-18: Analysis of common targets for the 15 differentially expressed proteins. Analysis performed using Pathway Studio 8.0. Proteins highlighted in blue are from the list of altered proteins.

6.7 Validation of altered proteins

Six of the differentially expressed proteins were selected for validation by immunoblotting [Table 6-13]. These proteins were selected after literature mining suggested an association between these proteins and signalling pathways downstream of HER2.

Table 6-13: Proteins selected for validation by immunoblotting

Protein ID.	**SILAC Ratio (H/L)**	**% Dev**
Phospho – Cyclin dependent kinase 1	1:6.40	129.11
Glyceraldehyde-3-phosphate dehydrogenase	1:1.5	14.3
Selenium-binding protein 1	1.5:1	16.7
Receptor tyrosine-protein kinase erbB-2	1.6:1	14.5
Protein SET	1.9:1	14.2
Proliferation-associated protein 2G4	1:1.6	12.9

6.7.1 Validation of phospho-CDK1

Cyclin-dependent kinase 1 (CDK1) is a protein that function as a serine/threonine kinase and plays a key role in the regulation of cell cycle progression. SILAC phospho-proteomic profiling of SKBR3-par and SKBR3-L cells revealed a 6.4-fold increase in the levels of phospho-CDK1 in SKBR3-L cells compared to SKBR3-par cells. Immunoblotting confirmed the increased phosphorylation of CDK1 in SKBR3-L cells compared to SKBR3-par cells ($p = 0.006$) [Figure 6-19]. In addition lapatinib treatment resulted in decreased levels of phosphorylation in both cell lines, and also decreased the expression of total CDK1 in both cell lines.

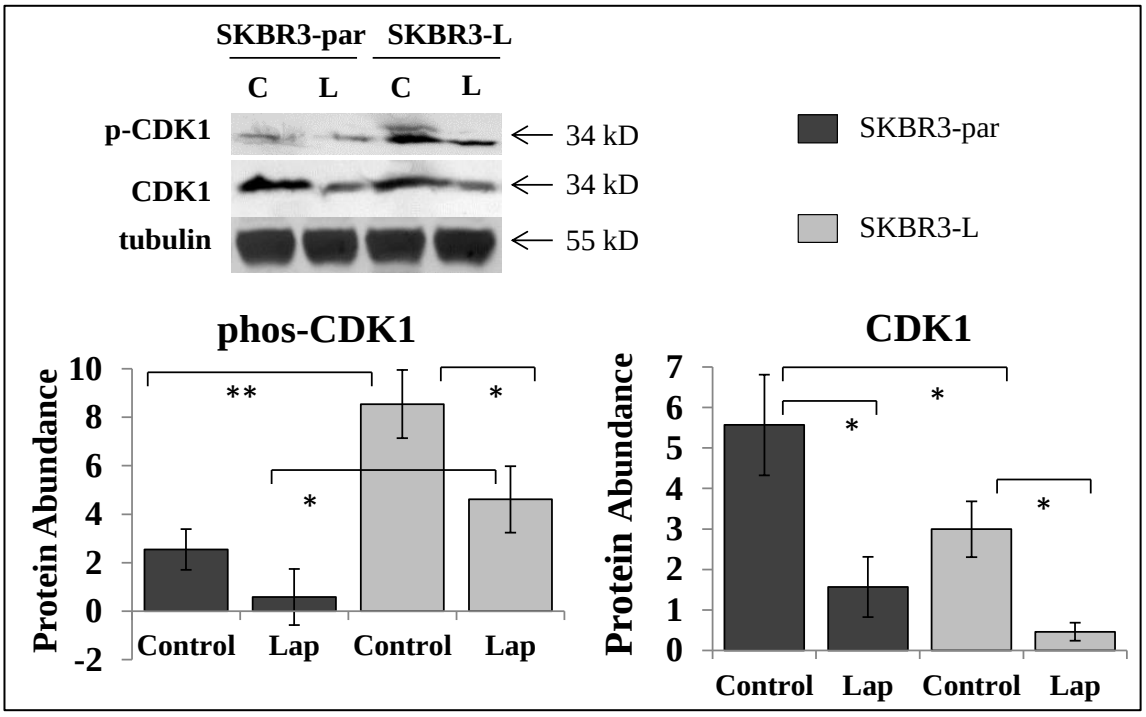

Figure 6-19: Immunoblotting for phospho- (Tyr15) and total CDK1 in SKBR3-par and SKBR3-L cells. α-tubulin was used as a loading control on each gel. Images are representative of triplicate experiments. Densitometry analysis of triplicate immunoblots was performed using ImageQuant software. * denotes $p \leq 0.05$, ** denotes $p \leq 0.001$.

6.7.2 Validation of Glyceraldehyde-3-phosphate dehydrogenase

Glyceraldehyde-3-phosphate dehydrogenase (GAPDH) is an enzyme which catalyses the conversion of glyceraldehyde-3-phosphate to D-glycerate 1,3-bisphosphate, a key step required in the breakdown on glucose to supply energy to cells. Total proteomic analysis revealed that SKBR3-L cells have higher levels of GAPDH compared to SKBR3-par cells. Immunoblotting confirmed a small, yet significant difference in the levels of GAPDH between the two cell lines. SKBR3-L cells have 1.3-fold higher levels of GAPDH protein compared to SKBR3-par cells ($p = 0.013$) [Figure 6-20].

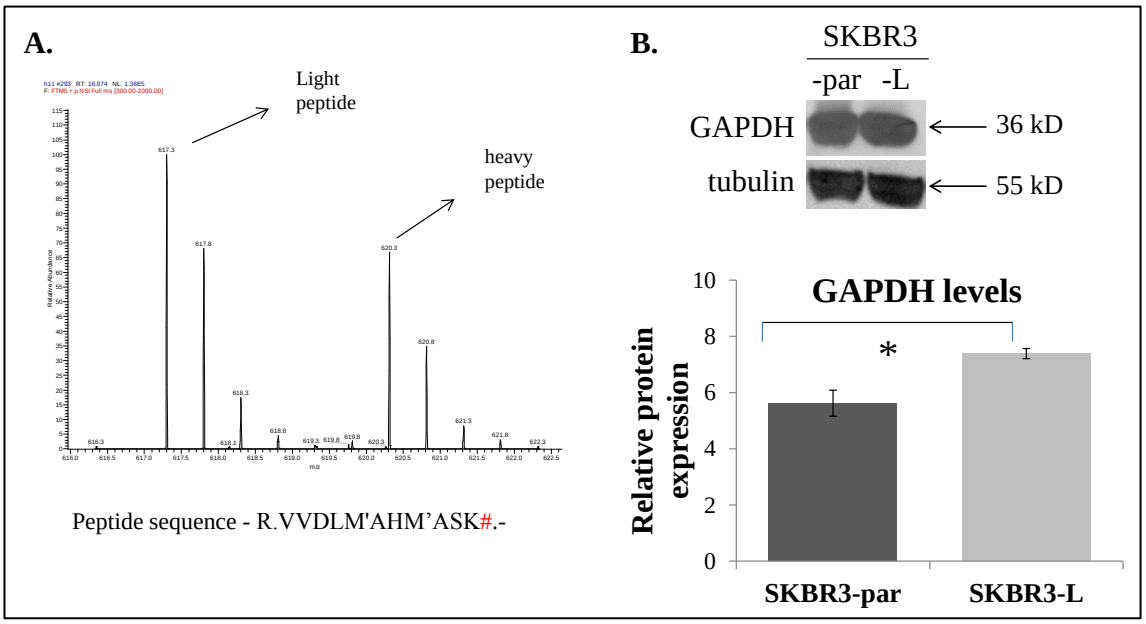

Figure 6-20: A) Full-MS revealing an alteration in matched heavy and light peptide sequence (-.VVDLM'AHM'ASK#.-) which corresponds to GAPDH protein, where # indicates labeled lysine and M' indicates methylation B) Immunoblotting for GAPDH protein in SKBR3-par and SKBR3-L cells. α-tubulin was used as a loading control on each gel. Images are representative of triplicate experiments. Densitometry analysis of triplicate immunoblots was performed using ImageQuant software. * denotes $p \leq 0.05$, ** denotes $p \leq 0.001$.

6.7.3 Validation of HER2

Total proteomic analysis revealed decreased expression of HER2 in SKBR3-L cells following lapatinib treatment compared to SKBR3-par cells. SKBR3-L cells have higher levels of HER2 following lapatinib treatment compared to SKBR3-par cells following lapatinib treatment ($p = 0.06$), however, the altered expression of HER2 did not achieve significance [Figure 6-21].

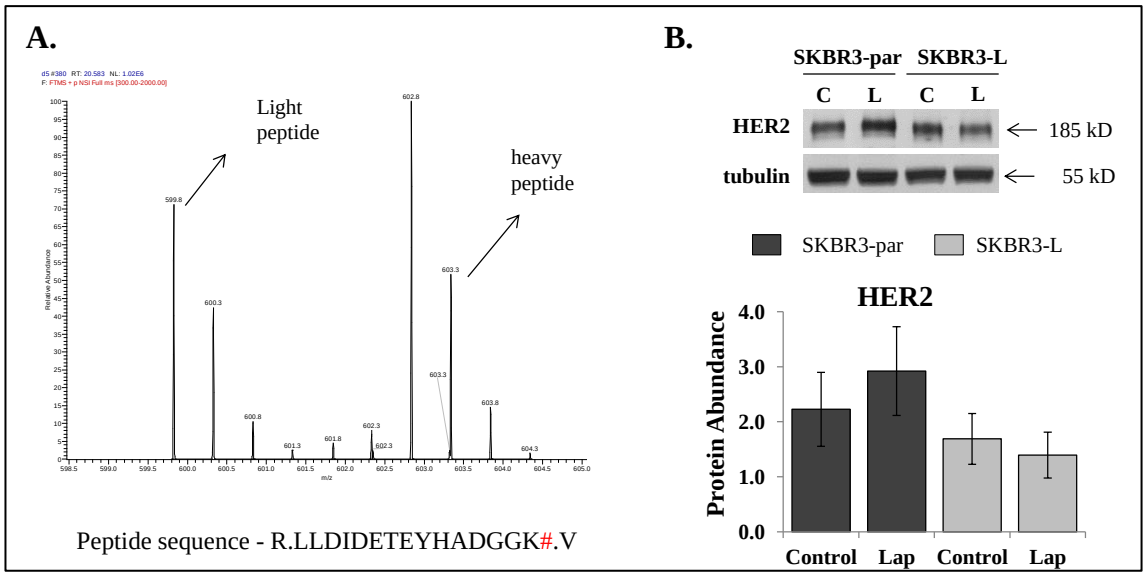

Figure 6-21: A) Full-MS revealing an alteration in matched heavy and light peptide sequence (R.LLDIDETEYHADGGK#.) which corresponds to HER2 protein, where # indicates labeled lysine, B) Immunoblotting for HER2 protein in SKBR3-par and SKBR3-L cells using 5 µg of protein. α-tubulin was used as a loading control on each gel. Images are representative of triplicate experiments. Densitometry analysis of triplicate immunoblots was performed using ImageQuant software.

6.7.4 Validation of Selenium-binding protein 1

Total proteomic analysis revealed that following lapatinib treatment the levels of selenium-binding protein 1 (SELENBP1) were higher in SKBR3-par cells compared to SKBR3-L cells. Selenium is an essential trace element which has been proposed to have an anti-cancer effect. A link between insufficient selenium and increased risk of cancer has been suggested [284, 285]. Immunoblotting confirmed that the expression of SELENBP1 was unaltered between untreated SKBR3-par and SKBR3-L cells, however following lapatinib treatment there was no significant change in the expression of SELENBP1 in SKBR3-par cells, while the expression of SELENBP1 was decreased in SKBR3-L cells following lapatinib treatment ($p = 0.017$) [Figure 6-22]. Thus, the levels of SELENBP1 were higher in SKBR3-L cells compared to SKBR3-par cells following lapatinib treatment ($p = 0.002$).

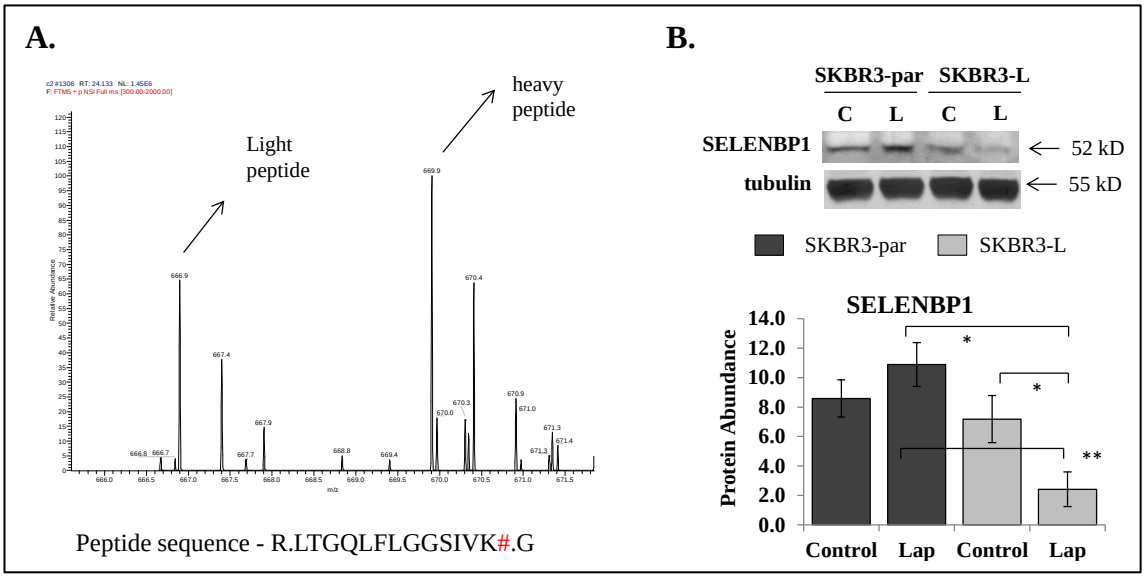

Figure 6-22: A) Full-MS revealing an alteration in matched heavy and light peptide sequence (R.LTGQLFLGGSIVK#.G) which corresponds to SELENBP1 protein, where # indicates labeled lysine, B) Immunoblotting for SELENBP1 protein in SKBR3-par and SKBR3-L cells. α-tubulin was used as a loading control on each gel. Images are representative of triplicate experiments. Densitometry analysis of triplicate immunoblots was performed using ImageQuant software. * denotes $p \leq 0.05$, ** denotes $p \leq 0.001$.

6.7.5 Validation of Protein SET

SET, more commonly known as I^2PP2A, is an oncoprotein with diverse cellular functions including cell cycle control, apoptosis and cell migration. SET was differentially expressed in SKBR3-par and SKBR3-L cells following treatment with lapatinib and this result was confirmed using immunoblotting. SKBR3-L cells treated with 1 µM lapatinib have 1.5-fold lower levels of I^2PP2A compared to SKBR3-par cells treated with lapatinib ($p = 0.03$) [Figure 6-23]. Lapatinib treatment had no effect on I^2PP2A expression in SKBR3-par cells, but resulted in decreased expression of I^2PP2A in SKBR3-L cells ($p = 0.02$). There was no significant difference in the expression of I^2PP2A between the untreated controls of each cell line.

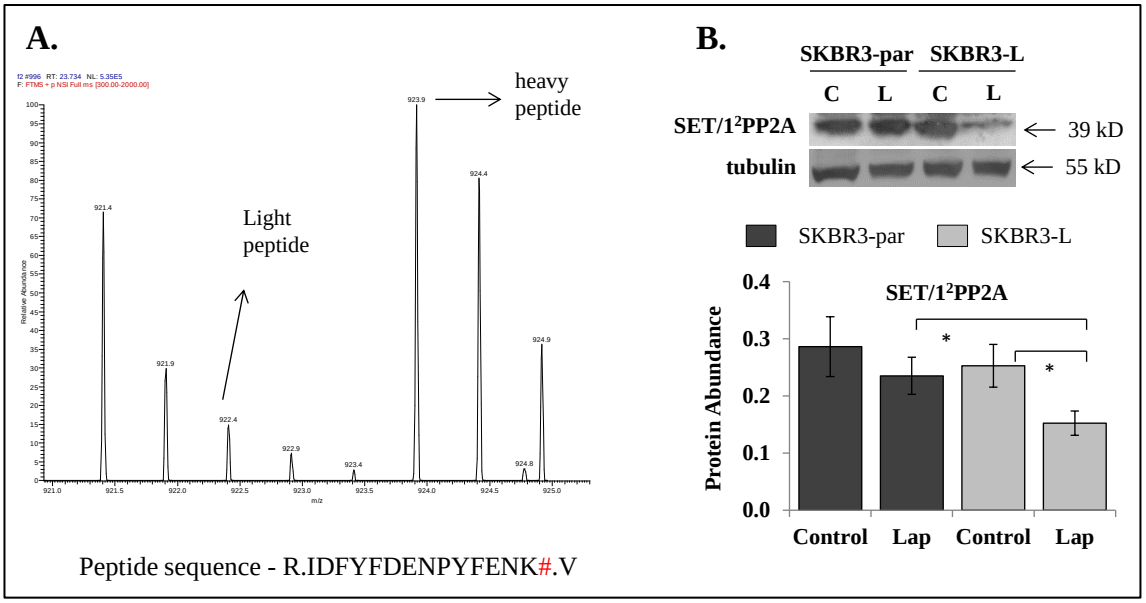

Figure 6-23: A) Full-MS revealing an alteration in matched heavy and light peptide sequence (R.IDFYFDENPYFENK#.V) which corresponds to SET/I^2PP2A protein, where # indicates labeled lysine, B) Immunoblotting for SET/I^2PP2A protein in SKBR3-par and SKBR3-L cells. α-tubulin was used as a loading control on each gel. Images are representative of triplicate experiments. Densitometry analysis of triplicate immunoblots was performed using ImageQuant software. * denotes $p \leq 0.05$, ** denotes $p \leq 0.001$.

6.7.6 Validation of Proliferation-associated protein 2G4

SILAC analysis revealed a 1.6-fold increase in the levels of Proliferation-associated protein 2G4, also known as EBP1, in SKBR3-L cells compared to SKBR3-par cells following treatment with lapatinib. EBP1 can interact with the cytoplasmic domain of HER3 and may contribute to transducing growth regulatory signals. EBP1 has been implicated in growth inhibition and the induction of differentiation of human cancer cells. Where there was no difference in the expression of EBP1 between SKBR3-par and SKBR3-L control untreated samples (p = 0.94) [Figure 6-24], treatment of the cells with lapatinib resulted in a significant decrease in EBP1 expression in SKBR3-par cells (p = 0.03), but no significant change in EBP1 expression in SKBR3-L cells. This resulted in SKBR3-L lapatinib treated cells having 2.5-fold higher expression of EBP1 compared to SKBR3-par lapatinib treated cells (p = 0.01).

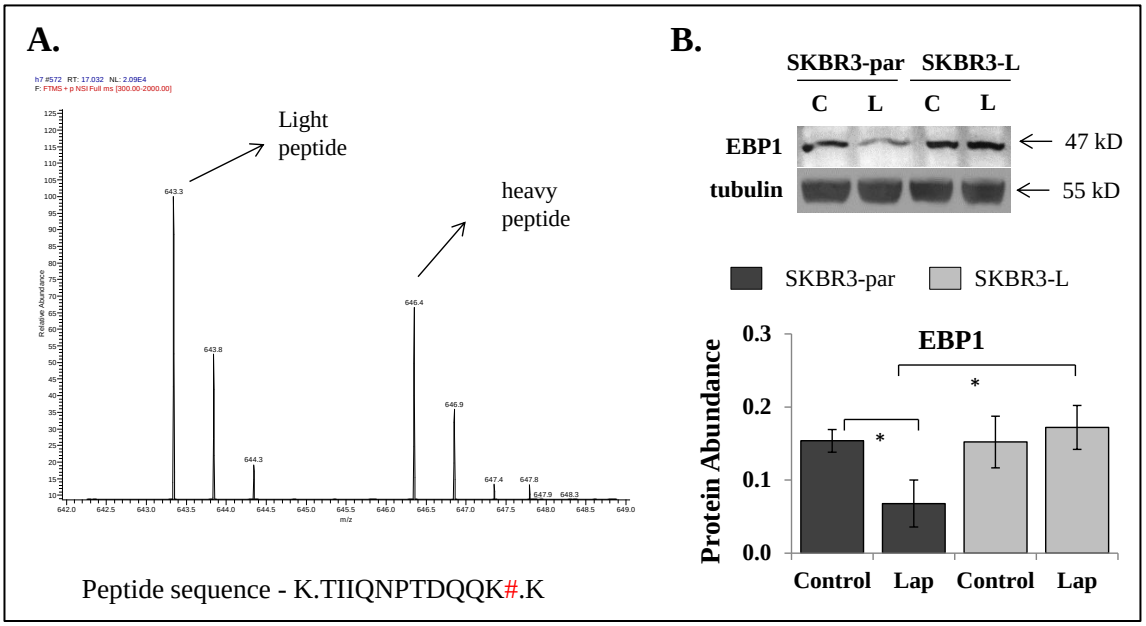

Figure 6-24: A) Full-MS revealing an alteration in matched heavy and light peptide sequence (K.TIIQNPTDQQK#.K) which corresponds to EBP1 protein, where # indicates labeled lysine, B) Immunoblotting for EBP1 protein in SKBR3-par and SKBR3-L cells. α-tubulin was used as a loading control on each gel. Images are representative of triplicate experiments. Densitometry analysis of triplicate immunoblots was performed using ImageQuant software. * denotes $p \leq 0.05$, ** denotes $p \leq 0.001$.

6.7 Summary

Metabolic labelling of cells using [U-$^{13}C^{6}$]-L-Lysine in SILAC media was achieved in SKBR3-par cells. The phospho-proteome of SKBR3-par cells was compared to SKBR3-L cells, both as untreated controls and in response to 1 µM lapatinib treatment. While the phospho-protein enrichment experiment was inefficient, CDK1 was identifed as a protein with increased phosphorylation in SKBR3-L cells compared to SKBR3-par cells. Lapatinib treatment resulted in decreased expression and phosphorylation of CDK1 in both cell lines. In addition to comparing the phospho-proteome of SKBR3-par and SKBR3-L cells, total proteomic analysis was also performed with the SILAC labelled protein extracts. A total of 20 proteins were detected that were altered between SKBR3-par and SKBR3-L cells, of these 20, the expression of 8 proteins were higher in SKBR3-par cells and the expression of 12 proteins was higher in SKBR3-L cells. The detected proteins encompass a range of different biological processes, functions and pathways. By comparing both cell lines following 24 hours treatment with 1 µM lapatinib a total of 15 proteins were detected that were altered between SKBR3-par and SKBR3-L cells (the expression of 13 proteins were higher in SKBR3-par cells and the expression of 2 proteins was higher in SKBR3-L cells). Significant alterations in the expression of GAPDH, HER2, SELENBP1 SET/I^{2}PP2A and EBP1 between SKBR3-par and SKBR3-L cells were confirmed using immunoblotting.

Chapter 7

Role of P13K, MAPK, mTOR and HER family signalling in innate lapatinib resistance

7.1 Introduction

Through collaboration with Dr Neil O'Brien in UCLA this study utilised a panel of 15 HER2-amplified cell lines which have under-gone extensive characterisation in their laboratory. The sensitivity of these cells lines to lapatinib has been published previously [194]. Ten of the cell lines are sensitive to lapatinib with IC_{50}s of less than 1 µM while 5 of the cell lines are resistant to lapatinib with IC_{50}s greater than 1 µM. Key signalling pathways which may contribute to innate lapatinib resistance were examined using this cell line panel. The key pathways involved in HER2 signalling and lapatinib response and resistance are the HER family members themselves, the downstream signalling pathways MAPK and P13K/AKT, and as demonstrated in SKBR3-L cells, the mTOR pathway. The basal levels of phospho-HER2, phospho-HER3 and phospho-EGFR have been shown to correlate with response to lapatinib [194]. Therefore in addition to examining the basal levels of proteins, the effect of lapatinib treatment on key members of these signalling pathways was examined and alterations of these proteins were correlated with response to lapatinib based on the IC_{50} data described in Table 7-1.

Table 7-1: The panel of HER2-amplified cell lines with lapatinib IC_{50} values ± the standard deviation of triplicate experiments. The responsiveness of each cell line to lapatinib is also described where S indicates sensitive while R indicates resistant. The lapatinib-resistant cell lines are highlighted in red. The assays in this table were performed by Dr Neil O'Brien and the data is reproduced from [194] with his permission.

Cell Line	**Lapatinib**	
	IC_{50} ± SD (μM)	Response
BT-474	0.016 ± 0.011	S
SUM-190	0.038 ± 0.003	S
HCC-1419	0.050 ± 0.021	S
SKBR3	0.054 ± 0.008	S
EFM192A	0.075 ± 0.002	S
HCC-202	0.074 ± 0.026	S
SUM-225	0.089 ± 0.052	S
ZR75-30	0.271 ± 0.136	S
MDA-361	0.295 ± 0.064	S
HCC-1954	0.358 ± 0.064	S
UACC-893	1.211 ± 0.251	R
JIMT-1	2.374 ± 0.246	R
UACC-732	2.629 ± 0.480	R
HCC-1569	3.550 ± 0.715	R
MDA-453	5.997 ± 1.103	R

7.2 Alterations in HER family members and lapatinib response

Lapatinib is a dual inhibitor of HER2 and EGFR; therefore the effect of lapatinib treatment on the phosphorylation of these proteins was examined. HER3 and HER2 heterodimers lead to activation of downstream signalling cascades. Thus the levels of phospho-HER3 following lapatinib treatment was also examined.

7.2.1 Expression and phosphorylation of HER2 and innate lapatinib sensitivity

The basal expression and phosphorylation of HER2 was examined in a panel of HER2-amplified cell lines. In addition, each cell line was treated with 1 μM lapatinib for 24

hours and examined alterations in phospho- and total HER2 levels [Figure 7-1]. Phospho-HER2 was detected in all cell lines, with the exception of JIMT-1 cells which had undetectable phospho-HER2 and UACC732 cells which had extremely low levels. An association was found between basal levels of phospho-HER2 and lapatinib response ($p = 0.094$), with higher levels of phospho-HER2 in lapatinib sensitive cells [Figure 7-2]. An association was also found between loss of phospho-HER2 following lapatinib treatment and lapatinib response ($p = 0.054$), with lapatinib sensitive cells exhibiting a greater decrease in phospho-HER2 levels following lapatinib treatment. Total HER2 was detected in all 15 cell lines. The basal expression of HER2 significantly correlates with lapatinib response ($p = 0.03$), with lapatinib sensitive cell lines expressing higher levels of HER2 compared to lapatinib-resistant cells, however there was no relationship between increased levels of HER2 following lapatinib treatment and lapatinib response ($p = 0.267$).

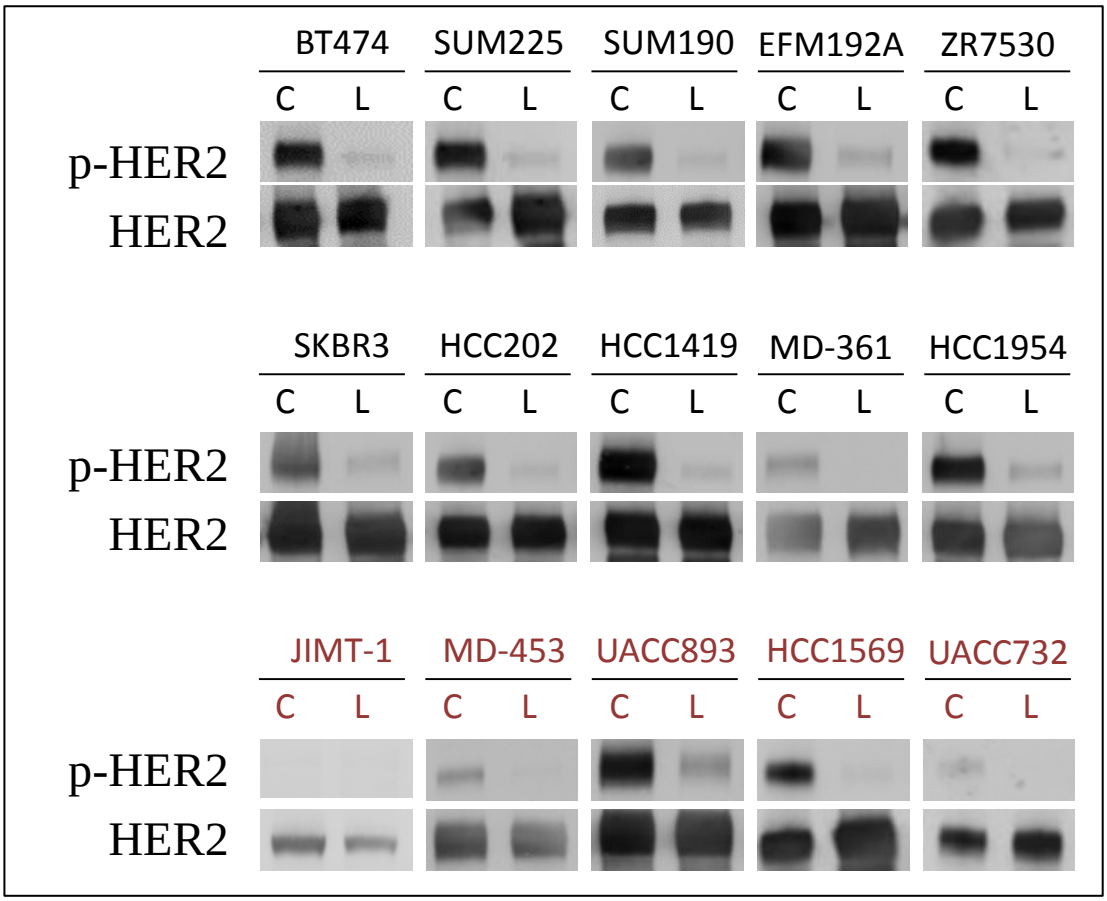

Figure 7-1: Immunoblotting for phospho-HER2 (Tyr1221/1222) and total HER2 in BT474, SUM225, SUM190, EFM192A, ZR7530, SKBR3, HCC202, HCC1419, MDA-MB-361, HCC1954, JIMT-1, MD-MBA-453, UACC893, HCC1569 and UACC732 cells treated with 1 μM lapatinib for 24 hours. α-tubulin was used as a loading control on each gel (not shown). Images are representative of triplicate experiments. Densitometry analysis of triplicate immunoblots was performed using ImageQuant software. Cell lines in red indicate innate lapatinib resistance.

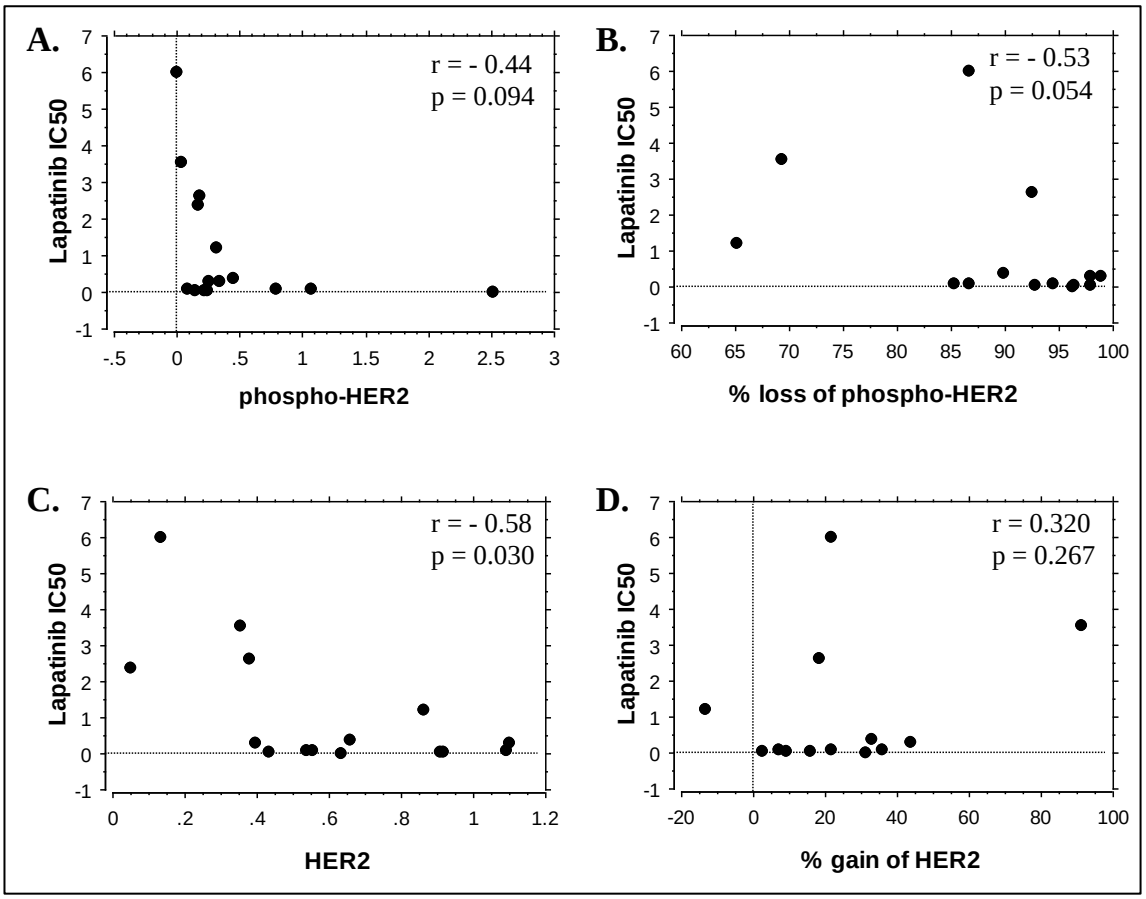

Figure 7-2: Bi-variant scattergraphs of lapatinib IC_{50} values compared to A) basal expression of phospho-HER2, B) percentage loss of phospho-HER2 following 24 hour 1 µM lapatinib treatment, C) basal expression of HER2 and D) percentage gain of HER2 following 24 hour 1 µM lapatinib treatment in a panel of HER2-amplified breast cancer cell lines.. Correlations performed using Speatman rank correlation (Statview).

7.2.2 Expression and phosphorylation of HER3 and innate lapatinib sensitivity

The basal expression and phosphorylation of HER3 was examined in the panel of HER2-amplified cell lines, and in response to 1 µM lapatinib (24 hours) [Figure 7-3]. Several cell lines had very low expression of phospho-HER3. A correlation between basal levels of phospho-HER3 and lapatinib response ($p = 0.049$) was found, with lapatinib sensitive cell lines exhibiting higher levels of phospho-HER3 compared to lapatinib-resistant cells [Figure 7-4]. There was no correlation between loss of phospho-HER3 following lapatinib treatment and lapatinib response ($p = 0.921$). Total HER3 was detected in all 15 cell lines; however, several cell lines had very low expression levels. There was no correlation between the basal expression of HER3 and lapatinib

response (p = 0.721). There was also no correlation between increased expression of HER3 following lapatinib treatment and lapatinib response (p = 0.401).

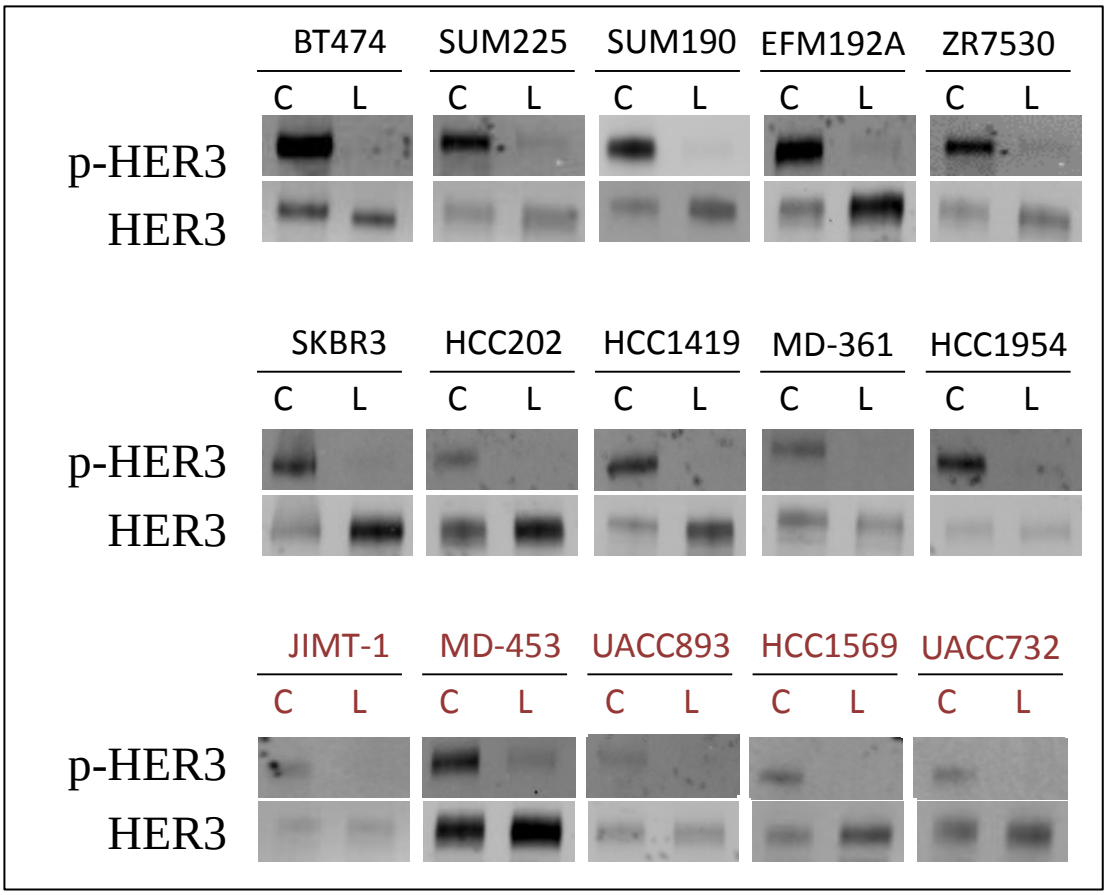

Figure 7-3: Immunoblotting for phospho-HER3 (Tyr1289) and total HER3 in BT474, SUM225, SUM190, EFM192A, ZR7530, SKBR3, HCC202, HCC1419, MDA-MB-361, HCC1954, JIMT-1, MD-MBA-453, UACC893, HCC1569 and UACC732 cells treated with 1 μM lapatinib for 24 hours. α-tubulin was used as a loading control on each gel (not shown). Images are representative of triplicate experiments. Densitometry analysis of triplicate immunoblots was performed using ImageQuant software. Cell lines in red indicate innate lapatinib resistance.

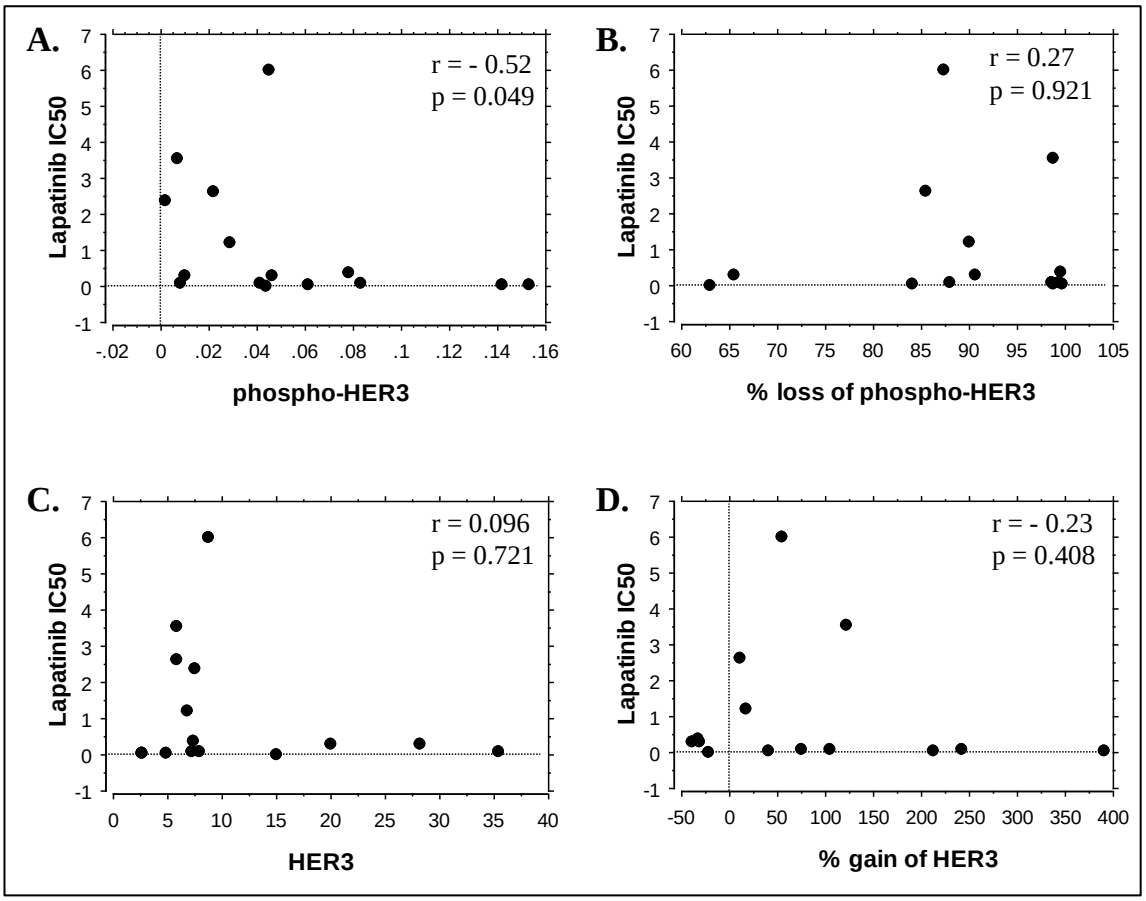

Figure 7-4: Bi-variant scattergraphs of lapatinib IC_{50} values compared to A) basal expression of phospho-HER3, B) percentage loss of phospho-HER3 following 24 hour 1 µM lapatinib treatment, C) basal expression of HER3 and D) percentage gain of HER3 following 24 hour 1 µM lapatinib treatment in a panel of HER2-amplified breast cancer cell lines. Correlations performed using Speatman rank correlation (Statview).

7.2.3. Expression and phosphorylation of EGFR and innate lapatinib sensitivity

Levels of phospho-EGFR were either very low or undetectable in the panel of cell lines, thus correlations between phospho-EGFR and lapatinib response were not performed [Figure 7-5]. EGFR was not detected in 3 of the cell lines tested. There was no correlation between basal expression of EGFR and lapatinib response ($p = 0.299$), nor was there a correlation between decreased EGFR expression following lapatinib treatment and lapatinib response ($p = 0.420$) [Figure 7-6].

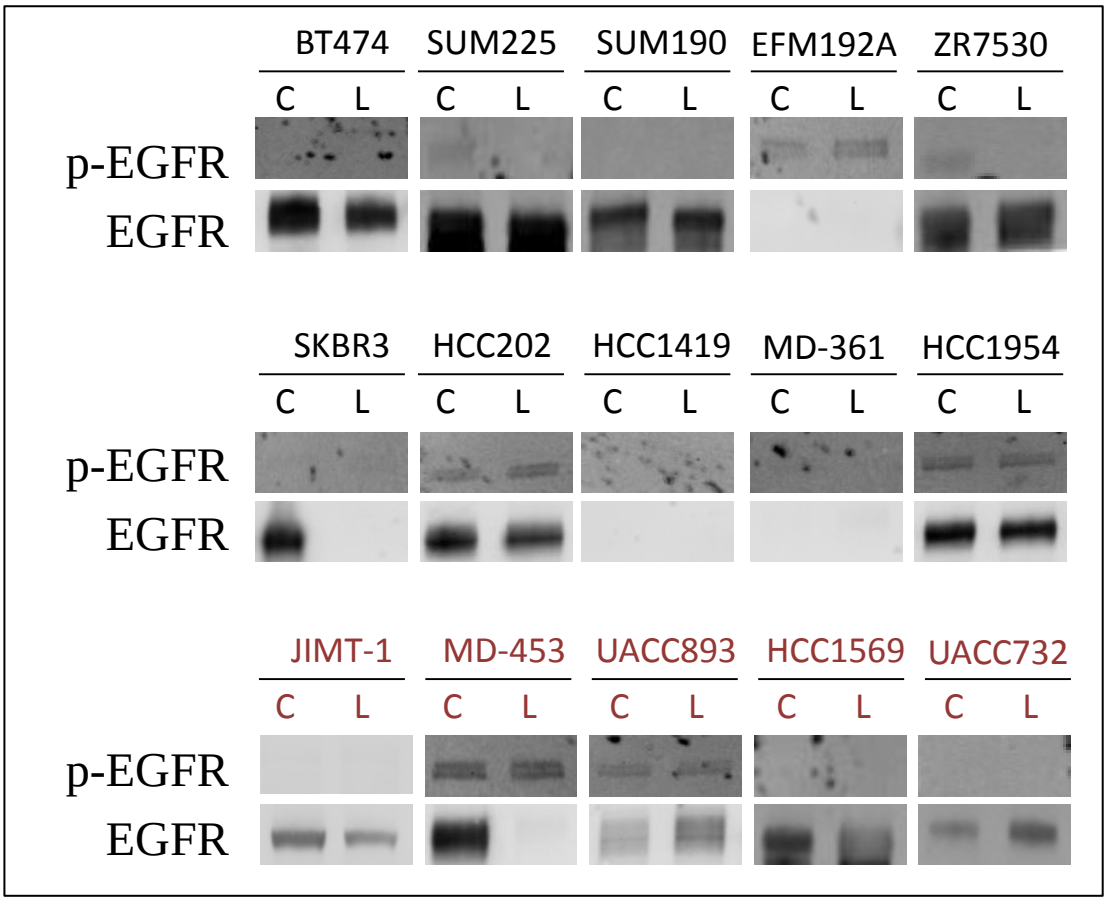

Figure 7-5: Immunoblotting for phospho-EGFR (Tyr1173) and total EGFR in BT474, SUM225, SUM190, EFM192A, ZR7530, SKBR3, HCC202, HCC1419, MDA-MB-361, HCC1954, JIMT-1, MD-MBA-453, UACC893, HCC1569 and UACC732 cells treated with 1 μM lapatinib for 24 hours. α-tubulin was used as a loading control on each gel (not shown). Images are representative of triplicate experiments. Densitometry analysis of triplicate immunoblots was performed using ImageQuant software. Cell lines in red indicate innate lapatinib resistance.

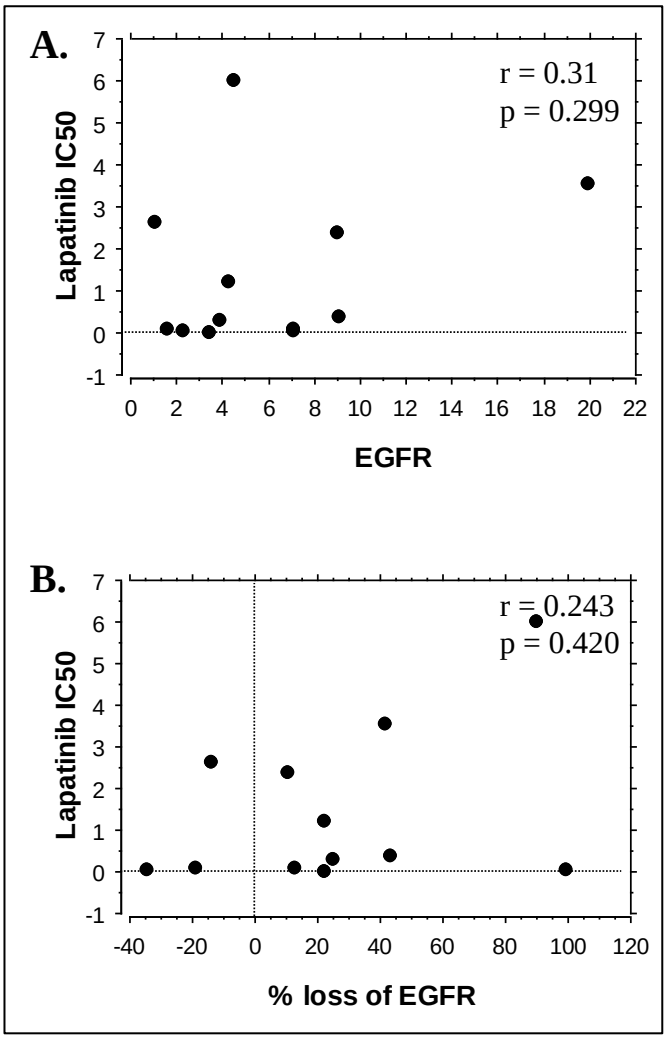

Figure 7-6: Bi-variant scattergraphs of lapatinib IC_{50} values compared to A) basal expression of EGFR, and B) percentage loss of EGFR following 24 hour 1 µM lapatinib treatment in a panel of HER2-amplified breast cancer cell lines. Correlations performed using Speatman rank correlation (Statview).

7.3 Alterations in signalling pathways downstream of HER2 and lapatinib response

The key signalling pathways activated by HER2 signalling are the P13K/AKT, MAPK and mTOR pathways, thus the expression and phosphorylation of key members of the above signalling pathways were examined in a panel of HER2-amplified breast cancer cell lines.

7.3.1 Expression and phosphorylation of AKT and innate lapatinib sensitivity

Phospho-AKT was detected in all cell lines with the exception of UACC732 cells [Figure 7-7]. No correlation was found between basal levels of phospho-AKT and lapatinib response ($p = 0.595$) [Figure 7-8]. There was a correlation between loss of phospho-AKT following lapatinib treatment and lapatinib response ($p = 0.035$), with lapatinib sensitive cells exhibiting a greater reduction in phospho-AKT levels compared to lapatinib-resistant cells following lapatinib treatment. Total AKT was detected in all cell lines and there was no association between basal AKT expression and lapatinib response ($p = 0.628$). There were no statistically significant alterations in the expression of AKT following lapatinib treatment.

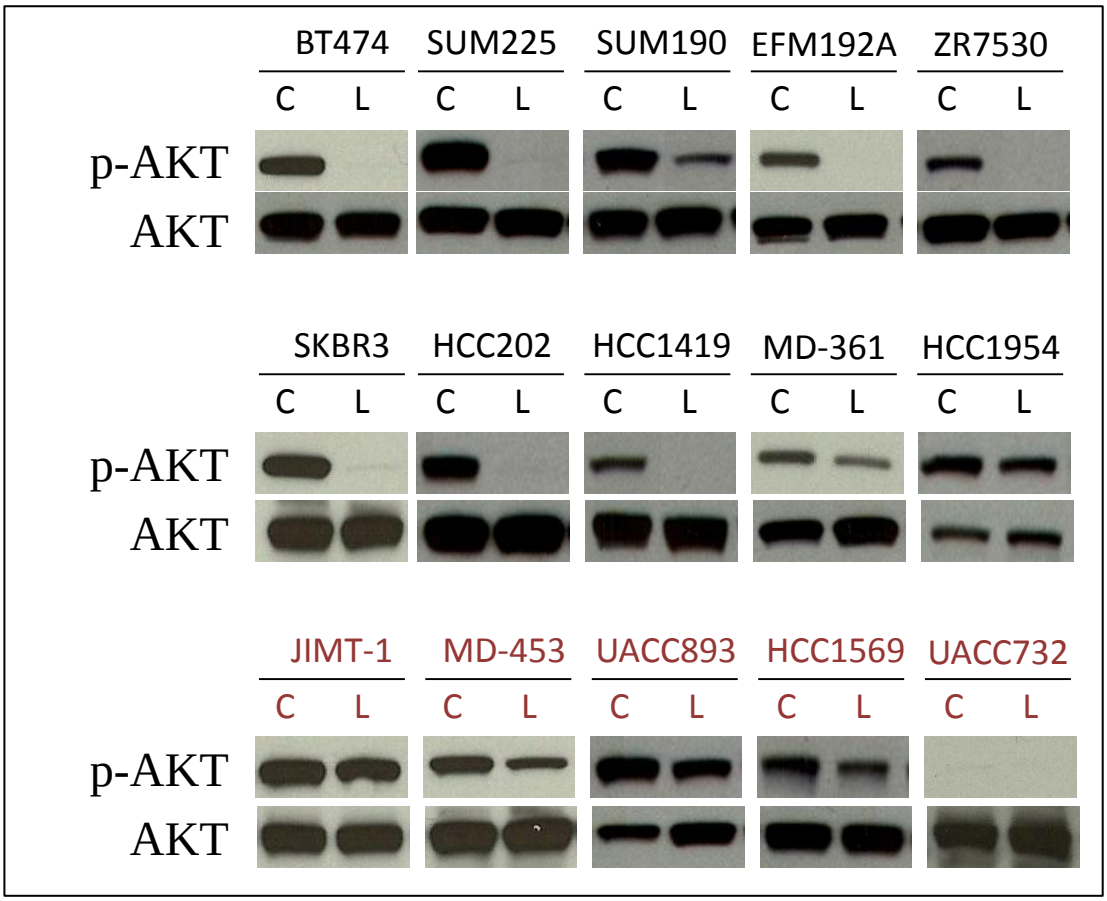

Figure 7-7: Immunoblotting for phospho-AKT (Ser473) and total AKT in BT474, SUM225, SUM190, EFM192A, ZR7530, SKBR3, HCC202, HCC1419, MDA-MB-361, HCC1954, JIMT-1, MD-MBA-453, UACC893, HCC1569 and UACC732 cells treated with 1 μM lapatinib for 24 hours. α-tubulin was used as a loading control on each gel (not shown). Images are representative of triplicate experiments. Densitometry analysis of triplicate immunoblots was performed using ImageQuant software. Cell lines in red indicate innate lapatinib resistance.

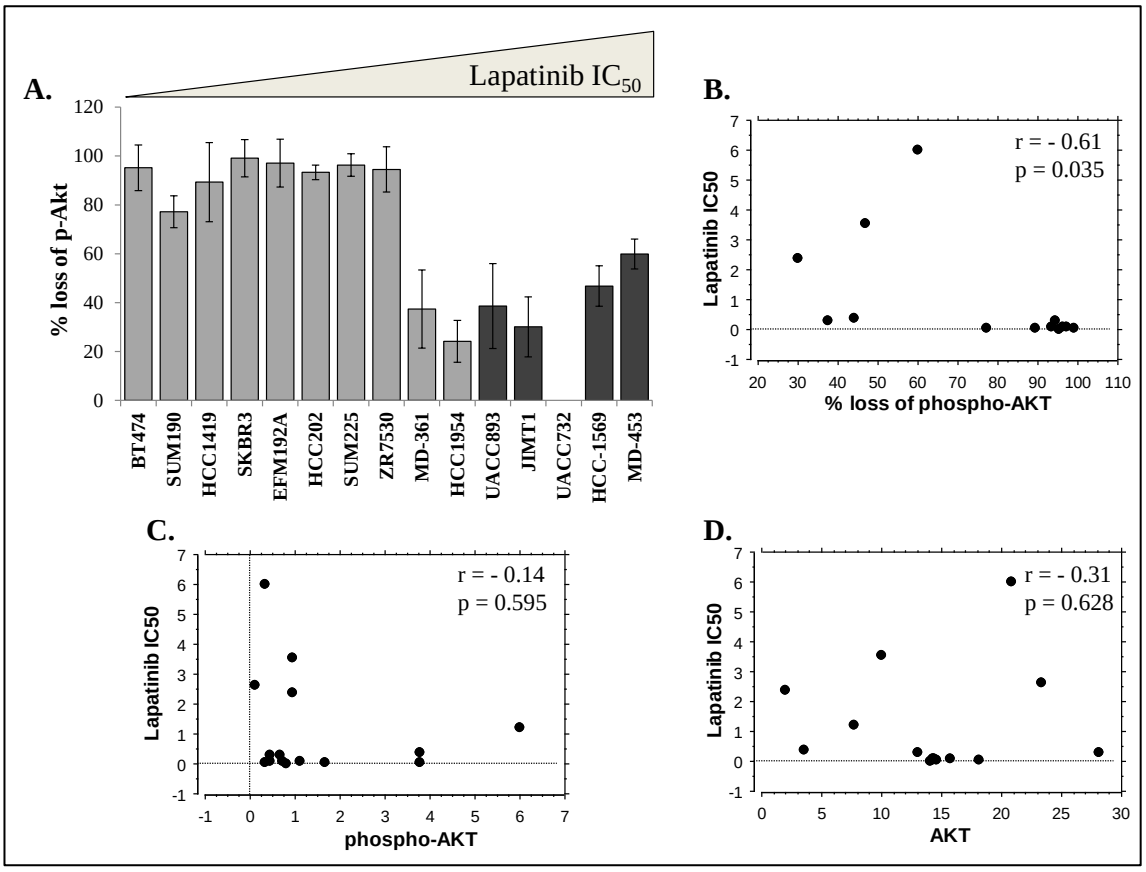

Figure 7-8: A) Percentage loss of phospho-AKT (± standard deviation) in the panel of HER2-amplified cells followed 24 hour treatment with 1 µM lapatinib, ordered from lowest to highest lapatinib IC_{50} value (left to right). Bi-variant scattergraphs of lapatinib IC_{50} values compared to B) percentage loss of phospho-AKT following lapatinib treatment, C) basal expression of phospho-AKT and D) basal expression of AKT in a panel of HER2-amplifed cell lines. Correlations performed using Spearman rank correlation (Statview).

7.3.2 Expression and phosphorylation of ERK and innate lapatinib sensitivity

Phospho-ERK was detected in all cell lines at differing levels [Figure 7-9]. No correlation was found between basal levels of phospho-ERK and lapatinib response (p = 0.986) however there was a correlation between loss of phospho-ERK following lapatinib treatment and lapatinib response (p = 0.014) with the more sensitive cell lines showing a greater decrease in phospho-ERK levels following lapatinib treatment [Figure 7-10]. Total ERK was detected in all cell lines and there was a weak correlation between basal ERK expression and lapatinib response (p = 0.093), with a trend towards

higher expression of ERK in lapatinib-resistant cell lines. There were no statistically significant alterations in the expression of ERK following lapatinib treatment.

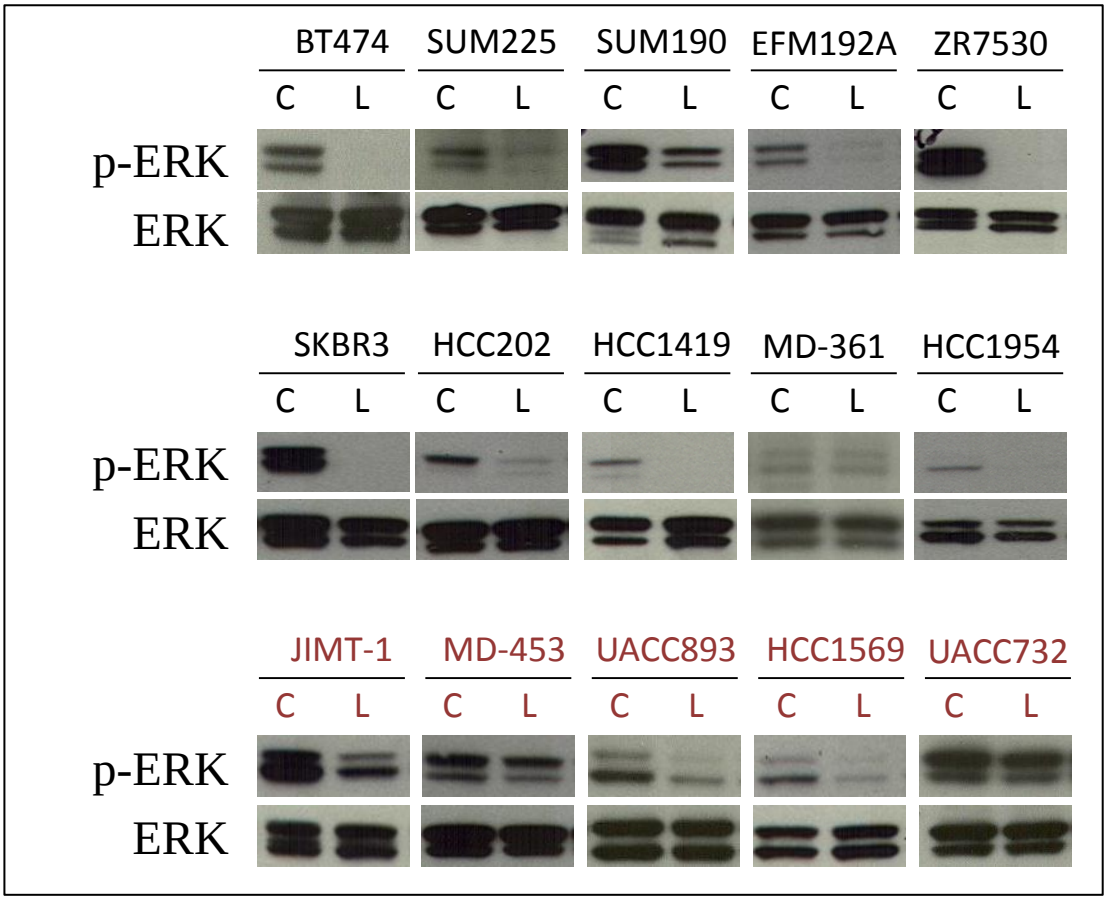

Figure 7-9: Immunoblotting for phospho-ERK (Thr202/204) and total ERK in BT474, SUM225, SUM190, EFM192A, ZR7530, SKBR3, HCC202, HCC1419, MDA-MB-361, HCC1954, JIMT-1, MD-MBA-453, UACC893, HCC1569 and UACC732 cells treated with 1 μM lapatinib for 24 hours. α-tubulin was used as a loading control on each gel (not shown). Images are representative of triplicate experiments. Densitometry analysis of triplicate immunoblots was performed using ImageQuant software. Cell lines in red indicate innate lapatinib resistance.

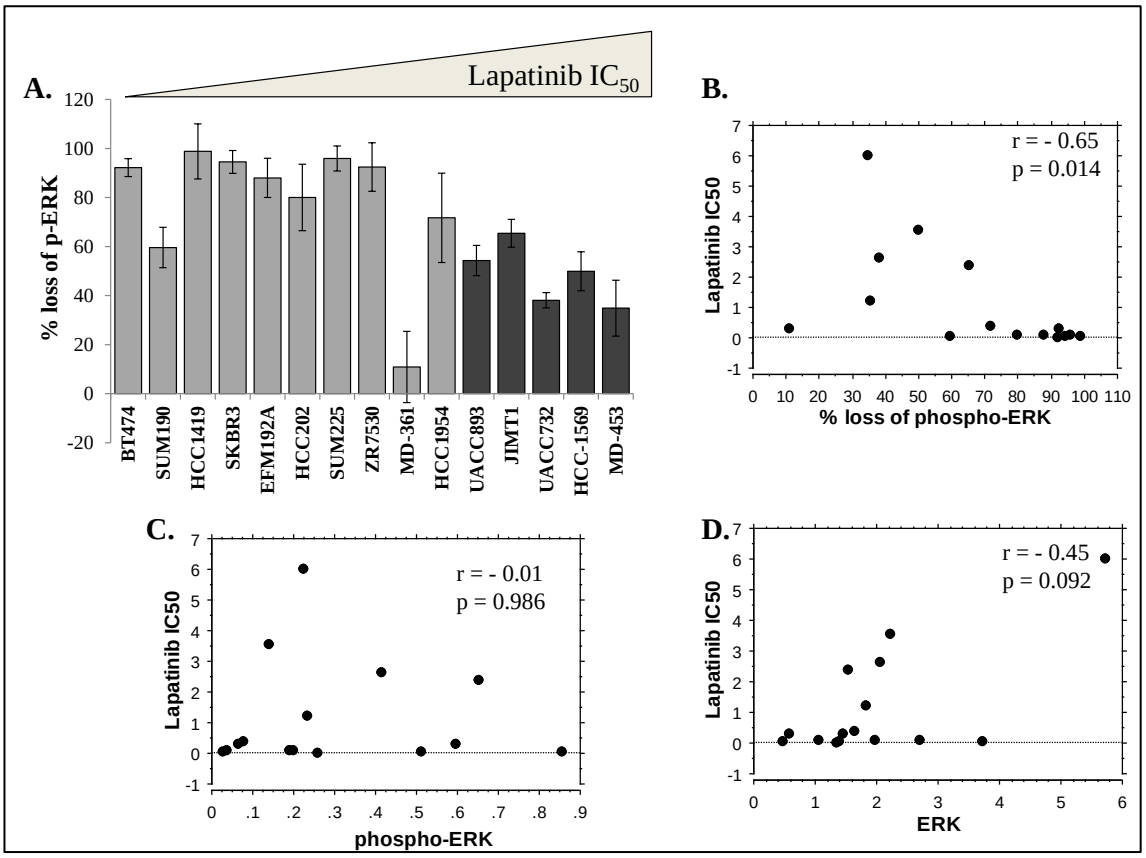

Figure 7-10: A) Percentage loss of phospho-ERK (± standard deviation) in the panel of HER2-amplified cells followed 24 hour treatment with 1 µM lapatinib, ordered from lowest to highest lapatinib IC_{50} value (left to right). Bi-variant scattergraphs of lapatinib IC_{50} values compared to B) percentage loss of phospho-ERK following lapatinib treatment, C) basal expression of phospho-ERK and D) basal expression of ERK in a panel of HER2-amplifed cell lines. Correlations performed using Spearman rank correlation (Statview).

7.3.3 Expression and phosphorylation of p70S6k and innate lapatinib sensitivity

Experiments described in Chapter 5 show that alterations in the mTOR pathway, specifically alterations in phospho-p70S6k and phospho-eEF2 correlate with lapatinib resistance in a model of acquired lapatinib resistance. The effect of lapatinib treatment was examined in the panel of HER2-amplified cell lines to see if alterations in these proteins would correlate with innate lapatinib resistance also.

Phospho-p70S6k was detected in all of the cell lines at varying levels [Figure 7-11]. The basal levels of phospho-p70S6k did not correlate with lapatinib response (p = 0.997),

however, loss of phospho-70S6k following lapatinib treatment correlated significantly ($p = 0.046$), with the more sensitive cell lines showing a greater decrease in phospho-p70S6k levels following lapatinib treatment [Figure 7-12]. Total p70S6k was expressed in all of the cell lines and the basal expression of p70S6k, was higher in lapatinib sensitive cell lines, however, this result failed to reach statistical significance ($p = 0.057$). There were no statistically significant alterations in the expression of p70S6k following lapatinib treatment.

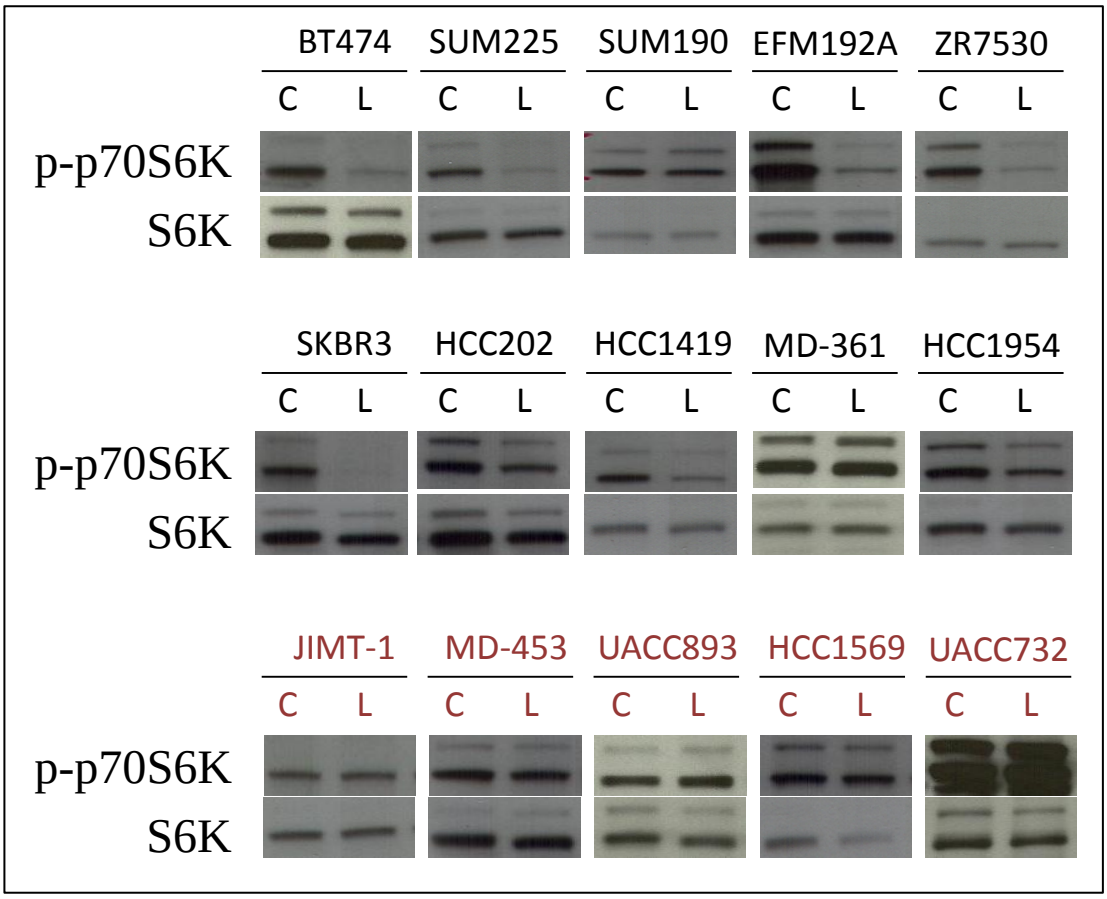

Figure 7-11: Immunoblotting for phospho- p70S6k (Thr389) and total p70S6k in BT474, SUM225, SUM190, EFM192A, ZR7530, SKBR3, HCC202, HCC1419, MDA-MB-361, HCC1954, JIMT-1, MD-MBA-453, UACC893, HCC1569 and UACC732 cells treated with 1 μM lapatinib for 24 hours. α-tubulin was used as a loading control on each gel (not shown). Images are representative of triplicate experiments. Densitometry analysis of triplicate immunoblots was performed using ImageQuant software. Cell lines in red indicate innate lapatinib resistance.

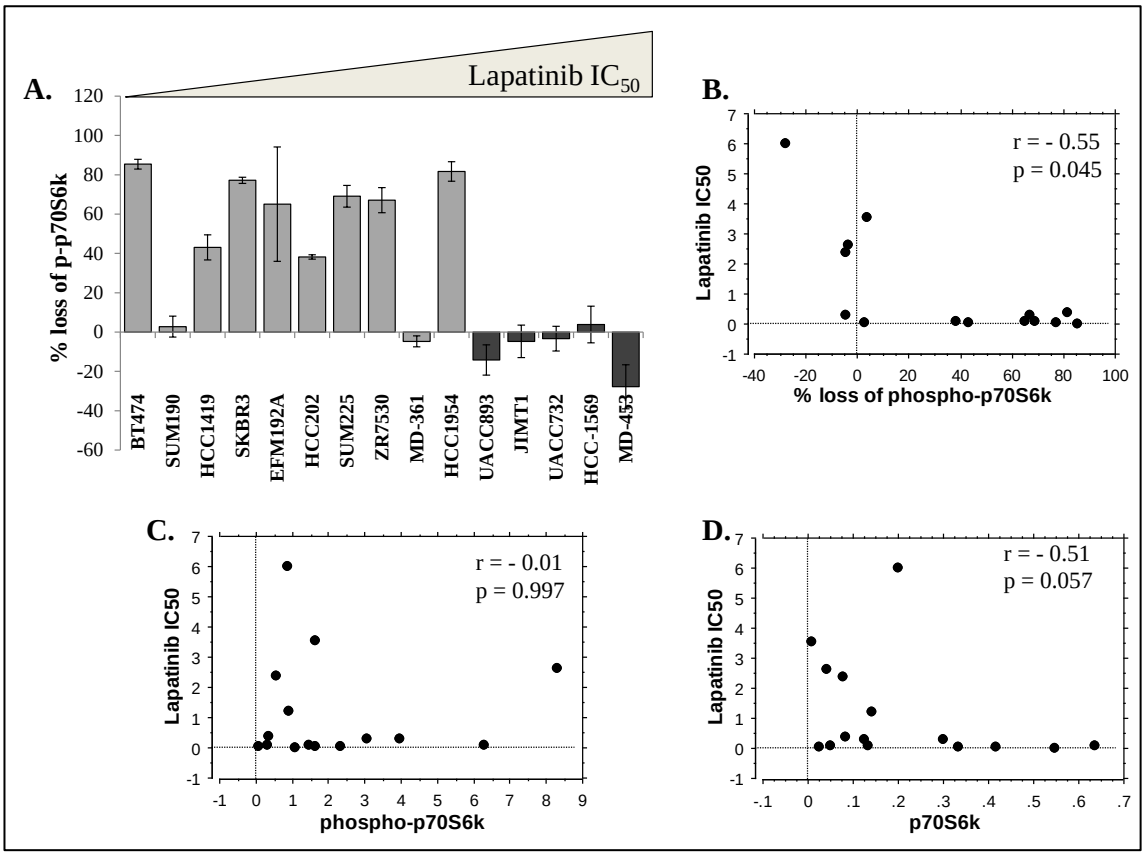

Figure 7-12: A) Percentage loss of phospho-p70S6k (± standard deviation) in the panel of HER2-amplified cells followed 24 hour treatment with 1 µM lapatinib, ordered from lowest to highest lapatinib IC_{50} value (left to right). Bi-variant scattergraphs of lapatinib IC_{50} values compared to B) percentage loss of phospho- p70S6k following lapatinib treatment, C) basal expression of phospho- p70S6k and D) basal expression of p70S6k in a panel of HER2-amplifed cell lines. Correlations performed using Spearman rank correlation (Statview).

7.3.4 Expression and phosphorylation of eEF2 and innate lapatinib sensitivity

Phospho-eEF2 was detected in all of the cell lines, with the exception of UACC732 cells [Figure 7-13]. The basal levels of phospho-eEF2 did not correlate with lapatinib response (p = 0.513), however, gain of phospho-eEF2 following lapatinib treatment correlated significantly with lapatinib response (p = 0.011), with the more sensitive cell lines showing a greater increase in phospho-eEF2 levels following lapatinib treatment [Figure **7-14**]. Total eEF2 was expressed in all of the cell lines however, there was no correlation between the basal expression of eEF2 and lapatinib response (p = 0.912). There were no statistically significant alterations in the expression of eEF2 following lapatinib treatment.

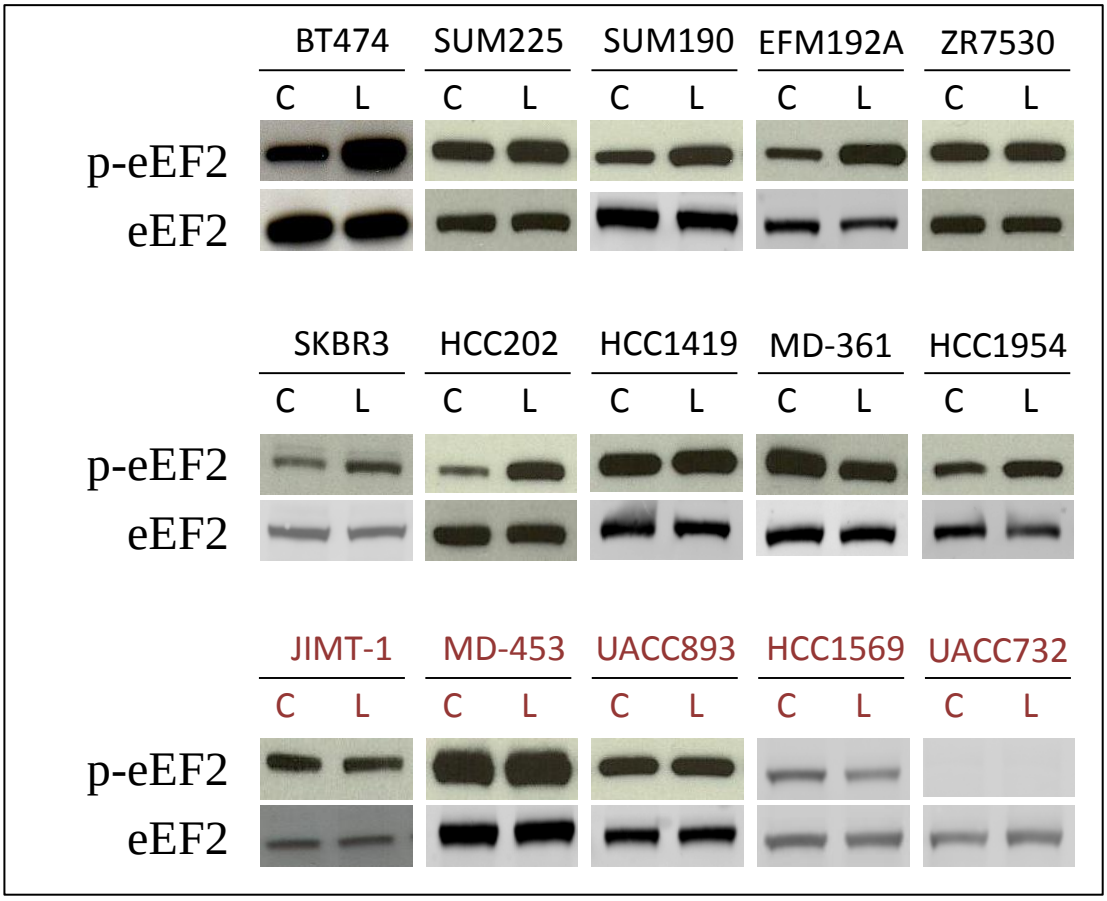

Figure 7-13: Immunoblotting for phospho-eEF2 (Thr56) and total eEF2 in BT474, SUM225, SUM190, EFM192A, ZR7530, SKBR3, HCC202, HCC1419, MDA-MB-361, HCC1954, JIMT-1, MD-MBA-453, UACC893, HCC1569 and UACC732 cells treated with 1 μM lapatinib for 24 hours. α-tubulin was used as a loading control on each gel (not shown). Images are representative of triplicate experiments. Densitometry analysis of triplicate immunoblots was performed using ImageQuant software. Cell lines in red indicate innate lapatinib resistance.

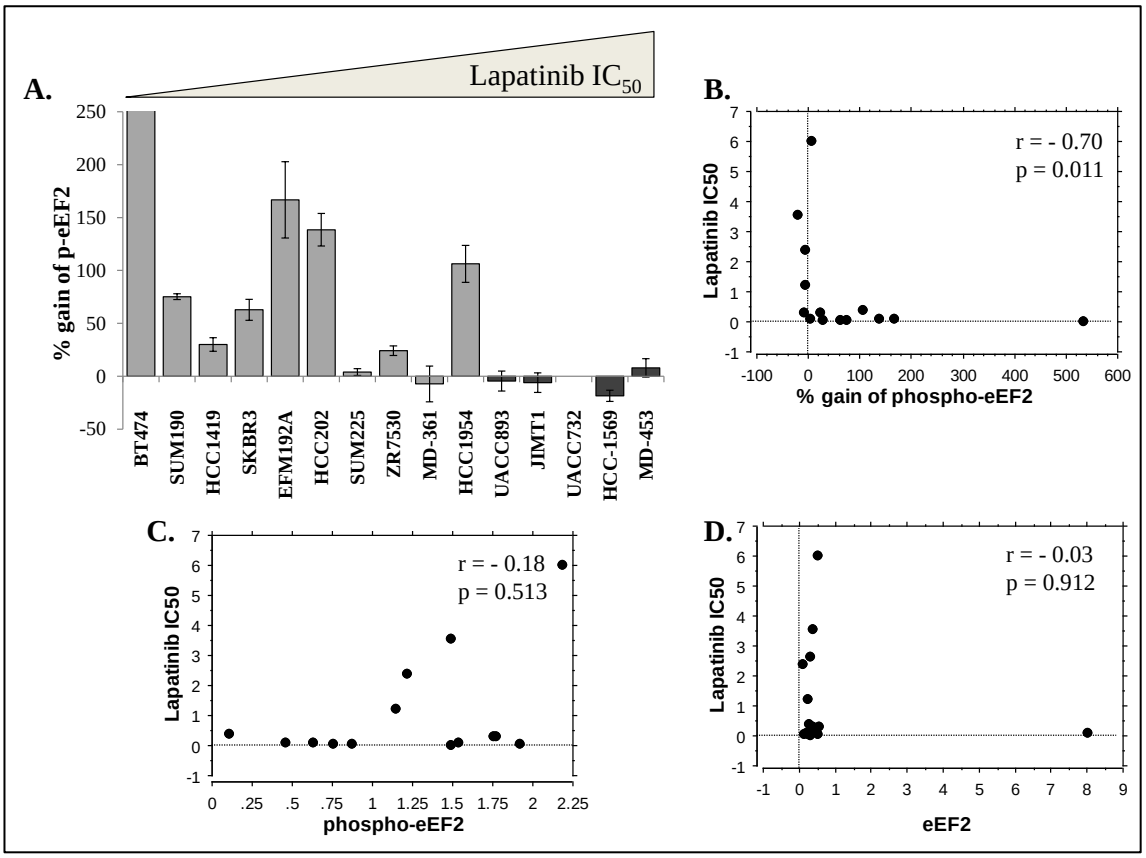

Figure 7-14: A) Percentage loss of phospho-eEF2 (± standard deviation) in the panel of HER2-amplified cells followed 24 hour treatment with 1 µM lapatinib, ordered from lowest to highest lapatinib IC_{50} value (left to right). Bi-variant scattergraphs of lapatinib IC_{50} values compared to B) percentage loss of phospho-eEF2 following lapatinib treatment, C) basal expression of phospho-eEF2 and D) basal expression of eEF2 in a panel of HER2-amplifed cell lines. Correlations performed using Spearman rank correlation (Statview).

Lapatinib treatment resulted in significant alterations in the phosphorylation of AKT, ERK, p70S6k and eEF2 [summarised in Table 7-2]. These results suggest that although the majority of cell lines exhibit uniform alterations dependent on their classification as a lapatinib sensitive or lapatinib-resistant cell line, there are several cell lines which do not respond as expected. For example, SUM190 and MDA-MB-361 cells exhibit alterations in the phosphorylation of the above proteins which are more characteristic of lapatinib-resistant cells rather than lapatinib sensitive cells, in addition MDA-MB-453 cells exhibit a small increase in peEF2 levels following lapatinib treatment in contrast to the other lapatinib-resistant cell lines which all exhibit either decreased levels or not change. Thus, these results suggest that when studying innate lapatinib resistance

SUM190, MDA-MB and MDA-MB-453 cell lines should not be studied in isolation, but rather only as part of a larger panel of cell lines.

Table 7-2: Summary of alterations in phosphorylation of AKT, ERK, p70S6k and eEF2 in lapatinib treated HER2-amplified breast cancer cell lines. Results are represented as either greater than or less than the average decrease in levels of phosphorylated protein for AKT, ERK and p70S6k, and as an increase or decrease in the phosphorylation of eEF2. Innate lapatinib-resistant cell lines are depicted in red. Italics indicate atypical cell lines.

Cell line	loss of p-AKT	loss of p-p70S6k	loss of p-ERK	p-eEF2 levels
BT474	≥ 70 %	≥ 35 %	≥ 65 %	increase
SUM190	*≤ 70 %*	*≤ 35 %*	*≤ 65 %*	*increase*
HCC1419	≥ 70 %	≥ 35 %	≥ 65 %	increase
SKBR3	≥ 70 %	≥ 35 %	≥ 65 %	increase
EFM192A	≥ 70 %	≥ 35 %	≥ 65 %	increase
HCC202	≥ 70 %	≥ 35 %	≥ 65 %	increase
SUM225	≥ 70 %	≥ 35 %	≥ 65 %	increase
ZR7530	≥ 70 %	≥ 35 %	≥ 65 %	increase
M361	*≤ 70 %*	*≤ 35 %*	*≤ 65 %*	*decrease*
HCC1954	≤ 70 %	≥ 35 %	≥ 65 %	increase
UACC893	≤ 70 %	≤ 35 %	≤ 65 %	decrease
JIMT1	≤ 70 %	≤ 35 %	≤ 65 %	decrease
UACC732	≤ 70 %	≤ 35 %	≤ 65 %	decrease
HCC-1569	≤ 70 %	≤ 35 %	≤ 65 %	decrease
MDA453	*≤ 70 %*	*≤ 35 %*	*≤ 65 %*	*increase*

7.4 Summary

The basal phosphorylation and expression of members of the HER family and several key members of signalling pathways downstream of HER2 were examined in a panel of HER2-amplified breast cancer cell lines. In addition the effects of lapatinib treatment on the expression and phosphorylation of these proteins was examined and correlations with the lapatinib IC_{50} value of each cell line were performed. High basal levels of

phospho-HER3 significantly correlated with sensitivity to lapatinib and there was a weak association between higher levels of phospho-HER2, HER2, and p70S6k and lapatinib sensitivity. Lower basal levels of ERK weakly associated with lapatinib sensitivity also. In contrast, there was no correlation between the levels of HER3, EGFR, phospho- or total AKT, phospho-ERK, phospho-p70S6k, phospho-or total eEF2 and sensitivity to lapatinib in the panel of HER2-amplifed cell lines. Each cell line was treated with 1 μM lapatinib for 24 hours and alterations in the expression and phosphorylation of the proteins were correlated with lapatinib IC_{50} values. There were no significant alterations in the expression of AKT, ERK, p70S6k or eEF2, and alterations on the levels of HER2, phospho-HER3, HER3 or EGFR did not correlate with response to lapatinib. However, there were significant correlations between lapatinib sensitivity and decreased levels of phospho-HER2, phospho-AKT, phospho-ERK and phospho-p70S6k. In addition, lapatinib sensitivity also correlated with increased levels of phospho-eEF2.

Chapter 8

Discussion

8.1 Introduction

Lapatinib, a dual HER2/EGFR tyrosine kinase inhibitor, in combination with capecitabine is approved for the treatment of HER2-positive trastuzumab refractory metastatic breast cancer. However, lapatinib has limited response as a single agent and many patients treated with lapatinib fail to respond to therapy, *de novo* (innate) resistance, or after a period of response develop resistance to lapatinib, acquired resistance [131]. A major stumbling block in the study and treatment of acquired lapatinib resistance is the limited number of published and characterised cell line models of resistance. This study sought to address this by developing new cell line models of acquired lapatinib resistance and characterising the resistance phenotype, with a view to identifying mechanisms of acquired lapatinib resistance. The use of *in vitro* cell line models of cancer, derived from patient tumour samples has long been the primary method used for the preclinical study of cancer. Promising *in vitro* data is frequently examined using *in vivo* cancer models, prior to evaluation using patient samples – successful hypotheses are then subject to analysis in clinical cancer trials. However, a recent study has suggested that *in vitro* models of cancer are not reflective of the heterogeneity seen in cancer patients, and those *in vitro* models more closely resemble each other rather than the cancer they are modelling [286]. The authors advise that investigators exercise caution when interpreting results derived from established cell lines used for the study of drug resistance, and call for use of primary tumour models to more closely mimic *in vivo* tumour environments and avoid cell culture mediated changes in gene expression. While this represents the ideal scenario for modelling cancer, established cell line models of cancer remain the standard method used to examine mechanisms of resistance, particularly resistance to inhibitors for which the supply of primary patient tumour is limited (e.g. lapatinib).

8.2 Comparison of newly developed cell line models to the published models of acquired lapatinib resistance

SKBR3, HCC1419 and HCC1954 cells are HER2-amplified, lapatinib-sensitive cell lines which were conditioned with lapatinib containing media for 6 months. SKBR3 lapatinib-resistant cells (SKBR3-L) were established by Dr. Brigid Browne [255]. HCC1954 lapatinib conditioned cells (HCC1954-L) and SKBR3-L cells began active proliferation in the presence of lapatinib. In contrast, HCC1419 cells did not actively

proliferate in lapatinib and thus may represent an alternative model of acquired lapatinib resistance (further discussed in section 8.3.1).

8.2.1 Methods of lapatinib conditioning

Of the published models of acquired lapatinib resistance there is very little commonality in the procedures used to condition the cells, in either the concentrations of lapatinib used or in the determination of resistance status [see Chapter 1, Table 1-3]. For instance, the procedures used to develop models of acquired lapatinib resistance included a single cell cloning technique [229, 232], fixed dose conditioning [233] and dose escalation conditioning [231, 235, 236]. There was significant variation in the concentrations of lapatinib used to condition the cells; many studies began with a low dose of lapatinib (e.g. 100 nM) which was dose-escalated to upwards of 2 μM. Fixed concentration conditioning was performed with concentrations of lapatinib ranging from 3 μM to 10 μM. The length of conditioning required to achieve resistance varied from study to study with the majority of studies taking approximately 12 weeks to achieve resistance, whereas other studies took up to 1 year to achieve resistance. Another variation in different models of lapatinib resistance was the definition of lapatinib resistance. Most of the studies defined their conditioned cell lines as resistant based on their ability to grow in the presence of the concentration of lapatinib used to condition the cells, only one study used an IC_{50} method while a number of studies did not quantify the level of resistance. In contrast to the previously published models of acquired lapatinib resistance, the resistant models described in this study were developed using a relatively low dose of lapatinib relative to the IC_{50} of the resulting cell line. To our knowledge our models of acquired lapatinib resistance, HCC1954-L and SKBR3-L are the first to show that extended exposure to low dose lapatinib results in significant lapatinib resistance, with resulting lapatinib IC_{50} values significantly higher than the concentration used for conditioning.

8.2.2 Stability of lapatinib-resistant phenotype

The stability of the resistance phenotype was examined by performing freeze-thaw cycles and drug-withdrawal assays to ensure that the cells did not revert back to a lapatinib sensitive phenotype following freezing, or while being cultured in the absence of lapatinib, as the cells were routinely cultured without lapatinib prior to all experiments. HCC1954-L and SKBR3-L cells exhibited stable resistance to lapatinib following a freeze-thaw cycle and drug-withdrawal experiments. HCC1954-L cells were stably-resistant in the absence of lapatinib for 3 months, while SKBR3-L cells were

stable for 2 months but then regained sensitivity to lapatinib after 4 months in the absence of drug. A recent study provided a model whereby a drug-tolerant phenotype was transiently acquired and relinquished by individual cells within a population. Treatment of a NSCLC-derived cell line (PC9) cells with gefitinib resulted in the outgrowth of "drug-tolerant expanded persistor" (DTEP) cells which were insensitive to the effects of gefitinib. Notably the authors found that the resistance of the cells was stable until passage 30 of the cells, after this point the sensitivity of the cells to gefitinib was restored. This suggests that the drug-tolerant (resistant) state was only stable for 90 doublings of the cells [287]. For SKBR3-L cells, 90 doublings equated to approximately 4 months [255] which would correlate with the results we have seen in the drug withdrawal experiments for the SKBR3-L cells. Only one other study reported data on the stability of the lapatinib resistant phenotype, and they noted that removal of lapatinib from HCT116 lapatinib-resistant cells did not cause a reversion of the resistant phenotype after 2 months drug absence [233].

8.2.3 Alterations in HER/P13K/MAPK signalling pathways in lapatinib resistance

An important question to address when characterising a model of acquired lapatinib resistance, is whether or not a sub-population of HER2-negative lapatinib-resistant cells has been cloned out of the HER2 positive lapatinib sensitive total population or if there are any alterations in the expression or phosphorylation of HER2.

Innate lapatinib sensitivity has been correlated with increased expression of HER2 [194], however, our cell line models of acquired lapatinib resistance exhibited either no significant change in HER2 expression (SKBR3-L) or increased HER2 expression (HCC1954-L) compared to parental cells. This suggests that acquired lapatinib resistance is not associated with loss of expression of HER2. While HCC1954-L cells have higher levels of phospho-HER2 compared to parental cells, there was no difference in the levels of phospho-HER2 between SKBR3-par and SKBR3-L cells, and lapatinib treatment resulted in a decrease in phospho-HER2 levels in all four of the cell lines, suggesting that in contrast to previous studies of innate response/resistance to lapatinib [134, 194], phosphorylation of HER2 does not correlate with response to lapatinib in acquired lapatinib resistance models. These results also indicate that HCC1954-L and SKBR3-L cells have retained HER2 overexpression, and that the ability of lapatinib to inhibit the phosphorylation of HER2 is unaltered in these cells. Thus altered expression and/or phosphorylation of HER2 do not mediate lapatinib resistance in these cells.

Treatment of SKBR3-par, SKBR3-L and HCC1954-L cells with lapatinib resulted in increased expression of total HER3, while the expression of HER3 was unaffected by lapatinib treatment in HCC1954-par cells. In another study, BT474, SKBR3 and SUM225 cells treated with 1 μM lapatinib for 24 hours exhibited increased HER3 at the mRNA and protein level [288], and these authors proposed that up-regulated HER3 is phosphorylated by HER2, resulting in the maintenance of phospho-AKT, thus limiting the efficacy of lapatinib. Another study, examining the effects of gefitinib and erlotinib, two EGFR TKIs, found that the dephosphorylation of HER3 following TKI treatment was a transient event and was accompanied by increased expression of HER3 [289]. In contrast to the above studies, while 24 hour treatment with 1 μM lapatinib in SKBR3-L and HCC1954-L cells increased the expression of HER3, it did not result in a corresponding increase in the phosphorylation of HER3. This suggests that altered expression and/or phosphorylation of HER3 may not be key mediators of lapatinib resistance in these cells. However, examining the effect of lapatinib treatment at different time-points on the expression and phosphorylation of HER3 may shed more light on the role of HER3 in acquired lapatinib resistance.

SKBR3-L cells have significantly less HER4 than SKBR3-par cells. HER4 expression has been correlated with favourable prognostic factors and improved survival in breast cancer patients [290]. The reintroduction of HER4 into HER4-negative cell lines resulted in apoptosis in breast cancer cell lines [291]. HER4 is thought to have a tumour suppressor function in breast cancer and epigenetic silencing of HER4 is mediated by promoter hypermethylation. Reactivation of epigenetically silenced HER4 using a DNA demethylating agent resulted in apoptosis [292], as did reintroduction of HER4 expression in several breast cancer cell lines [291]. Interestingly, expression of HER4 has been correlated with response to trastuzumab in breast cancer patients [293] and the loss of HER4 expression has been associated with tamoxifen resistance both *in vitro* and *in vivo* [294]. To date alterations in HER4 expression have not been associated with lapatinib sensitivity or resistance. It is possible that the loss of HER4 may potentially be an important mechanism of lapatinib resistance in our SKBR3-L cells. Examining the effect of HER4 knockdown on lapatinib response in HER2-amplified lapatinib sensitive cells and re-introducing HER4 into SKBR3-L cells would help determine whether or not altered HER4 expression plays a causative role in acquired lapatinib resistance.

As lapatinib is a dual inhibitor of HER2 and EGFR, it is important to determine if cells with acquired resistance to lapatinib are resistant to EGFR inhibition also. SKBR3-L

cells displayed a marked decrease in sensitivity to gefitinib, an anti-EGFR targeted agent, compared to SKBR3-par cells. Cross-resistance to lapatinib and another HER2-targeted agent, trastuzumab, has been shown in innate lapatinib-resistant cells [194]. However, to our knowledge SKBR3-L cells are the first model of acquired lapatinib resistance which has been shown to have cross-resistance to an EGFR targeted therapy as cross-resistance to EGFR inhibition has been tested in reported in published models of acquired lapatinib resistance. SKBR3-L cells also have increased levels of phospho- and total EGFR compared to SKBR3-par cells. Several mechanisms for resistance to EGFR targeted therapy have already been proposed including mutations in EGFR, MET amplification and an escape mechanism mediated by HER3 phosphorylation [289, 295-297]. Alterations in EGFR have also been implicated in resistance to trastuzumab [214]. However, in this study lapatinib treatment inhibits phosphorylation of EGFR in both the parental and resistant cells. As previously mentioned, the lapatinib resistance cells did not exhibit increased phosphorylation of HER3, suggesting that lapatinib and gefitinib resistance is not mediated by a HER3-dependent escape mechanism. These results suggest that, rather than alterations in the expression and/or phosphorylation of EGFR, HER2 and HER3, the mechanism(s) of resistance to lapatinib and gefitinib are likely to be either downstream of the HER family, or through activation of alternative signalling pathways. A recent study has shown that activating MET, using HGF, results in lapatinib resistance in a panel of HER2-postive gastric cancer cell lines [298], and MET amplification is associated with gefitinib resistance [296], suggesting the potential for an overlapping mechanism of resistance. Examining the role of MET in SKBR3-par and SKBR3-L cells, either by stimulating activity using HGF, or inhibiting activity using a specific MET inhibitor would determine if MET plays a role in acquired lapatinib and gefitinib resistance.

The key signalling pathways which are activated by HER2 are the P13K/AKT pathway and MAPK pathway leading to cell proliferation and survival. Treatment of lapatinib sensitive cells has been shown to decrease the levels of phospho-AKT and phospho-ERK, indicating inhibition of signalling through both the P13K/AKT and the MAPK pathway [134]. Treatment of both HCC1954-par and HCC1954-L cells with lapatinib resulted in a decrease in the levels of phospho-AKT and phospho-ERK, however the steady state levels of these two phospho-proteins were significantly higher in HCC1954-L cells compared to HCC1954-par cells. However, inhibition of phospho-AKT and phospho-ERK following lapatinib treatment was also seen in SUM190 [231]

and BT474 [229] lapatinib-resistant cells. In contrast to HCC1954-L cells, in which phospho-AKT and phospho-ERK are inhibited by lapatinib, using a different BT474 model of acquired lapatinib resistance, lapatinib treatment did not affect the levels of phospho-AKT or phospho-ERK [232]. This maintenance of phospho-AKT and phospho-ERK in response to lapatinib treatment is also shown in several other models of acquired lapatinib resistance [235].

In contrast to HCC1954-L cells, SKBR3-L cells had lower levels of both phospho-AKT and phospho-ERK; in fact the levels of phospho-AKT were barely detectable by immunoblotting. This suggests that the lapatinib-resistant cells are no longer dependent on AKT signalling for survival. Alterations in the PI3K/AKT pathway are frequent in human cancer, either due to amplification of the genes encoding either PI3K or AKT, PI3K mutations or loss of PTEN all of which result in increased activation of AKT [reviewed in [50]]. While alterations in the PI3K pathway have been implicated in resistance to trastuzumab [82, 299], the role of P13K mutations and pathway alteration in lapatinib resistance is still controversial. It has been reported that loss of PTEN expression and/or P13K mutations conferred resistance to lapatinib and trastuzumab, using BT474 breast cancer cell line [224]. However another study, using a panel of HER2 positive breast cancer cell lines, reported that loss of PTEN and/or P13K mutations is associated with innate resistance to trastuzumab but not lapatinib [194]. While mutations in PI3K are commonly thought to result in downstream activation of AKT, there is also evidence to suggest that P13K mutation may result in diminished AKT signalling [300]. Therefore, examination of the mutation status of PI3K, and the levels of PTEN, in the SKBR3-L cells may help to elucidate the mechanism of the decreased phospho-AKT in these cells.

8.2.4 Previously reported mechanisms of lapatinib resistance

8.2.4.1 Upregulation of ER signalling

Gene expression profiling comparing a BT474 model of acquired lapatinib resistance to its parent cell line revealed increased dependence on ER signalling for survival, and combining lapatinib with anti-ER therapy prevented the emergence of lapatinib-resistant cells [229]. Importantly, this study also showed that lapatinib treatment of HER2 positive breast tumours resulted in increased ER expression. Upregulation of ER signalling has also been shown in several other models of acquired lapatinib resistance.

In another BT474 model of acquired lapatinib resistance, in addition to showing upregulation of AXL as a novel mechanism of acquired lapatinib resistance, the lapatinib resistance cells had higher levels of ER and were sensitive to lapatinib when combined with fulvestrant or estrogen deprivation [232]. A recent study using BT474 and UACC812 models of lapatinib resistance also showed upregulated ER signalling and sensitivity to fulvestrant following acquisition of lapatinib resistance [236]. The above studies suggest that when HER2 signalling is inhibited by long-term lapatinib treatment in ER positive cells, ER becomes the dominant driver of growth in these cells. The expression of ER was measured in HCC1954-L and SKBR3-L cell lines and the levels of ER were found to be undetectable in both parental and resistant cell lines, indicating that upregulation of ER signalling was not a mechanism of lapatinib resistance in these cell lines. Thus, upregulation of ER signalling in lapatinib-resistant cells appears to be limited to HER2/ER positive cell lines and a switch from HER2 to ER signalling does not function as an escape mechanism for ER negative cell lines [231, 236, 301].

8.2.4.2 Upregulation of SRC family kinases

Phospho-proteomic profiling of lapatinib-resistant cells suggested that SRC (or a SRC family kinase) activity was upregulated in lapatinib-resistant cells compared to parental cells. BT474 resistant cells exhibited increased activity of YES while HCC1954 resistant cells exhibited increased activity of LYN and SRC was more ubiquitously expressed in all lapatinib-resistant cell lines tested [235]. Their study also showed that treatment of lapatinib-resistant cells with SRC inhibitors resulted in growth inhibition, and more importantly they showed that mRNA expression of several SRC family members was upregulated in a small cohort of primary HER2 positive tumours following lapatinib treatment. The levels of total and phosphorylated SRC were examined in HCC1954-L and SKBR3-L cells. While there was no change in the expression of SRC in SKBR3-L cells compared to SKBR3-par cells, HCC1954-L cells exhibited a small yet significant increase in SRC compared to HCC1954-par cells. The levels of phospho-SRC were practically undetectable in all four cell lines. The increased expression of SRC in HCC1954-L cells may indicate an alteration in sensitivity to SRC inhibition and further work to investigate the role altered SRC may play in acquired lapatinib resistance is warranted.

8.2.4.3 Upregulation of XIAP

XIAP, an inhibitor of apoptosis protein, has been linked to therapeutic resistance in multiple cancer types [245], and it has been reported to be expressed in breast tumour samples [302]. The expression of XIAP correlates with shorter overall survival and may act as an independent prognostic biomarker for invasive ductal carcinoma [246]. Trastuzumab treatment results in increased XIAP expression [303], and using IAP inhibitors in combination with either trastuzumab or lapatinib, increased apoptosis compared to either agent alone [304]. Notably, upregulation of XIAP has been seen in a SUM190 cell line model of lapatinib-resistant inflammatory breast cancer [231]. These studies suggested a strong interaction between HER2 signalling, resistance to anti-HER2 targeted therapy and expression of XIAP. The expression of XIAP was measured in HCC1954-L and SKBR3-L cells and found no change in expression between SKBR3-L and SKBR3-par cells. Interestingly, the steady state levels of XIAP were slightly lower in HCC1954-L cells compared to HCC1954-par, but when treated with lapatinib HCC1954-L cells exhibited a significant increase in XIAP expression, while the parental cells exhibited a decrease in XIAP. Decreased XIAP following lapatinib treatment has been reported previously in SUM190 lapatinib sensitive cells [303], however other studies have noted that lapatinib treatment did not affect the expression of XIAP in a panel breast cancer cell lines [144, 150]. In addition, XIAP expression was unaltered in HCT116 lapatinib-resistant cells [233]. The study identifying up-regulated XIAP in lapatinib resistance stated that the lapatinib-resistant cells were routinely cultured in lapatinib-containing medium; therefore it is unclear whether the change in XIAP expression represents a change in the steady-state expression levels or a change in expression in response to lapatinib, as seen in the case of HCC1954-L cells. Also of note, Aird *et al.*, use GW583340, a lab grade analogue of lapatinib, rather than GW572016. These results suggest that at present XIAP may not represent a common mechanism of acquired lapatinib resistance.

8.2.4.4 Upregulation of MCL-1

HCT116 cells, a colon cancer cell line conditioned with lapatinib, over-expresses MCL-1, an anti-apoptotic member of the BCL-2 family. Knockdown of MCL-1 in lapatinib-resistant cells enhanced lapatinib activity [233, 244]. The interaction between lapatinib treatment and altered MCL-1 expression is not limited to colon cancer. Treatment of HER2 positive breast cancer cell lines with lapatinib in combination with CDK inhibitors resulted in inhibition of MCL-1 expression, and combining lapatinib with an inhibitor of MCL-1 (obatoclax) enhanced the activity of lapatinib both *in vitro* and *in*

vivo [145]. Treatment of cell lines with trastuzumab has also been shown to alter MCL-1 expression levels [305]. The expression of MCL-1 was examined in HCC1954-L and SKBR3-L cells; SKBR3-L cells exhibit higher levels of MCL-1 compared to SKBR3-par cells. In contrast, HCC1954-L cells exhibit a decrease in steady-state MCL-1 levels compared to parental cells. The altered expression of MCL-1 in both resistant cells lines suggests that alterations in MCL-1 and possibly other members of the BCL-2 family may play a role in lapatinib resistance in these cell lines, and inhibition of MCL-1 has the potential to restore sensitivity to SKBR3-L cells. In fact, recent work from our laboratory has shown that in addition to increased expression of MCL-1, SKBR3-L cells exhibit decreased expression of BAX and are sensitive to combined inhibition with lapatinib and obatoclax [306].

8.2.4.5 Additional mechanisms of acquired lapatinib resistance

There are a number of other reported mechanisms of acquired lapatinib resistance including; up regulation of AXL [232], up regulation of β1 integrin [234], increased autophagy [252], RelA regulation [230], and increased expression of truncated HER2 [307]. Future work examining the possible role that these mechanisms may play in SKBR3-L and HCC1954-L cells would help elucidate mechanisms of lapatinib resistance.

In summary, this study reports the development and characterisation of two newly established cell line models of acquired lapatinib resistance; HCC1954-L cells and SKBR3-L cells. The lapatinib-resistant phenotype was stable in both cell lines following freeze-thaw cycles and for up to 2 months in the absence of lapatinib (3 months for HCC1954-L cells). Both cell lines retained their HER2 overexpression status following lapatinib conditioning and treatment of the cells with lapatinib inhibited the phosphorylation of HER2. SKBR3-L cells expressed significantly less HER4 compared to SKBR3-par cells, and thus, lack of HER4 expression may be mechanism of acquired lapatinib resistance in SKBR3-L cells. SKBR3-L cells also exhibited cross-resistance to EGFR targeted therapy, and have increased expression and phosphorylation of EGFR. Interestingly, the phosphorylation status of AKT and ERK were not associated with lapatinib response in HCC1954-L cells, however, SKBR3-L cells exhibited a lack of phospho-AKT in untreated cells. Future work will be required to determine the effect of lack of phospho-AKT and its relationship to lapatinib resistance in these cells. Published mechanisms of acquired lapatinib resistance were examined in HCC1954-L and SKBR3-L cells. Neither cell line exhibited increased

expression of ER suggesting that while ER upregulation has been shown as a mechanism of lapatinib resistance in HER2 positive cell lines which co-express ER, it is not a mechanism of lapatinib resistance in HER2 positive ER negative breast cancer. Upregulation of SRC was found in HCC1954-L cells only, upregulation of MCL-1 was found in SKBR3-L cells only and increased expression of XIAP was found in HCC1954-L cells following treatment with lapatinib. These results suggest that the published mechanisms of lapatinib resistance may contribute to lapatinib resistance in HCC1954-L and SKBR3-L cells and further investigation of these alterations would increase our understanding of acquired lapatinib resistance.

8.3 Novel mechanisms of acquired lapatinib resistance

8.3.1 Senescence – a novel effect of lapatinib conditioning

HCC1954-L and SKBR3-L cells, two cell line models of acquired resistance to lapatinib were developed. In contrast, HCC1419 cells conditioned with lapatinib did not result in the development of an actively proliferating cell line model of acquired lapatinib resistance. HCC1419 cells conditioned with lapatinib ceased proliferation and cells remaining after 6 months of conditioning displayed an altered morphology and arrested growth rate which lead us to hypothesise that lapatinib induced a senescent-like phenotype in HCC1419 cells. Senescence is a state of permanent cell cycle arrest characterised by a distinct and recognisable flattened and enlarged cellular morphology with a prominent nucleus and increased cytoplasmic granularity. Senescent cells remain viable and metabolically active but are permanently growth arrested in either the G1 or G2/M stage of the cell cycle [281]. A study showing that senescent cells had β-galactosidase activity, detectable at pH 6.0, that was not detectable in quiescent cells [308], led to the development of senescence-associated β-galactosidase activity as the most widely used biomarker in studies of cellular senescence *in vitro* and *in vivo* [309]. Lapatinib conditioning of HCC1419 cells, either short term (1 week), or long term (6 months), resulted in increased activity of senescence-associated β-galactosidase, suggesting that lapatinib induces a senescent-like phenotype in HCC1419 cells. This is the first to report of induction of senescence-associated β-galactosidase activity following lapatinib treatment.

Replicative or cellular senescence is a mechanism whereby aging cells exhaust their replicative potential and remain viable but become permanently growth arrested [310].

Human cells cultured *in vitro* displayed limited proliferation over an extended period [311], and the mechanism which controls the limited proliferative potential of cells was discovered to be the shortening of telomeres [312]. One of the hallmarks of cancer is increased and dysregulated proliferation [74], thus replicative senescence has a tumour suppressor function in normal cells [reviewed in [313, 314]]. Cells can also undergo senescence in response to stress which is independent of telomerase shortening, commonly referred to as therapy-induced senescence, or accelerated cellular senescence (ACS) [281]. Chemotherapeutic agents and several antibiotic compounds induced ACS in response to DNA damage, in multiple types of cancer both *in vitro* and *in vivo* [315-317]. Hydroxyurea, pyrithione and resveratrol induced reactive oxygen species (ROS)-mediated ACS in colon cancer and neuroblastoma cell lines [318-320]. Inhibition of PTEN, with a specific PTEN inhibitor (VO-OHpic) induced ACS in prostate cancer cells [321], and inhibition of aurora kinase A with MLN8054 induced ACS in multiple cancer cell lines *in vitro* and *in vivo* [322]. These studies show that in addition to playing a role in controlling the replicative potential of cells, induction of senescence may be a mode of action of several therapeutic interventions, including lapatinib.

The mechanism of how lapatinib induces a senescent-like phenotype in HCC1419 cells is not fully understood, however, specific inhibitors of both ERK and AKT show that inhibition of either pathway was sufficient to induce a senescent-like-phenotype in these cells. This suggests that the induction of a senescent-like-phenotype is not dependent on combined inhibition of P13K and MAPK signalling in HCC1419 cells. There is evidence to suggest that induction of ACS is dependent on the concentration of the inducing agent. Lower concentrations of the agent may trigger a senescence response without activating the cascade of caspase activity that commits the cell to apoptosis [315]. High dose doxorubicin induces apoptosis in cardiomyocytes, whereas low dose doxorubicin induces ACS [323]. Consistent with this result HCC1419 cells treated with low dose lapatinib (50 – 500 nM) induced stronger senescence-associated β-galactosidase activity compared to concentrations of lapatinib in excess of 500 nM. Interestingly, senescence-associated β-galactosidase activity was induced following combined treatment with trastuzumab and lapatinib in HCC1419 cells but not following treatment with trastuzumab alone. This result suggests lapatinib-induced senescence may be mediated by direct inhibition of the HER2 kinase domain.

The tumour suppressor p53 plays a key role in promoting senescence [reviewed in [324]], and has been reported to be critical for the establishment of senescence in human

cells [325, 326]. However, other studies have shown that transformed cells that lack p53 retain the capacity to develop senescence in response to anti-cancer agents [327, 328]. Intriguingly, our study reports lapatinib-induced senescent-like phenotype in HCC1419 cells which are p53 negative [329]. In contrast SKBR3 cells which have mutant p53 (p53R175H), which has a gain of function effect on p53 [330], do not undergo lapatinib induced senescence.

p16 ^{Ink4A} (CDKN2A) is a cyclin-dependent kinase (CDK) inhibitor whose expression is often increased in senescent cells [331], along with increased expression of p15^{Ink4B} (CDKN2B) [332], p21^{Waf1} (CDKN1A) [333] and p27^{Kip1} (CDKN1B) [334] [reviewed in [281, 283, 335]]. Treatment of SKBR3 and HCC1419 cells with lapatinib had a similar effect on the expression of these CDKs; the levels of p21 were unchanged in both cell lines, and the levels of p15 and p27 increased in both cell lines. However, only HCC1419 cells exhibited increased β-galactosidase activity. This may be due to HCC1419 cells having much higher levels of p15, p21 and p27 than SKBR3 cells when the cells were treatment naive, therefore following lapatinib treatment the levels of p15, p21 and p27 were significantly higher in HCC1419 cells compared to SKBR3. Interestingly p16 levels were undetectable in both SKBR3 and HCC1419 cells; this is consistent with reports that loss of p16 expression is a frequent occurrence in tumour-derived cell lines [336-338]. Thus, lapatinib induced a senescent-like phenotype in HCC1419 cells characterised by increased β-galactosidase activity and high levels of p15, p21 and p27.

Based on these results we propose the induction of a senescent-like phenotype as a novel mechanism of action of lapatinib. Recently there has been increasing interest in senescence-induction as a mechanism for inhibiting the growth of cancer cells. This type of strategy would result in tumour cytostatis rather than tumour regression or ablation. Senescence can be induced in tumour models that have inactivated apoptotic pathways leading to improved survival following chemotherapy [339]. In addition, evidence suggesting that senescence is induced with lower doses of drugs than that required for apoptosis induction suggests reduced toxicity related side effects for patients [320, 323]. Taken together these results suggest senescence induction may play an increasing role in cancer-therapy and the ability of lapatinib to induce senescence warrants further investigation as a mechanism of lapatinib action.

In addition to the discovery that lapatinib induces a senescent-like phenotype in HCC1419 cells, there is evidence suggesting that the senescent-like phenotype induced by lapatinib is reversible. The senescent-like phenotype was reversed when lapatinib was removed from the media; the previously senescent cells began to actively proliferate and retained their initial sensitivity to lapatinib. Senescence is defined as a being the permanent and irreversible loss of proliferative potential, given that growth factors cannot stimulate senescent cells to divide [313, 340]. However, several other studies have suggested that senescence can be reversed [317, 341, 342]. A model of reversible senescence has been proposed where the reversibility of senescence is dependent on the expression of p16 and p53 [341]. Senescence induced in cells which expressed low levels of p16 was reversible when p53 was inactivated or when oncogenic RAS was expressed in the cells. In contrast, inactivation of p53 and/or expression of RAS were incapable of reversing senescence induced in cells expressing high levels of p16 [341]. Studies show that p21 plays an important role in arresting cell growth in the early stages of senescence whereas p16 is the key effector in the maintaining long-term growth arrest, known as terminal senescence [316, 343]. In another model, senescence induced in response to a variety of chemotherapeutic agents was reversible in the p53-null, p16-deficient lung cancer cell line [317]. The cells that "escaped" senescence were found to overexpress CDK1 and targeting these cells with a CDK1 inhibitor prevented the cells from escaping senescence. A subsequent study with the same cells found that survivin is phosphorylated by CDK1, and that phosphorylated survivin is necessary for the reversibility of senescence and for viability of the cells following senescence escape [342]. Thus, suggesting that combining senescence-induction with inhibition of survivin, is a means of preventing reversible senescence. Taken together these studies suggest a mechanism for the reversibility of the senescence phenotype induced in HCC1419 cells following lapatinib treatment [Figure 8-1]. The lack of detectable p16 expression coupled with p53 negativity suggests that the senescence induced by lapatinib in HCC1419 cells is reversed when the repression of oncogenic HER2 signalling by lapatinib is removed. Restoration of HER2 signalling provides a mechanism for senescent HCC1419 cells to escape senescence and re-establish active proliferation in response to growth factor signalling. As the cells are once again dependent on HER2 for proliferation and survival, treating the cells with lapatinib inhibits their growth. Lapatinib-induced expression was examined in several additional models of HER2 positive lapatinib sensitive breast cancer but to date another cell line has not yet been identified which undergoes senescence in response to lapatinib

treatment. Future work examining the induction of senescence in response to lapatinib in HER2 positive cells should be focused on p53 and p16 negative cell lines.

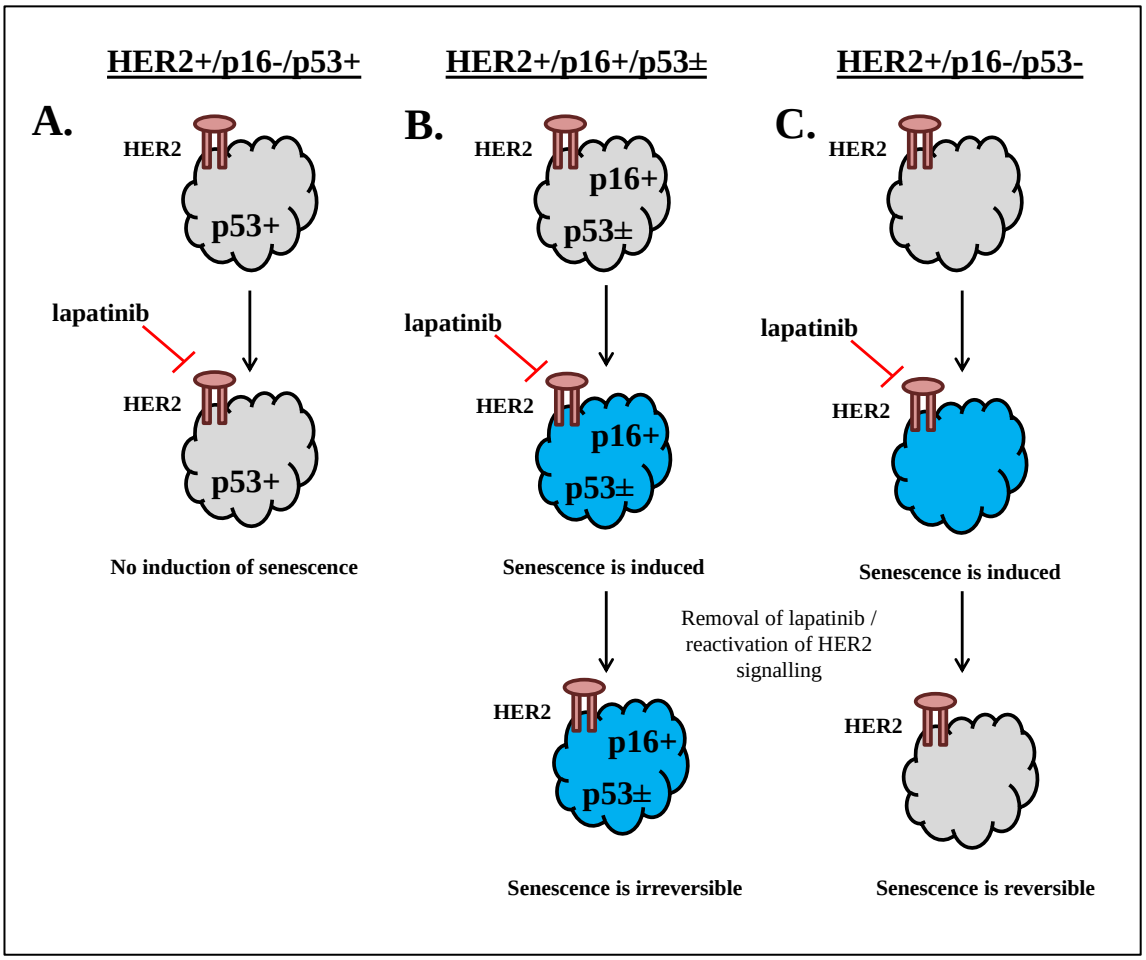

Figure 8-1: Proposed model of induction of reversible and/or irreversible senescence following lapatinib treatment. (A) HER2 positive cells expressing p53, but lacking p16 expression do not undergo senescence following lapatinib treatment (e.g. SKBR3 cells). (B) Senescence can be induced by lapatinib in HER2 positive cells with high levels of p16 and/or p53 expression; however, due to the expression of p16 the induced senescence is irreversible, despite reactivation of HER2 signalling. (C) HER2 positive cells lacking p53 and p16 expression undergo senescence in response to lapatinib treatment (e.g. HCC1419 cells). Without expression of p16 to maintain the senescence phenotype, reactivation of HER2 signalling reverses the senescence.

The induction of senescence in cancer cells following lapatinib treatment may represent a clinically relevant model of lapatinib resistance. Senescence has been identified in 41 % of patient breast tumours following treatment with cyclophosphamide, doxorubicin, and 5-fluorouracil [316]. The staining was confined to tumour cells with no detection in normal tissues. Senescent markers have also been observed in lung tumours after

treatment with carboplatin and docetaxel [317]. These studies suggest that senescence may be a more prevalent tumour response to current anti-cancer therapy than previously thought.

In summary, lapatinib induces senescence in HCC1419 cells following either short or long term treatment with lapatinib. HCC1419 cells are p53 negative, do not express p16, and express higher levels of p15, p21 and p27 compared to p53 positive SKBR3 cells, which do not exhibit senescence-associated β-galactosidase activity following lapatinib treatment. Lapatinib, but not trastuzumab, induced senescence in a dose-dependent manner, an effect which is simulated inhibition of AKT or ERK. Interestingly, lapatinib induced senescence in HCC1419 cells is reversible; following removal of lapatinib from the media HCC1419 cells began active proliferation and retain their initial sensitivity to lapatinib. Thus, the induction of senescence is being proposed as a novel mechanism of lapatinib action. In addition, p53 negativity coupled with lack of p16 expression may prevent induction of terminal senescence. Therefore the escape from lapatinib-induced senescence may be a novel mechanism of resistance to lapatinib in HCC1419 cells. Furthermore, loss of p53 and p16 may be potential biomarkers to identify tumours likely to undergo this reversible senescence in response to lapatinib treatment.

8.3.2 Chromosomal alterations

Alterations at the genetic level are quite common in cancer cells and reflect changes in biological process and signalling pathways that lead to cancer development and progression. Array Comparative Genomic Hybridisation (aCGH) is a technique that detects genome–wide copy number alterations which allows for the detection of cancer-associated genes [reviewed in [257]]. aCGH technology was used to interrogate HCC1954-L cells for gene copy number alterations compared to the parental cell line. The alterations that found span several different chromosomes. Array CGH has previously been used to identify changes and characterise newly derived trastuzumab-resistant cells [266], [267]. To our knowledge, aCGH has not yet been used to characterise a model of acquired lapatinib resistance.

Amplification of chr17q12

HCC1954-L cells have increased amplification of chr17q12 compared to HCC1954-par cells. This region corresponds to multiple genes, the most instantly recognisable of which is HER2. The amplification of HER2 in HCC1954-L cells detectable at the genomic level, was also detectable at the protein level. A small but significant increase in HER2 levels was found in HCC1954-L cells compared to the parental cells which already have high levels of HER2. This increased amplification of HER2 was also detectable by FISH. However, given that the phosphorylation of HER2 is inhibited by lapatinib in HCC1954-L cells, it is unlikely that the increased expression and amplification of HER2 is playing a causative role in lapatinib resistance in these cells. Chromosome 17q12-21 contains the HER2 gene which is frequently amplified in breast cancer, however, the other genes from this region which are often co-amplified with HER2 have recently come under scrutiny. The genes associated with the HER2 amplicon are depicted in Figure 8-2. TOP2A has aroused particular interest as it is frequently co-amplified with HER2 and has been associated with response to anthracycline-based chemotherapy in breast cancer [344, 345]. There was no increase in TOP2A amplification in HCC1954-L compared to HCC1954-par cells, however there was an increase in other genes from the chr17q12-21 region, including STARD3, GRB7 and GSDMA**.** GSDMA, also known as GSDM1 and Gasdermin, is frequently suppressed in gastric cancer and associates with TGF-β in apoptotic regulation [346]. Upregulation of GRB7, growth factor receptor-bound protein 7, has been implicated in response to lapatinib therapy using *in vitro* and *in vivo* models [254]. Knockdown of GRB7 in HER2-amplified cells results in decreased cell proliferation [347]. Validating whether or not amplification of these genes corresponds to increased expression at the protein level will be important in determining the significance of these alterations.

Intriguingly, using immunoblotting, the increased amplification of STARD3 (StAR-related lipid transfer (START) domain containing 3) was also associated with a dramatic increase in STARD3 protein expression. STARD3, often referred to as MLN64 (metastatic lymph node 64), was initially identified from a breast-cancer-derived metastatic lymph node cDNA library as a gene that was overexpressed and amplified in breast cancer [280]. STARD3 is frequently co-amplified with HER2 and over-expressed in breast cancer [348-350]. Studies also show its over-expression in prostate cancer [351]. HER2 and STARD3 share common transcriptional control

mechanisms [348]. In addition, overexpression of STARD3 in breast cancer correlates with poorer prognosis and survival [350]. Knockdown of STARD3 resulted in decreased cell proliferation and decreased cell-cycle progression in HER2 positive breast cancer cell lines which co-express STARD3 [347, 350]. Taken together these studies suggest that amplification and over-expression of STARD3 in HCC1954-L cells may contribute to lapatinib-resistant phenotype and also suggest that STARD3 could be promoting proliferation in HCC1954-L cells.

Interestingly, while the co-amplification of GRB7, STARD3 and GSDMA with HER2 has been reported previously [253, 347, 350], increased amplification of these genes has not previously been reported in lapatinib resistance.

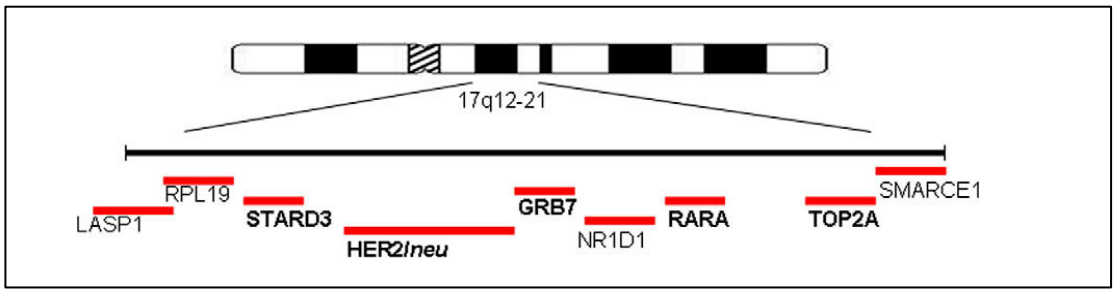

Figure 8-2: The HER2 amplicon on chromosome 17. LASP1, LIM and SH3 protein 1; RPL19, ribosomal protein L19; STARD3, StAR-related lipid transfer (START) domain containing 3; GRB7, growth factor receptor-bound protein 7; NR1D1, nuclear receptor subfamily 1, group D, member 1; RARA, retinoic acid receptor alpha; TOP2A, Topoisomerase 2-alpha; SMARCE1, SWI/SNF related, matrix associated, actin dependent regulator of chromatin, subfamily e, member 1. This figure and legend were reproduced from [352].

Amplification of chr12p12.1-12.2

There were several other amplifications and deletions in the HCC1954-L cell line compared to HCC1954-par cells which warrant further investigation. HCC1954-L cells have an amplification in the region of chr12p12.1-12.2 compared to HCC1954-par cells. This region encodes multiple genes including all four members of the OATP1 (organic anion transporting polypeptide 1) family. OATPs belong to the superfamily of solute carrier anion transporters (SLCO), and HCCC1954-L cells have amplification of

OAPT1C1 (SLCO1C1), OATP1B3, (SLCO1B3), OATP1B1 (SLCO1B1) and OATP1A2 (SLCO1A2), [for review see [353]]. Altered expression of these OATPs has been reported in several cancer types including breast cancer [354]. OATPs transport a wide range of compounds into cells, OATP substrates include substrates include antibiotics, anti-diabetic drugs, anti-inflammatory drugs, antifungals, antivirals, antihistamines, anti-hypertensives, fibrates, statins, cardiac glycosides, immunosuppressants, and anti-cancer drugs [353, 355]. While the transport of lapatinib by OATPs has not been reported, OATP1B1 can transport CP724-714, a potent HER2 tyrosine kinase inhibitor [356]. The OATP1 family amplified in HCC1954-L cells transport several anti-cancer drugs into the cell, including imatinib, methotrexate, SN-38, docetaxel, paclitaxel and rapamycin [353]. This suggests that treating the lapatinib-resistant cells with any of the above agents may be an effective treatment strategy as more of the drug would be transported into the cells, however, the increased amplification of the OATP1 family would need to confirmed at the protein level and the increased activity of the transporters validated.

In summary, aCGH analysis of HCC1954-L cells compared to HCC1954-par cells revealed increased amplification of chr17q12, corresponding to several genes including HER2 and STARD3. The amplification of HER2 and STARD3 at the genomic level also translated into increased expression at the protein level. Of particular interest is the amplification and increased expression of STARD3 as several studies have highlighted the potential of STARD3 knockdown as a means of inhibiting the growth of cancer cells. Future work investigating the role of STARD3 amplification and protein expression in lapatinib resistance is warranted.

8.3.3 Decreased phosphorylation of eEF2

Previous work in our laboratory included the development of the SKBR3-L model of acquired lapatinib resistance, and phospho-proteomic profiling of SKBR3-L cells and their parent cell line, SKBR3-par [255]. The results of the phospho-proteomic analysis revealed alterations in the levels of phospho-eEF2, showing down regulation of 6 forms of phospho-eEF2 in SKBR3-L cells compared to SKBR3-par.

Eukaryotic elongation factor 2 (eEF2) is a monomeric GTPase that plays an essential role in protein synthesis, whereby it catalyses the coordinated movement of two tRNA

molecules and the mRNA, and catalyses conformational changes in the ribosome. The activity of eEF2 regulates protein synthesis and the activity of eEF2 is inhibited upon phosphorylation. Phosphorylation of eEF2 at Thr56 inhibits its activity by preventing eEF2 binding to the ribosome [reviewed in [60, 256]]. Phospho-proteomic analysis revealed that SKBR3-L cells have significantly lower levels of phospho-eEF2 compared to SKBR3-par cells and this result was confirmed using immunoblotting with an antibody specific to the Thr56 phosphorylation site of eEF2. In addition, treatment of SKBR3-par cells with lapatinib resulted in a significant increase in phospho-eEF2 levels, suggesting inhibition of protein synthesis. In contrast, there was no change in the levels of phospho-eEF2 in SKBR3-L cells following lapatinib treatment, suggesting that lapatinib does not inhibit protein synthesis in SKBR3-L cells. These results suggest that alterations in the levels of phospho-eEF2 may play a role in acquired lapatinib resistance. eEF2 was found to be highly expressed in lung adenocarcinoma where its expression was associated with an increased incidence of tumour recurrence and a significantly worse prognosis [357]. eEF2 is also expressed in gastrointestinal and colorectal cancer, where eEF2 promoted G2/M progression and enhanced cell growth [358]. Although the expression of eEF2 has previously been associated with cancer, it has not previously been studied in acquired lapatinib resistance. We therefore sought to determine the mechanism responsible for the altered phosphorylation of eEF2 in SKBR3-L cells.

eEF2 kinase (eEF2k), also known as calmodulin-dependent protein kinase III, is a calcium/calmodulin-dependent enzyme that inhibits protein synthesis by phosphorylating and inactivating eEF2 [359]. The expression of eEF2k was increased in SKBR3-L cells compared to SKBR3-par cells, which correlates with the decreased phosphorylation of eEF2 in SBR3-L cells. A previous study has shown that eEF2k expression and activity was increased in breast tumours compared to normal adjacent breast tissue [360]. eEF2k is a substrate for p70S6k, a kinase which is activated in an mTOR-dependent manner. p70S6k phosphorylates eEF2k at Ser366 resulting in the inactivation of eEF2k, thus preventing the phosphorylation of eEF2 [361]. SKBR3-L cells have higher levels of Ser366 phosphorylation of eEF2k compared to SKBR3-par cells. Based on this result, it was hypothesised that phosphorylation of eEF2k at Ser366 may regulate the phosphorylation of eEF2, and that the increased Ser366 phosphorylation of eEF2k in SKBR3-L cells may be responsible for decreased phospho-eEF2 levels in SKBR3-L cells compared to SKBR3-par cells. However, while

treatment of SKBR3-L cells with lapatinib had no effect on the levels of Ser366 phosphorylation of eEF2k, treatment of SKBR3-par cells with lapatinib resulted in a small, yet significant increase in Ser366 phosphorylation of eEF2k. Increased phosphorylation of Ser366 should decrease the activity of eEF2k, however, in SKBR3-par cells phospho-eEF2 is significantly increased following lapatinib treatment. These results suggest that phosphorylation of eEF2k at Ser366 does not regulate the activity of eEF2k on the phosphorylation of eEF2 in these cells.

The activity of eEF2k is also regulated by phosphorylation of Ser359 by SAPK4/p38MAPKδ (SAPK4), whereby phosphorylation of eEF2k at Ser359 results in the inactivation of eEF2k leading to reduced phosphorylation of eEF2 (activation) [362]. In addition, cdc2, also known as CDK1, phosphorylates eEF2k at Ser359 [363]. Phosphorylation of eEF2k at Ser359 was significantly increased in SKBR3-L cells compared to SKBR3-par cells. Treatment of SKBR3-par cells with lapatinib resulted in decreased levels of phospho-eEF2k at Ser359. This suggests that phosphorylation of Ser359, rather than Ser366, regulates the activity of eEF2k in SKBR3-par cells. While there was a small decrease in phospho-eEF2k (Ser359) in SKBR3-L cells following lapatinib treatment, the decrease was not significant. To summarise, we propose that increased phosphorylation of Ser359 of eEF2k contributes to the decrease in eEF2 phosphorylation observed in SKBR3-L cells [Figure 8-3].

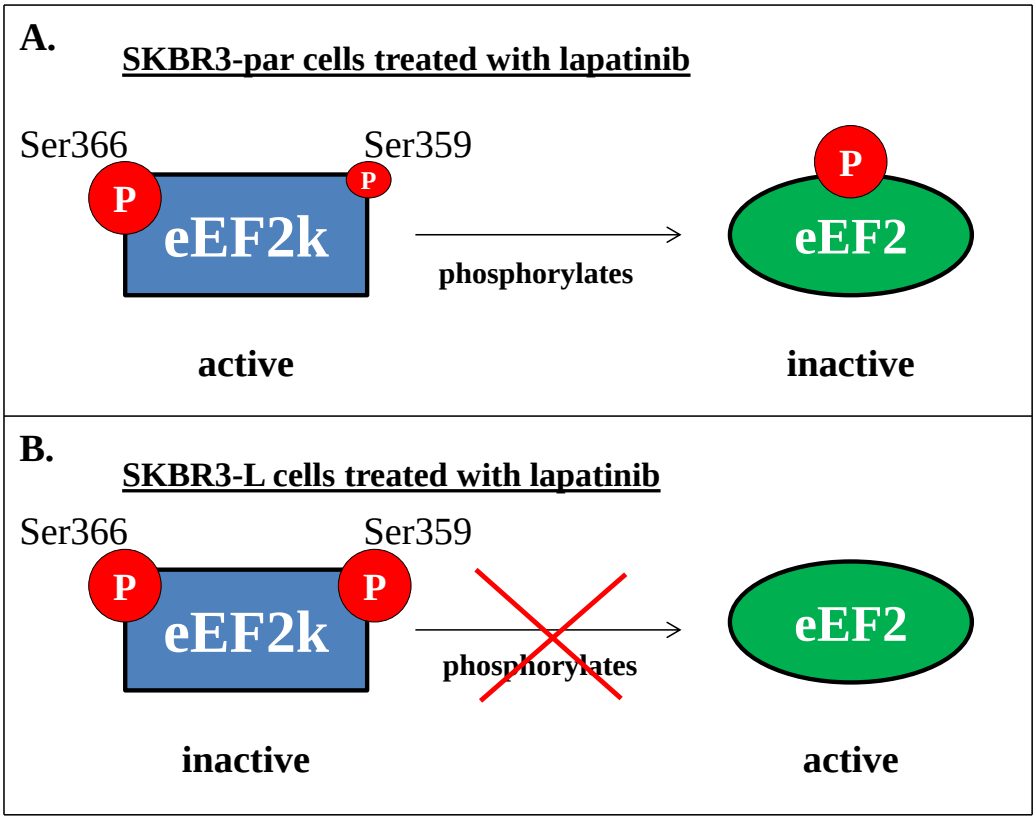

Figure 8-3: Regulation of eEF2 phosphorylation: (A) lapatinib-induced dephosphorylation of eEF2k at Ser359 results in the activation of eEF2k and the subsequent phosphorylation and inactivation of eEF2 in SKBR3-par cells. (B) Maintained phosphorylation at Ser359 of eEF2k prevents lapatinib-induced activation of eEF2k and thus, eEF2 remains un-phosphorylated and active in SKBR3-L cells.

By showing that the activity of eEF2k is not regulated via phosphorylation of Ser366, a mechanism is proposed whereby the phosphorylation of eEF2 is regulated in an mTOR-independent manner. However, it has been reported that insulin-like growth factor 1 (IGF-1) can phosphorylate eEF2k at Ser359 and treatment with the mTOR inhibitor rapamycin prevents this effect [362]. SAPK4 is not activated by IGF-1, nor thought to be regulated by mTOR, suggesting that the phosphorylation of Ser359 may occur via both mTOR dependent and independent mechanisms. To determine whether or not mTOR signalling plays a role in the regulation of eEF2 signalling, SKBR3-par and SKBR3-L cells were treated with lapatinib and examined the phosphorylation and expression of mTOR. The phosphorylation of mTOR at Ser2448 was lower in SKBR3-L cells compared to SKBR3-par cells; however, lapatinib treatment of both cell lines resulted in the inhibition of Ser2448 phosphorylation. This indicates that lapatinib inhibits mTOR signalling in both cell lines and thus the alteration in eEF2 phosphorylation is not likely to be mediated by mTOR. This result was further

confirmed by treating SKBR3-par and SKBR3-L cells with rapamycin; rapamycin treatment increased the phosphorylation of eEF2 in SKBR3-par but had no effect on eEF2 phosphorylation in SKBR3-L cells. Thus, inhibition of mTOR signalling by either lapatinib or rapamycin leads to increased phospho-eEF2 in the SKBR3-par cells but not in the SKBR3-L cells. Although lapatinib inhibits mTOR signalling in SKBR3-L cells, our results suggest alterations in other pathways that regulate eEF2k phosphorylation are responsible for the dephosphorylation and activation of eEF2 in SKBR3-L cells.

After identifying a mechanism whereby the phosphorylation of eEF2k at Ser359 regulates the phosphorylation of eEF2, the effect of inhibition of eEF2k activity on phosphorylation of eEF2 and on the sensitivity of SKBR3-par cells to lapatinib was examined. NH125 is a potent and selective inhibitor of eEF2k activity, with an IC_{50} of 60 nM for eEF2k *in vitro* [364]. Treatment of SKBR3-par cells with concentrations of NH125 ranging from 100 to 500 nM, resulted in the inhibition of eEF2k activity, measured as the dephosphorylation of eEF2 at Thr56. NH125 treatment dephosphorylated eEF2 without affecting signalling through AKT or ERK. Following confirmation that NH125 treatment resulted in the inactivity of eEF2k, and dephosphorylation of eEF2, the combined treatment of SKBR3-par cells with NH125 and lapatinib was examined to test whether it would decrease the sensitivity of SKBR3-par cells to lapatinib, suggesting the development of lapatinib resistance. Under very specific conditions, (ie. 100 nM NH125 pre-treatment, followed by 250 nM lapatinib treatment for 5 days), combining NH125 with lapatinib resulted in a small, yet significant decrease in sensitivity of SKBR3-par cells to lapatinib. However, the same effect was not seen using different concentrations of either NH125 or lapatinib. In addition, pre-treatment of SKBR3-par cells with 100 nM NH125 resulted in a decrease in lapatinib IC_{50} in SKBR3-par cells. Therefore it seems that NH125 can affect the sensitivity of SKBR3-par cells to lapatinib but its effects on lapatinib sensitivity are concentration dependent. Interestingly, although NH125 is a potent inhibitor of eEF2k, thus activating eEF2 (dephosphorylating) and enhancing protein synthesis, it has also been reported have anti-proliferative and pro-apoptotic effects in cancer cell lines [364-366]. There are also conflicting reports on the effects of NH125 on the phosphorylation of eEF2, our study and others have shown that treatment with NH125 results in the dephosphorylation of eEF2 [364, 366]. This is in contrast to a recent study which reports that the anti-cancer activity of NH125 is correlated with induction of phospho-eEF2 rather than inhibition of eEF2k [365]. For this reason the authors of the study

warn against the use of NH125 as an eEF2k inhibitor, although it should be noted that the concentration of NH125 used in the study were significantly higher (1 – 10 μM) than the concentrations used here (100 nM) to successfully dephosphorylate eEF2 and decrease lapatinib sensitivity in SKBR3-par cells. Inhibition of eEF2k activity, via NH125 treatment may not represent the most effective means of altering eEF2 phosphorylation in SKBR3-par cells, or indeed give the most accurate representation of the effects of reduced eEF2k activity and phospho-eEF2 on the efficacy of lapatinib. Further work utilising eEF2k shRNA, to give sustained knockdown eEF2k expression and activity, or alternatively using a different inhibitor of eEF2k, such as the small molecule inhibitor A-484954, would be required to confirm the effect of eEF2k inhibition on lapatinib sensitivity.

Inhibition of eEF2k activity via NH125 resulted in the dephosphorylation of eEF2 but was not sufficient to reliably alter the sensitivity of SKBR3-par cells to lapatinib. Indirectly targeting the activity of eEF2k, via inhibition of the protein/pathway regulating its phosphorylation at Ser359, could provide a more effective means of altering lapatinib sensitivity. We have proposed that phosphorylation of eEF2k at Ser359, possibly mediated by SAPK4 [362], or CDK1 [363], may be responsible for the regulation of eEF2 phosphorylation. Immunoblotting revealed that SKBR3-L cells have increased phosphorylation of CDK1 at Tyr15 (which is associated with decreased CDK1 activity), despite having decreased expression of CDK1 compared to SKBR3-par cells. This result suggests that CDK1 activity may play a role in eEF2 phosphorylation, as CDK1 phosphorylates eEF2k at Ser359. However, treatment of the cell lines with lapatinib revealed decreased expression and phosphorylation of CDK1 in both cells, suggesting that lapatinib treatment has a similar effect on CDK1 activity in both cell lines. Thus, the role that CDK1 may play in the regulation of eEF2 phosphorylation is unclear and future work examining the effect of CDK1 activation and suppression on eEF2 signalling is warranted.

SAPK4 signalling may also play a role in the regulation of eEF2 phosphorylation. If SAPK4 is the kinase regulating the phosphorylation of eEF2k at Ser359, then pharmacological inhibition of SAPK4 would result in the phosphorylation and inactivation of eEF2 in SKBR3-L cells. SAPK4 is a member of the 38MAPK family, of which there are four member (p38α, p38β, p38γ and p38δ (SAPK4)). In additional to its role in the phosphorylation of eEF2k, SAPK4 is thought to play a role in cytoskeletal regulation [367, 368]. The chemical inhibitors SB203580 and SB202190 inhibit p38α

and p38β but do not inhibit p38γ and SAPK4 [369], and although BIRB0796 can inhibit SAPK4, it also inhibits the other members of the p38MAPk family [370]. Therefore, at present specific pharmacological inhibition of SAPK4 is not feasible. A possible method of examining the role SAPK4 plays in regulating eEF2 phosphorylation would be to knockdown SAPK4 expression using siRNA in SKBR3-L cells and examine the phosphorylation of eEF2 and activity of lapatinib in the cells.

Described above is a mechanism whereby eEF2 phosphorylation is mediated by increased eEF2k (Ser359) phosphorylation, however, future work will be required to determine the alteration(s) upstream of eEF2k causing its inactivation in SKBR3-L cells. In addition it is important to note that several other proteins/pathway can directly or indirectly regulate the phosphorylation of eEF2, as depicted in Figure 8-4. These include MEK, AMPK, PKC and PP2A. An activated form of MEK has been shown to dephosphorylate eEF2 via PI3K/mTOR dependent [371] and independent mechanisms [372]. Interestingly, SKBR3 cells overexpressing Ras develop resistance to lapatinib which can be overcome via MEK inhibition [373]. SKBR3-L cells exhibit lower levels of phospho-ERK compared to SKBR3-par cells and ERK is the only known substrate for MEK [374], thus, it is unlikely that decreased phosphorylation of eEF2 in SKBR3-L cells is mediated by activated MEK. AMP-activated protein kinase (AMPK) plays a key role in cellular energy homeostasis; depletion of ATP leads to a rise in the levels of AMP which activates AMPK [375]. AMPK phosphorylates eEF2k at Ser398, resulting in phosphorylation and inactivation of eEF2 via a non-mTOR mediated mechanism [376], and a generic HER1/2 inhibitor (GW-2974) activated AMPK in cancer cells [138]. It was not possible to examine phosphorylation at this site as there is currently no Ser398 phospho-eEF2k antibody commercially available. Oxytocin can induce dephosphorylation of eEF2 via the protein kinase C (PKC) pathway and Ser359 of eEF2k has been suggested to be a putative PKC phosphorylation site [377]. There is also evidence that PKC activation leads to increased PP2A activity [378, 379]. PP2A is a ubiquitously expressed protein phosphatase that functions to reverse the action of kinases in most major signalling cascades. Transgenic mice overexpressing PP2A exhibit increased eEF2 dephosphorylation [380] and inhibitors of PP2A attenuate the effects of angiotensin II on eEF2 dephosphorylation [371]. Tyrosine phosphorylation of PP2A results in inactivation of its phosphatase activity and loss of function as a tumour suppressor. Treatment of BT474 cells with heregulin resulted in increased phosphorylation of PP2A on Thr307 and treatment with a HER2 kinase inhibitor

(AG825) resulted in a decrease in PP2A phosphorylation thus increasing its activity. In breast tumour specimens, phosphorylated PP2A was high in HER2 positive breast tumours and significantly correlated with tumour progression [381]. This indicates that in HER2 positive cancer cells, signalling through HER2 is associated with phosphorylated PP2A and thus phosphorylated eEF2 and when signalling through HER2 is inhibited then PP2A is activated resulting in a dephosphorylation of eEF2. PP2A can also inactivate SAPK4 [382]. It is tempting to speculate that there could potentially be an alteration in PP2A activity leading to the constitutive dephosphorylation of eEF2 in SKBR3-L cells as a result of lapatinib conditioning.

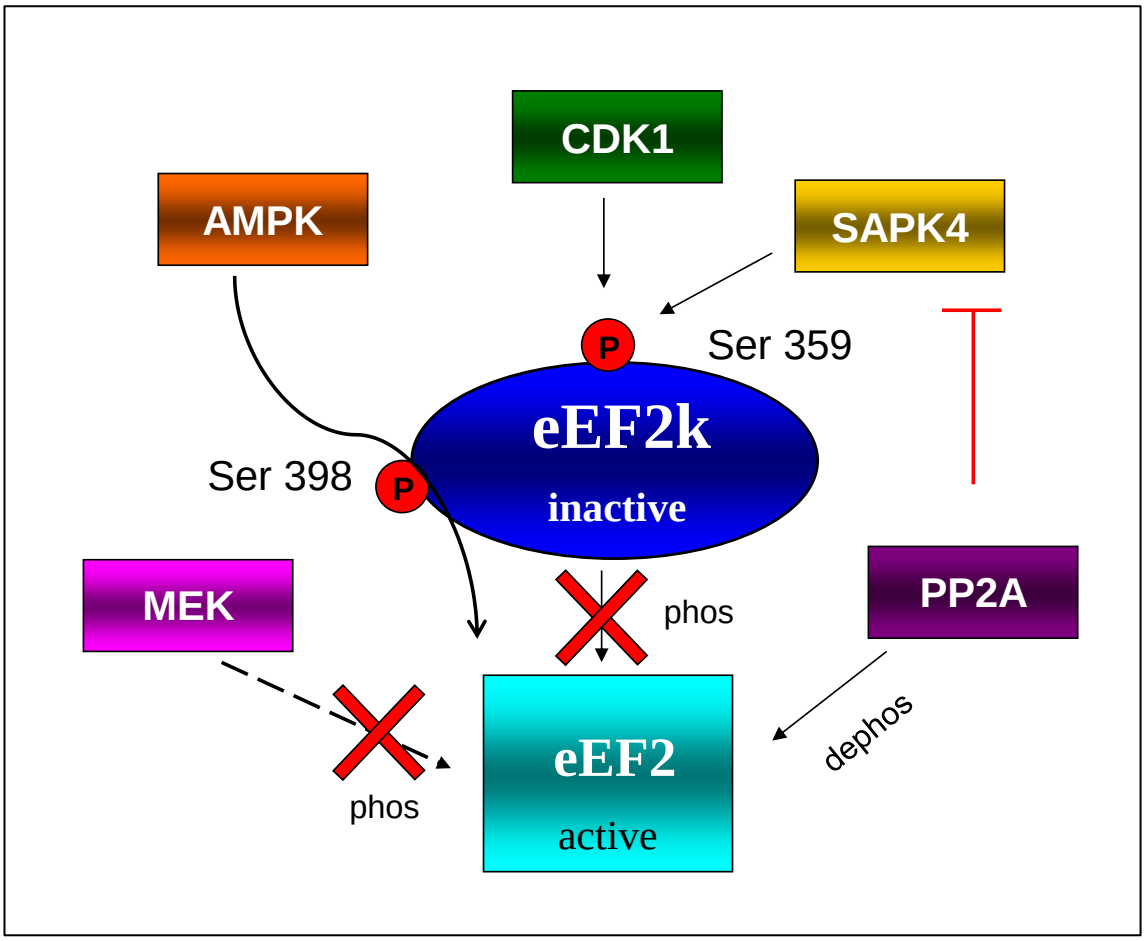

Figure 8-4: mTOR-independent signalling pathways which interact with eEF2k or eEF2 to regulate the phosphorylation of eEF2.

Acquired lapatinib resistance in SKBR3-L cells is associated with decreased phosphorylation of eEF2. The phosphorylation of eEF2 is regulated by phosphorylation of Ser359 of eEF2k and the activity of eEF2k is independent of mTOR signalling in these cells. Although inhibition of eEF2k activity, with NH125, did not reliably affect the sensitivity of lapatinib, it did result in the dephosphorylation of eEF2. Thus we propose that the alterations in the activity of eEF2k and eEF2 represent potential, novel, biomarkers of acquired lapatinib resistance. Validation in additional models of acquired lapatinib resistance would be required prior to pursuing this in tumour samples.

Although a role for mTOR in the regulation of eEF2 phosphorylation in SKBR3-L cells has been ruled out, an interesting alteration was uncovered in the phosphorylation of p70S6k, a kinase directly phosphorylated by mTOR. The levels of phosphorylated p70S6k (Thr389) are unaltered between SKBR3-par and SKBR3-L cells, however, while treatment of SKBR3-par cells with lapatinib inhibits the phosphorylation of

p70S6k, there was no effect on the levels of phospho-p70S6k in SKBR3-L cells. Phosphorylated p70S6k regulates the activity of eEF2k via phosphorylation at Ser366, however, the phosphorylation of eEF2k at Ser366 does not affect the activity of eEF2k towards eEF2. Thus suggesting that the alteration in the phosphorylation of p70S6k is independent of the alteration in eEF2 phosphorylation. The phosphorylation of p70S6k at Thr389 has been shown to be dependent on mTORC1 signalling, as rapamycin treatment results in the inhibition of p70S6k phosphorylation [383]. The phosphorylation of mTOR at Ser2448 has been reported to correlate with the activity of mTORC1 whereas phosphorylation at Ser2148 correlates with the activity of mTORC2 [384]. Interestingly, although mTOR signalling is inhibited in SKBR3-L cells following lapatinib treatment, the phosphorylation of p70S6k was unaffected. This result suggests that the phosphorylation of p70S6k in SKBR3-L cells is maintained independently of mTORC1. mTORC1 was thought to be the sole kinase which phosphorylated p70S6k at Thr389 until experiments using cells with mutant p70S6k, revealed continued phosphorylation of p70S6k following mTORC1 inhibition with rapamycin [385]. The discovery that mTORC2, which is insensitive to acute rapamycin, can phosphorylate p70S6k in an mTORC1-independent manner, suggests a mechanism whereby the phosphorylation of p70S6k is maintained despite inhibition of mTORC1 signalling [386]. This suggests that mTORC2 may be responsible for maintaining the phosphorylation of p70S6k in SKBR3-L cells.

Although alterations in p70S6k phosphorylation are not responsible for the dephosphorylation and activation of eEF2 via Ser359 phosphorylation and inactivation of eEF2k, maintenance of p70S6k phosphorylation in SKBR3-L cells may be an independent marker of acquired lapatinib resistance in SKBR3-L cells. Overexpression and/or amplification of p70S6k is associated with a worse prognosis, decreased overall survival and increased risk or recurrence in breast cancer patients [387, 388], and the expression of p70S6k has been correlated with HER2 overexpression [389]. A recent study has reported that sensitivity to lapatinib is associated with its ability to inhibit the phosphorylation of p70S6k in breast cancer cell lines [390], and an association between hyper-phosphorylation of p70S6k and lapatinib resistance in an MCF-7-HER2 transfected model of acquired lapatinib resistance [391]. These studies support the hypothesis that altered phosphorylation of p70S6k may be a marker of acquired lapatinib resistance, and the mechanism maintaining phosphorylation of p70S6k in SKBR3-L cells warrants further investigation.

In summary, SKBR3-L cells have lower levels of phospho-eEF2 compared to SKBR3-par cells. Treatment of SKBR3-par cells with lapatinib resulted in increased phosphorylation of eEF2 but it had no effect on the phosphorylation of eEF2 in SKBR3-L cells. Phosphorylation of eEF2k at Ser359 but not the mTOR dependent Ser366 site, correlated with eEF2k activity. Lapatinib treatment inhibited mTOR activity in both cell lines, as indicated by inhibition of Ser2448 phosphorylation, and rapamycin treatment was incapable of phosphorylating eEF2 in SKBR3-L cells. These results confirm that eEF2k regulation of eEF2 phosphorylation is independent of mTOR, and represent a novel association between alterations in the eEF2 phosphorylation and acquired lapatinib resistance. SKBR3-L cells also exhibited mTOR-independent maintenance of phospho-p70S6k which may be an eEF2-independent marker of acquired lapatinib resistance.

8.3.4 SILAC phospho- and total proteomics

SILAC labelling coupled with phospho-tyrosine enrichment was performed to compare the tyrosine phospho-proteome of SKBR3-par cells to SKBR3-L cells. The quantification and identification of alterations in tyrosine phosphorylation is hindered by the low abundance of phospho-proteins, particularly tyrosine-phosphorylated proteins in human cells. A major break-through in the study of altered phospho-tyrosine signalling came with the development of a phospho-peptide enrichment procedure utilising an immunoaffinity-based based method [272]. This enrichment procedure revealed more than 300 distinct tyrosine phosphorylation sites in protein extracts from three different human cancer cell lines. Since then, this enrichment procedure has been used to study tyrosine phosphorylation in multiple different settings including in the study of human cancer [273, 392-395], and also in the study of drosophila [396] and plants [397]. The technique has also been utilised to examine alterations in phospho-tyrosine signalling in a BT474 cell lines model of acquired lapatinib resistance [235].

Unfortunately, despite positive indications from optimisation experiments, the same tyrosine phosphorylation enrichment procedure was inefficient in the identification of alterations in tyrosine phosphorylation between SKBR3-par and SKBR3-L cells. In fact, only a single tyrosine-phosphorylated protein (CDK1) was identified which was present in all three biological replicates and had quantitative data associated with it. Why the tyrosine-enrichment procedure was inefficient in identifying alteration in phospho-

tyrosine signalling between SKBR3-par and SKBR3-L cells remains unclear. However, it is possible that inefficient binding of phospho-tyrosine peptides to the antibody beads and/or loss of sample during the concentration and clean-up steps may be contributing factors. If this procedure was to be repeated analysis of a small quantity of the sample by LC-MS prior to and following the antibody-binding step and clean-up steps would be recommended.

Although the volume of results generated from the phospho-tyrosine analysis were disappointing CDK1 was identified as a tyrosine phosphorylated protein whose level was significantly higher in untreated SKBR3-L cells compared to untreated SKBR3-par cells. Immunoblotting for phospho-CDK1 with an antibody which targets Tyr15 confirmed increased levels of phospho-CDK1 in SKBR3-L cells. Cyclin dependent kinase 1(CDK1), also known as cdc2, is a protein which plays a key role in regulating the mammalian cell cycle [reviewed in [398]]. CDK1, forms a complex with cyclin-B but is held in an inactive state by phosphorylation of CDK1 at Tyr15 and Thr14 by the protein kinases Wee1 and Myt1. Dephosphorylation of the CDK1-cyclin B complex at Thr14, following by Tyr15 by Cdc25 phosphatases results in activation and cell cycle progression [399]. The phosphorylation of CDK1 at Tyr15 is higher in SKBR3-L cells compared to SKBR3-par, despite SKBR3-L cells having decreased expression of CDK1 compared to SKBR3-par cells. Lapatinib treatment decreases the expression and phosphorylation of CDK1 in both cell lines. Thus, at present, the impact of CDK1 phosphorylation and expression on sensitivity and/or resistance to lapatinib has not been elucidated and future work examining additional phosphorylation sites and CDK1 activity assays and cell cycle assays may more clearly define a role for CDK1 in lapatinib resistance. However, validation of the altered phosphorylation of CDK1, suggests that the SILAC labelling procedure and phospho-tyrosine enrichment worked as identification of an alteration in phospho-tyrosine signalling was detected, suggesting that the labelling and enrichment procedure worked but was extremely inefficient.

In addition to analysing alterations in tyrosine phosphorylation between SKBR3-par and SKBR3-L cells changes in total protein expression were analysed using the SILAC-labelled protein. Several statistically significant changes were detected in the levels of proteins in SKBR3-L cells compared to SKBR3-par cells, and also between both of the cell lines treated with lapatinib (GAPDH, SET, HER2, EBP1 and SELENBP1) and the altered levels of these proteins were confirmed using immunoblotting.

8.3.4.1 GAPDH

Glyceraldehyde-3-phosphate dehydrogenase (GAPDH) is an enzyme which plays a pivotal role in metabolism and is generally considered a housekeeping gene, however, this enzyme is actually very tightly regulated and is involved in numerous cellular functions [reviewed in [400]]. GAPDH has also been shown to have both a proapoptotic and antiapoptotic role in cell fate. Overexpression of GAPDH in ovarian cancer cells resulted in an increase in H_20_2-induced apoptosis, and the phosphorylation of GAPDH by AKT2 is an essential step in GAPDH-mediated apoptosis [401]. Knockdown of GAPDH in A549 cells results in accelerated cellular senescence with increased signalling through the AMPK pathway suggesting a role for GAPDH in the control of tumour cell proliferation [402]. SKBR3-L cells have lower levels of GAPDH compared to SKBR3-par cells. Whether or not the altered expression of GAPDH is as a result of, or indeed plays any role in acquired lapatinib resistance has yet to be determined. Interestingly GAPDH interacts with SET protein (see discussion below) both *in vitro* and *in vivo* and together they regulate cell cycle progression by modulating cyclin B-CDK-1 activity [403].

8.3.4.2 SET / I2PP2A

The SET domain is a 130-amino-acid sequence which was initially identified in the protein products of three regulatory genes in *Drosophila*, whose names account for the name SET, i.e, SU(VAR)3-9, enhancer of Zeste [E(Z)], and trithorax (Trx) [404]. SET protein, which is named for its SET domain, is also referred to as I^2PP2A and TAF1β. SKBR3-par and SKBR3-L cells express SET protein, however SKBR3-L cells treated with 1 μM lapatinib have lower levels of SET compared to untreated cells, whereas the levels of SET in SKBR3-par cells are unaffected by lapatinib treatment. SET is an oncoprotein with diverse cellular functions including cell cycle control, via inhibition of CDK1 activity [405], histone acetylation [406], gene transcription [407], apoptosis [408], and cell migration [409]. SET interacts with nm23-H1, a metastasis suppressor [410]. SET is a potent inhibitor of PP2A [411], a tumour suppressor protein which when active, negatively regulates the activity of several proteins including Akt, β-catenin and c-Myc and eEF2 [412-414]. Taken together this data suggests that SET plays a key role in numerous pathways that lead to more aggressive phenotypes and therefore represents an attractive target in the treatment of cancer. COG112, has been shown to bind SET and increase the activity of PP2A and nm23-H1 and also Rac-1 [415]. The role of SET as an inhibitor of PP2A is of particular interest in SKBR3-L cells as the phosphorylation

of AKT and eEF2 is inhibited in SKBR3-L cells. It is possible that increased PP2A activity, mediated by alterations in SET, which is a negative regulator of PP2A activity, may play a role in the dephosphorylation of AKT and eEF2 in SKBR3-L cells. Further work will be required to elucidate the roles of SET and PP2A in lapatinib resistance.

8.3.4.3 HER2

The SILAC proteomic experiment revealed increased HER2 expression in SKBR3-par cells following lapatinib treatment compared to SKBR3-L cells. Immunoblotting with 30 µg of protein did not reveal any alterations in HER2 expression. However, by reducing the quantity of protein to 5 µg, increased HER2 expression was detected in SKBR3-par cells compared to SKBR3-L cells following lapatinib treatment. The increased HER2 expression following lapatinib treatment in SKBR3-par cells is consistent with previous reports suggesting that lapatinib increases the expression and accumulation of HER2 [416, 417].Yet as previously discussed with regard to the increased HER2 amplification and expression of HER2 in HCC1954-L cells, this alteration in HER2 expression is unlikely to be causative of lapatinib resistance as lapatinib inhibits the phosphorylation of HER2 in all cell lines regardless of lapatinib sensitivity.

8.3.4.4 EBP1

Proliferation-associated protein 2G4, also known as ERBB3-binding protein one (EBP1), was initially identified as a HER3-binding protein using a yeast two-hybrid screen for HER3 interacting proteins [418]. Overexpression of EBP1 inhibits the growth of breast cancer cells [419]. Ectopic expression of EBP1 in breast cancer cells reduces the levels of HER2 protein, HER2 promoter activity and reduces HER2 protein stability [420, 421]. EBP1 also interacts with AKT via the PKC pathway to regulate cell survival and suppress apoptosis [422]. There are two different isoforms of EBP1, the longer form p48, suppresses apoptosis whereas the shorter from p42 promotes cell differentiation. In addition, EGF strongly stimulates p42 binding to HER3, whereas p48 does not bind to HER3 regardless of EGF treatment [423]. This suggests that EBP1 has different effects on cell growth on survival depending on the expression of its isoforms. SKBR3-par and SKBR3-L cells express EBP1 and treatment of SKBR3-par cells with lapatinib results in a decrease in the expression of EBP1, in contrast there is no change in the levels of EBP1 in SKBR3-L when treated with lapatinib. The differential expression of EBP1 in response to lapatinib in these cells lines warrants further

investigation to determine whether EBP1 is playing a role in acquired lapatinib resistance.

8.3.4.5 SELENBP1

Selenium is an essential trace element which has been proposed to have an anti-cancer effect. A link between insufficient selenium and increased risk of cancer has been suggested [284, 285]. The anticancer action of selenium is thought to be mediated by selenium-binding protein 1 (SELENBP1). However, there is very limited data on the significance of selenium binding to SELENBP1 or indeed on the molecular function of SELENBP1. Interestingly, the expression of SELENBP1 is reduced in multiple cancer types including; gastric [424], prostate [425], lung [426], ovarian [427], thyroid [428], colorectal [429], uterine [430], esophageal adenocarcinoma [431] and hepatocellular [432], and has been associated with poor survival in gastric [424] and colorectal carcinoma [429]. Stable overexpression of SELENBP1 in esophageal adenocarcinoma cells resulted in increased sensitivity to cisplatin [431]. It has been proposed that SELENBP1 has tumour-suppressor function as the overexpression of SELENBP1sensitied colon cancer cells to H_2O_2-induced apoptosis, inhibited cancer cell migration *in vitro* and inhibited tumour growth in nude mice [433]. The expression of SELENBP1 was altered in SKBR3-L cells; SELENP1expression is significantly lower in SKBR3-L cells, treated with lapatinib, compared to SKBR3-par cells treated with lapatinib. The role that altered SELENBP1 may play in the response of SKBR3-par and SKBR3-L cells to lapatinib is yet unknown, this is the first study to report an alteration in SELENBP1 in breast cancer or in response to a targeted therapeutic agent.

8.3.4.6

As previously discussed the tyrosine-phosphorylation protein enrichment procedure was disappointing in that the yield of phosphorylated proteins identified for which matched SILAC data was calculated was extremely low. When the total proteome of the samples was examined using the un-enriched SILAC-labelled samples several alterations in total protein expression were identified between the two cell lines. However, several alterations which had previously been confirmed using western blotting were not detected as being altered between the two cell lines for example, eEF2k, IGF-IR, EGFR, HER4 etc. It’s possible that some of these proteins, like the HER receptors, have been

harder to detect due to the fact that they are not as readily separated on a 10 % gel as lower molecular weight proteins. Thus, if the experiment was to be repeated a gradient gel may provide more information than a 10 % gel. However, new developments in the field of proteomics are occurring at an accelerated pace and one of the more recently developed proteomic techniques is label-free MS. Label-free MS overcomes many of the limitations associated with SILAC technology such as increased time and complexity of sample preparation, requirement for higher sample concentration, high cost of the reagents, incomplete labeling, and the requirement for specific quantification software. Thus, label-free MS represents a fast and low-cost method of measuring protein expression levels in complex biological samples [434].

In summary, SILAC labelling coupled with phospho-tyrosine enrichment produced limited results on alterations in phospho-tyrosine signalling between SKBR3-par and SKBR3-L cells. However, it was possible to validate an alteration in the phosphorylation of CDK1, which was higher in SKBR-L cells compared to SKBR3-par cells. CDK1 plays an integral role in cell cycle progression and phosphorylation at Tyr15 regulates its activity. The expression of total proteins was analysed using SILAC-labelled protein and significant alterations in the expression of GAPDH, SET protein, EBP1 and SELENBP1 were found. Functional validation of these proteins may reveal new targets or biomarkers of acquired lapatinib resistance.

8.4 Innate lapatinib resistance

In addition to examining alterations in HER family proteins and downstream signalling pathways activated by HER2 signalling in acquired lapatinib resistance, the expression and phosphorylation of these proteins were examined in innate lapatinib resistance. Using a panel of 15 HER2-amplified breast cancer cells, including 5 cell lines with innate lapatinib resistance the basal levels of phospho- and total HER2, HER3, EGFR, AKT, ERK, p70S6k and eEF2 were examined. Lapatinib sensitivity correlated with levels of phospho-HER2, total HER2, phospho-HER3, ERK and p70S6k. While lapatinib sensitivity has previously been correlated with the basal expression of HER2 and the phosphorylation of HER2, HER3 and EGFR [134, 194], a correlation between levels of ERK or p70S6k and lapatinib sensitivity has not been reported previously. Quantifiable phospho-EGFR was not detected by immunoblotting thus correlations with

lapatinib sensitivity were not possible. This is in contrast to the above studies which measured phospho- and total EGFR by ELISA which is more sensitive.

In addition, as the phosphorylation of AKT, ERK, p70S6k and eEF2 in response to lapatinib treatment differs between lapatinib sensitive and acquired lapatinib-resistant cells, alterations in the phosphorylation of these proteins were examined in a panel of HER2-amplifed cell lines. Reduced phosphorylation of HER2, AKT, p70S6k and ERK correlated with sensitivity to lapatinib, and increased phosphorylation of eEF2 also correlated with lapatinib sensitivity. Innate lapatinib-resistant cells exhibit maintained phosphorylation of AKT, ERK and p70S6k and do not exhibit increased eEF2 phosphorylation in response to lapatinib treatment. The relationship between decreased phosphorylation of HER2 AKT, p70S6k and ERK and lapatinib sensitivity have previously been reported [134, 194, 390]. However, phosphorylation of eEF2 has not previously been correlated with sensitivity to lapatinib. Evaluation of the phosphorylation of eEF2, p70S6k, AKT, ERK and HER2 in lapatinib-treated breast tumours would be required to test the robust nature of these phospho-proteins as early pharmacodynamic biomarkers of lapatinib response.

Interestingly, our results also suggest that several of the cell lines (SUM190, MDA-MB-453 and MDA-MB-361) exhibit atypical alterations in the phosphorylation of eEF2, p70S6k, AKT and ERK compared to other lapatinib-sensitive/lapatinib-resistant cell lines. This suggests that these cell lines should not be utilised in isolation as cell line models of lapatinib sensitive and/or lapatinib-resistant cells as the results may not be indicative of global alterations.

8.5 Summary and conclusions

HCC1954-L and SKBR3-L cells represent novel cell line models of acquired lapatinib resistance. These cell lines were stably resistant and retained HER2 positivity. A summary of the alterations between SKBR3-par and SKBR3-L cells is listed in Table 8-1. Several alterations were found in HER family members and members of downstream signalling pathways which may contribute to lapatinib resistance including, inhibition of HER4 expression, decreased levels of phospho-AKT and cross-resistance to EGFR targeted therapy in SKBR3-L cells. HCC1954-L cells also exhibited alterations in the phosphorylation of AKT and ERK. Published mechanisms of acquired lapatinib

resistance were examined in HCC1954-L and SKBR3-L cells. Increased ER expression has been reported as a mechanism of resistance to lapatinib however, it is not a resistance mechanism in HCC1954-L and SKBR3-L cells as there are ER negative. This study also reports upregulation of SRC in HCC1954-L cells only, upregulation of MCL-1 in SKBR3-L cells only and increased expression of XIAP in HCC1954-L cells following treatment with lapatinib. These results suggest that these mechanisms may contribute to lapatinib resistance in HCC1954-L and SKBR3-L cells and further investigation of these alterations is warranted.

Table 8-1: List of alterations in protein phosphorylation and expression in SKBR3-L cells compared in SKBR3-par cells.

Alteration	Condition
↑ phospho-HER2 in SKBR3-L cells	Untreated cells
↑ phospho- and total EGFR in SKBR3-L cells	Untreated cells
↑ HER3 in SKBR3-L cells	following 1 μM lapatinib treatment
↓ HER4 in SKBR3-L cells	Untreated cells
↓ phospho-AKT in SKBR3-L cells	Untreated cells
↓ phospho-ERK in SKBR3-L cells	Untreated cells
↑ phospho- and total IGF-IR in SKBR3-L cells	Untreated cells
↑ MCL-1 in SKBR3-L cells	Untreated cells
↓ phospho-eEF2 in SKBR3-L cells	Untreated cells
↑ phospho-eEF2 in SKBR3-par cells only	following 1 μM lapatinib treatment
↑ phospho-eEF2k (Ser359) in SKBR3-L cells	Untreated cells
↓ phospho-eEF2k (Ser359) in SKBR3-par cells	following 1 μM lapatinib treatment
↑ phospho-eEF2k (Ser366) in SKBR3-L cells	Untreated cells
↑ phospho-eEF2k (Ser366) in SKBR3-par cells	following 1 μM lapatinib treatment
↑ eEF2k in SKBR3-L cells	Untreated cells
↓ phospho-mTOR in SKBR3-L cells	Untreated cells
↓ phospho-p70S6k in SKBR3-par cells	following 1 μM lapatinib treatment
↑ phospho-CDK1 in SKBR3-L cells	Untreated cells
↓ CDK1 in SKBR3-L cells	Untreated cells
↑ GAPDH in SKBR3-L cells	Untreated cells
↓ SELENBP1 in SKBR3-L cells	SILAC LAP vs LAP comparison
↓ SET in SKBR3-L cells	SILAC LAP vs LAP comparison
↑ EBP1 in SKBR3-L cells	SILAC LAP vs LAP comparison
↓ sensitivity to gefitinib in SKBR3-L cells	0.8 ± 0.2 μM versus 4.9 ± 1.1 μM

Lapatinib conditioning of HCC1419 cells revealed a novel potential mechanism of lapatinib action – the induction of a senescent-like phenotype. The induction of senescence was independent of p53 and p16 expression and associated with high levels of p15 and p27 mRNA. The senescent-like phenotype induced by lapatinib was reversed when lapatinib was removed from the media. We propose a model whereby lack of p53 and p16 expression in HCC1419 cells prevented the cells from undergoing terminal

senescence in response to lapatinib treatment and thus the de-repression of HER2 oncogenic signalling, following removal of lapatinib from the media, provided an escape from senescence. Therefore lapatinib induced senescence may not only be a novel mechanism of lapatinib action but also a novel mechanism of lapatinib resistance. These mechanisms warrant further investigation in *in vitro* and *in vivo* models of HER2 positive breast cancer. However, to date this phenotype has not yet been replicated in any other models of lapatinib-sensitive cells. Future work will be required to identify another model of lapatinib-induced senescence. In addition, model based on p53 and p16 expression requires validation using over-expression and knock-down experiments in HCC1419 and SKBR3 cells.

In addition, the lapatinib-resistant phenotype of HCC1954-L and SKBR3-L cells were examined and characterised using several different screening techniques, including; aCGH technology and proteomics.

Array CGH comparison of HCC1954-L cells to HCC1954-par cells revealed amplification of chr17q12, corresponding to several genes including HER2 and STARD3. There was amplification of all 4 members of the OATP family of influx pumps. The amplification of HER2 and STARD3 at the genomic level also translated into increased expression at the protein level. The increased expression of STARD3 is particularly interesting as it has not been reported in lapatinib resistance previously.

Previous phospho-proteomic analysis revealed decreases levels of phospho-eEF2 in SKBR3-L cells compared to SKBR3-par cells. The phosphorylation and activity of eEF2 was found to be regulated by phosphorylation of eEF2k at Ser359, in an mTOR independent manner. This suggests a role for SAPK4 signalling in lapatinib resistance. In addition SKBR3-L exhibit maintained phosphorylation of p70S6k following lapatinib treatment. Examining the phosphorylation of eEF2 and p70S6k in a panel of HER2 positive lapatinib resistance cell lines revealed that alterations in the phosphorylation of eEF2 and p70S6k, in addition to the alteration in phospho-HER2, phospho-AKT and phospho-ERK, correlated with lapatinib sensitivity. Thus suggesting that these phosphorylated proteins have the potential to be biomarkers of lapatinib response. In addition the basal levels of phospho-HER2, HER2, phospho-HER3, ERK and p70S6k predicted lapatinib sensitivity in the panel of cell lines.

SILAC phospho-tyrosine proteomic analysis of SKBR3-par and SKBR3-L cells revealed an alteration in phospho-CDK1, which may play a role in lapatinib resistance. In addition, performing total proteomic analysis of the cell lines revealed significant alterations in several proteins including, GADPH, SET protein, EBP1 and SELENBP1. Many of these protein alterations have not been previously reported in breast cancer and/or in lapatinib resistance.

Further validation of all of the above results, using *in vitro* and *in vivo* models of lapatinib sensitivity and resistance, will be required to elucidate the roles of these alterations in a clinical setting.

References

[1] Cooper, G. Elements of Human Cancer. **1992**.

[2] The National Cancer Registry of Ireland *http://www.ncri.ie/ncri/index.shtml* (accessed 01/03, 2012).

[3] American Cancer Society
Breast Cancer Facts & Figures 2011-2012. **2011**.

[4] Therese, S. Molecular portraits of breast cancer: tumour subtypes as distinct disease entities. *Eur. J. Cancer* **2004**, *40*, 2667-2675.

[5] Cleator, S.; Heller, W.; Coombes, R. C. Triple-negative breast cancer: therapeutic options. *The Lancet Oncology* **2007**, *8*, 235-244.

[6] Perou, C. M., *et al.* Molecular portraits of human breast tumours. *Nature* **2000**, *406*, 747-752.

[7] Carey, L. A., *et al.* Race, Breast Cancer Subtypes, and Survival in the Carolina Breast Cancer Study. *JAMA: The Journal of the American Medical Association* **2006**, *295*, 2492-2502.

[8] Sørlie, T., *et al.* Gene expression patterns of breast carcinomas distinguish tumor subclasses with clinical implications. *Proceedings of the National Academy of Sciences* **2001**, *98*, 10869-10874.

[9] Sørlie, T., *et al.* Repeated observation of breast tumor subtypes in independent gene expression data sets. *Proceedings of the National Academy of Sciences* **2003**, *100*, 8418-8423.

[10] Hu, Z., *et al.* The molecular portraits of breast tumors are conserved across microarray platforms. *BMC Genomics* **2006**, *7*, 96.

[11] Akiyama, T., *et al.* The product of the human c-erbB-2 gene: a 185-kilodalton glycoprotein with tyrosine kinase activity. *Science* **1986**, *232*, 1644-1646.

[12] Hynes, N. E.; Lane, H. A. ERBB receptors and cancer: the complexity of targeted inhibitors. *Nat Rev Cancer* **2005**, *5*, 341-354.

[13] Morris, J. K., *et al.* Rescue of the Cardiac Defect in ErbB2 Mutant Mice Reveals Essential Roles of ErbB2 in Peripheral Nervous System Development. *Neuron* **1999**, *23*, 273-283.

[14] Özcelik, C., *et al.* Conditional mutation of the ErbB2 (HER2) receptor in cardiomyocytes leads to dilated cardiomyopathy. *Proceedings of the National Academy of Sciences* **2002**, *99*, 8880-8885.

[15] Crone, S. A., *et al.* ErbB2 is essential in the prevention of dilated cardiomyopathy. *Nat. Med.* **2002**, *8*, 459-465.

[16] Negro, A.; Brar, B. K.; Lee, K. Essential Roles of Her2/erbB2 in Cardiac Development and Function. *Recent Prog. Horm. Res.* **2004**, *59*, 1-12.

[17] Slamon, D., *et al.* Human breast cancer: correlation of relapse and survival with amplification of the HER-2/neu oncogene. *Science* **1987**, *235*, 177-182.

[18] Wolff, A. C., *et al.* American Society of Clinical Oncology/College of American Pathologists Guideline Recommendations for Human Epidermal Growth Factor Receptor 2 Testing in Breast Cancer. *Journal of Clinical Oncology* **January 20, 2006**, *25*, 118-145.

[19] Konecny, G., *et al.* HER-2/neu and Urokinase-Type Plasminogen Activator and Its Inhibitor in Breast Cancer. *Clinical Cancer Research* **2001**, *7*, 2448-2457.

[20] Ménard, S., *et al.* Role of HER2 gene overexpression in breast carcinoma. *J. Cell. Physiol.* **2000**, *182*, 150-162.

[21] Olayioye, M. A., *et al.* The ErbB signaling network: receptor heterodimerization in development and cancer. *EMBO J.* **2000**, *19*, 3159-3167.

[22] Borrell-Pages, M., *et al.* TACE is required for the activation of the EGFR by TGF-[alpha] in tumors. *EMBO J.* **2003**, *22*, 1114-1124.

[23] Harris, R. C.; Chung, E.; Coffey, R. J. EGF receptor ligands. *Exp. Cell Res.* **2003**, *284*, 2-13.

[24] Franklin, M. C., *et al.* Insights into ErbB signaling from the structure of the ErbB2-pertuzumab complex. *Cancer Cell* **2004**, *5*, 317-328.

[25] Cho, H., *et al.* Structure of the extracellular region of HER2 alone and in complex with the Herceptin Fab. *Nature* **2003**, *421*, 756-760.

[26] Burgess, A. W., *et al.* An Open-and-Shut Case? Recent Insights into the Activation of EGF/ErbB Receptors. *Mol. Cell* **2003**, *12*, 541-552.

[27] Guy, P. M., *et al.* Insect cell-expressed p180erbB3 possesses an impaired tyrosine kinase activity. *Proc. Natl. Acad. Sci. U. S. A.* **1994**, *91*, 8132-8136.

[28] Jura, N., *et al.* Structural analysis of the catalytically inactive kinase domain of the human EGF receptor 3. *Proceedings of the National Academy of Sciences* **2009**, *106*, 21608-21613.

[29] Zhang, X., *et al.* An Allosteric Mechanism for Activation of the Kinase Domain of Epidermal Growth Factor Receptor. *Cell* **2006**, *125*, 1137-1149.

[30] Campbell, M. R.; Amin, D.; Moasser, M. M. HER3 Comes of Age: New Insights into Its Functions and Role in Signaling, Tumor Biology, and Cancer Therapy. *Clinical Cancer Research* **2010**, *16*, 1373-1383.

[31] Y, Y. The EGFR family and its ligands in human cancer: signalling mechanisms and therapeutic opportunities. *Eur. J. Cancer* **2001**, *37, Supplement 4*, 3-8.

[32] Citri, A.; Skaria, K. B.; Yarden, Y. The deaf and the dumb: the biology of ErbB-2 and ErbB-3. *Exp. Cell Res.* **2003**, *284*, 54-65.

[33] Citri, A.; Yarden, Y. EGF-ERBB signalling: towards the systems level. *Nat. Rev. Mol. Cell Biol.* **2006**, *7*, 505-516.

[34] Garrett, T. P. J., *et al.* The Crystal Structure of a Truncated ErbB2 Ectodomain Reveals an Active Conformation, Poised to Interact with Other ErbB Receptors. *Mol. Cell* **2003**, *11*, 495-505.

[35] Graus-Porta, D., *et al.* ErbB-2, the preferred heterodimerization partner of all ErbB receptors, is a mediator of lateral signaling. *EMBO J.* **1997**, *16*, 1647-1655.

[36] Baselga, J.; Swain, S. M. Novel anticancer targets: revisiting ERBB2 and discovering ERBB3. *Nat Rev Cancer* **2009**, *9*, 463-475.

[37] Browne, B. C., *et al.* HER-2 signaling and inhibition in breast cancer. *Curr. Cancer. Drug Targets* **2009**, *9*, 419-438.

[38] Pronk, G. J., *et al.* Insulin-induced phosphorylation of the 46- and 52-kDa Shc proteins. *Journal of Biological Chemistry* **1993**, *268*, 5748-5753.

[39] Rozakis-Adcock, M., *et al.* Association of the Shc and Grb2/Sem5 SH2-containing proteins is implicated in activation of the Ras pathway by tyrosine kinases. *Nature* **1992**, *360*, 689-692.

[40] Buday, L.; Downward, J. Epidermal growth factor regulates p21ras through the formation of a complex of receptor, Grb2 adapter protein, and Sos nucleotide exchange factor. *Cell* **1993**, *73*, 611-620.

[41] Schulze, W. X.; Deng, L.; Mann, M. Phosphotyrosine interactome of the ErbB-receptor kinase family. *Mol Syst Biol* **2005**, *1*.

[42] Fruman, D. A.; Meyers, R. E.; Cantley, L. C. PHOSPHOINOSITIDE KINASES. *Annu. Rev. Biochem.* **1998**, *67*, 481-507.

[43] Chan, T. O.; Rittenhouse, S. E.; Tsichlis, P. N. AKT/PKB AND OTHER D3 PHOSPHOINOSITIDE-REGULATED KINASES: Kinase Activation by Phosphoinositide-Dependent Phosphorylation. *Annu. Rev. Biochem.* **1999**, *68*, 965-1014.

[44] Sarbassov, D. D., *et al.* Phosphorylation and regulation of Akt/PKB by the rictor-mTOR complex. *Science* **2005**, *307*, 1098-1101.

[45] Dong, L. Q.; Liu, F. PDK2: the missing piece in the receptor tyrosine kinase signaling pathway puzzle. *American Journal of Physiology - Endocrinology And Metabolism* **2005**, *289*, E187-E196.

[46] Hresko, R. C.; Mueckler, M. mTOR·RICTOR Is the Ser473 Kinase for Akt/Protein Kinase B in 3T3-L1 Adipocytes. *Journal of Biological Chemistry* **2005**, *280*, 40406-40416.

[47] Zhang, Z., *et al.* mTOR-rictor is the Ser^{473} kinase for AKT1 in mouse one-cell stage embryos. *Molecular and Cellular Biochemistry* **2012**, *361*, 249-257.

[48] Glidden, E. J., *et al.* Multiple Site Acetylation of Rictor Stimulates Mammalian Target of Rapamycin Complex 2 (mTORC2)-dependent Phosphorylation of Akt Protein. *Journal of Biological Chemistry* **2012**, *287*, 581-588.

[49] Calvo, E.; Bolos, V.; Grande, E. Multiple roles and therapeutic implications of Akt signaling in cancer. *Onco Targets Ther.* **2009**, *2*, 135-150.

[50] Osaki, M.; Oshimura, M.; Ito, H. PI3K-Akt pathway: its functions and alterations in human cancer. *Apoptosis* **2004**, *9*, 667-676.

[51] Luo, J.; Manning, B. D.; Cantley, L. C. Targeting the PI3K-Akt pathway in human cancer: Rationale and promise. *Cancer Cell* **2003**, *4*, 257-262.

[52] Goncharenko-Khaider, N., *et al.* The inhibition of Bid expression by Akt leads to resistance to TRAIL-induced apoptosis in ovarian cancer cells. *Oncogene* **2010**, *29*, 5523-5536.

[53] Cross, D. A. E., *et al.* Inhibition of glycogen synthase kinase-3 by insulin mediated by protein kinase B. *Nature* **1995**, *378*, 785-789.

[54] Plas, D. R.; Thompson, C. B. Akt Activation Promotes Degradation of Tuberin and FOXO3a via the Proteasome. *Journal of Biological Chemistry* **2003**, *278*, 12361-12366.

[55] Huang, J.; Manning, B. D. A complex interplay between Akt, TSC2 and the two mTOR complexes. *Biochem. Soc. Trans.* **2009**, *37*, 217-222.

[56] Huang, H., *et al.* Skp2 inhibits FOXO1 in tumor suppression through ubiquitin-mediated degradation. *Proceedings of the National Academy of Sciences of the United States of America* **2005**, *102*, 1649-1654.

[57] Inoki, K.; Guan, K. Complexity of the TOR signaling network. *Trends Cell Biol.* **2006**, *16*, 206-212.

[58] Dos D. Sarbassov, *et al.* Rictor, a Novel Binding Partner of mTOR, Defines a Rapamycin-Insensitive and Raptor-Independent Pathway that Regulates the Cytoskeleton. *Current Biology* **2004**, *14*, 1296-1302.

[59] Menon, S.; Manning, B. D. Common corruption of the mTOR signaling network in human tumors. *Oncogene* **2008**, *27 Suppl 2*, S43-51.

[60] Kaul, G.; Pattan, G.; Rafeequi, T. Eukaryotic elongation factor-2 (eEF2): its regulation and peptide chain elongation. *Cell Biochem. Funct.* **2011**, *29*, 227-234.

[61] Hay, N.; Sonenberg, N. Upstream and downstream of mTOR. *Genes & Development* **2004**, *18*, 1926-1945.

[62] Dobashi, Y., *et al.* Mammalian target of rapamycin: a central node of complex signaling cascades. *Int. J. Clin. Exp. Pathol.* **2011**, *4*, 476-495.

[63] Dershaw, D. D. Mammography in patients with breast cancer treated by breast conservation (lumpectomy with or without radiation). *American Journal of Roentgenology* **1995**, *164*, 309-316.

[64] van Nes, J. G. H.; van de Velde, C. J. H. The preferred treatment for young women with breast cancer - mastectomy versus breast conservation. *The Breast* **2006**, *15, Supplement 2*, S3-S10.

[65] Dollinger, M.; Rosenbaum, E.; Tempero, M. Everyone's guide to cancer therapy : how cancer is diagnosed, treated, and managed day to day. **2002**, *Fourth*.

[66] Beitsch, P. D.; Shaitelman, S. F.; Vicini, F. A. Accelerated partial breast irradiation. *J. Surg. Oncol.* **2011**, *103*, 362-368.

[67] Lehman, M.; Hickey, B. The less than whole breast radiotherapy approach. *The Breast* **2010**, *19*, 180-187.

[68] Pratt, W.; Ruddon, R. The Anticancer Drugs. **1979**.

[69] Chabner, B. A.; Roberts, T. G., Chemotherapy and the war on cancer. *Nat Rev Cancer* **2005**, *5*, 65-72.

[70] Shah, M. A.; Schwartz, G. K. The relevance of drug sequence in combination chemotherapy. *Drug Resistance Updates* **2000**, *3*, 335-356.

[71] Yeh, E. T. H. Cardiotoxicity Induced by Chemotherapy and Antibody Therapy. *Annu. Rev. Med.* **2006**, *57*, 485-498.

[72] Elsevier The Elsevier Guide to Oncology Drugs & Regimes. **2006**.

[73] Widakowich, C., *et al.* Molecular targeted therapies in breast cancer: Where are we now? *Int. J. Biochem. Cell Biol.* **2007**, *39*, 1375-1387.

[74] Hanahan, D.; Weinberg, R. A. The Hallmarks of Cancer. *Cell* **2000**, *100*, 57-70.

[75] Cole, M. P.; Jones, C. T. A.; Todd, I. D. H. A new anti-oestrogenic agent in late breast cancer. An early clinical appraisal of ICI46474. *Br. J. Cancer* **1971**, *25*, 270.

[76] Carter, P., *et al.* Humanization of an anti-p185HER2 antibody for human cancer therapy. *Proceedings of the National Academy of Sciences* **1992**, *89*, 4285-4289.

[77] Tokuda, Y., *et al.* In vitro and in vivo anti-tumour effects of a humanised monoclonal antibody against c-erbB-2 product. *Br. J. Cancer* **1996**, *73*, 1362-1365.

[78] Baselga, J., *et al.* Phase II study of weekly intravenous recombinant humanized anti-p185HER2 monoclonal antibody in patients with HER2/neu-overexpressing metastatic breast cancer. *Journal of Clinical Oncology* **1996**, *14*, 737-744.

[79] Cobleigh, M. A., *et al.* Multinational Study of the Efficacy and Safety of Humanized Anti-HER2 Monoclonal Antibody in Women Who Have HER2-Overexpressing Metastatic Breast Cancer That Has Progressed After

Chemotherapy for Metastatic Disease. *Journal of Clinical Oncology* **1999**, *17*, 2639-2639.

[80] Vogel, C. L., *et al.* Efficacy and Safety of Trastuzumab as a Single Agent in First-Line Treatment of HER2-Overexpressing Metastatic Breast Cancer. *Journal of Clinical Oncology* **2002**, *20*, 719-726.

[81] Slamon, D. J., *et al.* Use of Chemotherapy plus a Monoclonal Antibody against HER2 for Metastatic Breast Cancer That Overexpresses HER2. *N. Engl. J. Med.* **2001**, *344*, 783-792.

[82] Nagata, Y., *et al.* PTEN activation contributes to tumor inhibition by trastuzumab, and loss of PTEN predicts trastuzumab resistance in patients. *Cancer Cell* **2004**, *6*, 117-127.

[83] Molina, M. A., *et al.* NH(2)-terminal truncated HER-2 protein but not full-length receptor is associated with nodal metastasis in human breast cancer. *Clin. Cancer Res.* **2002**, *8*, 347-353.

[84] Xia, W., *et al.* Truncated ErbB2 receptor (p95ErbB2) is regulated by heregulin through heterodimer formation with ErbB3 yet remains sensitive to the dual EGFR//ErbB2 kinase inhibitor GW572016. *Oncogene* **2004**, *23*, 646-653.

[85] Molina, M. A., *et al.* Trastuzumab (Herceptin), a Humanized Anti-HER2 Receptor Monoclonal Antibody, Inhibits Basal and Activated HER2 Ectodomain Cleavage in Breast Cancer Cells. *Cancer Research* **2001**, *61*, 4744-4749.

[86] Kostler, W. J., *et al.* Monitoring of serum Her-2/neu predicts response and progression-free survival to trastuzumab-based treatment in patients with metastatic breast cancer. *Clin. Cancer Res.* **2004**, *10*, 1618-1624.

[87] Gennari, R., *et al.* Pilot Study of the Mechanism of Action of Preoperative Trastuzumab in Patients with Primary Operable Breast Tumors Overexpressing HER2. *Clinical Cancer Research* **2004**, *10*, 5650-5655.

[88] Mohsin, S. K., *et al.* Neoadjuvant Trastuzumab Induces Apoptosis in Primary Breast Cancers. *Journal of Clinical Oncology* **2005**, *23*, 2460-2468.

[89] Lee, S., *et al.* Enhanced Sensitization to Taxol-induced Apoptosis by Herceptin Pretreatment in ErbB2-overexpressing Breast Cancer Cells. *Cancer Research* **2002**, *62*, 5703-5710.

[90] Cuello, M., *et al.* Down-Regulation of the erbB-2 Receptor by Trastuzumab (Herceptin) Enhances Tumor Necrosis Factor-related Apoptosis-inducing Ligand-mediated Apoptosis in Breast and Ovarian Cancer Cell Lines that Overexpress erbB-2. *Cancer Research* **2001**, *61*, 4892-4900.

[91] Pietras, R. J., *et al.* Antibody to HER-2/neu receptor blocks DNA repair after cisplatin in human breast and ovarian cancer cells. *Oncogene* **1994**, *9*, 1829-1838.

[92] Konecny, G. E., *et al.* Association between HER-2/neu and Vascular Endothelial Growth Factor Expression Predicts Clinical Outcome in Primary Breast Cancer Patients. *Clinical Cancer Research* **2004**, *10*, 1706-1716.

[93] Izumi, Y., *et al.* Tumour biology: Herceptin acts as an anti-angiogenic cocktail. *Nature* **2002**, *416*, 279-280.

[94] Clynes, R. A., *et al.* Inhibitory Fc receptors modulate in vivo cytoxicity against tumor targets. *Nat. Med.* **2000**, *6*, 443-446.

[95] Collins, D. M., *et al.* Trastuzumab induces antibody-dependent cell-mediated cytotoxicity (ADCC) in HER-2-non-amplified breast cancer cell lines. *Annals of Oncology* **2011**.

[96] Mendoza, N., *et al.* Inhibition of Ligand-mediated HER2 Activation in Androgen-independent Prostate Cancer. *Cancer Research* **2002**, *62*, 5485-5488.

[97] Wehrman, T. S., *et al.* A system for quantifying dynamic protein interactions defines a role for Herceptin in modulating ErbB2 interactions. *Proceedings of the National Academy of Sciences* **2006**, *103*, 19063-19068.

[98] Agus, D. B., *et al.* Targeting ligand-activated ErbB2 signaling inhibits breast and prostate tumor growth. *Cancer Cell* **2002**, *2*, 127-137.

[99] Baselga, J., *et al.* Pertuzumab plus Trastuzumab plus Docetaxel for Metastatic Breast Cancer. *N. Engl. J. Med.* **2011**.

[100] Gianni, L., *et al.* Efficacy and safety of neoadjuvant pertuzumab and trastuzumab in women with locally advanced, inflammatory, or early HER2-positive breast cancer (NeoSphere): a randomised multicentre, open-label, phase 2 trial. *The Lancet Oncology* **2012**, *13*, 25-32.

[101] Lewis Phillips, G. D., *et al.* Targeting HER2-Positive Breast Cancer with Trastuzumab-DM1, an Antibody–Cytotoxic Drug Conjugate. *Cancer Research* **2008**, *68*, 9280-9290.

[102] Krop, I. E., *et al.* Phase I study of trastuzumab-DM1, an HER2 antibody-drug conjugate, given every 3 weeks to patients with HER2-positive metastatic breast cancer. *J. Clin. Oncol.* **2010**, *28*, 2698-2704.

[103] Burris, H. A., *et al.* Phase II Study of the Antibody Drug Conjugate Trastuzumab-DM1 for the Treatment of Human Epidermal Growth Factor Receptor 2 (HER2) – Positive Breast Cancer After Prior HER2-Directed Therapy. *Journal of Clinical Oncology* **2011**, *29*, 398-405.

[104] Perez, E.; Dirix, L.; Kocsis, J. e. a. In *In Efficacy and safey of trastuzumab-DM1 versus trastuzumab plus docetaxel in HER2-postive metastatic breast cancer patients with no prior chemotherapy for metastatic disease: preliminary results of a randomized, multicenter, open-label phase 2 study.* Program and abstracts of the 35th European Society of Medical Oncology Congress; October 8-12, 2010; Milan, Italy. Abstract LBA3; 2010; .

[105] Hurvitz, S., *et al.* In *In Transtuzumab emtansine (T-DM1) vs trastuzumab plus docetaxel (H+T) in previously untreated HER-2 positive metastatic breast cancer (MBC): primary results of a randomized, multicenter, open-label phase II study (TDM4450g/BO21976).* Program and abstracts of the 2011 European Multidisciplinary Cancer Congress; 2011; .

[106] Barok, M., *et al.* Trastuzumab-DM1 causes tumour growth inhibition by mitotic catastrophe in trastuzumab-resistant breast cancer cells in vivo. *Breast Cancer Res.* **2011**, *13*, R46.

[107] Barok, M., *et al.* Trastuzumab-DM1 is highly effective in preclinical models of HER2-positive gastric cancer. *Cancer Lett.* **2011**, *306*, 171-179.

[108] Junttila, T., *et al.* Trastuzumab-DM1 (T-DM1) retains all the mechanisms of action of trastuzumab and efficiently inhibits growth of lapatinib insensitive breast cancer. *Breast Cancer Research and Treatment* **2011**, *128*, 347-356.

[109] clinicaltrials.gov A Study of Trastuzumab-Emtasine (T-DM1) Plus Pertuzumab/Pertuzumab Placebo Versus Trastuzumab [Herceptin] Plus a Taxane in Patients With Metastatic Breast Cancer (MARIANNE) NCT01120184. *http://clinicaltrials.gov/ct2/show/NCT01120184* (accessed 01/04, 2012).

[110] clinicaltrials.gov An Open-Label Study of Trastuzumab-MCC-DM1 (T-DM1) vs Capecitabine+Lapatinib in Patients With HER2-Positive Locally Advanced or Metastatic Breast Cancer (EMILIA) NCT00829166. *http://clinicaltrials.gov/ct2/show/NCT00829166* (accessed 01/04, 2012).

[111] Nielsen, D. L.; Andersson, M.; Kamby, C. HER2-targeted therapy in breast cancer. Monoclonal antibodies and tyrosine kinase inhibitors. *Cancer Treat. Rev.* **2009**, *35*, 121-136.

[112] Xia, W., *et al.* Anti-tumor activity of GW572016: a dual tyrosine kinase inhibitor blocks EGF activation of EGFR/erbB2 and downstream Erk1/2 and AKT pathways. *Oncogene* **2002**, *21*, 6255-6263.

[113] Fabian, M. A., *et al.* A small molecule-kinase interaction map for clinical kinase inhibitors. *Nat Biotech* **2005**, *23*, 329-336.

[114] Rusnak, D. W., *et al.* The Effects of the Novel, Reversible Epidermal Growth Factor Receptor/ErbB-2 Tyrosine Kinase Inhibitor, GW2016, on the Growth of Human Normal and Tumor-derived Cell Lines in Vitro and in Vivo. *Molecular Cancer Therapeutics* **2001**, *1*, 85-94.

[115] Scheffler, M., *et al.* Clinical Pharmacokinetics of Tyrosine Kinase Inhibitors: Focus on 4-Anilinoquinazolines. *Clin. Pharmacokinet.* **2011**, *50*.

[116] GlaxoSmithKline Perscribing information for Tykerb. *http://us.gsk.com/products/assets/us_tykerb.pdf* (accessed 02/03, 2012).

[117] Burris, H. A., *et al.* Phase I Safety, Pharmacokinetics, and Clinical Activity Study of Lapatinib (GW572016), a Reversible Dual Inhibitor of Epidermal Growth Factor

Receptor Tyrosine Kinases, in Heavily Pretreated Patients With Metastatic Carcinomas. *Journal of Clinical Oncology* **August 10, 2005**, *23*, 5305-5313.

[118] Araki, K., *et al.* In *In Lapatinib Resistance Confers Cross-Resistance to Microtubule Inhibitors in ErbB2-Overexpressing Breast Cancer Cells [P4-01-05];* San Antonio Breast Cancer Symposium; 2010; .

[119] Chang, J., *et al.* Survival of patients with metastatic breast carcinoma. *Cancer* **2003**, *97*, 545-553.

[120] Pestalozzi, B. C., *et al.* Identifying breast cancer patients at risk for Central Nervous System (CNS) metastases in trials of the International Breast Cancer Study Group (IBCSG). *Annals of Oncology* **June 2006**, *17*, 935-944.

[121] Pestalozzi, B. C.; Brignoli, S. Trastuzumab in CSF. *J. Clin. Oncol.* **2000**, *18*, 2349-2351.

[122] Ceresoli, G. L., *et al.* Gefitinib in patients with brain metastases from non-small-cell lung cancer: a prospective trial. *Annals of Oncology* **2004**, *15*, 1042-1047.

[123] Gril, B., *et al.* Effect of Lapatinib on the Outgrowth of Metastatic Breast Cancer Cells to the Brain. *Journal of the National Cancer Institute* **2008**, *100*, 1092-1103.

[124] Lin, N. U., *et al.* Multicenter Phase II Study of Lapatinib in Patients with Brain Metastases from HER2-Positive Breast Cancer. *Clinical Cancer Research* **2009**, *15*, 1452-1459.

[125] Spector, N. L., *et al.* Study of the Biologic Effects of Lapatinib, a Reversible Inhibitor of ErbB1 and ErbB2 Tyrosine Kinases, on Tumor Growth and Survival Pathways in Patients With Advanced Malignancies. *Journal of Clinical Oncology* **2005**, *23*, 2502-2512.

[126] Gomez, H. L., *et al.* Efficacy and Safety of Lapatinib As First-Line Therapy for ErbB2-Amplified Locally Advanced or Metastatic Breast Cancer. *Journal of Clinical Oncology* **June 20, 2008**, *26*, 2999-3005.

[127] Blackwell, K. L., *et al.* Single-agent lapatinib for HER2-overexpressing advanced or metastatic breast cancer that progressed on first- or second-line trastuzumab-containing regimens. *Annals of Oncology* **2009**, *20*, 1026-1031.

[128] Burstein, H. J., *et al.* A phase II study of lapatinib monotherapy in chemotherapy-refractory HER2-positive and HER2-negative advanced or metastatic breast cancer. *Annals of Oncology* **2008**, *19*, 1068-1074.

[129] Ishitsuka, H., *et al. Capecitabine: an orally available fluoropyrimidine with tumor selective activity*. *Proc. Am. Assoc. Cancer. Res* **1995**, *36*, 407.

[130] Schwartz, G.; Chu, Q.; Hammond, L. In *In Phase I clinical, biology, and pharmacokinetic study of the combination of GW572016 and capecitabine in patients with advanced solid tumors.* 2004; Vol. 23, pp 212.

[131] Geyer, C. E., *et al.* Lapatinib plus Capecitabine for HER2-Positive Advanced Breast Cancer. *N. Engl. J. Med.* **2006**, *355*, 2733-2743.

[132] Cameron, D., *et al.* A phase III randomized comparison of lapatinib plus capecitabine versus capecitabine alone in women with advanced breast cancer that has progressed on trastuzumab: updated efficacy and biomarker analyses. *Breast Cancer Research and Treatment* **2008**, *112*, 533-543.

[133] Cameron, D., *et al.* Lapatinib Plus Capecitabine in Women with HER-2–Positive Advanced Breast Cancer: Final Survival Analysis of a Phase III Randomized Trial. *The Oncologist* **2010**, *15*, 924-934.

[134] Konecny, G. E., *et al.* Activity of the Dual Kinase Inhibitor Lapatinib (GW572016) against HER-2-Overexpressing and Trastuzumab-Treated Breast Cancer Cells. *Cancer Research* **2006**, *66*, 1630-1639.

[135] Tan-Chiu, E., *et al.* Assessment of Cardiac Dysfunction in a Randomized Trial Comparing Doxorubicin and Cyclophosphamide Followed by Paclitaxel, With or Without Trastuzumab As Adjuvant Therapy in Node-Positive, Human Epidermal Growth Factor Receptor 2–Overexpressing Breast Cancer: NSABP B-31. *Journal of Clinical Oncology* **2005**, *23*, 7811-7819.

[136] Slamon, D., *et al.* Adjuvant Trastuzumab in HER2-Positive Breast Cancer. *N. Engl. J. Med.* **2011**, *365*, 1273-1283.

[137] Perez, E. A., *et al.* Cardiac Safety of Lapatinib: Pooled Analysis of 3689 Patients Enrolled in Clinical Trials. *Mayo Clinic Proceedings* **2008**, *83*, 679-686.

[138] Shell, S. A., *et al.* Activation of AMPK is necessary for killing cancer cells and sparing cardiac cells. *Cell Cycle* **2008**, *7*, 1769-1775.

[139] Fletcher, J. I., *et al.* ABC transporters in cancer: more than just drug efflux pumps. *Nat Rev Cancer* **2010**, *10*, 147-156.

[140] Perry, J., *et al.* A Synergistic Interaction between Lapatinib and Chemotherapy Agents in a Panel of Cell Lines Is Due to the Inhibition of the Efflux Pump BCRP. *Molecular Cancer Therapeutics* **2010**, *9*, 3322-3329.

[141] Dunne, G., *et al.* Modulation of P-gp expression by lapatinib. *Investigational New Drugs* **2011**, *29*, 1284-1293.

[142] Xia, W., *et al.* Combining lapatinib (GW572016), a small molecule inhibitor of ErbB1 and ErbB2 tyrosine kinases, with therapeutic anti-ErbB2 antibodies enhances apoptosis of ErbB2-overexpressing breast cancer cells. *Oncogene* **2005**, *24*, 6213-6221.

[143] O'Donovan, N., *et al.* Synergistic interaction between trastuzumab and EGFR/HER-2 tyrosine kinase inhibitors in HER-2 positive breast cancer cells. *Investigational New Drugs* **2011**, *29*, 752-759.

[144] Tanizaki, J., *et al.* Roles of BIM induction and survivin downregulation in lapatinib-induced apoptosis in breast cancer cells with HER2 amplification. *Oncogene* **2011**, *30*, 4097-4106.

[145] Mitchell, C., *et al.* Inhibition of MCL-1 in breast cancer cells promotes cell death in vitro and in vivo. *Cancer. Biol. Ther.* **2010**, *10*, 903-917.

[146] Altieri, D. C. Survivin, cancer networks and pathway-directed drug discovery. *Nat. Rev. Cancer.* **2008**, *8*, 61-70.

[147] Xia, W., *et al.* Regulation of Survivin by ErbB2 Signaling: Therapeutic Implications for ErbB2-Overexpressing Breast Cancers. *Cancer Research* **2006**, *66*, 1640-1647.

[148] Oliveras-Ferraros, C., *et al.* Inhibitor of Apoptosis (IAP) survivin is indispensable for survival of HER2 gene-amplified breast cancer cells with primary resistance to HER1/2-targeted therapies. *Biochem. Biophys. Res. Commun.* **2011**, *407*, 412-419.

[149] Kim, J. W., *et al.* The growth inhibitory effect of lapatinib, a dual inhibitor of EGFR and HER2 tyrosine kinase, in gastric cancer cell lines. *Cancer Lett.* **2008**, *272*, 296-306.

[150] Diaz, R., *et al.* Antitumor and antiangiogenic effect of the dual EGFR and HER-2 tyrosine kinase inhibitor lapatinib in a lung cancer model. *BMC Cancer* **2010**, *10*, 188.

[151] McHugh, L. A., *et al.*
Lapatinib, a dual inhibitor of ErbB-1/-2 receptors, enhances effects of combination of chemotherapy in bladder cancer cells. *Int. J. Oncol.* **2009**, *34*, 1155-1163.

[152] Kondo, Y., *et al.* The role of autophagy in cancer development and response to therapy. *Nat Rev Cancer* **2005**, *5*, 726-734.

[153] Cheng, Y., *et al.* Cytoprotective Effect of the Elongation Factor-2 Kinase-Mediated Autophagy in Breast Cancer Cells Subjected to Growth Factor Inhibition. *PLoS ONE* **2010**, *5*, e9715.

[154] Tang, Y., *et al.* Obatoclax and Lapatinib Interact to Induce Toxic Autophagy Through NOXA. *Molecular Pharmacology* **2012**.

[155] Di Leo, A., *et al.* Phase III, Double-Blind, Randomized Study Comparing Lapatinib Plus Paclitaxel With Placebo Plus Paclitaxel As First-Line Treatment for Metastatic Breast Cancer. *Journal of Clinical Oncology* **December 1, 2008**, *26*, 5544-5552.

[156] Jagiello-Gruszfeld, A., *et al.* A single-arm phase II trial of first-line paclitaxel in combination with lapatinib in HER2-overexpressing metastatic breast cancer. *Oncology* **2010**, *79*, 129-135.

[157] Boussen, H., *et al.* Phase II Study to Evaluate the Efficacy and Safety of Neoadjuvant Lapatinib Plus Paclitaxel in Patients With Inflammatory Breast Cancer. *Journal of Clinical Oncology* **2010**, *28*, 3248-3255.

[158] Park, I., *et al.* A phase Ib study of preoperative lapatinib, paclitaxel, and gemcitabine combination therapy in women with HER2 positive early breast cancer. *Investigational New Drugs* **2011**, 1-6.

[159] LoRusso, P. M., *et al.* Phase I and pharmacokinetic study of lapatinib and docetaxel in patients with advanced cancer. *J. Clin. Oncol.* **2008**, *26*, 3051-3056.

[160] clinicaltrials.gov Lapatinib in Combination With Docetaxel in Patients With HER-2 Positive Advanced or Metastatic Breast Cancer (LapDoc) NCT01044485. *http://clinicaltrials.gov/ct2/show/NCT01044485* (accessed 02/03, 2012).

[161] clinicaltrials.gov A Phase II Neo-adjuvant Study Assessing TCH (Docetaxel, Carboplatin and Trastuzumab), TCL (Docetaxel, Carboplatin and Lapatinib) and the Combination of TCHL (Docetaxel,Carboplatin, Trastuzumab and Lapatinib) in HER-2 Positive Breast Cancer Patients. (TCHL Phase II). *http://clinicaltrials.gov/ct2/show/NCT01485926* (accessed 02/03, 2012).

[162] Osborne, C. K.; Schiff, R. Mechanisms of endocrine resistance in breast cancer. *Annu. Rev. Med.* **2011**, *62*, 233-247.

[163] Chu, Q. S. C., *et al.* A Phase I and Pharmacokinetic Study of Lapatinib in Combination with Letrozole in Patients with Advanced Cancer. *Clinical Cancer Research* **2008**, *14*, 4484-4490.

[164] Johnston, S., *et al.* Lapatinib Combined With Letrozole Versus Letrozole and Placebo As First-Line Therapy for Postmenopausal Hormone Receptor–Positive Metastatic Breast Cancer. *Journal of Clinical Oncology* **2009**, *27*, 5538-5546.

[165] Schwartzberg, L. S., *et al.* Lapatinib plus Letrozole as First-Line Therapy for HER-2+ Hormone Receptor–Positive Metastatic Breast Cancer. *The Oncologist* **2010**, *15*, 122-129.

[166] Blackwell, K. L., *et al.* Randomized Study of Lapatinib Alone or in Combination With Trastuzumab in Women With ErbB2-Positive, Trastuzumab-Refractory Metastatic Breast Cancer. *Journal of Clinical Oncology* **2010**, *28*, 1124-1130.

[167] Baselga, J., *et al.* In *In First Results of the NeoALTTO Trial (BIG 01-06 / EGF 106903): a phase III, randomized, open label, neoadjuvant study of lapatinib, trastuzumab, and their combination plus paclitaxel in women with HER2-positive primary breast cancer.* 2010; .

[168] clinicaltrials.gov ALTTO (Adjuvant Lapatinib And/Or Trastuzumab Treatment Optimisation) Study; BIG 2-06/N063D) NCT00490139. *http://clinicaltrials.gov/ct2/show/NCT00490139* (accessed 01/09, 2012).

[169] Rabindran, S. K., *et al.* Antitumor Activity of HKI-272, an Orally Active, Irreversible Inhibitor of the HER-2 Tyrosine Kinase. *Cancer Research* **2004**, *64*, 3958-3965.

[170] Burstein, H. J., *et al.* Neratinib, an Irreversible ErbB Receptor Tyrosine Kinase Inhibitor, in Patients With Advanced ErbB2-Positive Breast Cancer. *Journal of Clinical Oncology* **2010**, *28*, 1301-1307.

[171] clinicaltrials.gov Study Evaluating The Effects Of Neratinib After Adjuvant Trastuzumab In Women With Early Stage Breast Cancer (ExteNET) NCT00878709. *http://clinicaltrials.gov/ct2/show/NCT00878709* (accessed 01/04, 2012).

[172] clinicaltrials.gov A Phase 1/2 Study of HKI-272 (Neratinib) in Combination With Paclitaxel (Taxol) in Subjects With Solid Tumors and Breast Cancer NCT00445458. *http://clinicaltrials.gov/ct2/show/NCT00445458* (accessed 01/04, 2012).

[173] clinicaltrials.gov A Phase 1/2 Study Of HKI-272 (Neratinib) in Combination With Trastuzumab (Herceptin) In Subjects With Advanced Breast Cancer NCT00398567. *http://clinicaltrials.gov/ct2/show/NCT00398567* (accessed 01/04, 2012).

[174] clinicaltrials.gov Study Evaluating Neratinib Plus Paclitaxel VS Trastuzumab Plus Paclitaxel In ErbB-2 Positive Advanced Breast Cancer (NEFERTT) NCT00915018. *http://clinicaltrials.gov/ct2/show/NCT00915018* (accessed 01/04, 2012).

[175] clinicaltrials.gov Study Evaluating Neratinib Versus Lapatinib Plus Capecitabine For ErbB2 Positive Advanced Breast Cancer NCT00777101. *http://clinicaltrials.gov/ct2/show/NCT00777101* (accessed 01/04, 2012).

[176] Li, D., *et al.* BIBW2992, an irreversible EGFR/HER2 inhibitor highly effective in preclinical lung cancer models. *Oncogene* **2008**, *27*, 4702-4711.

[177] Ioannou, N., *et al.* Anti-tumour activity of afatinib, an irreversible ErbB family blocker, in human pancreatic tumour cells. *Br. J. Cancer* **2011**, *105*, 1554-1562.

[178] Hirsh, V. Afatinib (BIBW 2992) development in non-small-cell lung cancer. *Future Oncology* **2011**, *7*, 817-825.

[179] Metro, G.; CrinÃ², L. The LUX-Lung clinical trial program of afatinib for non-small-cell lung cancer. *Expert Rev Anticancer Ther* **2011**, *11*, 673-682.

[180] Quesnelle, K. M.; Grandis, J. R. Dual Kinase Inhibition of EGFR and HER2 Overcomes Resistance to Cetuximab in a Novel In Vivo Model of Acquired Cetuximab Resistance. *Clinical Cancer Research* **2011**, *17*, 5935-5944.

[181] clinicaltrials.gov LUX-Breast 2; Afatinib in HER2 (Human Epidermal Growth Factor Receptor)-Treatment Failures NCT01271725. *http://www.clinicaltrials.gov/ct2/show/NCT01271725* (accessed 02/02, 2012).

[182] clinicaltrials.gov 6 Weeks Treatment of Locally Advanced Breast Cancer With BIBW 2992 (Afatinib) or Lapatinib or Trastuzumab NCT00826267. *http://www.clinicaltrials.gov/ct2/show/NCT00826267* (accessed 02/02, 2012).

[183] clinicaltrials.gov Afatinib (BIBW2992) in HER2-overexpressing Inflammatory Breast Cancer NCT01325428. *http://clinicaltrials.gov/ct2/show/NCT01325428* (accessed 02/02, 2012).

[184] clinicaltrials.gov LUX-Breast 1: BIBW 2992 (Afatinib) in HER2-positive Metastatic Breast Cancer Patients After One Prior Herceptin Treatment NCT01125566. *http://clinicaltrials.gov/ct2/show/NCT01125566* (accessed 01/04, 2012).

[185] McDonagh, C. F., *et al.* Antitumor activity of a novel bispecific antibody that targets the ErbB2/ErbB3 oncogenic unit and inhibits heregulin-induced activation of ErbB3. *Mol. Cancer. Ther.* **2012**.

[186] clinicaltrials.gov A Study of MM-111 in Patients With Advanced, Refractory Her2 Amplified, Heregulin Positive Cancers (Monotherapy) NCT00911898. *http://clinicaltrials.gov/ct2/show/NCT00911898* (accessed 01/04, 2012).

[187] clinicaltrials.gov A Study of MM-111 in Combination With Multiple Treatments in Patients With HER2 Positive Cancer NCT01304784. *http://clinicaltrials.gov/ct2/show/NCT01304784* (accessed 01/04, 2012).

[188] clinicaltrials.gov Phase 1b/2 Study of U3-1287 in Combination With Trastuzumab Plus Paclitaxel in Newly Diagnosed Metastatic Breast Cancer (MBC) NCT01512199. *http://clinicaltrials.gov/ct2/show/NCT01512199* (accessed 01/04, 2012).

[189] de La Motte Rouge, T., *et al.* A novel epidermal growth factor receptor inhibitor promotes apoptosis in non-small cell lung cancer cells resistant to erlotinib. *Cancer Res.* **2007**, *67*, 6253-6262.

[190] Ahn, E. R.; Vogel, C. L. Dual HER2-targeted approaches in HER2-positive breast cancer. *Breast Cancer Res. Treat.* **2012**, *131*, 371-383.

[191] Depowski, P. L.; Rosenthal, S. I.; Ross, J. S. Loss of Expression of the PTEN Gene Protein Product Is Associated with Poor Outcome in Breast Cancer. *Mod. Pathol.* **2001**, *14*, 672-676.

[192] Bachman, K. E., *et al.* The PIK3CA gene is mutated with high frequency in human breast cancers. *Cancer Biology & Therapy* **2004**, *3*, 772-775.

[193] Razis, E., *et al.* Evaluation of the association of PIK3CA mutations and PTEN loss with efficacy of trastuzumab therapy in metastatic breast cancer. *Breast Cancer Research and Treatment* **2011**, *128*, 447-456.

[194] O'Brien, N. A., *et al.* Activated Phosphoinositide 3-Kinase/AKT Signaling Confers Resistance to Trastuzumab but not Lapatinib. *Molecular Cancer Therapeutics* **2010**, *9*, 1489-1502.

[195] Berns, K., *et al.* A Functional Genetic Approach Identifies the PI3K Pathway as a Major Determinant of Trastuzumab Resistance in Breast Cancer. *Cancer Cell* **2007**, *12*, 395-402.

[196] Zagozdzon, R.; Gallagher, W. M.; Crown, J. Truncated HER2: implications for HER2-targeted therapeutics. *Drug Discov. Today* **2011**, *16*, 810-816.

[197] Liu, P. C. C., *et al.* Identification of ADAM10 as a major source of HER2 ectodomain sheddase activity in HER2 overexpressing breast cancer cells. *Cancer Biology & Therapy* **2006**, *5*, 657-664.

[198] Scott, G. K., *et al.* A truncated intracellular HER2/neu receptor produced by alternative RNA processing affects growth of human carcinoma cells. *Mol. Cell. Biol.* **1993**, *13*, 2247-2257.

[199] Sáez, R., *et al.* p95HER-2 Predicts Worse Outcome in Patients with HER-2-Positive Breast Cancer. *Clinical Cancer Research* **2006**, *12*, 424-431.

[200] Scaltriti, M., *et al.* Expression of p95HER2, a Truncated Form of the HER2 Receptor, and Response to Anti-HER2 Therapies in Breast Cancer. *Journal of the National Cancer Institute* **2007**, *99*, 628-638.

[201] Sperinde, J., *et al.* Quantitation of p95HER2 in Paraffin Sections by Using a p95-Specific Antibody and Correlation with Outcome in a Cohort of Trastuzumab-Treated Breast Cancer Patients. *Clinical Cancer Research* **2010**, *16*, 4226-4235.

[202] Junttila, T. T., *et al.* Ligand-Independent HER2/HER3/PI3K Complex Is Disrupted by Trastuzumab and Is Effectively Inhibited by the PI3K Inhibitor GDC-0941. *Cancer Cell* **2009**, *15*, 429-440.

[203] Motoyama, A. B.; Hynes, N. E.; Lane, H. A. The Efficacy of ErbB Receptor-targeted Anticancer Therapeutics Is Influenced by the Availability of Epidermal Growth Factor-related Peptides. *Cancer Research* **2002**, *62*, 3151-3158.

[204] Huang, X., *et al.* Heterotrimerization of the Growth Factor Receptors erbB2, erbB3, and Insulin-like Growth Factor-I Receptor in Breast Cancer Cells Resistant to Herceptin. *Cancer Research* **2010**, *70*, 1204-1214.

[205] Narayan, M., *et al.* Trastuzumab-induced HER reprogramming in "resistant" breast carcinoma cells. *Cancer Res.* **2009**, *69*, 2191-2194.

[206] Smith, B. L., *et al.* The efficacy of Herceptin therapies is influenced by the expression of other erbB receptors, their ligands and the activation of downstream signalling proteins. *Br. J. Cancer* **2004**, *91*, 1190-1194.

[207] Lu, Y., *et al.* Insulin-Like Growth Factor-I Receptor Signaling and Resistance to Trastuzumab (Herceptin). *Journal of the National Cancer Institute* **2001**, *93*, 1852-1857.

[208] Nahta, R., *et al.* Insulin-like Growth Factor-I Receptor/Human Epidermal Growth Factor Receptor 2 Heterodimerization Contributes to Trastuzumab Resistance of Breast Cancer Cells. *Cancer Research* **2005**, *65*, 11118-11128.

[209] Browne, B. C., *et al.* Inhibition of IGF1R activity enhances response to trastuzumab in HER-2-positive breast cancer cells. *Annals of Oncology* **2011**, *22*, 68-73.

[210] Dokmanovic, M., *et al.* Trastuzumab regulates IGFBP-2 and IGFBP-3 to mediate growth inhibition: implications for the development of predictive biomarkers for trastuzumab resistance. *Mol. Cancer. Ther.* **2011**, *10*, 917-928.

[211] Köstler, W., *et al.* Insulin-like growth factor-1 receptor (IGF-1R) expression does not predict for resistance to trastuzumab-based treatment in patients with Her-2/*neu* overexpressing metastatic breast cancer. *Journal of Cancer Research and Clinical Oncology* **2006**, *132*, 9-18.

[212] Ritter, C. A., *et al.* Human Breast Cancer Cells Selected for Resistance to Trastuzumab In vivo Overexpress Epidermal Growth Factor Receptor and ErbB Ligands and Remain Dependent on the ErbB Receptor Network. *Clinical Cancer Research* **2007**, *13*, 4909-4919.

[213] Scaltriti, M., *et al.* Cyclin E amplification/overexpression is a mechanism of trastuzumab resistance in HER2+ breast cancer patients. *Proceedings of the National Academy of Sciences* **2011**, *108*, 3761-3766.

[214] Shattuck, D. L., *et al.* Met Receptor Contributes to Trastuzumab Resistance of Her2-Overexpressing Breast Cancer Cells. *Cancer Research* **2008**, *68*, 1471-1477.

[215] Zhuang, G., *et al.* Elevation of Receptor Tyrosine Kinase EphA2 Mediates Resistance to Trastuzumab Therapy. *Cancer Research* **2010**, *70*, 299-308.

[216] Gong, C., *et al.* Up-regulation of miR-21 Mediates Resistance to Trastuzumab Therapy for Breast Cancer. *Journal of Biological Chemistry* **2011**, *286*, 19127-19137.

[217] Kawaguchi, Y., *et al.* Mechanisms of escape from trastuzumab-mediated ADCC in esophageal squamous cell carcinoma: relation to susceptibility to perforin-granzyme. *Anticancer Res.* **2009**, *29*, 2137-2146.

[218] Zhao, Y., *et al.* Overcoming Trastuzumab Resistance in Breast Cancer by Targeting Dysregulated Glucose Metabolism. *Cancer Research* **2011**, *71*, 4585-4597.

[219] Nagy, P., *et al.* Decreased Accessibility and Lack of Activation of ErbB2 in JIMT-1, a Herceptin-Resistant, MUC4-Expressing Breast Cancer Cell Line. *Cancer Research* **2005**, *65*, 473-482.

[220] Bourguignon, L. Y. W., *et al.* Hyaluronan Promotes CD44v3-Vav2 Interaction with Grb2-p185HER2 and Induces Rac1 and Ras Signaling during Ovarian Tumor Cell Migration and Growth. *Journal of Biological Chemistry* **2001**, *276*, 48679-48692.

[221] Ghatak, S.; Misra, S.; Toole, B. P. Hyaluronan Oligosaccharides Inhibit Anchorage-independent Growth of Tumor Cells by Suppressing the Phosphoinositide 3-Kinase/Akt Cell Survival Pathway. *Journal of Biological Chemistry* **2002**, *277*, 38013-38020.

[222] Johnston, S., *et al.* Phase II Study of Predictive Biomarker Profiles for Response Targeting Human Epidermal Growth Factor Receptor 2 (HER-2) in Advanced

Inflammatory Breast Cancer With Lapatinib Monotherapy. *Journal of Clinical Oncology* **March 1, 2008**, *26*, 1066-1072.

[223] Xia, W., *et al.* Lapatinib Antitumor Activity Is Not Dependent upon Phosphatase and Tensin Homologue Deleted on Chromosome 10 in ErbB2-Overexpressing Breast Cancers. *Cancer Research* **2007**, *67*, 1170-1175.

[224] Eichhorn, P. J., *et al.* Phosphatidylinositol 3-kinase hyperactivation results in lapatinib resistance that is reversed by the mTOR/phosphatidylinositol 3-kinase inhibitor NVP-BEZ235. *Cancer Res.* **2008**, *68*, 9221-9230.

[225] Wang, L., *et al.* PI3K pathway activation results in low efficacy of both trastuzumab and lapatinib. *BMC Cancer* **2011**, *11*, 11:248-2407-11-248.

[226] Scaltriti, M., *et al.* Clinical Benefit of Lapatinib-Based Therapy in Patients with Human Epidermal Growth Factor Receptor 2–Positive Breast Tumors Coexpressing the Truncated p95HER2 Receptor. *Clinical Cancer Research* **2010**, *16*, 2688-2695.

[227] Pedersen, K., *et al.* A Naturally Occurring HER2 Carboxy-Terminal Fragment Promotes Mammary Tumor Growth and Metastasis. *Mol. Cell. Biol.* **2009**, *29*, 3319-3331.

[228] Nahta, R., *et al.* Lapatinib induces apoptosis in trastuzumab-resistant breast cancer cells: effects on insulin-like growth factor I signaling. *Mol. Cancer. Ther.* **2007**, *6*, 667-674.

[229] Xia, W., *et al.* A model of acquired autoresistance to a potent ErbB2 tyrosine kinase inhibitor and a therapeutic strategy to prevent its onset in breast cancer. *Proceedings of the National Academy of Sciences* **2006**, *103*, 7795-7800.

[230] Xia, W., *et al.* Resistance to ErbB2 Tyrosine Kinase Inhibitors in Breast Cancer Is Mediated by Calcium-Dependent Activation of RelA. *Molecular Cancer Therapeutics* **2010**, *9*, 292-299.

[231] Aird, K. M., *et al.* X-Linked Inhibitor of Apoptosis Protein Inhibits Apoptosis in Inflammatory Breast Cancer Cells with Acquired Resistance to an ErbB1/2 Tyrosine Kinase Inhibitor. *Molecular Cancer Therapeutics* **2010**, *9*, 1432-1442.

[232] Liu, L., *et al.* Novel mechanism of lapatinib resistance in HER2-positive breast tumor cells: activation of AXL. *Cancer Res.* **2009**, *69*, 6871-6878.

[233] Martin, A. P., *et al.* Lapatinib Resistance in HCT116 Cells Is Mediated by Elevated MCL-1 Expression and Decreased BAK Activation and Not by ERBB Receptor Kinase Mutation. *Molecular Pharmacology* **2008**, *74*, 807-822.

[234] Huang, C., *et al.* Beta1 Integrin Mediates an Alternative Survival Pathway in Breast Cancer Cells Resistant to Lapatinib. *Breast Cancer Res.* **2011**, *13*, R84.

[235] Rexer, B. N., *et al.* Phosphoproteomic mass spectrometry profiling links Src family kinases to escape from HER2 tyrosine kinase inhibition. *Oncogene* **2011**, *30*, 4163-4174.

[236] Wang, Y. C., *et al.* Different mechanisms for resistance to trastuzumab versus lapatinib in HER2-positive breast cancers - role of estrogen receptor and HER2 reactivation. *Breast Cancer Res.* **2011**, *13*, R121.

[237] Clark, G. M.; Osborne, C. K.; McGuire, W. L. Correlations between estrogen receptor, progesterone receptor, and patient characteristics in human breast cancer. *Journal of Clinical Oncology* **1984**, *2*, 1102-1109.

[238] Guo, S.; Sonenshein, G. E. Forkhead Box Transcription Factor FOXO3a Regulates Estrogen Receptor Alpha Expression and Is Repressed by the Her-2/neu/Phosphatidylinositol 3-Kinase/Akt Signaling Pathway. *Molecular and Cellular Biology* **2004**, *24*, 8681-8690.

[239] Hafizi, S.; Dahlbäck, B. Signalling and functional diversity within the Axl subfamily of receptor tyrosine kinases. *Cytokine Growth Factor Rev.* **2006**, *17*, 295-304.

[240] Korshunov, V. A. Axl-dependent signalling: a clinical update. *Clin. Sci. (Lond)* **2012**, *122*, 361-368.

[241] Zhang, Y., *et al.* AXL Is a Potential Target for Therapeutic Intervention in Breast Cancer Progression. *Cancer Research* **2008**, *68*, 1905-1915.

[242] Hutterer, M., *et al.* Axl and Growth Arrest–Specific Gene 6 Are Frequently Overexpressed in Human Gliomas and Predict Poor Prognosis in Patients with Glioblastoma Multiforme. *Clinical Cancer Research* **2008**, *14*, 130-138.

[243] Kang, M. H.; Reynolds, C. P. Bcl-2 inhibitors: targeting mitochondrial apoptotic pathways in cancer therapy. *Clin. Cancer Res.* **2009**, *15*, 1126-1132.

[244] Martin, A. P., *et al.* Inhibition of MCL-1 enhances lapatinib toxicity and overcomes lapatinib resistance via BAK-dependent autophagy. *Cancer. Biol. Ther.* **2009**, *8*, 2084-2096.

[245] Dubrez-Daloz, L.; Dupoux, A.; Cartier, J. IAPs: more than just inhibitors of apoptosis proteins. *Cell. Cycle* **2008**, *7*, 1036-1046.

[246] Zhang, Y., *et al.* X-linked inhibitor of apoptosis positive nuclear labeling: a new independent prognostic biomarker of breast invasive ductal carcinoma. *Diagn. Pathol.* **2011**, *6*, 49.

[247] Finn, R. S. Targeting Src in breast cancer. *Ann. Oncol.* **2008**, *19*, 1379-1386.

[248] Karin, M.; Lin, A. NF-kappaB at the crossroads of life and death. *Nat. Immunol.* **2002**, *3*, 221-227.

[249] Cordes, N.; Park, C. C. beta1 integrin as a molecular therapeutic target. *Int. J. Radiat. Biol.* **2007**, *83*, 753-760.

[250] Wang, F., *et al.* Reciprocal interactions between beta1-integrin and epidermal growth factor receptor in three-dimensional basement membrane breast cultures: a

different perspective in epithelial biology. *Proc. Natl. Acad. Sci. U. S. A.* **1998**, *95*, 14821-14826.

[251] Lesniak, D., *et al.* β1-Integrin Circumvents the Antiproliferative Effects of Trastuzumab in Human Epidermal Growth Factor Receptor-2–Positive Breast Cancer. *Cancer Research* **2009**, *69*, 8620-8628.

[252] Chen, S., *et al.* Autophagy facilitates the Lapatinib resistance of HER2 positive breast cancer cells. *Med. Hypotheses* **2011**, *77*, 206-208.

[253] Staaf, J., *et al.* High-resolution genomic and expression analyses of copy number alterations in HER2-amplified breast cancer. *Breast Cancer Res.* **2010**, *12*, R25.

[254] Nencioni, A., *et al.* Grb7 Upregulation Is a Molecular Adaptation to HER2 Signaling Inhibition Due to Removal of Akt-Mediated Gene Repression. *PLoS ONE* **2010**, *5*, e9024.

[255] Browne, B. C. The role of receptor tyrosine kinase signalling in HER-2-positive cells and Trastuzumab (Herceptin) Resistance in Breast Cancer. **2008**.

[256] Jorgensen, R.; Merrill, A. R.; Andersen, G. R. The life and death of translation elongation factor 2. *Biochem. Soc. Trans.* **2006**, *34*, 1-6.

[257] Shinawi, M.; Cheung, S. W. The array CGH and its clinical applications. *Drug Discov. Today* **2008**, *13*, 760-770.

[258] Fejzo, M. S., *et al.* Knockdown of ovarian cancer amplification target ADRM1 leads to downregulation of GIPC1 and upregulation of RECK. *Genes Chromosom. Cancer* **2011**, *50*, 434-441.

[259] Konecny, G. E., *et al.* Expression of p16 and Retinoblastoma Determines Response to CDK4/6 Inhibition in Ovarian Cancer. *Clinical Cancer Research* **2011**, *17*, 1591-1602.

[260] Ishkanian, A. S., *et al.* High-resolution array CGH identifies novel regions of genomic alteration in intermediate-risk prostate cancer. *Prostate* **2009**, *69*, 1091-1100.

[261] Gao, K., *et al.* Genomic analyses identify gene candidates for acquired irinotecan resistance in melanoma cells. *Int. J. Oncol.* **2008**, *32*, 1343-1349.

[262] Baik, S., *et al.* DNA profiling by array comparative genomic hybridization (CGH) of peripheral blood mononuclear cells (PBMC) and tumor tissue cell in non-small cell lung cancer (NSCLC). *Molecular Biology Reports* **2009**, *36*, 1767-1778.

[263] Kreisel, F., *et al.* High resolution array comparative genomic hybridization identifies copy number alterations in diffuse large B-cell lymphoma that predict response to immuno-chemotherapy. *Cancer Genetics* **2011**, *204*, 129-137.

[264] Johnson, N., *et al.* A comparative study of genome-wide SNP, CGH microarray and protein expression analysis to explore genotypic and phenotypic mechanisms

of acquired antiestrogen resistance in breast cancer. *Breast Cancer Research and Treatment* **2008**, *111*, 55-63.

[265] Callagy, G., *et al.* Identification and validation of prognostic markers in breast cancer with the complementary use of array-CGH and tissue microarrays. *J. Pathol.* **2005**, *205*, 388-396.

[266] Barok, M., *et al.* Characterization of a novel, trastuzumab resistant human breast cancer cell line. *Front. Biosci. (Elite Ed)* **2010**, *2*, 627-640.

[267] Rennstam, K., *et al.* Cytogenetic characterization and gene expression profiling of the trastuzumab-resistant breast cancer cell line JIMT-1. *Cancer Genet. Cytogenet.* **2007**, *172*, 95-106.

[268] Ong, S.; Mann, M. A practical recipe for stable isotope labeling by amino acids in cell culture (SILAC). *Nat. Protocols* **2007**, *1*, 2650-2660.

[269] Uitto, P. M., *et al.* Comparing SILAC and Two-Dimensional Gel Electrophoresis Image Analysis for Profiling Urokinase Plasminogen Activator Signaling in Ovarian Cancer Cells. *J. Proteome Res.* **2007**, *6*, 2105-2112.

[270] Gygi, S. P., *et al.* Evaluation of two-dimensional gel electrophoresis-based proteome analysis technology. *Proceedings of the National Academy of Sciences* **2000**, *97*, 9390-9395.

[271] Gafken, P. R.; Lampe, P. D. Methodologies for Characterizing Phosphoproteins by Mass Spectrometry. *Cell Commun Adhes* **2006**, *13*, 249-262.

[272] Rush, J., *et al.* Immunoaffinity profiling of tyrosine phosphorylation in cancer cells. *Nat Biotech* **2005**, *23*, 94-101.

[273] Hammond, D. E., *et al.* Quantitative Analysis of HGF and EGF-Dependent Phosphotyrosine Signaling Networks. *J. Proteome Res.* **2010**, *9*, 2734-2742.

[274] Liu, H., *et al.* CUB-domain–containing protein 1 (CDCP1) activates Src to promote melanoma metastasis. *Proceedings of the National Academy of Sciences* **2011**, *108*, 1379-1384.

[275] Comuzzi, B.; Sadar, M. D. Proteomic analyses to identify novel therapeutic targets for the treatment of advanced prostate cancer. *Cellscience* **2006**, *3*, 61-81.

[276] Dolai, S., *et al.* Quantitative chemical proteomics in small-scale culture of phorbol ester stimulated basal breast cancer cells. *Proteomics* **2011**, *11*, 2683-2692.

[277] Yan, G. R., *et al.* Global identification of miR-373-regulated genes in breast cancer by quantitative proteomics. *Proteomics* **2011**, *11*, 912-920.

[278] Chen, H., *et al.* Proteomic characterization of Her2/neu-overexpressing breast cancer cells. *Proteomics* **2010**, *10*, 3800-3810.

[279] Thomas, P. D., *et al.* PANTHER: a browsable database of gene products organized by biological function, using curated protein family and subfamily classification. *Nucleic Acids Research* **2003**, *31*, 334-341.

[280] Tomasetto, C., *et al.* Identification of Four Novel Human Genes Amplified and Overexpressed in Breast Carcinoma and Localized to the q11-q21.3 Region of Chromosome 17. *Genomics* **1995**, *28*, 367-376.

[281] Ewald, J. A., *et al.* Therapy-Induced Senescence in Cancer. *Journal of the National Cancer Institute* **2010**, *102*, 1536-1546.

[282] Michishita, E., *et al.* 5-Bromodeoxyuridine induces senescence-like phenomena in mammalian cells regardless of cell type or species. *J. Biochem.* **1999**, *126*, 1052-1059.

[283] Bringold, F.; Serrano, M. Tumor suppressors and oncogenes in cellular senescence☆. *Exp. Gerontol.* **2000**, *35*, 317-329.

[284] Clark, L. C., *et al.* Effects of selenium supplementation for cancer prevention in patients with carcinoma of the skin. A randomized controlled trial. Nutritional Prevention of Cancer Study Group. *JAMA* **1996**, *276*, 1957-1963.

[285] Whanger, P. D. Selenium and its relationship to cancer: an update. *Br. J. Nutr.* **2004**, *91*, 11-28.

[286] Gillet, J., *et al.* Redefining the relevance of established cancer cell lines to the study of mechanisms of clinical anti-cancer drug resistance. *Proceedings of the National Academy of Sciences* **2011**, *108*, 18708-18713.

[287] Sharma, S. V., *et al.* A chromatin-mediated reversible drug-tolerant state in cancer cell subpopulations. *Cell* **2010**, *141*, 69-80.

[288] Garrett, J. T., *et al.* Transcriptional and posttranslational up-regulation of HER3 (ErbB3) compensates for inhibition of the HER2 tyrosine kinase. *Proceedings of the National Academy of Sciences* **2011**, *108*, 5021-5026.

[289] Sergina, N. V., *et al.* Escape from HER-family tyrosine kinase inhibitor therapy by the kinase-inactive HER3. *Nature* **2007**, *445*, 437-441.

[290] Witton, C. J., *et al.* Expression of the HER1-4 family of receptor tyrosine kinases in breast cancer. *J. Pathol.* **2003**, *200*, 290-297.

[291] Naresh, A., *et al.* The ERBB4/HER4 Intracellular Domain 4ICD Is a BH3-Only Protein Promoting Apoptosis of Breast Cancer Cells. *Cancer Research* **2006**, *66*, 6412-6420.

[292] Das, P. M., *et al.* Reactivation of epigenetically silenced HER4/ERBB4 results in apoptosis of breast tumor cells. *Oncogene* **2010**, *29*, 5214-5219.

[293] Sassen, A., *et al.* Presence of HER4 associates with increased sensitivity to Herceptin in patients with metastatic breast cancer. *Breast Cancer Res.* **2009**, *11*, R50.

[294] Naresh, A., *et al.* The HER4/4ICD Estrogen Receptor Coactivator and BH3-Only Protein Is an Effector of Tamoxifen-Induced Apoptosis. *Cancer Research* **2008**, *68*, 6387-6395.

[295] Paez, J. G., *et al.* EGFR mutations in lung cancer: correlation with clinical response to gefitinib therapy. *Science* **2004**, *304*, 1497-1500.

[296] Engelman, J. A., *et al.* MET Amplification Leads to Gefitinib Resistance in Lung Cancer by Activating ERBB3 Signaling. *Science* **2007**, *316*, 1039-1043.

[297] Bean, J., *et al.* MET amplification occurs with or without T790M mutations in EGFR mutant lung tumors with acquired resistance to gefitinib or erlotinib. *Proceedings of the National Academy of Sciences* **2007**, *104*, 20932-20937.

[298] Chen, C., *et al.* Met activation mediates resistance to lapatinib inhibition of HER2-amplified gastric cancer cells. *Molecular Cancer Therapeutics* **2012**.

[299] Berns, K., *et al.* A Functional Genetic Approach Identifies the PI3K Pathway as a Major Determinant of Trastuzumab Resistance in Breast Cancer. *Cancer Cell* **2007**, *12*, 395-402.

[300] Vasudevan, K. M., *et al.* AKT-independent signaling downstream of oncogenic PIK3CA mutations in human cancer. *Cancer. Cell.* **2009**, *16*, 21-32.

[301] Aird, K. M., *et al.* ErbB1/2 tyrosine kinase inhibitor mediates oxidative stress-induced apoptosis in inflammatory breast cancer cells. *Breast Cancer Res. Treat.* **2011**.

[302] Jaffer, S., *et al.* Immunohistochemical detection of antiapoptotic protein X-linked inhibitor of apoptosis in mammary carcinoma. *Hum. Pathol.* **2007**, *38*, 864-870.

[303] Aird, K. M., *et al.* Trastuzumab signaling in ErbB2-overexpressing inflammatory breast cancer correlates with X-linked inhibitor of apoptosis protein expression. *Molecular Cancer Therapeutics* **2008**, *7*, 38-47.

[304] Foster, F. M., *et al.* Targeting inhibitor of apoptosis proteins in combination with ErbB antagonists in breast cancer. *Breast Cancer Res.* **2009**, *11*, R41.

[305] Henson, E. S.; Hu, X.; Gibson, S. B. Herceptin Sensitizes ErbB2–Overexpressing Cells to Apoptosis by Reducing Antiapoptotic Mcl-1 Expression. *Clinical Cancer Research* **2006**, *12*, 845-853.

[306] Eustace, A. J., *et al.* In *In Acquired resistance to lapatinib in HER2-positive breast cancer cells results in alterations to the Bcl-2 family members MCL-1 and BAX, which sensitizes cells to treatment with the Bcl-2 inhibitor obatoclax and lapatinib.* ASCO 2012 - submitted abstract #96277; 2012; .

[307] Xia, W., *et al.* Truncated ErbB2 Expressed in Tumor Cell Nuclei Contributes to Acquired Therapeutic Resistance to ErbB2 Kinase Inhibitors. *Molecular Cancer Therapeutics* **2011**, *10*, 1367-1374.

[308] Dimri, G. P., *et al.* A biomarker that identifies senescent human cells in culture and in aging skin in vivo. *Proceedings of the National Academy of Sciences* **1995**, *92*, 9363-9367.

[309] Debacq-Chainiaux, F., *et al.* Protocols to detect senescence-associated beta-galactosidase (SA-[beta]gal) activity, a biomarker of senescent cells in culture and in vivo. *Nat. Protocols* **2009**, *4*, 1798-1806.

[310] Campisi, J.; d'Adda, d. F. Cellular senescence: when bad things happen to good cells. *Nat. Rev. Mol. Cell Biol.* **2007**, *8*, 729-740.

[311] HAYFLICK, L.; MOORHEAD, P. S. The serial cultivation of human diploid cell strains. *Exp. Cell Res.* **1961**, *25*, 585-621.

[312] Harley, C. B.; Futcher, A. B.; Greider, C. W. Telomeres shorten during ageing of human fibroblasts. *Nature* **1990**, *345*, 458-460.

[313] Judith, C. Cellular senescence as a tumor-suppressor mechanism. *Trends Cell Biol.* **2001**, *11*, S27-S31.

[314] Reddy, J.; Li, Y. Oncogene-Induced Senescence and its Role in Tumor Suppression. *Journal of Mammary Gland Biology and Neoplasia* **2011**, *16*, 247-256.

[315] Chang, B. D., *et al.* A senescence-like phenotype distinguishes tumor cells that undergo terminal proliferation arrest after exposure to anticancer agents. *Cancer Res.* **1999**, *59*, 3761-3767.

[316] te Poele, R. H., *et al.* DNA Damage Is Able to Induce Senescence in Tumor Cells in Vitro and in Vivo. *Cancer Research* **2002**, *62*, 1876-1883.

[317] Roberson, R. S., *et al.* Escape from Therapy-Induced Accelerated Cellular Senescence in p53-Null Lung Cancer Cells and in Human Lung Cancers. *Cancer Research* **2005**, *65*, 2795-2803.

[318] Heiss, E. H.; Schilder, Y. D. C.; Dirsch, V. M. Chronic Treatment with Resveratrol Induces Redox Stress- and Ataxia Telangiectasia-mutated (ATM)-dependent Senescence in p53-positive Cancer Cells. *Journal of Biological Chemistry* **2007**, *282*, 26759-26766.

[319] Narath, R., *et al.* Induction of senescence in MYCN amplified neuroblastoma cell lines by hydroxyurea. *Genes, Chromosomes and Cancer* **2007**, *46*, 130-142.

[320] Ewald, J. A., *et al.* A High-Throughput Method to Identify Novel Senescence-Inducing Compounds. *Journal of Biomolecular Screening* **2009**, *14*, 853-858.

[321] Alimonti, A., *et al.* A novel type of cellular senescence that can be enhanced in mouse models and human tumor xenografts to suppress prostate tumorigenesis. *J. Clin. Invest.* **2010**, *120*, 681-693.

[322] Huck, J. J., *et al.* MLN8054, an Inhibitor of Aurora A Kinase, Induces Senescence in Human Tumor Cells Both In vitro and In vivo. *Molecular Cancer Research* **2010**, *8*, 373-384.

[323] Spallarossa, P., *et al.* Doxorubicin induces senescence or apoptosis in rat neonatal cardiomyocytes by regulating the expression levels of the telomere binding factors 1 and 2. *American Journal of Physiology - Heart and Circulatory Physiology* **2009**, *297*, H2169-H2181.

[324] Zuckerman, V., *et al.* Tumour suppression by p53: the importance of apoptosis and cellular senescence. *J. Pathol.* **2009**, *219*, 3-15.

[325] Atadja, P., *et al.* Increased activity of p53 in senescing fibroblasts. *Proceedings of the National Academy of Sciences* **1995**, *92*, 8348-8352.

[326] Gire, V.; Wynford-Thomas, D. Reinitiation of DNA Synthesis and Cell Division in Senescent Human Fibroblasts by Microinjection of Anti-p53 Antibodies. *Molecular and Cellular Biology* **1998**, *18*, 1611-1621.

[327] Chang, B. D., *et al.* Role of p53 and p21waf1/cip1 in senescence-like terminal proliferation arrest induced in human tumor cells by chemotherapeutic drugs. *Oncogene* **1999**, *18*, 4808-4818.

[328] Gewirtz, D. A.; Holt, S. E.; Elmore, L. W. Accelerated senescence: An emerging role in tumor cell response to chemotherapy and radiation. *Biochem. Pharmacol.* **2008**, *76*, 947-957.

[329] Gazdar, A. F., *et al.* Characterization of paired tumor and non-tumor cell lines established from patients with breast cancer. *International Journal of Cancer* **1998**, *78*, 766-774.

[330] Runnebaum, I. B., *et al.* Mutations in p53 as potential molecular markers for human breast cancer. *Proceedings of the National Academy of Sciences* **1991**, *88*, 10657-10661.

[331] Dai, C. Y.; Enders, G. H. p16 INK4a can initiate an autonomous senescence program. *Oncogene* **2000**, *19*, 1613-1622.

[332] Fuxe, J., *et al.* Adenovirus-mediated Overexpression of p15INK4B Inhibits Human Glioma Cell Growth, Induces Replicative Senescence, and Inhibits Telomerase Activity Similarly to p16INK4A. *Cell Growth Differ.* **2000**, *11*, 373-384.

[333] Fang, L., *et al.* p21Waf1/Cip1/Sdi1 induces permanent growth arrest with markers of replicative senescence in human tumor cells lacking functional p53. *Oncogene* **1999**, *18*, 2789-2797.

[334] Majumder, P. K., *et al.* A Prostatic Intraepithelial Neoplasia-Dependent p27Kip1 Checkpoint Induces Senescence and Inhibits Cell Proliferation and Cancer Progression. *Cancer Cell* **2008**, *14*, 146-155.

[335] Jeanblanc, M., *et al.* Parallel pathways in RAF-induced senescence and conditions for its reversion. *Oncogene* **2011**.

[336] Okamoto, A., *et al.* Mutations and altered expression of p16INK4 in human cancer. *Proceedings of the National Academy of Sciences* **1994**, *91*, 11045-11049.

[337] WHITAKER, N., *et al.* Involvement of Rb-1, P53, P16(ink4) and Telomerase in Immortalization of Human-Cells. *Oncogene* **1995**, *11*, 971-976.

[338] Tsutsui, T., *et al.* Association of p16INK4a and pRb inactivation with immortalization of human cells. *Carcinogenesis* **2002**, *23*, 2111-2117.

[339] Schmitt, C. A., *et al.* A senescence program controlled by p53 and p16INK4a contributes to the outcome of cancer therapy. *Cell* **2002**, *109*, 335-346.

[340] Duan, J., *et al.* Irreversible cellular senescence induced by prolonged exposure to H2O2 involves DNA-damage-and-repair genes and telomere shortening. *Int. J. Biochem. Cell Biol.* **2005**, *37*, 1407-1420.

[341] Beausejour, C. M., *et al.* Reversal of human cellular senescence: roles of the p53 and p16 pathways. *EMBO J.* **2003**, *22*, 4212-4222.

[342] Wang, Q., *et al.* Survivin and escaping in therapy-induced cellular senescence. *International Journal of Cancer* **2011**, *128*, 1546-1558.

[343] Schwarze, S. R., *et al.* Role of cyclin-dependent kinase inhibitors in the growth arrest at senescence in human prostate epithelial and uroepithelial cells. *Oncogene* **2001**, *20*, 8184-8192.

[344] O'Malley, F. P., *et al.* Topoisomerase II Alpha and Responsiveness of Breast Cancer to Adjuvant Chemotherapy. *Journal of the National Cancer Institute* **2009**, *101*, 644-650.

[345] Leo, A. D., *et al.* HER2 and TOP2A as predictive markers for anthracycline-containing chemotherapy regimens as adjuvant treatment of breast cancer: a meta-analysis of individual patient data. *The Lancet Oncology* **2011**, *12*, 1134-1142.

[346] Saeki, N., *et al.* GASDERMIN, suppressed frequently in gastric cancer, is a target of LMO1 in TGF-[beta]-dependent apoptotic signalling. *Oncogene* **2007**, *26*, 6488-6498.

[347] Kao, J.; Pollack, J. R. RNA interference-based functional dissection of the 17q12 amplicon in breast cancer reveals contribution of coamplified genes. *Genes, Chromosomes and Cancer* **2006**, *45*, 761-769.

[348] Alpy, F., *et al.* Metastatic lymph node 64 (MLN64), a gene overexpressed in breast cancers, is regulated by Sp//KLF transcription factors. *Oncogene* **2003**, *22*, 3770-3780.

[349] Moog-Lutz, C., *et al.* MLN64 exhibits homology with the steroidogenic acute regulatory protein (STAR) and is over-expressed in human breast carcinomas. *International Journal of Cancer* **1997**, *71*, 183-191.

[350] Cai, W., *et al.* Expression of MLN64 influences cellular matrix adhesion of breast cancer cells, the role for focal adhesion kinase. *Int. J. Mol. Med.* **2010**, *25*, 573-580.

[351] Stigliano, A., *et al.* Increased metastatic lymph node 64 and CYP17 expression are associated with high stage prostate cancer. *Journal of Endocrinology* **2007**, *194*, 55-61.

[352] Glynn, R. W.; Miller, N.; Kerin, M. J. 17q12-21 – The pursuit of targeted therapy in breast cancer. *Cancer Treat. Rev.* **2010**, *36*, 224-229.

[353] Obaidat, A.; Roth, M.; Hagenbuch, B. The Expression and Function of Organic Anion Transporting Polypeptides in Normal Tissues and in Cancer. *Annu. Rev. Pharmacol. Toxicol.* **2012**.

[354] Miki, Y., *et al.* Expression of the Steroid and Xenobiotic Receptor and Its Possible Target Gene, Organic Anion Transporting Polypeptide-A, in Human Breast Carcinoma. *Cancer Research* **2006**, *66*, 535-542.

[355] Hagenbuch, B.; Gui, C. Xenobiotic transporters of the human organic anion transporting polypeptides (OATP) family. *Xenobiotica* **2008**, *38*, 778-801.

[356] Feng, B., *et al.* Role of Hepatic Transporters in the Disposition and Hepatotoxicity of a HER2 Tyrosine Kinase Inhibitor CP-724,714. *Toxicological Sciences* **2009**, *108*, 492-500.

[357] Chen, C., *et al.* Sumoylation of eukaryotic elongation factor 2 is vital for protein stability and anti-apoptotic activity in lung adenocarcinoma cells. *Cancer Science* **2011**, *102*, 1582-1589.

[358] Nakamura, J., *et al.* Overexpression of eukaryotic elongation factor eEF2 in gastrointestinal cancers and its involvement in G2/M progression in the cell cycle. *Int. J. Oncol.* **2009**, *34*, 1181-1189.

[359] Ryazanov, A. G.; Shestakova, E. A.; Natapov, P. G. Phosphorylation of elongation factor 2 by EF-2 kinase affects rate of translation. *Nature* **1988**, *334*, 170-173.

[360] Parmer, T. G., *et al.* Activity and regulation by growth factors of calmodulin-dependent protein kinase III (elongation factor 2-kinase) in human breast cancer[ast]. *Br. J. Cancer* **1998**, *79*, 59-64.

[361] Browne, G. J.; Proud, C. G. Regulation of peptide-chain elongation in mammalian cells. *European Journal of Biochemistry* **2002**, *269*, 5360-5368.

[362] Knebel, A.; Morrice, N.; Cohen, P. A novel method to identify protein kinase substrates: eEF2 kinase is phosphorylated and inhibited by SAPK4/p38delta. *EMBO J.* **2001**, *20*, 4360-4369.

[363] Smith, E. M.; Proud, C. G. cdc2-cyclin B regulates eEF2 kinase activity in a cell cycle- and amino acid-dependent manner. *EMBO J.* **2008**, *27*, 1005-1016.

[364] Arora, S., *et al.* Identification and Characterization of an Inhibitor of Eukaryotic Elongation Factor 2 Kinase against Human Cancer Cell Lines. *Cancer Research* **2003**, *63*, 6894-6899.

[365] Chen, Z., *et al.* 1-Benzyl-3-cetyl-2-methylimidazolium iodide (NH125) Induces Phosphorylation of Eukaryotic Elongation Factor-2 (eEF2). *Journal of Biological Chemistry* **2011**, *286*, 43951-43958.

[366] Zhang, Y., *et al.* Inhibition of eEF-2 kinase sensitizes human glioma cells to TRAIL and down-regulates Bcl-xL expression. *Biochem. Biophys. Res. Commun.* **2011**, *414*, 129-134.

[367] Parker, C. G., *et al.* Identification of Stathmin as a Novel Substrate for p38 Delta. *Biochem. Biophys. Res. Commun.* **1998**, *249*, 791-796.

[368] Cuenda, A.; Rousseau, S. p38 MAP-Kinases pathway regulation, function and role in human diseases. *Biochimica et Biophysica Acta (BBA) - Molecular Cell Research* **2007**, *1773*, 1358-1375.

[369] Goedert, M., *et al.* Activation of the novel stress-activated protein kinase SAPK4 by cytokines and cellular stresses is mediated by SKK3 (MKK6); comparison of its substrate specificity with that of other SAP kinases. *EMBO J.* **1997**, *16*, 3563-3571.

[370] Kuma, Y., *et al.* BIRB796 Inhibits All p38 MAPK Isoforms in Vitro and in Vivo. *Journal of Biological Chemistry* **2005**, *280*, 19472-19479.

[371] Everett, A. D., *et al.* Angiotensin II regulates phosphorylation of translation elongation factor-2 in cardiac myocytes. *American Journal of Physiology - Heart and Circulatory Physiology* **2001**, *281*, H161-H167.

[372] Wang, L.; Proud, C. G. Regulation of the phosphorylation of elongation factor 2 by MEK-dependent signalling in adult rat cardiomyocytes. *FEBS Lett.* **2002**, *531*, 285-289.

[373] Zoppoli, G., *et al.* Ras-induced resistance to lapatinib is overcome by MEK inhibition. *Curr. Cancer. Drug Targets* **2010**, *10*, 168-175.

[374] Roberts, P. J.; Der, C. J. Targeting the Raf-MEK-ERK mitogen-activated protein kinase cascade for the treatment of cancer. *Oncogene* **2007**, *26*, 3291-3310.

[375] Hardie, D. G., *et al.* Management of cellular energy by the AMP-activated protein kinase system. *FEBS Lett.* **2003**, *546*, 113-120.

[376] Browne, G. J.; Finn, S. G.; Proud, C. G. Stimulation of the AMP-activated Protein Kinase Leads to Activation of Eukaryotic Elongation Factor 2 Kinase and to Its Phosphorylation at a Novel Site, Serine 398. *Journal of Biological Chemistry* **2004**, *279*, 12220-12231.

[377] Devost, D.; Carrier, M.; Zingg, H. H. Oxytocin-Induced Activation of Eukaryotic Elongation Factor 2 in Myometrial Cells Is Mediated by Protein Kinase C. *Endocrinology* **2008**, *149*, 131-138.

[378] Guan, L., *et al.* Protein Kinase C-mediated Down-regulation of Cyclin D1 Involves Activation of the Translational Repressor 4E-BP1 via a Phosphoinositide 3-Kinase/Akt-independent, Protein Phosphatase 2A-dependent Mechanism in Intestinal Epithelial Cells. *Journal of Biological Chemistry* **2007**, *282*, 14213-14225.

[379] Zhang, D., *et al.* Protein kinase C delta negatively regulates tyrosine hydroxylase activity and dopamine synthesis by enhancing protein phosphatase-2A activity in dopaminergic neurons. *J. Neurosci.* **2007**, *27*, 5349-5362.

[380] Gergs, U., *et al.* Overexpression of the Catalytic Subunit of Protein Phosphatase 2A Impairs Cardiac Function. *Journal of Biological Chemistry* **2004**, *279*, 40827-40834.

[381] Wong, L. L., *et al.* Tyrosine phosphorylation of PP2A is regulated by HER-2 signalling and correlates with breast cancer progression. *Int. J. Oncol.* **2009**, *34*, 1291-1301.

[382] Sundaresan, P.; Farndale, R. W. p38 mitogen-activated protein kinase dephosphorylation is regulated by protein phosphatase 2A in human platelets activated by collagen. *FEBS Lett.* **2002**, *528*, 139-144.

[383] Price, D., *et al.* Rapamycin-induced inhibition of the 70-kilodalton S6 protein kinase. *Science* **1992**, *257*, 973-977.

[384] Copp, J.; Manning, G.; Hunter, T. TORC-Specific Phosphorylation of Mammalian Target of Rapamycin (mTOR): Phospho-Ser2481 Is a Marker for Intact mTOR Signaling Complex 2. *Cancer Research* **2009**, *69*, 1821-1827.

[385] Dennis, P. B., *et al.* The principal rapamycin-sensitive p70(s6k) phosphorylation sites, T-229 and T-389, are differentially regulated by rapamycin-insensitive kinase kinases. *Molecular and Cellular Biology* **1996**, *16*, 6242-6251.

[386] Ali, S. M.; Sabatini, D. M. Structure of S6 Kinase 1 Determines whether Raptor-mTOR or Rictor-mTOR Phosphorylates Its Hydrophobic Motif Site. *Journal of Biological Chemistry* **2005**, *280*, 19445-19448.

[387] Bärlund, M., *et al.* Detecting Activation of Ribosomal Protein S6 Kinase by Complementary DNA and Tissue Microarray Analysis. *Journal of the National Cancer Institute* **2000**, *92*, 1252-1259.

[388] van der Hage, ,J.A., *et al.* Overexpression of P70 S6 kinase protein is associated with increased risk of locoregional recurrence in node-negative premenopausal early breast cancer patients. *Br. J. Cancer* **2004**, *90*, 1543-1550.

[389] Klos, K. S., *et al.* ErbB2 Increases Vascular Endothelial Growth Factor Protein Synthesis via Activation of Mammalian Target of Rapamycin/p70S6K Leading to Increased Angiogenesis and Spontaneous Metastasis of Human Breast Cancer Cells. *Cancer Research* **2006**, *66*, 2028-2037.

[390] Gayle, S. S., *et al.* Pharmacologic Inhibition of mTOR Improves Lapatinib Sensitivity in HER2-Overexpressing Breast Cancer Cells with Primary Trastuzumab Resistance. *Anticancer Agents Med. Chem.* **2011**.

[391] Vazquez-Martin, A., *et al.* Low-scale phosphoproteome analyses identify the mTOR effector p70 S6 kinase 1 as a specific biomarker of the dual-HER1/HER2 tyrosine kinase inhibitor lapatinib (Tykerb®) in human breast carcinoma cells. *Annals of Oncology* **2008**, *19*, 1097-1109.

[392] Boersema, P. J., *et al.* In-depth Qualitative and Quantitative Profiling of Tyrosine Phosphorylation Using a Combination of Phosphopeptide Immunoaffinity Purification and Stable Isotope Dimethyl Labeling. *Molecular & Cellular Proteomics* **2010**, *9*, 84-99.

[393] Guha, U., *et al.* Comparisons of tyrosine phosphorylated proteins in cells expressing lung cancer-specific alleles of EGFR and KRAS. *Proceedings of the National Academy of Sciences* **2008**, *105*, 14112-14117.

[394] Guo, A., *et al.* Signaling networks assembled by oncogenic EGFR and c-Met. *Proceedings of the National Academy of Sciences* **2008**, *105*, 692-697.

[395] Rikova, K., *et al.* Global Survey of Phosphotyrosine Signaling Identifies Oncogenic Kinases in Lung Cancer. *Cell* **2007**, *131*, 1190-1203.

[396] Krishnamoorthy, S. Receptor Tyrosine Kinase (RTK) Mediated Tyrosine Phosphor-Proteome from Drosophila S2 (ErbB1) Cells Reveals Novel Signaling Networks. *PLoS ONE* **2008**, *3*, e2877.

[397] Mithoe, S. C., *et al.* Targeted Quantitative Phosphoproteomics Approach for the Detection of Phospho-tyrosine Signaling in Plants. *J. Proteome Res.* **2012**, *11*, 438-448.

[398] Satyanarayana, A.; Kaldis, P. Mammalian cell-cycle regulation: several Cdks, numerous cyclins and diverse compensatory mechanisms. *Oncogene* **2009**, *28*, 2925-2939.

[399] Takizawa, C. G.; Morgan, D. O. Control of mitosis by changes in the subcellular location of cyclin-B1–Cdk1 and Cdc25C. *Curr. Opin. Cell Biol.* **2000**, *12*, 658-665.

[400] Colell, A.; Green, D. R.; Ricci, J. Novel roles for GAPDH in cell death and carcinogenesis. *Cell Death Differ.* **2009**, *16*, 1573-1581.

[401] Huang, Q., *et al.* Akt2 Kinase Suppresses Glyceraldehyde-3-phosphate Dehydrogenase (GAPDH)-mediated Apoptosis in Ovarian Cancer Cells via Phosphorylating GAPDH at Threonine 237 and Decreasing Its Nuclear Translocation. *Journal of Biological Chemistry* **2011**, *286*, 42211-42220.

[402] Phadke, M., *et al.* Accelerated cellular senescence phenotype of GAPDH-depleted human lung carcinoma cells. *Biochem. Biophys. Res. Commun.* **2011**, *411*, 409-415.

[403] Carujo, S., *et al.* Glyceraldehyde 3-phosphate dehydrogenase is a SET-binding protein and regulates cyclin B-cdk1 activity. *Oncogene* **2006**, *25*, 4033-4042.

[404] Krajewski, W. A., *et al.* A Motif within SET-Domain Proteins Binds Single-Stranded Nucleic Acids and Transcribed and Supercoiled DNAs and Can Interfere with Assembly of Nucleosomes. *Molecular and Cellular Biology* **2005**, *25*, 1891-1899.

[405] Canela, N., *et al.* The SET Protein Regulates G2/M Transition by Modulating Cyclin B-Cyclin-dependent Kinase 1 Activity. *Journal of Biological Chemistry* **2003**, *278*, 1158-1164.

[406] Seo, S., *et al.* Regulation of Histone Acetylation and Transcription by INHAT, a Human Cellular Complex Containing the Set Oncoprotein. *Cell* **2001**, *104*, 119-130.

[407] Compagnone, N. A., *et al.* Novel Role for the Nuclear Phosphoprotein SET in Transcriptional Activation of P450c17 and Initiation of Neurosteroidogenesis. *Molecular Endocrinology* **2000**, *14*, 875-888.

[408] Madeira, A., *et al.* SET protein (TAF1β, I2PP2A) is involved in neuronal apoptosis induced by an amyloid precursor protein cytoplasmic subdomain. *The FASEB Journal* **2005**.

[409] ten Klooster, J. P., *et al.* Rac1-induced cell migration requires membrane recruitment of the nuclear oncogene SET. *EMBO J.* **2007**, *26*, 336-345.

[410] Fan, Z., *et al.* Tumor Suppressor NM23-H1 Is a Granzyme A-Activated DNase during CTL-Mediated Apoptosis, and the Nucleosome Assembly Protein SET Is Its Inhibitor. *Cell* **2003**, *112*, 659-672.

[411] Li, M.; Makkinje, A.; Damuni, Z. Molecular Identification of I1PP2A, a Novel Potent Heat-Stable Inhibitor Protein of Protein Phosphatase 2Aâ€ . *Biochemistry (N. Y.)* **1996**, *35*, 6998-7002.

[412] Arnold, H.; Sears, R. A tumor suppressor role for PP2A-B56α through negative regulation of c-Myc and other key oncoproteins. *Cancer and Metastasis Reviews* **2008**, *27*, 147-158.

[413] Götz, J., *et al.* Distinct role of protein phosphatase 2A subunit Cα in the regulation of E-cadherin and β-catenin during development. *Mech. Dev.* **2000**, *93*, 83-93.

[414] Resjö, S., *et al.* Protein phosphatase 2A is the main phosphatase involved in the regulation of protein kinase B in rat adipocytes. *Cell. Signal.* **2002**, *14*, 231-238.

[415] Switzer, C. H., *et al.* Targeting SET/I(2)PP2A oncoprotein functions as a multi-pathway strategy for cancer therapy. *Oncogene* **2011**, *30*, 2504-2513.

[416] Mimura, K., *et al.* Lapatinib inhibits receptor phosphorylation and cell growth and enhances antibody-dependent cellular cytotoxicity of EGFR- and HER2-overexpressing esophageal cancer cell lines. *Int. J. Cancer* **2011**, *129*, 2408-2416.

[417] Scaltriti, M., *et al.* Lapatinib, a HER2 tyrosine kinase inhibitor, induces stabilization and accumulation of HER2 and potentiates trastuzumab-dependent cell cytotoxicity. *Oncogene* **2008**, *28*, 803-814.

[418] Yoo, J. Y., *et al.* Interaction of the PA2G4 (EBP1) protein with ErbB-3 and regulation of this binding by heregulin. *Br. J. Cancer* **2000**, *82*, 683-690.

[419] Lessor, T. J., *et al.* Ectopic expression of the ErbB-3 binding protein Ebp1 inhibits growth and induces differentiation of human breast cancer cell lines. *J. Cell. Physiol.* **2000**, *183*, 321-329.

[420] Lu, Y., *et al.* The ErbB3 binding protein EBP1 regulates ErbB2 protein levels and tamoxifen sensitivity in breast cancer cells. *Breast Cancer Research and Treatment* **2011**, *126*, 27-36.

[421] Zhang, Y.; Akinmade, D.; Hamburger, A. W. Inhibition of heregulin mediated MCF-7 breast cancer cell growth by the ErbB3 binding protein EBP1. *Cancer Lett.* **2008**, *265*, 298-306.

[422] Ahn, J., *et al.* Nuclear Akt associates with PKC-phosphorylated Ebp1, preventing DNA fragmentation by inhibition of caspase-activated DNase. *EMBO J.* **2006**, *25*, 2083-2095.

[423] Liu, Z., *et al.* Ebp1 isoforms distinctively regulate cell survival and differentiation. *Proceedings of the National Academy of Sciences* **2006**, *103*, 10917-10922.

[424] Zhang, J.; Dong, W. G.; Lin, J. Reduced selenium-binding protein 1 is associated with poor survival rate in gastric carcinoma. *Med. Oncol.* **2011**, *28*, 481-487.

[425] Yang, M.; Sytkowski, A. J. Differential Expression and Androgen Regulation of the Human Selenium-binding Protein Gene hSP56 in Prostate Cancer Cells. *Cancer Research* **1998**, *58*, 3150-3153.

[426] Chen, G., *et al.* Reduced selenium-binding protein 1 expression is associated with poor outcome in lung adenocarcinomas. *J. Pathol.* **2004**, *202*, 321-329.

[427] Schaner, M. E., *et al.* Gene Expression Patterns in Ovarian Carcinomas. *Molecular Biology of the Cell* **2003**, *14*, 4376-4386.

[428] Brown, L. M., *et al.* Quantitative and qualitative differences in protein expression between papillary thyroid carcinoma and normal thyroid tissue. *Mol. Carcinog.* **2006**, *45*, 613-626.

[429] Kim, H., *et al.* Suppression of human selenium-binding protein 1 is a late event in colorectal carcinogenesis and is associated with poor survival. *Proteomics* **2006**, *6*, 3466-3476.

[430] Zhang, P., *et al.* The expression of selenium-binding protein 1 is decreased in uterine leiomyoma. *Diagn. Pathol.* **2010**, *5*, 80.

[431] Silvers, A. L., *et al.* Decreased Selenium-Binding Protein 1 in Esophageal Adenocarcinoma Results from Posttranscriptional and Epigenetic Regulation and Affects Chemosensitivity. *Clinical Cancer Research* **2010**, *16*, 2009-2021.

[432] Raucci, R., *et al.* Structural and functional studies of the human selenium binding protein-1 and its involvement in hepatocellular carcinoma. *Biochim. Biophys. Acta* **2011**, *1814*, 513-522.

[433] Pohl, N. M., *et al.* Transcriptional Regulation and Biological Functions of Selenium-Binding Protein 1 in Colorectal Cancer In Vitro and in Nude Mouse Xenografts. *PLoS ONE* **2009**, *4*, e7774.

[434] Zhu, W.; Smith, J. W.; Huang, C. M. Mass spectrometry-based label-free quantitative proteomics. *J. Biomed. Biotechnol.* **2010**, *2010*, 840518.

Appendix

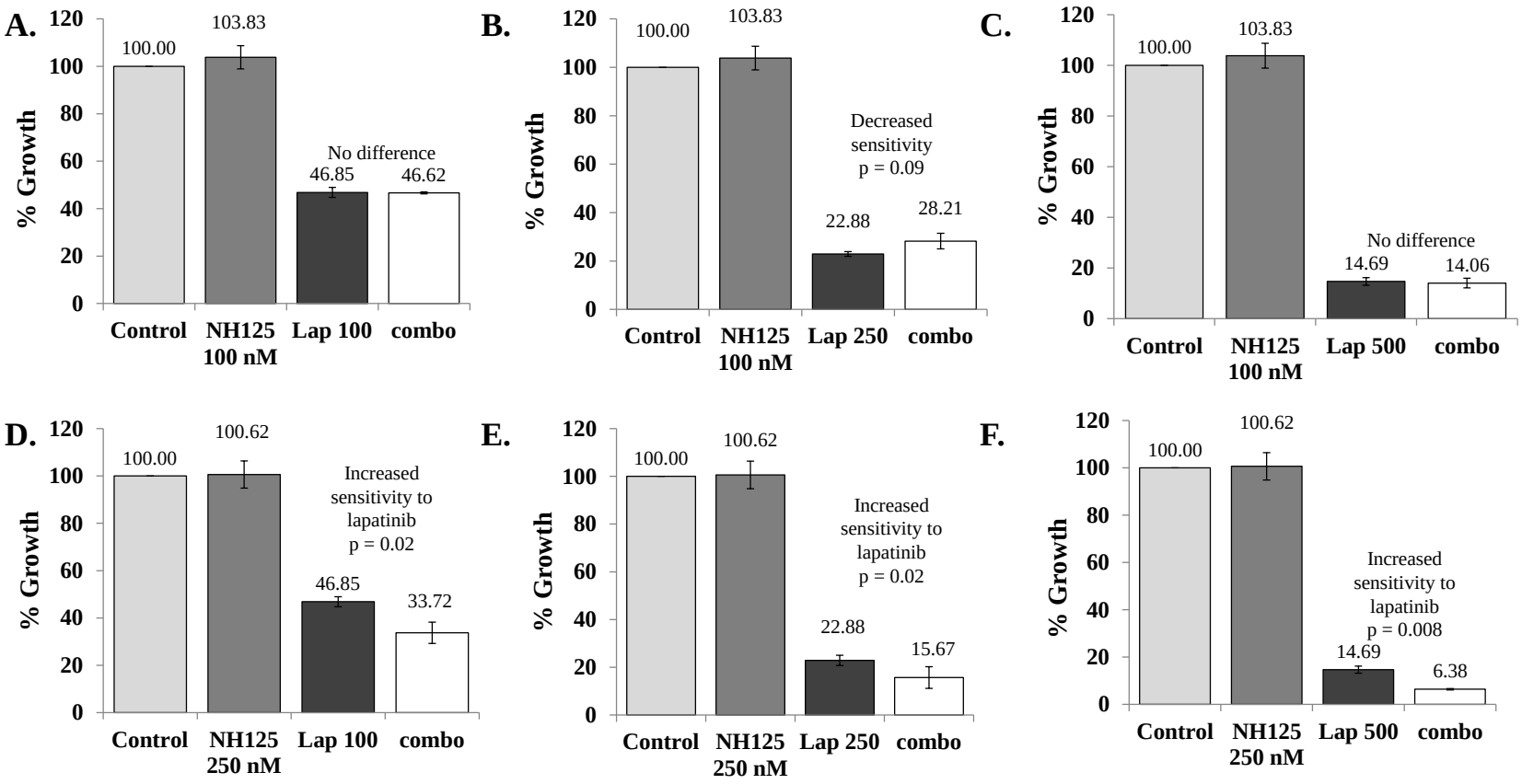

Figure 9-1: SKBR3-par cells were pre-treated with either 100 nM (A, B and C) or 250 nM (D, E and F) NH125 for 24 hours, after which time NH125 was removed from the cells and they were treated with either 100 nM lapatinib (A and D), 250 nM lapatinib (B and E) or 500 nM lapatinib (C and F) and the percentage growth of the cells was compared cells treated with lapatinib only. Growth is expressed relative to control untreated cells. Error bars represent the standard deviation of triplicate experiments.

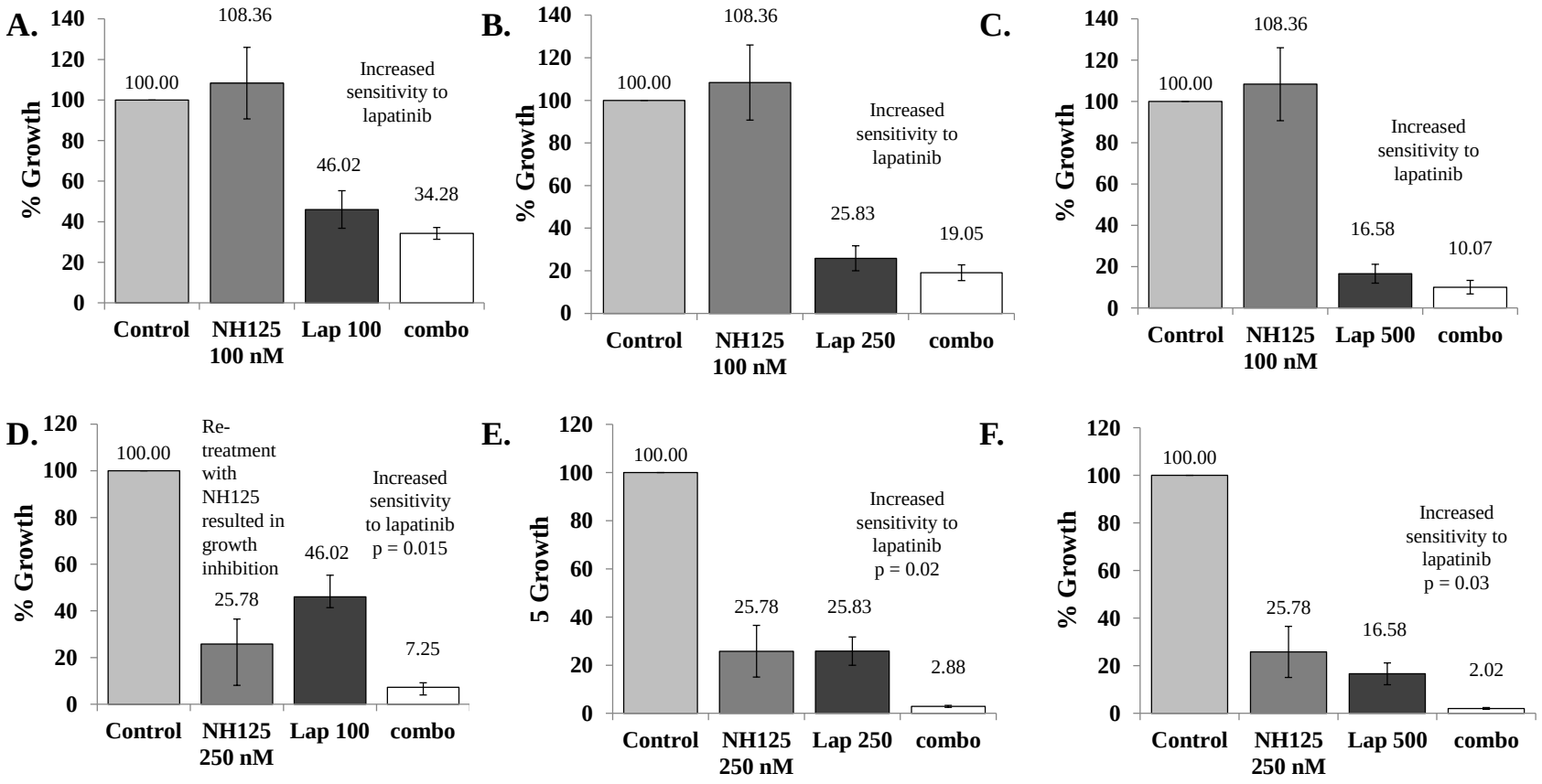

Figure 9-2: SKBR3-par cells were pre-treated with either 100 nM (A, B and C) or 250 nM (D, E and F) NH125 for 24 hours, after which time NH125 was removed from the cells and they were re-treated with NH125 and with either 100 nM lapatinib (A and D), 250 nM lapatinib (B and E) or 500 nM lapatinib (C and F) and the percentage growth of the cells was compared cells treated with lapatinib only. Growth is expressed relative to control untreated cells. Error bars represent the standard deviation of triplicate experiments.

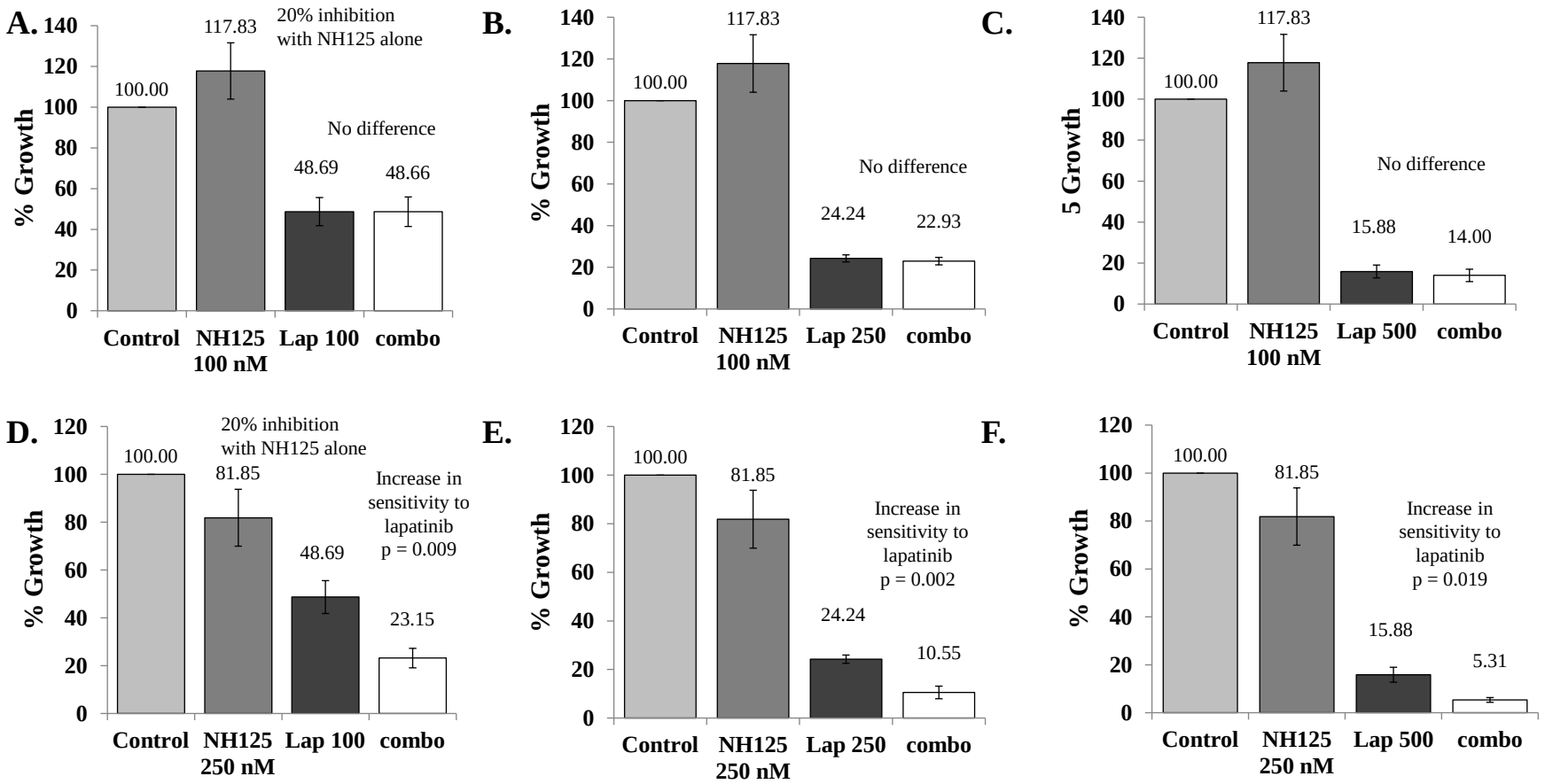

Figure 9-3: SKBR3-par cells were treated with either 100 nM (A, B and C) or 250 nM (D, E and F) NH125 in combination with either 100 nM lapatinib (A and D), 250 nM lapatinib (B and E) or 500 nM lapatinib (C and F) and the percentage growth of the cells was compared cells treated with lapatinib only. Growth is expressed relative to control untreated cells. Error bars represent the standard deviation of triplicate experiments.